annual report 1971

nuclear physics laboratory
university of washington

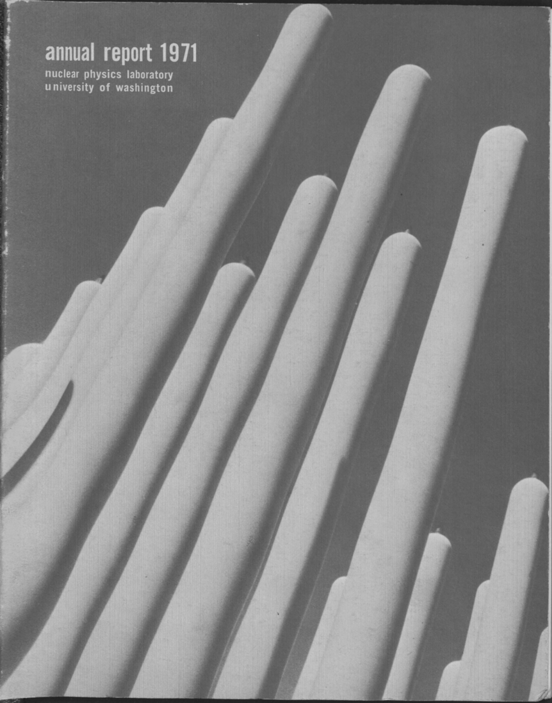

ANNUAL REPORT

Nuclear Physics Laboratory
University of Washington
June, 1971

Program "A" --
Experimental Nuclear Physics
Program (Cyclotron)
under
U.S. Atomic Energy Commission
Contract A.T.(45-1)-1388

THE COVER DESIGN

Each year we endeavor to find a cover picture which has interest for both the physicist and non-physicist, and which might be classed as somewhat unique to our laboratory.

This year we have used the same cover picture as we did last year; viz., the high pressure gas cylinders which store the nitrogen and carbon dioxide mixture used for insulating the high potential terminals of the two Van de Graaff machines.

The architect of our building managed to turn the knotty problem of where to put the cylinders into an architectural conversation piece. They form a group of towers which front on the Van de Graaff building and have aroused considerable local interest and curiosity. A faculty wife from Madrid, whose English is minimal but delightful, is convinced they are gigantic candles.

The reader can best appreciate the design by opening both front and back covers. The visitor can best observe the towers by lying on the grass and gazing at the yellow-colored tanks against a blue sky background.

There are several reasons why we did not change the cover design. First, it was cheaper to make no change; second, some of our more enthusiastic photographer-graduate students have departed; third, we rather liked the design anyway.

INTRODUCTION

The research and technical work described in this report was performed at the Nuclear Physics Laboratory of the University of Washington during the year ending April 15, 1971. It was directed and executed by faculty and graduate students from the Departments of Physics and Chemistry, by the staff of the Laboratory, and by visitor groups from both within and outside the University community.

The principal facilities of the Laboratory are a three-stage Model-FN tandem Van de Graaff accelerator, constructed by the High Voltage Engineering Company and completed in 1967, and a conventional cyclotron -- the "Sixty-Inch"-- constructed by laboratory personnel, and completed in 1952. The three-stage Van de Graaff accelerator produces a direct current beam of protons with energies variable up to 24.6 MeV. It is also used for deuteron, alpha particle, and heavy ion acceleration. The cyclotron accelerates protons, deuterons, and alpha particles to essentially fixed energies of 11, 22, and 44 MeV, respectively.

Financial support for the laboratory and for operations conducted with the Van de Graaff accelerator is provided by the Atomic Energy Commission under Contract A.T.(45-1)-1388, Program "A", and the State of Washington. Cyclotron operations are supported by State funds and by financial assistance from outside user groups. A National Science Foundation grant provided funds for the purchase of the Van de Graaff accelerator, a portion of the associated equipment, and approximately one half the construction costs of the laboratory building. The remainder of the building funds came from state sources. The State also provided considerable financial assistance for the initial construction of the cyclotron and building facilities.

The research in the Laboratory involves a wide range of current problems in the study of nuclear structure, nuclear reactions, related nuclear studies such as beta decay, and nuclear medicine. Within the limitations imposed by facilities and time, we encourage individuals and groups to pursue any avenue of research appropriate to the facilities we have available.

Each individual report is intended to describe the status of experiments or developments which in some cases are incomplete. Although many are continuations of work described in earlier Annual Reports, an effort has been made to insure that enough background material is included so that the *raison d'etre* of the work is clear to the reader. The appearance of specific numerical results and conclusions here does not constitute publication, and should not be quoted without permission of the investigators. All names are listed in alphabetical order.

Most of the reports have been written by graduate students and are chiefly their responsibility. We regard this chore as important in their training. The act of writing encourages one to focus upon objectives, and the completed sum of reports provides excellent intra-laboratory communication. We therefore feel that our Annual Report is of value both internally and externally. The editors have expressed no value judgments, and therefore we've chosen in this introduction to not single out any particular portions of the report.

Again this year, in recognition of the logic that all good experimental work must begin with good equipment, we have inverted our former subject order by placing the instrumentation sections at the beginning. However, it should not be construed that order denotes importance or even always logic. For example, the high regard we hold for our staff is not reflected in the fact that our group picture, an innovation begun last year, appears at the end of the report.

Section 14 of this report contains brief descriptions of a wide variety of research projects conducted at the Sixty-Inch Cyclotron by groups from outside the Laboratory. These visitor groups, which come from other organizations within the University, from other universities and colleges, and from industrial organizations, have provided the material contained in this section, and we appreciate their contributions. Because of the obvious benefits of this work both to the Laboratory, and to the scientific community in general, such groups will continue to be welcomed here to the fullest extent possible within the limitations of time, maintenance, and safety.

TABLE OF CONTENTS

Page

Page

1. ACCELERATOR DEVELOPMENT

1. Van de Graaff Accelerator Improvements and Operations

Laboratory Staff

This year saw the first acceleration of polarized proton and deuteron beams with our Van de Graaff. The polarized ion source, which is described in detail in Secs. 2.1,2.2 and 2.3 of this report, was installed on the machine last September, 1970 and began producing beams shortly thereafter. Difficulties were encountered in obtaining adequate reliability in control systems, in obtaining stable operation, and in matching source optics to the requirements of the accelerator. These problems have for the most part been overcome, and the source has recently been used to take experimental data (see Sec. 6.7).

In addition to the ion source installation, and to improvements listed in Secs. 1,2, and 3 of this report, the following are among the improvements that have been made this year:

a. The pumping system on the direct ion source has been revised to give lower back streaming.

b. The direct extraction source gas handling system has been modified to permit easier operation with ^{18}O.

c. The gas handling system for the Li exchange source has been revised to make it easier to operate and more reliable.

d. A larger pump for evacuating the accelerator tank has been installed.

e. A removable aperture was added in front of the 90° magnet to permit experimenters to reduce the accelerator emittance if desired.

f. A new corona head drive mechanism was installed to permit tandem operation at low voltages.

Statistics of Van de Graaff operations are given in Table 1.1-1. The tank was opened 14 times and the injector twice during the period of this report. With the exception of a belt replacement in February, maintenance in the tank was of a minor nature.

Table 1.1-1. Statistics of Van de Graaff Operation from April 16, 1970 to April 15, 1971

		Time (Hrs)	Per Cent
1.	Division of time among activities		
	Normal operation[a]	6261	71
	Scheduled Maintenance[b]	399	5
	Unscheduled Maintenance[b]	820	9
	Unrequested time	1280	15
	Total[c]	8760	100.
2.	Division of beam-on time among particles		
	a. Two-stage operation		
	Polarized protons	83	1
	Protons	1027	18
	Deuterons	374	6
	^{3}He	510	9
	^{4}He	870	15
	^{16}O	654	11
	^{18}O	191	3
	^{6}Li	385	7
	Total	4094	71
	b. Three-stage operation		
	Protons	999	17
	Deuterons	708	12
	Total	1707	29
	TOTAL BEAM TIME	5801	100

a. Includes all time accelerator was under control of an experimenter.
b. Includes time the accelerator is idle on account of these activities.
c. This is the number of hours in one year.

1.2 Terminal Ripple Remover

H. Fauska, G. Roth, F.H. Schmidt, W.G. Weitkamp

The Terminal Ripple Remover is designed to sense a signal from the tandem image slits and transmit it to the terminal of the accelerator where it is amplified to kilovolt level and applied to the stripper in such a manner as to be out of phase with terminal fluctuations.

Last year it was reported[1] that a microwave link, using a klystron transmitter outside the tank and a diode at the terminal, was used to convey information to the terminal. This system had several problems. The microwave diode was very susceptible to damage from sparks and also the klystron was unstable and difficult to keep tuned. For these reasons a light coupled system was planned.

This year such a system has been developed using a gallium arsenide light emitting diode at the tank base and a light sensitive phototransistor at the terminal. Very inexpensive diodes are now on the market which can be driven at 2 amps continuously with a light output of 18 mw. Such quantity of light is available that the diode was driven with an analog signal rather than the much more complicated analog-to-digital converter.

To couple the diode to transistor, a PVC jacketed fiber optics bundle was tried. A 25 foot length was successfully tested in the injector stage to a terminal voltage of 6.5 MV for several weeks. However, a second 25 foot length was installed in the tandem section and after a week at 8.5 MV with considerable sparking the glass fiber bundle splintered. A lens system has been substituted for the fiber optics although it is not clear that fiber optics cannot be made to operate in this environment. The lens coupled system, which has been in service several months, seems very reliable and satisfactory. Tests using a signal generator to modulate the diode have shown that the beam on the image slits is also modulated, with no appreciable phase shift, to a frequency of about 1000 Hz.

We are presently working on a system to drive the corona from the generating voltmeter to stabilize the terminal to within range of the light system. Tests of the entire system are due to begin shortly.

---

1. Nuclear Physics Laboratory Annual Report, University of Washington (1970), p. 14.

1.3 Beam Transport Calculations

J.D. Larson* and H. Willenberg

A method was found to expand the standard, linear beam-transport matrix by an additional row and column to permit first-order beam transit time calculations. Elapsed-time coefficients were derived for the common transport elements and also for electrostatic acceleration tubes. Time dispersion coefficients which include effects due to pole tip rotation were derived for bending magnets. The method preserves all traditional matrix manipulations so that spatial and temporal calculations occur simultaneously.

Work was begun on the problem of finding the phase space ellipse of larges area which survives the passage of an arbitrary ellipse through a defining aperture. A solution based on this initial effort has since been found for the symmetric aperture and this work is being continued under another contract.

The beam transport program OPTIC II was adapted to operate on the CDC 6400 computer. This program was then modified, using procedures outlined above, to perform calculations of beam transit times and time dispersion. Studies were made of the time spread contributed to pulsed beams of finite phase space area as they pass through the analyzing and beam switching magnets. Beam transport into the tandem accelerator from the negative ion sources was also examined.

---

* Brookhaven National Laboratory, Upton, New York.

1.4 Cyclotron Improvements and Operations

Laboratory Staff

Cyclotron maintenance during the period of this report was routine; no major problems were encountered and no major improvements were begun.

Statistics on cyclotron operations are given in Table 1.4-1. Total normal operating time is down somewhat from past years, a trend that will be reversed in the near future when the recently funded ^{18}F Production Project and the Fast Neutron Cancer Therapy Program begin utilizing cyclotron time.

Table 1.4-1. Statistics of Cyclotron Time from April 16, 1970 to April 15, 1971

		Time (Hrs)	Per Cent
1.	Division of time among activities[a]		
	Normal operation	2442	55
	Scheduled maintenance	284	6
	Unscheduled maintenance	211	5
	Unrequested time	1483	34
	Total[b]	4420	100
2.	Division of beam-on time among particles		
	Alpha particles	1065	80
	Deuterons	256	19
	Protons	13	1
	Total	1334	100
3.	Division of normal operation time among users		
	University of Washington Nuclear Physics Laboratory	1306	53
	University of Washington Department of Nuclear Medicine		
	(Fast Neutron Activation Analysis)	908	37
	(^{18}F Production)	47	2
	University of Washington Physics Department	74	3
	Atomics International	63	3
	University of Washington Department of Fisheries	17	1
	Western Washington State College	15	1
	Oregon State University	12	-
	Total	2442	100

a. These categories are defined in the same way as those in Table 1.1-1.
b. This equals 52 5-day weeks of 17 hours per day.

2. ION SOURCE DEVELOPMENT

2.1 Operation of the Lamb-Shift Polarized Ion Source

H. Fauska, E. Preikschat, G.W. Roth, and W.G. Weitkamp

The Lamb-shift polarized ion source has been installed at the tandem accelerator and preliminary measurements of beam intensity and polarization have been made.

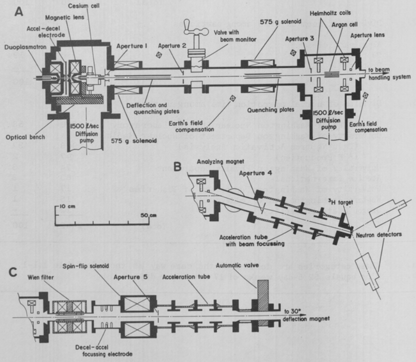

Fig. 2.1-1. (A) Cross sectional view of the polarized ion source, (B) the source configuration used during initial tests, and (C) the configuration presently used to inject beam into the tandem.

The operational principle of this type of source has already been described in a number of papers.[1-3] The construction of the source has been discussed to some extent in previous Annual Reports.[4-5]

This report will cover some details which have proven important for reliable operation of the source, and those factors which might still be limiting the beam intensity and polarization. Figure 2.1-1A is a cross sectional view of the source. Figure 2.1-1B shows the configuration used for initial testing and Fig. 2.1-1C the beam optics as presently installed.

A duoplasmatron of the Los Alamos type is used as a source of H^+ or D^+ ions, which are neutralized in the cesium exchange cell. A fraction of the neutral beam is left in the metastable $2S_{\frac{1}{2}}$ state. The beam is subsequently polarized by inducing, in a magnetic field, the electron metastables with electron spin anti-parallel to decay to the ground state via the short-lived $2P_{\frac{1}{2}}$ state. The remaining metastables are then selectively charge exchanged in the argon exchange cell (see Sec. 2.3 of this report).

The output from the duoplasmatron once optimized is very stable. The arc current is typically 6-8A and the total output 10-30 mA. The extraction geometry was varied to optimize the beam output (see Fig. 2.1-2). The on-axis alignment was found to have the most significant effect on the source output. For this reason two manual adjustments allow for moving the whole duoplasmatron relative to the magnetic lens, and the bottle relative to the extraction aperture. The latter adjustment can be made while observing the heating pattern produced by the arc on the extraction plate aperture through a glass filament holder.

The third of the three types of

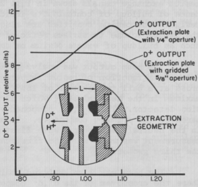

Fig. 2.1-2. The beam intensity shown as a function of the distance between the magnetic lens and the duoplasmatron (in inches).

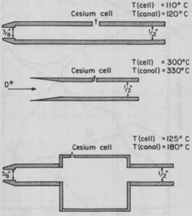

Fig. 2.1-3. Various cesium exchange canal geometries used.

cesium exchange canals shown in Fig. 2.1-3 is presently used. There is no evidence of buildup of contaminants inside the canal as was the case with the first design. The cesium densities are also more reproducible. This is attributed to the larger volume to surface ratio of the canal, which reduces surface effects such as buildup of excess cesium or contaminants.

The beam output was analyzed behind the cesium canal and is shown in Fig. 2.1-4 as a function of cesium temperature. For deuterium the d^+,d^- components cross at a cell temperature of 165°C. This approximately corresponds to the maximum in the neutral beam, which is measured using a secondary electron emission detector. The d_2^+,d_2^- components were down by at least a factor of 10 compared to the primary components. Figure 2.1-4 also shows evidence of hysteresis in the neutral beam output when first heating the cell and then cooling it. The measurement was made with the first canal geometry. The effect was not seen with the third geometry.

The beam was also analyzed behind the argon exchange cell (see Fig.2.1-5). There the crossover of the d^+,d^- components occurs at a lower cesium temperature, around 145°C. One explanation for this is that poor pumping conditions give

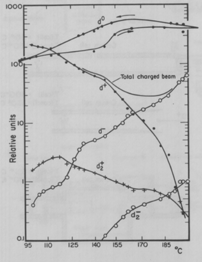

Fig. 2.1-4. Beam output (using deuterium) measured behind the cesium canal as a function of cesium cell temperature.

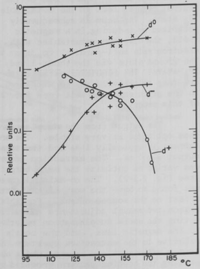

Fig. 2.1-5. Beam output measured behind the argon cell as a function of cesium cell temperature.

rise to an appreciable density of the charge exchange gas and source gas along the beam path, causing additional charge exchange reactions which increase the d^-/d^+ ratio and also reduce the polarization. To overcome this problem we have ordered a better diffusion pump with a pumping speed of 2500 ℓ/sec instead of the present 500 ℓ/sec.

The argon exchange cell has a 1" diameter and is 3" long. It is made up of a number of stainless steel tubes of 1/8" diameter. The array has an optical transparency of about 70%. The argon cell can also be heated to drive off contaminants. A pair of Helmholtz coils provide a solenoidal field at the argon cell for strong field ionization as needed for vector polarization.

Initial source tests indicated a beam instability, which was attributed to the formation of an insulating layer on many of the conductors, in particular the quenching plates. The problem was eliminated by gridding and baffling the plates. Any charge building up on the top surface of the grid is effectively drained away by the large electric field gradients present near small diameter wires.

This same technique was also used to cover defining aperture 5 and the electrodes of the Wien filter, all of which are hit by charged beam. This made the beam more stable and has reduced service requirements.

To achieve maximum polarization the source utilizes the Sona[6] cross-over scheme, which doubles the vector polarization for both protons and deuterons and increases the tensor polarization from -.33 to -1.0. To avoid depolarization the crossing time of the atoms must be fast enough so that the electron spin cannot follow the reversal of the magnetic field. In addition care must be taken to minimize the transverse magnetic field components. The transverse magnetic field $H_\perp$ associated with any magnetic field gradient $H_{\parallel}'$ is given by

$$H_\perp = \frac{r}{2} H_{\parallel}'$$

where r is the distance off axis. In our case $H_{\parallel}' = .9$ g/cm and the radius of the defining aperture is equal to 0.6 cm, i.e., $H_\perp = .27$ gauss at the rim of the aperture. The magnetic field at the sudden crossing region has to satisfy the inequality

$$\frac{4 H_\perp^2}{14 \text{ G-cm}} << H_{\parallel}' << \frac{14 \text{ G-cm}}{r^2}$$

i.e., in our case $.021$ G/cm $<< H_{\parallel}' <<$ 39 G/cm for protons

and $.014$ G/cm $<< H_{\parallel}' <<$ 59 G/cm for deuterons.

Both of these conditions are well satisfied by choosing $H_{\parallel}' \sim 1$ G/cm. Other developments have shown[7] that the two solenoidal magnetic fields can be magnetically shielded and also that the field gradient in the crossing region can be as large as 1.9 G/cm without reducing polarization.

This means that the distance between the two solenoids can be reduced from 60 cm to 25.5 cm, effectively increasing the beam transmission by a factor of 1.9.

Because of the requirement of small transverse magnetic fields mentioned above, care has been taken to eliminate the earth's field in the crossover region. The resulting tensor polarization, however, measured as a function of this compensating field did not show a strong peak as expected for complete compensation of the earth's field. This can be attributed to a number of factors, the most important being the inferior pumping speed of the diffusion pumps presently used. The largest tensor polarization measured via the $T(\vec{d},n)^4He$ reaction was .787 ± .020 of that theoretically expected, discounting the 20% unpolarized background contribution. The maximum net tensor polarization measured previously with the source configuration shown in Fig. 2.1-1B was -.763 ± .027.

The argon exchange cell is followed by the two spin precessing elements, the Wien filter and the spin flip solenoid.

The Wien filter, consisting of a crossed electric and magnetic field, is preceded and followed by aperture lenses (see Fig. 2.1-1C). The lenses are adjusted to bring the beam to a focus within the Wien filter, in order to minimize the aberrational effects. The magnetic field is shielded to increase the field gradient at the end of the filter and match it to the gradient of the electric field. The electric field plates are shaped to provide a uniform field across the filter and the necessary falloff at the ends. The transmission of the filter is nearly 100% for the polarized beam. No attempt has as yet been made to reduce the cylindrical lens effect of the filter.

The spin flip solenoid produces a spin precession around the beam axis (see Sec. 2.2 of this report). A 1/4" aperture is mounted behind the solenoid. The polarized component of the beam is brought to a second focus at that point thereby substantially reducing the unpolarized beam which has a larger emittance. the unpolarized beam then makes up about 16% to 25% of the total (polarized and unpolarized) beam, i.e., the quenching ratio is 4-6.

Table 2.1-1. Polarized ion source beam currents.

	Deuteron beam (doubly quenched)	Proton beam (singly quenched with zero field crossing
Largest beams measured during original source tests, using source configuration B	300 nA	150 nA
Typical beams measured after installing source at tandem, using configuration C	150 nA	80 nA
Typical beams measured at low energy end of tandem	100 nA	30-60 nA
Typical beams obtained on target	20-60 nA	10-25 nA

Table 2.1-1 shows the beam intensities measured at various locations. At the present time we are still trying to match the optics of the source to that of the tandem. The beam instabilities encountered earlier have been eliminated by shielding the glass of the acceleration tube and gridding the aperture plates and electrodes. For the case of a proton beam it is clear that a single (or double) accelerating gap followed by a strong Einzel lens is preferable to the present multi-gap accelerating tube.

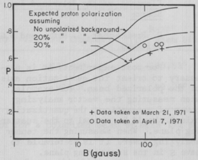

Fig. 2.1-6. Measured polarization as a function of magnetic field in the ionization region compared to expected polarization assuming various background contributions.

The polarization of a proton beam has been measured via elastic scattering from ^{12}C at 7.99 MeV and a lab angle of 70°. Figure 2.1-6 shows the measured values for the polarizations as a function of the strong field in the argon cell. The expected polarization values are also shown assuming different background contributions. The proton polarization was measured to be .701 ± .004 assuming a polarization asymmetry for this particular scattering geometry and target of 1.00. The polarization remained constant to within three standard deviations over a period of two days. Even though the source was overhauled and cleaned between two sets of measurements, the source output has remained relatively constant at about 10 nA of proton beam on target with 70% polarization. Higher beam currents have now been obtained.

The source performance should be substantially improved by using higher quality diffusion pumps and by improving the geometry of the sudden zero crossing region and the source optics. Even without these changes the present performance is sufficient for many types of experiments.

1. W. Haeberli, Ann. Rev. Nucl. Sci. *17*, 373 (1967).
2. A. Cesati, F. Cristofori, L. Milazzo-Colli and P.G. Sona, Progr. Nucl. Phys. *10*, 119 (1969).
3. G. Michel, K. Corrigan, H. Meiner, R.M. Prior, and S.E. Darden, Nucl. Instr. and Meth., *78*, 261 (1970).
4. Nuclear Physics Laboratory Annual Report, University of Washington (1969), p. 156.
5. Nuclear Physics Laboratory Annual Report, University of Washington (1970), p. 7.
6. P.G. Sona, Energia Nucleare *14*, 295 (1967).
7. V. Bechtold, H. Brückmann, D. Finken, and L. Friedrich, Z. Physik *231*, 98 (1970).

2.2 Calibrating the Spin Precessing Elements of the Polarized Ion Source

E. Preikschat, G. Roth, and W.G. Weitkamp

For most experiments it is necessary to orient the quantization axis of the polarized beam. For example, when measuring the vector analyzing power of a reaction, the quantization axis $\hat{S}$ should be normal to the scattering plane. When measuring the tensor analyzing powers it is preferable to have S in the scattering plane.

To position $\hat{S}$ in two different planes the spin has to be precessed around two separate axes. A Wien filter, consisting of a crossed electric and magnetic field is used for precession around a vertical axis, and a solenoidal field for precession around the beam axis. As the solenoid does not contain any ferromagnetic material, the magnetic field is accurately reproducible. The spin can be flipped merely by reversing the direction of the solenoid current.

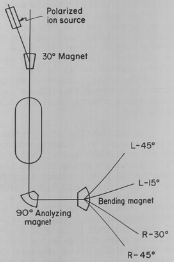

Fig. 2.2-1. Various beam lines commonly used.

For the purpose of describing the scattering of polarized protons and deuterons we are using the Madison convention, where $\hat{z}$ is along the incident beam axis $\vec{k}_1$, $\hat{y}$ is along $\vec{k}_i \times \vec{k}_0$, where $\vec{k}_0$ is in the direction of the scattered beam, and x, y, and z make up a right-handed coordinate system. The spin orientation is given by angles β and ϕ. β is the angle between $\hat{S}$ and $\vec{k}_i$, ϕ is the angle between the spin projected onto the x-y plane and the y-axis.

Before the spin is processed by the various deflection magnets of the accelerator the quantization axis $\hat{S}$ lies along the beam axis. The amount of spin precession is directly proportional to the angle through which the beam is deflected. The ratio between the Larmor precession frequency and the cyclotron frequency is 2.793 for the proton and 0.857 for the deuteron. Figure 2.2-1 shows the magnets through which the beam must pass in traversing the accelerator and the various beam lines commonly used. Table 2.2-1 gives the angle β, between $\hat{S}$ and the beam axis, for the different target locations.

The Wien filter and spin flip solenoid were calibrated using the $^{12}C(p,p)$ reaction, for which the asymmetries have already been previously measured[1] at

Table 2.2-1. The angle β between $\hat{S}$ and the beam axis for various target locations.

Beam	L-45° (spectrometer)	L-15° (60" Sc. Chamber)	R-30° (24" Sc. Chamber)	R-45° (10" Beam Line)
Proton	-4.15°	-57.95°	-138.63°	-165.53°
Deuteron	36.40°	40.70°	47.13°	49.28°

various proton energies. The cross section for a polarized beam of spin 1/2 particles is given by

$$I(\theta,\phi) = I_0(\theta)[1 + (P_z \sin \beta \cos \phi)A_y(\theta)],$$

where P_z is the polarization of the beam and A_y is the analyzing power of the particular reaction.

At 7.99 MeV and a lab angle of 70° the asymmetry A_y is given as 1.03 ± .05 and the cross section as 37.1 mb/ster. The measurements were made in the 24" scattering chamber with two detectors mounted in the x-z plane and two in the y-z plane with all the detectors at a lab angle of 10°. The Wien filter was calibrated using the up-down detectors to determine the periodicity of $P_z \sin \beta$. The measured polarization is shown in Fig. 2.2-2 plotted against the electrode voltage of the Wien filter. At 41.5 ± .3 volts the proton spin is precessed through 90°. The Wien filter is highly velocity-selective. The transmitted beam is reduced by half when changing the electric field by .2 volts while keeping the magnetic field constant. The Wien filter can thus be accurately set by applying a given voltage to the electrodes and adjusting the magnetic field for optimum transmission.

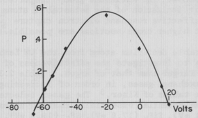

Fig. 2.2-2. Polarization plotted as a function of Wien filter setting.

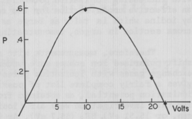

Fig. 2.2-3. Polarization plotted as a function of spin flip solenoid setting.

The spin flip solenoid was calibrated with the left-right detectors. At a Wien filter setting of 41.5 volts the spin is normal to the beam axis. In Fig. 2.2-3 the measured polarization is plotted against the supply voltage of the solenoid. The peak in the sine-curve corresponds to a spin alignment along the y-axis. The temperature of the solenoid is maintained constant to minimize the temperature drift in the voltage reading.

These results can readily be generalized for the case of a deuteron beam of the same velocity as the proton beam. In that case the fields have to be larger by a factor of 6.518 to precess the deuteron spin the same amount as the proton spin.

---

1. S.J. Moss and W. Haeberli, Nucl. Phys. *17*, 417 (1965).

2.3 Investigation of Alternative Exchange Gases for the Production of Negative Ions in Lamb-Shift Polarized Ion Sources

J.G. Cramer, E. Preikschat, and W. Trautmann

The yield and net polarization from a Lamb-shift type polarized ion source depend quite critically on two atomic cross sections, the cross section for electron capture by hydrogen or deuterium atoms in the metastable 2S state to form negative ions (which should be large) and the similar capture cross section for ground-state atoms (which should be small). Donnally and Sawyer[1] have measured these cross sections with 600 eV protons for a variety of exchange gases and have found argon to be clearly superior to others studied, both in having a large cross section for metastables and in having a small cross section for ground state atoms. Their results, expressed as cross section ratios, are shown in Fig. 2.3-1.

However, no gases were studied in this work which had ionization potentials greater than that of argon (15.68 eV) with the exception of helium (26.46 eV), and a clear trend was found in the data for increasing 2S/gs cross section ratios with increasing ionization potential. Moreover, the Karlsruhe group[2] reported an effective cross section for the resonant ionization of the metastable atoms by iodine which is twice as large as the effective resonant electron capture cross section in argon, demonstrating that higher cross sections are possible.

Therefore, measurements with metastable deuterium atoms from the UW Lamb-shift polarized ion source were undertaken to investigate the effectiveness of exchange gases with ionization potentials larger than that of argon. Table 2.3-1 gives a fairly complete list of possible exchange gases, in order of increasing ionization potential, as obtained from the tables of Kiser.[3] The gases selected for this investigation were air (ionization potential essentially that of nitrogen, or 15.51 eV), BF_3 (15.7 eV), Ar (15.68 eV), SiF_4 (17.8 eV), SF_6 (19.3 eV), Ne (21.47 eV), and He (26.46 eV).

There are two criteria for resonant electron capture from a given exchange gas: (a) the collision time d/v must be comparable to the transition time Q/h,

Table 2.3-1. Ionization Potentials of Gases and Vapors

MATERIAL	IONIZATION POTENTIAL (eV)	BOILING POINT (0)	MOLECULAR DIAMETER (Å)
He	26.46	-268.9	1.90
Ne	21.47	-245.9	
SF_6	19.3	-56	
F_2	17.8	-188	
CF_4	17.8	-128	
F	17.34	-188*	
SiF_4	16.9	-65	
BF_3	15.7	-99.9	
Ar	15.68	-186	2.94
H_2	15.6	-252	2.40
N_2	15.51	-195	3.15
UF_6	15.5	+56.2	
CH_4	14.5	-161.5	
CO_2	14.4	-78.5	3.34
CO	14.1	-190	3.19
CN	14.0	-20.5	
Kr	13.93	-152.9	3.2
CHF_3	13.84	-82.2	
O	13.550	-183.0*	
H	13.527	-252*	
Cl_2	13.2	-34.6	
NF_3	13.2	-128.2	
SO_2	13.1	-10.0	
Cl	12.952	-34.6*	
N_2O	12.9	-88.49	
CH_3F	12.8	-78.4	
$CClF_3$	12.8	-81.1	
O_3	12.8	-183.0*	
Br_2	12.8	+58.78	
C_2H_6	12.8	-88.63	
H_2O	12.56	+100.00	
CH_2F_2	12.55	-51.6	
O_2	12.5	-182.6	2.98

*Requires dissociation

MATERIAL	IONIZATION POTENTIAL (eV)	BOILING POINT (0)	MOLECULAR DIAMETER (Å)
C_2H_4	12.2	-88.3	
Xe	12.08	-107.1	3.42
Br	11.80	+58.78*	
CCl_2F_2	11.7	-29	
C_2H_2	11.6	-81.8	
CCl_4	11.47	+76.75	
$CHCl_3$	11.42	+61.2	
CH_2Cl_2	11.35	+40	
CH_2O	11.3	-21	
CH_3Cl	11.2	-23.76	
NH_3	11.2	-33.35	3.0
I	10.6	+184.3*	
H_2S	10.42		
CS_2	10.4	+46.3	
Hg	10.39	+356.6	3.01
S_2	10.0	+444.6	
CH_3Br	10.0	+3.56	
I_2	9.7	+184.3	
Benzene(C_6H_6)	9.6	+80	
NO	9.5	-151.8	
CH_3I	9.1	+42.5	
$B(C_2H_5)_3$	9.0	+95	
$B(CH_3)_3$	8.8	-20	
Toluene(C_7H_8)	8.5	+110.6	
Analine($C_6H_5NH_2$)	7.7	+184.4	
Triethylamine	7.7	+89.5	
Benzylamine	7.56	+185	
Perylene($C_{20}H_{12}$)	6.94	+350-400	
Pentacene	6.73	+290-300	
Ca	6.02	+1240	
Li	5.390	+1336	
Na	5.14	+880	
K	4.399	+760	
Cs	3.893	+670	

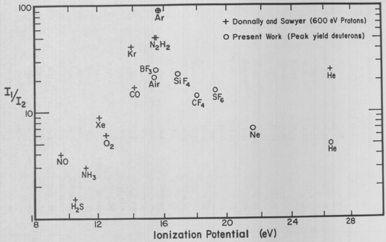

Fig. 2.3-1. Ratio of cross sections for electron capture of 2S metastable atoms to ground state hydrogen and deuterium atoms as a function of ionization potential. The absolute values of the ratios in the present work are normalized to those of Donnally and Sawyer[1] for argon to allow for differences in experimental geometry. The present work used deuterium atoms, with energies adjusted to give peak yield, while those of Donnally and Sawyer[1] used 600 eV protons. However, previous work has shown no important differences between proton and deuteron yields at the same velocities.[5]

i.e., $dQ/vh = 1$, where d is the atomic diameter, v is the velocity of the colliding ions in the center-of-mass system, Q is the absolute value of the reaction Q-value, and h is Planck's constant. This is called the Massey criterion.[4] (b) The cross-over point of the atomic pseudo-potentials occurs at an interaction radius which is smaller than the sum of the atomic radii.

Both of these conditions can usually be met by tuning the energy of the deuterium atoms to the appropriate value. Therefore, each exchange gas was tested over a range of deuteron acceleration potentials, and the peak yield was used. Figure 2.3-1 shows the results of the present measurements. Since the ratio of 2S/gs yields depends to some extent on the geometry of the source, our results are normalized to the proton measurements of Donnally and Sawyer for ease of comparison. Previous work[5] has shown that protons and deuterons of the same velocity give essentially the same yields.

It is seen that argon is clearly the best exchange gas of those tested. Thus we are satisfied that the performance of a Lamb-shift polarized ion source cannot be improved by using a different exchange gas.

1. B. Donnally and W. Sawyer, *Proc. Symp. Polarization Phenomena, Karlsruhe,* (Ed. by P. Huber and H. Schopper, Birkhauser, Basel, 1966) 2nd Edition, p. 71.
2. Private communication.
3. R. Kiser, *Tables of Ion Potentials,* AEC Document TID-6142, Kansas State University.
4. N.F. Mott and H.S.W. Massey, *The Theory of Atomic Collisions,* (Clarendon Press, Oxford, 1933).
5. B.L. Donnally and W. Sawyer, Phys. Rev. Letters *15*, 439 (1965).

2.4 The ^{3}He Recirculating System

D.L. Johnson and W.G. Weitkamp

The expense of isotopically pure ^{3}He combined with its routine use as an accelerated particle require that a method for salvaging it be incorporated into the ion source. A recirculating system similar to that at Stanford University has been built and partially tested. The system takes the gas pumped from the ion source box and passes it through a LN_2 cooled Zeolite trap. The remaining gas is mostly ^{3}He and is available for re-use by the ion source.

2.5 The Lithium Negative Ion Source

J.G. Cramer and W.R. Wharton

During the last year the lithium negative ion source[1] has progressed from the development stage to become a general workhorse for our Laboratory, not only supplying $^6Li^-$ and $^7Li^-$ beams but also replacing the old potassium-exchange source[2] as the regular α^- and $^3He^-$ source for our Laboratory.

The major breakthrough in development of the source came in placing an Einzel lens after the exchange canal so that the most intense part of the energy distribution of ions emerging from the canal could be selected and focused into the tandem accelerator. This modification of the source has resulted in beam outputs 4-10 times what can be obtained without the Einzel lens. The result is that the source provides maximum ^{6}Li and α beams larger than required in any current experiment. No attempt has been made to measure the maximum beam outputs, although we have easily obtained 1.2 μa of analyzed $^6Li^{+++}$ and 2.5 μa of analyzed $^4He^{++}$.

For maximum beam output, the temperature of the lithium cell must be around 600°C. At such high temperatures for prolonged periods (5 days to a week) the source begins having stability problems, the electrodes become coated with a thick layer of lithium, and the cell empties fairly rapidly. However, the lower beam requirements of the experimenter have allowed us to run the source as low as 320°C. The result has been a much more dependable source, and up to three weeks of operation without filling the lithium cell.

Our major problem has been the deterioration of electrical insulators. We use the same insulators to support the exchange canal, the extraction electrode, and two Einzel lenses. These insulators are unglazed alumina cylinders[3] with 3/4" O.D. and 4" long. Each insulator is protected from electron bombardment and heat radiation by two overlapping stainless steel cylindrical shields. The insulators supporting the new Einzel lens have cracked and broken down on three separate occasions and needed to be replaced. The same problem has arisen twice to one of the insulators supporting the extraction electrode. The other insulators have survived without incident. There is reason to suspect that some of the insulators are being bombarded by ions passing through a horizontal gap between the overlapping shields. Plans are now being made to correct this situation.

After several weeks of operation, the performance of the source begins to deteriorate. The lithium cell must run at higher temperatures for the same beam output and the insulators start to break down, making it necessary to take the source out, clean, and reassemble it. At the present rate, the source is being cleaned four times a year. To aid in aligning the source during reassembly, a special telescope mount has been made which mounts a telescope to the optical bench of the source. This makes possible the alignment of all electrodes, the exchange canal, and the extraction cone to within a few mils of the center of the optical bench. In turn, the position of the optical bench in the source box of the tandem has been set for proper alignment.

---

1. Nuclear Physics Laboratory Annual Report, University of Washington (1970), p. 9.
2. Nuclear Physics Laboratory Annual Report, University of Washington (1967), p. 97.
3. Superior Steatite and Ceramic Corp., 83-91 West Forest Ave., Englewood, N.J. 07631.

2.6 The Terminal Ion Source

H. Fauska, C. Linder, J. Orth, G. Roth, and W. Weitkamp

A preliminary design has been completed for a source of negative ions to be located in the high voltage terminal of the injector. The source will be similar to a terminal ion source recently installed at the Brookhaven National Laboratory.[1] The source is expected to increase the energy, intensity, and variety of beams available from the accelerator and should produce substantial savings in operating expenses for the injector.

---

1. J.D. Benjamin *et al.*, Proc. IEEE, to be published.

---

3. INSTRUMENTATION FOR RESEARCH

3.1 Pneumatic Target Transport System

R.E. Marrs

Interest in making accurate branching ratio measurements for several beta decays of short half-life (200 ms -- several minutes) has inspired the construction of a fast rabbit system. The rabbit has been installed between the 0° beam line in cave I and a counting station in cave II. Targets are mounted on the end of a 3/8" square × 1" long balsa wood plug and blown through the shielding wall between caves I and II in an aluminum tube of square cross section. The rabbit is intended for use with Ge(Li) gamma-ray detectors. The 5 foot thick shielding wall between the two caves effectively eliminates background and spares the detector from fast neutron damage.

The target is returned to the bombardment station (Fig. 3.1-1) by suction from a vacuum cleaner and stops against two metal pegs which straddle the target. The beam entrance and exit windows are .25 mil Havar foil and a 1/8" tantalum aperture is mounted in front of the entrance window. Using a ballast bottle and throttle valve in the pressurized air line provides for a strong

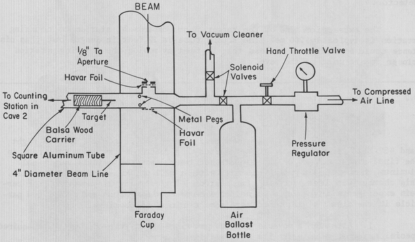

Fig. 3.1-1. Schematic diagram of the bombardment station. This assembly is mounted on the end of the 0° beam line which enters cave I near the wall between caves I and II.

initial acceleration. But as the target approaches the counting station and the air in the ballast bottle expands to fill the space behind it, the acceleration falls off and becomes a deceleration. This technique makes it possible to run with a short extraction time from bombardment station to counting station without damage to the balsa wood when it is stopped. The counting station end of the tube is open and the balsa wood target carrier stops against a padded piece of aluminum approximately 1/4" from the end of the tube.

Arrival of the target at the counting station is sensed by the interruption of the light beam between a light emitting diode and a phototransistor. The phototransistor is part of a trigger circuit which produces a start pulse to gate the electronics on and begin the collection of data.

The solenoid valves to the suction and pressure lines are opened and closed automatically under the control of a repeat cycle cam timer. The open and close times of the valves are continuously variable and the length of the complete cycle is variable in discrete steps over a wide range.

The system is capable of carrying almost any type of small target. Targets of Si, Al, S, and ^{15}N have already been made. At this writing only the ^{15}N target (adenine vacuum evaporated onto a 6 mil tantalum backing epoxied to the end of the balsa wood carrier) has actually been used in an experiment. In this case ^{16}N (7.1 sec half-life) was produced by the reaction $^{15}N(d,p)^{16}N$ and the gamma radiation following the beta decay of ^{16}N to ^{16}O was detected with a Ge(Li) detector.

The extraction time of the target from bombardment station to counting station is typically 200 ms. The square tube is 22 feet in length but this distance could be shortened to less than 12 feet by moving the counting station closer to the wall of the cave.

3.2 A New Scattering Chamber for Neutron Time of Flight Studies

J.R. Calarco

A new scattering chamber was designed and built for use on the right hand 45° beam line for the purpose of studying reactions involving neutrons in the final state. Previous experiments had been conducted using a spherical aluminum chamber 10 inches in diameter with a wall thickness of about 60 mils. This chamber was ideal for studying neutron singles spectra. However, for certain experiments involving a coincidence between the neutron and a charged particle in the final state, there were some serious shortcomings.

1. Although a movable arm was provided inside the chamber, it required special detector mounts for its use.

2. The small size of the chamber prevented the detector from being placed at a distance of more than about 3 inches from the target. This limited the use of double apertures in front of the detector.

3. The target changing mechanism was capable of holding only two targets mounted in the standard manner (or one if a blank position is desired) or three on special small frames (two plus a blank).

4. The detector angular readout was in error by about 1° and could not be accurately set to better than about 1/3°. Also there appears to be some stiffness in the mechanism causing it to relax back slightly after being changed.

5. The most serious problem was the lack of a suitable azimuthal alignment mechanism. Because the chamber was held onto the beam line by flanges free to slip around the tube, the chamber itself was also free to rotate about the beam axis. Thus it was difficult to define a reaction plane between the target and charged particle detector inside the chamber and the neutron counter outside except by using a transit or, empirically, by searching for coincidences.

6. The small size and the spherical geometry made access to the detectors and targets difficult. It was possible to gain entry only by removing the chamber from the beam line and working through the entrance and exit connections to the beam tube.

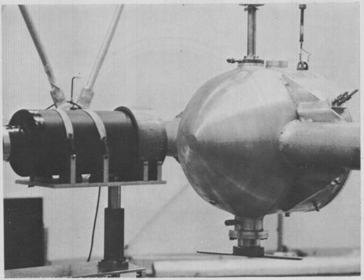

Fig. 3.2-1. A view of the chamber showing the hemispherical side and the neutron detector.

The new scattering chamber was designed to alleviate all the difficulties while keeping it thin to neutrons. The basic geometry is hemispherical on the side facing the neutron detector and cylindrical on the opposite side. The hemispherical side maintained a wall thickness of about 60 mils. The diameter was increased to 16 inches. Access to the chamber was made possible by removing the end plate on the cylindrical side. Detectors are supported on a rotatable table using standard laboratory mounts with the vertical support shortened by 7/8 inches. Angular readout is done by observing markings on the table through a small port. Angles can be set to 0.1°; absolute accuracy has not yet been checked experimentally. The target mount is a standard 5 position ladder. Azimuthal alignment is done using a bubble level mounted directly on the detector table which can be observed from above through a viewing port. It is hoped that the azimuthal angle (and the reaction plane) can be defined to ±1/2°.

Figures 3.2-1 and 3.2-2 show two views of the finished chamber. Figure 3.2-1 shows the hemispherical side being viewed by the neutron detector. Figure 3.2-2 shows the interior looking through the cylindrical side with the end plate removed. A detector mount is on the circular table.

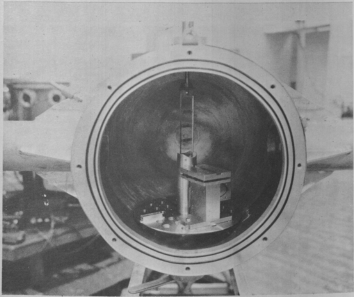

Fig. 3.2-2. The chamber interior as seen through the cylindrical side with the end plate removed. The target ladder and rotating table are clearly visible. A detector stand and the bubble level are mounted on the table.

3.3 Gamma Counter Carriage for Out-of-Plane Particle-Gamma Angular Correlation Measurements

J. Eenmaa

For the purpose of measuring out-of-plane particle-gamma angular correlations (described in Secs. 10.7 and 10.8 of this report), a new lid, gamma counter carriage, and shielding assembly was designed and fabricated for use on

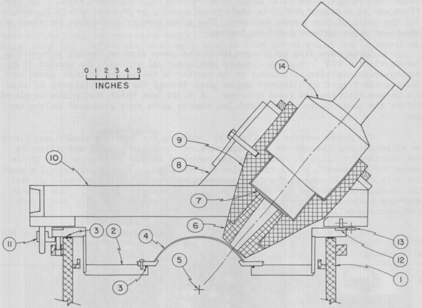

Fig. 3.3-1. Cross sectional view of out-of-plane gamma-counter carriage and assembly.

(1) 24-in. scattering chamber
(2) Chamber lid
(3) Vacuum seal
(4) Aluminum window
(5) Target source of gamma radiation
(6) Removable lead aperture
(7) Lead plate
(8) Support bracket
(9) Lead shielding
(10) Carriage rail
(11) Clamp
(12) Steel roller-bearing track
(13) Roller bearings
(14) Gamma-ray detector assembly

the general-purpose 24-inch scattering chamber. Figure 3.3-1 shows a cross-sectional view of this assembly. The standard lid for the 24-inch chamber is removed. The new aluminum lid is positioned on the chamber with pins and is marked at 5° intervals around its circumference for azimuthal positioning of the gamma detector. The carriage consists of two aluminum rails which bridge the opening of the chamber and thus support the gamma-ray detector and its shielding. The carriage can be rotated azimuthally about the axis of the chamber on roller bearings which run on a circumferential steel track along the rim of the lid. The aluminum bracket which supports the gamma counter on the rails of the carriage defines the fixed polar angle with respect to the chamber axis. The carriage was so designed that this angle could readily be changed merely by changing the angle of the support bracket. The gamma counter could thus be fixed at any polar angle between 0 and 45 degrees.

Gamma rays from the target enter the gamma counter through a removable vacuum-tight 0.032 inch thick aluminum hemispherical window. The center of the hemispherical section is located at the center of the target so that gamma rays leaving the target at different angles pass through the same thickness of aluminum before entering the gamma detector. A 0.125 inch thick lead plate is placed before the gamma detector to absorb low energy gamma rays generated in the target.

The gamma counter is aligned by removing the aluminum window and placing an alignment rod through the lead aperture of the gamma counter and adjusting the counter for lateral, radial and yaw movement so that the rod points at the center of the target at all times when the carriage is rotated azimuthally about the axis of the chamber. The lead aperture of the shield is removable so that the acceptance angle of the detector may be changed as necessary. The present aperture subtends a geometric half-angle of 5.5 degrees vertically and 4.0 degrees horizontally.

The gamma counter itself, a 4 × 5 in. NaI(Tℓ) crystal coupled to an RCA 4522 photomultiplier tube is surrounded by about one inch of lead shielding on all sides.

3.4 Target Fabrication

J. Heagney

Approximately 120 specifically requested target foils were prepared over the last fiscal year. In addition to this numerous thin foils for use as degraders and detector cover foils were prepared as needed. The tandem Van de Graaff foil stripper wheel containing 39 thin carbon foils was replaced 9 times.

Of particular interest is the fact that self-supporting ^{6}Li and ^{7}Li metal foils as thin as 150 μg/cm^2 were fabricated and used successfully with minimal oxidation.

3.5 ^{13}C Targets

J. Heagney and D. Oberg

^{13}C targets have been produced by a procedure similar to that described by V.L. Aquilar[1] by which enriched methyl iodide[2] is cracked onto heated 0.5 mil nickel foils[3] in an evacuated chamber.

The apparatus (Fig. 3.5-1) consists of a system of glass tubing, teflon stopcocks (1-4), a fixture for holding the foils (6), a thermocouple gauge (7) (P ∿ 10 mtorr - 1 torr), a Bourdon gauge (8)(P ∿ 30 in. - 1 atm.) and a cold trap (9). The cold trap was filled with liquid nitrogen to increase pumping speed and to keep the corrosive methyl iodide vapors from contaminating the mechanical pump oil. Teflon stopcocks were used so that grease would not be required, since the grease is attacked by the methyl iodide; however, this increased the leak rate slightly over that expected with glass stopcocks.

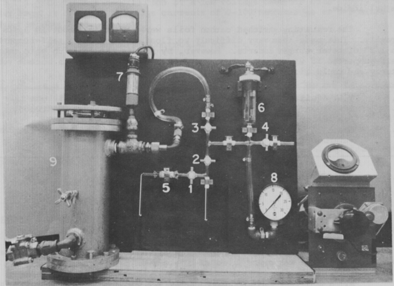

Fig. 3.5-1. Methyl iodide cracking apparatus for making ^{13}C targets.

In operation, methyl iodide was introduced via the tube (lower left) and the ground glass taper with a teflon sleeve (5), frozen, and pumped on. It was then distilled, the vapors passing to the lower right tube through valve 1 which was then closed. Since carefully controlled temperature distillation was not found to be helpful, quick freezing with liquid nitrogen and quick heating with hot air was used.

The nickel foils were cleaned in acetone, alcohol and distilled water and blown dry with argon. They were then clamped in a spring-loaded holder (6) to keep the foils from buckling when heated. The holder had insulated vacuum feed-throughs for supplying the heating current. The current was applied gradually by a motor-driven variac, thus improving the reproducibility in heating.

The system was evacuated to about 20 mtorr and isolated by valve 3. Valve 2 was opened and the methyl iodide was heated until the pressure reached about 5 inches (25 inches on the gauge) and then the foil was heated. The correct final temperature was found to correspond to a dull red glow. After 30 seconds, the current was then turned off and the foil allowed to cool. The uncracked methyl iodide was refrozen in the lower right reservoir and the system evacuated to 20 mtorr and then let up to air with valve 4. In this way little methyl iodide was wasted and several cycles were performed using only 0.5 ml of methyl iodide.

The resulting enriched carbon foils were very thin (about 10 $\mu g/cm^2$) and fragile. This made them very difficult to float and to pick up self-supporting on 1/2" diameter target inserts. However, by picking the foils up onto mounted, self-supported 15 $\mu g/cm^2$ natural carbon foils, the enriched foils became very sturdy and could withstand high beam currents.

---

1. V.L. Aquilar, Ph.D. Thesis, University of Maryland, 1965.
2. 60-65% enriched Methyl Iodide available from Isotopes, Westwood, New Jersey.
3. Grade "A" nickel foils available from Chromium Corp. of America, Waterbury, Conn.

3.6 Design and Construction of Electronic Equipment

L.H. Dunning, H. Fauska, K.H. Lee, R.E. Stowell, and N.G. Ward

Major electronic projects are discussed in Secs. 3.7 and 3.8 of this report. Additional projects completed during the last year include:

a. A saturable reactor regulating system for the 0-250 kv polarized ion source power supply was constructed and installed.

b. A constant-current power supply was designed and constructed for the coil compensating for the earth's field at the polarized ion source. A similar supply was constructed for vertical deflection magnets used in the polarized ion source.

c. A current-sensing reference circuit was designed and constructed to provide control of the corona needle current source from the generating voltmeter of the tandem Van de Graaff.

d. Provision was provided at the computer site to monitor the ion beam current and to have an audio signal whose rate is proportional to the scaling of the beam current.

e. Six voltage-sensitive preamplifiers capable of operation in vacuum were constructed for use with the position-sensitive proportional counter on the magnetic spectrometer.

f. An 8-channel computer gating logic driver with a variable delay feature was designed and constructed.

g. An automatic filament regulator for baking coated filaments for the direct extraction source was designed and constructed.

h. A sensing device was designed and constructed to actuate the counting room electronics upon the arrival of a rabbit carrying a radioactive target.

i. Design and construction of a low voltage detector bias supply with a meter capable of sensing leakage currents of 0-100 nanoamperes or 0-1 microamperes was completed.

j. A thermistor-sensed controller for the cell heater of the polarized ion source was constructed.

k. A high input impedance differential amplifier system was designed and constructed to provide a faster ratio-response of the Van de Graaff accelerator slit amplifiers.

l. A 0-10,000 volt supply was constructed to provide fine control and focusing of the polarized ion source beam.

m. To insure more resistance to breakdown from high voltage transients, six power supplies on the polarized ion source were modified.

Electronic items purchased during the last year include:

1	TENNELEC TC 137 preamplifier
2	ORTEC #453 discriminators
1	ORTEC #451 amplifier
5	TENNELEC 203BLR amplifiers
1	ORTEC #444 biased amplifier
2	ORTEC #125 preamplifiers
2	ORTEC #437A time to pulse height converters
1	Tektronix #7704 oscilloscope
2	AEC module power bins

3.7 A Laboratory Radiation Monitor

L.H. Dunning and H. Fauska

The Laboratory has designed and constructed five linear count rate meters to provide radiation level monitoring and an audio alert. The monitors, providing an audio signal whose volume rises with increased radiation, were attached to the wall at cave and accelerator entrance doors. The circuit diagram is shown in Fig. 3.7-1.

The count rate circuit is designed around the Quad. 2 input positive nand gate integrated circuit, and drives a 0-1 ma. meter with selectable ranges of 0-200, or 0-2000 counts per minute. The input sensitivity of 200 millivolts negative was designed for a Geiger Mueller tube. One integrated circuit provides a Schmitt trigger and a pulse time shaper. The time-shaped pulse gates on a constant-current source which provides the usual charge pump. The pump compensates for non-linearities due to the voltage buildup across the meter network. The large capacitor across the meter network provides a time constant to average out the count rate fluctuations.

The second integrated circuit provides a shaped audio signal which is coupled to an audio system by a transistor attenuator providing attenuation

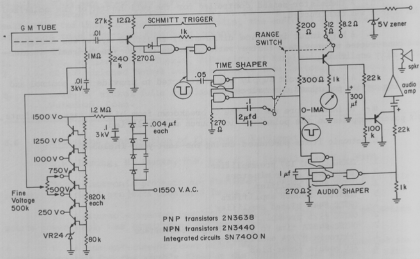

Fig. 3.7-1. Schematic of Laboratory Radiation Monitor

inversely with the meter deflection.

High voltage is obtained through a transistor divider string referenced to a Zener diode. Provision is made for a coarse and fine voltage adjustment. The transistor divider reduces the loading effects of the fine control.

3.8 Signal Sensing at Elevated Potentials Using Fiber Optics

G.W. Roth

The number of ion sources and other equipment in the Laboratory operating at high voltage has made it desirable to have an inexpensive and versatile means of transmitting signals across large potential differences. A system using gallium arsenide diodes and light sensitive transistors coupled by fiber optics bundles has been developed which is inexpensive and very versatile.

The system is entirely analog and linear. A small signal is sensed across a shunt and fed into one input of an inexpensive operational amplifier. The other input is used as an offset making it easy to accommodate different shunt signals and still keep the diode biased to conduction. The amplifier output drives a gallium arsenide diode. Thus a signal across the shunt produces a proportionate light output. The light is coupled to a phototransistor through a one foot length of .062" diameter fiber optics. The transistor drives one input of a second operational amplifier with the other input again used as an offset. The output of this operational amplifier drives a meter at ground potential. Figure 3.8-1 shows a complete unit with channels plugged into place and a spare channel.

Since the system is entirely linear, drifts must be minimized. The small aluminum cylinders at each end of the light pipes contain the diodes and transistors and hold them in rigid alignment with the light pipes. A well regulated supply and solid state operational amplifier reduce electrical drift to about 2% of full scale meter reading. An oscilloscope can be clipped across the meter at ground potential to observe the a.c. ripple on source power supplies or to note sparking or plasma oscillations in the source. Plug-in channels can be reversed to send contorl signals up to the ion source also. Cost per channel is about $5 plus meter.

At present a unit is operating at about 60 kV in the direct extraction ion source and units are being built for the injector neutral ion source (27 kV) and polarized ion source (90 kV).

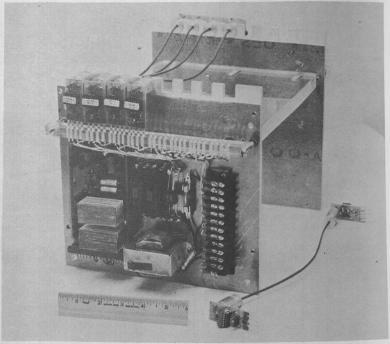

Fig. 3.8-1. Photograph of Analog Readouts Showing Complete Unit and a Spare Channel

3.9 Breit-Wigners Viewed Through Gaussians

D. H. Wilkinson

It often arises that a signal of Breit-Wigner form:

$$I_0(E) = \frac{\Gamma}{2\pi} \frac{1}{E^2 + \frac{1}{4}\Gamma^2}$$

is detected through an instrument whose response-function may be represented by a Gaussian:

$$D(E) = \frac{1}{\theta\sqrt{\pi}} e^{-(E/\theta)^2}$$

so that the recorded signal is the convolution of the two functions:

$$I(E) = \int_{-\infty}^{\infty} I_0(E') D(E - E')dE'$$

$$= \frac{1}{\theta\sqrt{\pi}} \frac{R}{-} \omega(\frac{E}{\theta} + i \frac{\Gamma}{2\theta}).$$

Here $\omega(z)$ is the complex error function.

The practical questions that must usually be answered following the determination of I(E) are:

(i) What is the form of I(E) outside the region of reliable observation?;

(ii) What is Γ?;

(iii) What is the area under the peak outside the part that has been reliably determined?

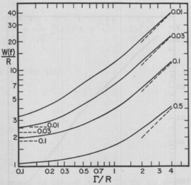

Fig. 3.9-1. A Breit-Wigner of width Γ is viewed through a Gaussian of FWHM R. The figure gives the full width W(f) of the resultant signal at a fraction f of its peak height. The f-values are the numbers at the right-hand ends of the lines. The dashed lines at the lower left are the Gaussian asymptotes ($\Gamma \to 0$); the sloping dashed lines are the Breit-Wigner asymptotes ($R \to 0$).

Question No. (i) is answered directly by R; it is interesting to present specimen results in graphical form in terms of the full width W(f) or I(E) at a given fraction f of its peak height. This is done in Fig. 3.9-1.

Question No. (ii) is of great practical concern since one must know how to extract Γ from the observed I(E); if $\Gamma >> R$ the problem is slight but if $\Gamma \leqslant 4R$ it is acute.

The answer to this question is conveniently given in terms of the width Γ_1 that would be deduced by a quadratic subtraction of the FWHM R of the Gaussian from the FWHM, W(0.5), of I(E):

$$\Gamma_1 = [W(0.5)^2 - R^2]^{\frac{1}{2}}.$$

The true width Γ of the Breit-Wigner is then given by

$$\Gamma = \Gamma_1/\xi$$

where ξ is given in Fig. 3.9-2.

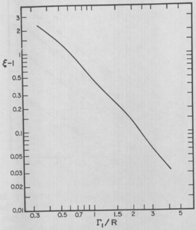

Fig. 3.9-2. Quadratic subtraction of the Gaussian FWHM R from the FWHM of the convoluted signal, W(0.5), gives a width Γ_1: $\Gamma_1^2 = W(0.5)^2 - R^2$. This is larger than the true width Γ of the Breit-Wigner by the factor $\xi = \Gamma_1/\Gamma$.

ξ is parameterized by:

$$\ln(\xi - 1) = a_0 + a_1 \ln(\Gamma_1/R) + a_2[\ln(\Gamma_1/R)]^2$$

with

$$a_0 = -0.774$$
$$a_1 = -1.652$$
$$a_2 = -0.153.$$

Question No. (iii) is also of great practical concern since we can usually reliably estimate the area under I(E) only over a finite range of E, say $\pm\Delta$, either side of the peak of I(E). In order to know the total area we must know the fraction $F(\Delta,\Gamma,R)$ that is not contained between $\pm\Delta$. This is given in Table 3.9-1.

Useful approximations to $\underline{R}\omega(z)$ are available. For small y, i.e., heavy smearing, we have:

Table 3.9-1

Breit-Wigner of width Γ viewed through a Gaussian of FWHM = R. $x = \Delta/\theta$; $y = \Gamma/2\theta$. $\theta = R/[2(\ln 2)^{\frac{1}{2}}] = 0.6006R$. The entries show the fraction $F(\Delta,\Gamma,R)$ of the line lying outside $\pm\Delta$ from its center. For the parts of the table beyond the entries (for $\Delta/\theta > 0.4$) the approximation given by expression (1) of the text is good to better than 1% of its own value.

$\Gamma/2\theta$ \ Δ/θ	0.4	0.6	0.8	1.0	1.2	1.4	1.6	2.0	2.4	2.8	3.2
0.1	0.614	0.452	0.321	0.222	0.151	0.104	0.073	0.043	0.031	0.025	0.021
0.2	0.650	0.500	0.376	0.279	0.207	0.155	0.120	0.079	0.060	0.049	0.042
0.3	0.680	0.542	0.425	0.330	0.257	0.203	0.164	0.115	0.089	0.073	
0.4	0.707	0.578	0.467	0.376	0.303	0.247	0.205	0.149	0.117		
0.5	0.730	0.610	0.505	0.417	0.345	0.288	0.243	0.182			
0.6	0.751	0.638	0.539	0.453	0.383	0.325	0.279	0.214			
0.7	0.769	0.663	0.569	0.486	0.417	0.359	0.312				
0.8	0.784	0.685	0.595	0.516	0.448						
0.9	0.798	0.705	0.619	0.543	0.477						
1.0	0.811	0.772	0.641								

$$\underline{R}\omega(x + iy) \approx e^{-x^2}[1 - \frac{2y}{\sqrt{\pi}} \{1 - \frac{x^2}{2\sqrt{\pi}} + \frac{2}{\sqrt{\pi}} \sum(x)\} + y^2(1 - 2x^2)].$$

Here

$$\sum(x) = \sum_{n=1}^{\infty} \frac{e^{-n^2/4}}{n^2} (1 - \cosh nx)$$

which is given in Table 3.9-2.

Table 3.9-2

The function $\sum(x) = \sum_{n=1}^{\infty} \frac{e^{-n^2/4}}{n^2} (1 - \cosh nx)$. For small x $\sum(x) \approx -\frac{1}{2} x^2(\sqrt{\pi}-\frac{1}{2})$; this approximation is good to better than 1% up to x = 0.20. For large x, $\sum(x) \approx \frac{\sqrt{\pi}}{4} e^{x^2}/x^2$; this approximation is still in error by 10% at x = 4, does not achieve an accuracy of 1% until $x \approx 12.5$.

x	$-\sum(x)$	x	$-\sum(x)$	x	$-e^{-x^2}\sum(x)$
0.1	0.00638	1.6	3.454	1	0.302
0.2	0.02569	1.7	4.417	2	0.180
0.3	0.05848	1.8	5.697	3	6.15×10^{-2}
0.4	0.1057	1.9	7.430	4	3.08
0.5	0.1688	2.0	9.823	5	1.89
0.6	0.2497	2.2	18.04	6	1.29
0.7	0.3510	2.4	35.87	7	9.34×10^{-3}
0.8	0.4764	2.6	78.14	8	7.09
0.9	0.6305	2.8	187.8	9	5.58
1.0	0.8197	3.0	498.6	10	4.50
1.1	1.052	3.2	1461	11	3.71
1.2	1.340	3.4	4714	12	3.11
1.3	1.697	3.6	16686	13	2.65
1.4	2.147	3.8	64671	14	2.28
1.5	2.718	4.0	273925	15	1.98

For larger values of y we have:

$$\underline{R}\omega(x + iy) \approx y\sum_{i}^{3} \frac{a_i(x^2 + y^2 + b_i)}{(x^2 - y^2 - b_i)^2 + 4x^2y^2}$$

with

$a_1 = 0.4613135$ $\qquad b_1 = 0.1901635$

$a_2 = 0.09999216$ $\qquad b_2 = 1.7844927$

$a_3 = 0.002883894$ $\qquad b_3 = 5.5253437.$

This approximation is useful for computing the "escape fraction" $F(\Delta,\Gamma,R)$ that was defined in our discussion of Question No.(iii). We have:

$$F(\Delta,\Gamma,R) = \frac{1}{\sqrt{\pi}} \sum_i a_i\{\pi - [\arctan \frac{2}{\Gamma}(\Delta + \sqrt{b_i}\ \theta) + \arctan \frac{2}{\Gamma}(\Delta - \sqrt{b_i}\ \theta)]\}. \quad (1)$$

This is the approximation referred to earlier as accurate to better than 1% of its own value outside the range of tabulation of the exact values in Table 3.9-1.

The accuracy of these two approximations has been evaluated in detail.

---

4. DETECTOR SYSTEMS

4.1 Purchase of Ge(Li) Detectors

R.H. Heffner, R.E. Marrs, J. Pedersen, P.A. Russo, and D.H. Wilkinson

During the past year the laboratory has purchased two Ge(Li) gamma-ray detectors. A 45cc detector was supplied by Princeton Gamma-Tech. It has 2.41 keV (FWHM) resolution and 7.2% relative efficiency at 1.33 MeV. The good efficiency of this detector makes it especially valuable for detection of high energy gamma-rays. Resolution at 7 MeV is approximately 7 keV (FWHM).

A smaller volume detector was purchased from Canberra. This 20cc coaxial crystal resolves 1.33 MeV lines to 2.7 keV (FWHM). The efficiency is approximately 3%. The time resolution capabilities of this detector have been shown to be better than 6 nsec (FWHM) with constant fraction techniques.

4.2 Silicon Detectors

S. Kellenbarger

For the past year we have made our lithium-drifted silicon detectors with silicon purchased from Nucleonic Products Co., (NPC), Canoga Park, California. This is zero etch pit density silicon and comes in ingots with diameters of 20 to 35 mm. We have made detectors up to 4 mm thick (as thick as we need) and 500 mm^2 area. We are not etching mesas or wells, cutting grooves, or double drifting to make shelf structures. With the proper silicon, these procedures do not seem necessary for us.

Detectors from the first two NPC ingots we used drifted slowly. About three weeks at 125°C for a 3 mm detector was required in our Berkeley air ovens. Therefore we tried drifting in FC-43, originally used by Miller, Pate, and Wagner.[1] At the same temperature, our detectors drift in about half the time in FC-43 as in air. If a temperature of about 140°C is used at the beginning of drifting and gradually decreased during the process, the detectors drift in about one-fourth the time required in air. Detectors drifted in air and in FC-43 seem to perform equally well.

NPC now classifies its silicon as to rate of drifting, but we do not have enough experience with the faster drifting silicon to comment on it.

When using Monsanto silicon, we found it necessary to "redrift" detectors (applying 500 volts reverse bias for 15 hours at 80°C) about every month in order to maintain the noise at a satisfactory level. During storage, either with or without reverse bias, the noise would gradually increase until another redrifting was needed. With the NPC silicon, redrifting is no longer necessary, nor does it seem to have any beneficial effect.

We have continued to make surface barrier fission fragment detectors as mentioned last year,[2] except that we now apply a narrow band of p-type epoxy[3] around the edge of the face ('p' side) of the detector after etching. The epoxy, with a pot life of 2-3 minutes, is applied with a plastic applicator which is dipped in the epoxy and then placed on the detector. The applicator has a hole in the center through which a little plastic rod can be put to hold the detector down when removing the applicator. A mask is used during gold evaporation so the edge of the evaporated gold layer lies on top of the ring of epoxy. Detectors with lower reverse current and less noise have resulted.

---

1. G.L. Miller, B.D. Pate, and S. Wagner, IEEE Trans. Nucl. Sci. *NS-10*, No. 1, 220 (1963).
2. Nuclear Physics Laboratory Annual Report, University of Washington (1970), p. 30.
3. Epoxylite Corporation, Box 3397, So. El Monte, California, 5 drops resin #69 + 1 drop C-323 catalyst.

4.3 A Si(Li) Counter for the Detection of X-Rays

J.G. Cramer, S. Kellenbarger, and C. Wilson

The success of the program of construction of lithium drifted silicon counters for the detection of charged particles[1] has prompted the extension of this program to the fabrication of Si(Li) detectors for X-ray detection. A 2.9 mm detector with an active area of 180 mm^2 which had been prepared originally for particle detection was selected because of its thickness and low noise characteristics. This detector was somewhat larger in area than is desirable for optimum resolution because of its larger capacitance, but no equivalent detector of smaller area was available at that time.

The detector was mounted in a copper housing inside a laboratory-constructed right-angle cryostat which has originally been constructed to house a Ge(Li) detector.[2] The entrance window of the cryostat was modified so that X-rays entering the detector need only pass through a curved 0.7 mil aluminum entrance window. The cryostat was evacuated, the molecular sieve material was activated by external heating, and the detector was cooled by immersing the lower end of the cryostat in liquid nitrogen. After one accident in which the thin aluminum entrance window was perforated, an annular lucite cylinder was constructed to slip over the end of the cryostat and protect the window from damage.

Various tests have been made with the detector using a variety of X-ray and low energy gamma ray sources. Resolution seems to depend strongly on the preamplifier and amplifier used. The best resolution so far has been obtained with a Tennelec TC137 preamplifier and TC203BLR amplifier, with the time constants of the latter set for four microseconds. With these devices, the X-rays from Cs and Ba, as produced by a ^{133}Ba source and a ^{137}Cs source, respectively, were observed. For Cs the $K_{\alpha 1}$ X-ray has an energy of 30.97 keV, the $K_{\alpha 2}$ an energy of 30.63 keV, and K_β X-rays an average energy of about 35.1 keV. For Ba the corresponding energies are: $K_{\alpha 1}$ = 32.19 keV, $K_{\alpha 2}$ = 31.82 keV, and K_β = 36.8 keV. A resolution of 1.7 keV FWHM has been measured for these X-rays as shown in Fig. 4.3-1.

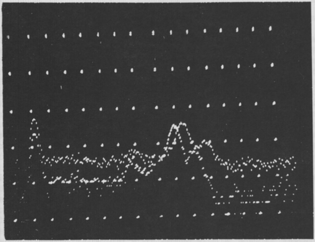

Fig. 4.3-1. Superimposed spectra of K X-rays from Cs and Ba with energies of about 31-32 keV.

This resolution, while respectable for a large area detector with an uncooled preamplifier, is considerably above "state-of-the-art" systems used elsewhere with resolutions of a few hundred electron-volts. We are now taking steps to improve on these preliminary measurements by the construction of a new detector system with a smaller Si(Li) detector with a thickness of 3.3 mm and an area of 50 mm^2 and the use of an Ortec 120-2B preamplifier which eliminates the noise of the bias resistor by bringing the bias voltage in on the "back side" of the detector. We are also considering the construction of a cooled-FET preamplifier to further improve resolution.

1. Nuclear Physics Laboratory Annual Report, University of Washington (1968), p. 158.
2. Nuclear Physics Laboratory Annual Report, University of Washington (1969), p. 137.

4.4 A Positron Annihilation Gamma Counter

W. Jacobs

It was desired to determine the cross-section for the reaction $^{14}N(p,\alpha)$ ^{11}C by activation methods.[1] ^{11}C is a positron emitter (half life of 20.3 minutes), suggesting the measurement of the activity by the well known method of detecting the annihilation gamma rays in coincidence.

A "positron counter" was built consisting of two 3" x 3" NaI(Tℓ) crystals to be used in 180° geometry, the activated target (or calibration source) is placed between the two gamma counters in an absorber sandwich sufficient to ensure annihilation of the positron near the target. The device was built to be compatible with use inside the 60" scattering chambers, that is, with the NaI crystals at beam height when the holders are placed on the scattering chamber arms.

For activities with relatively long half lives, as encountered in this experiment, it was thought that most efficient use of beam time would be made by counting the targets outside the scattering chamber. Therefore, a special arm was machined to serve as an optical bench giving a proper and reproducible alignment for the crystals. An adjustable stand (for fine centering of the source on the crystal axis) clamps between the crystals and holds a standard five-target target ladder. A hole burned in a thin polyethylene target, mounted in the ladder at the time of bombardment, together with a pointer device, allow one to center the bombarded area (usually a spot about 3/32" in diameter) on the counter axis to ± 1/32". If the crystals are about 11" apart, this reduces the geometric contribution to the error in the efficiency to less than 2%. A selection device allows one to select and position with precision the targets on the ladder to be counted. If targets are placed on alternate positions in the ladder, and appropriate lead shielding is used, several targets can be successively counted without removing them from the original target ladder.

---

1. See Section 7.1 of this Report.

4.5 A High Resolution NaI Detector for High Energy Gamma Rays

I. Halpern, D.L. Johnson, and D.F. Measday*

Several gamma ray experiments in the past have used a 3ϕ" x 5 1/4" NaI crystal as the central detector inside an 8ϕ" x 12" NaI anti-coincidence annulus. The resolution of this system for high energy gamma rays has been very poor. For 15 MeV gamma rays its resolution was about 12% whereas Drake[1] at Los Alamos has achieved better than 7% with a similar system. It was verified that the central crystal was the likely cause of poor resolution and that a new crystal could have superior resolution if it were manufactured according to certain rigid specifications[1] that take into account the deep penetration of high energy gamma rays. A new 3ϕ" x 6" NaI crystal was purchased from the Bicron Corporation[2] with funds available to Dr. David F. Measday of the University of British Columbia. The performance specifications were as follows:

a) Pulse height and resolution shall be uniform within 1% when measured along the side of the crystal with a well collimated low energy gamma source (eg. ^{22}Na). The resolution uniformity means that, for example, the resolution lies within the range of 8.5 to 7.5% everywhere along the length except within an inch of either end.

b) The extrapolated resolution at infinite energy* should be equal to or less than 3% when measured on the front face with low energy sources such as ^{22}Na, ^{137}Cs, ^{54}Mn and ^{207}Bi. (* obtained by plotting R^2 vs $1/E_\gamma$).

c) The resolution of ^{137}Cs on the front face should be equal to or less than 9%.

All specifications were met except that the extrapolated resolution at infinite energy was slightly high at ~3.65%. The ^{137}Cs resolution was 8.50%. When tested with 15.11 MeV gamma rays the detector-annulus system gave a resolution as good as 6.0%. The resolution was dependent upon the collinator size as is shown below.

Diameter of Gamma Illumination on Back Face of Crystal	15 MeV Resolution
~3/4"	6.0%
~1 1/2"	6.4%
~3"	7.9%

It is felt that the resolution is limited at present by the inability of the annulus detector to intercept all secondary gamma rays. Annihilation quanta from pair events and compton events are not detected by the annulus when they travel back towards the target direction (see Figure 4.5-1). Hence a shoulder appears on the low energy side of the gamma ray response function due to events that are not rejected by the annulus.

A plug of scintillating plastic placed in front of the 3ϕ" x 6" detector and used as part of the annulus should improve the best resolution to better than 5%.

* University of British Columbia, Vancouver, B.C.
1. D. Drake, private communication.
2. Bicron Corporation, 12345 Kinsman Road, Newbury, Ohio 44065

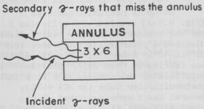

Fig. 4.5-1. Gamma ray detection geometry.

4.6 Description of a Tapered-Annulus Gamma Detector for Use in Particle-Gamma Correlation Studies

T. Lewellen and F. Schmidt

The study of the substrate cross sections of the 3.73 MeV 3^- state of ^{40}Ca currently in progress (see Sec. 10.1 of this report) has required the design of a new gamma detector system. The system has been designed to meet the following criteria:

1) Provide integration over ϕ_γ as defined in Fig. 1.
2) Emphasize the radiation from the even substates
3) Fit into the existing 60 inch scattering chamber
4) Be designed for reasonable data collection efficiency.
5) Use plastic or liquid scintillators.

The reason for criterion 1 is explained in Sec. 10.1 of this report. Criterion 5 reduces the cost of the scintillator and provides desirable fast timing characteristics.

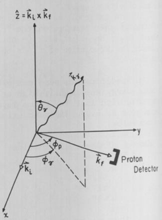

Fig. 4.6-1. The coordinate system used in particle-gamma correlation studies. The beam is along the x-axis.

It was decided to use a scintillator of sufficient size to perform the integration directly. Due to the geometrical restrictions imposed by the scattering chamber, a scintillator in the shape of a tapered annulus was chosen to make the calculation of solid angle corrections reasonably straightforward.

Octupole radiation patterns [Fig. 4.6-2] coupled with criterion 2 and the scattering chamber restrictions dictated a polar angle acceptance from 25° to 40°. Accordingly a small annulus was fabricated from NE102[1] plastic scintillator and coupled to a five inch photomultiplier tube (an RCA 4522). Several tests were performed which, along with some simple calculations involving detector efficiency and expected counting rates, indicated that

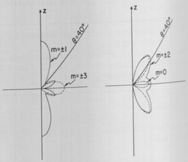

Fig. 4.6-2. Octupole Radiation patterns.

a design using a larger volume scintillator and multiple photomultiplier tubes would be advantageous.

A NE102 scintillator in the shape of a tapered annulus having a polar angle acceptance from 25° to 40° and a maximum outer diameter of nine inches was purchased from Nuclear Enterprises Inc. Eight RCA 8575 2" photomultiplier tubes used in the design were also purchased.

Tube bases for the photomultipliers have been designed and built. The schematic diagram for the tube bases is shown in Fig. 4.6-3 while the physical appearance is illustrated in Fig. 4.6-4. It was felt desirable to make each tube base independent of the others to allow their use in other experiments.

The design of the voltage divider was based on information supplied by RCA and designs by ORTEC, J. Calarco,[2] and J. Tesmer *et al.*[3] A split power supply system was used to allow a high divider string current for the last few dynodes in order to help minimize gain shifts due to count rate changes and yet keep the rest of the divider string current low to minimize heat problems. The split supply system also allows greater flexibility in selecting the gains and rise times at the various outputs when the base is used with different scintillators.

Three outputs are provided. The ninth dynode is to be used as the energy signal, the twelfth dynode for fast coincidence requirements between tubes, and the anode as a standard fast timing signal.

The physical design had to allow for the close spacing of the eight photomultipliers when they are in place on the scintillator. As shown in Fig. 4.6-4, magnetic shielding is provided by two concentric tubes separated by several layers of teflon tape. The outer tube is netic alloy[4] and the inner tube, which is also used as an electrostatic shield, is conetic alloy.[4] The inner tube is connected to the cathode potential by means of a small printed circuit board jack inserted in the blank space of the standard tube socket supplied by RCA (see Fig. 4.6-4).

Preliminary tests of the photomultiplier tubes and tube bases have been completed. A 2" x 2" NE102 scintillator, a ^{60}Co source, a negative voltage of -1600 VDC and a positive voltage of 1060 VDC were used. The average rise time for the eight assemblies was 3.0 nsec and the average anode pulse height was 10 volts. A rapid change in counting rate from 2500 cps to 45,000 cps produced a maximum gain shift of $\sim$2%.

One of the problems with using a plastic scintillator is the lack of resolution for gamma rays. This is a problem because a reference peak of known energy is needed to determine discriminator settings, check for gain shifts, and to determine the product $f\varepsilon\omega$ [fraction of gamma spectrum observed, times the detection efficiency for the gamma ray energy of interest times the effective solid angle].

We hope to use a light pulser system to generate such a reference peak and, at the same time, provide a convenient measure of the system dead time

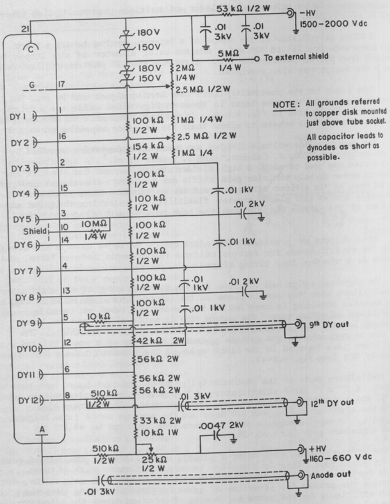

Fig. 4.6-3. Schematic diagram of tube base for RCA 8575 photomultiplier tube.

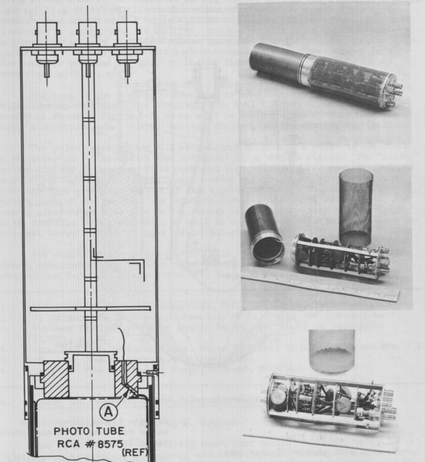

Fig. 4.6-4. Tube base for #8575 photomultiplier. A refers to printed circuit board jack used to make connection to external electrostatic shield.

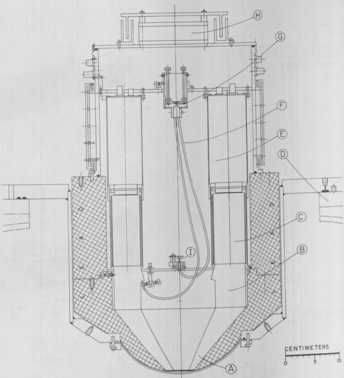

Fig. 4.6-5. Tapered Annulus Gamma Detector.

A. NE 102 scintillator

B. Lucite light pipe

C. RCA 8575 photomultiplier tube

D. 60-in. scattering chamber lid

E. Tube base

F. Multiple branch fiber optics bundle (one branch to each photomultiplier tube)

G. Gallium arsenide light-emitting diode

H. Exhaust fan

I. Phototransistor

during an experiment: As indicated in Fig. 4.6-5, we will use a gallium arsenide light emitting diode[5] to illuminate one end of a multiple branch fiber optics bundle.[5] One branch of the bundle will be coupled to each photomultiplier tube by means of a light pipe. In addition, one branch will go to a phototransistor to allow monitoring of the light pulser independent of the photomultiplier tubes. A single light source system with a phototransistor monitor was chosen to minimize possible problems of variation in the light output of the diode due to temperature effects, etc.

The rest of the housing is designed to keep the interior light-tight while allowing sufficient air circulation to cool the tube bases. In addition to what is shown in Fig. 4.6-5, there will be another chassis containing the pulser electronics, the "master" voltage divider, and the summing electronics.

The pulser electronics will be designed to provide a pulse to the diode on the order of 3-5 nsec wide when triggered by an outside signal. The "master" voltage divider is designed to be supplied high voltage by two positive and one negative voltage supplies [each supply having a 20 ma capacity]. The divider will then supply voltage to each of the eight tube bases with provision for adjusting each of the positive and negative voltages over a 500 volt range. The summing electronics will provide one energy signal and one fast timing signal to the counting room electronics as well as demanding a suitable coincidence requirement between adjacent tubes before allowing an output.

The design of the entire system, with the exceptions of the pulser and summing electronics, is complete. The fabrication of the system is now in progress and hopefully system tests will begin in early June.

---

1. Obtained from Nuclear Enterprises, Inc., San Carlos, California.
2. J. Calarco, Ph.D. Thesis, University of Illinois, 1969 (unpublished).
3. Nuclear Physics Laboratory Annual Report, University of Washington (1970), p. 32.
4. Obtained from Perfection Mica, Magnetic Shield Division, Bensenville, Ill.
5. Obtained from Monsanto Co., Caldwell, N.J.
6. Obtained from Don Corning Corp., Midland, Michigan.

4.7 Heavy Ion Identification Using a ΔE-E Telescope

M. Hasinoff, K.G. Nair, and W. Wharton

The possibility of identifying heavy ions in the mass range 12 to 24 using a single telescope arrangement was investigated. A transmission detector of thickness 11μ and an 87μ thick E-detector were placed at a distance of 7.5" from the target. A circular aperture of diameter 0.125" was used to define an azimuthal angular acceptance of about 1°. ^{16}O ions with energies varying from 50.0 MeV to 68.0 MeV provided the incident beam. Targets of ^{12}C, ^{50}Ti, ^{58}Ni and ^{140}Ce of approximate thicknesses varying from 50μg/cm^2 to 75μg/cm^2 were used to obtain heavy ion recoils and reaction products.

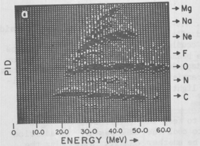

Fig. 4.7-1a. Plot of ID vs E for outgoing heavy ions from the oxygen bombardment of carbon. ^{16}O elastic from carbon is used as a normalization point in the energy calibration. The rest of the legend is self-explanatory. For details, see text.

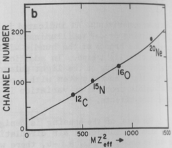

Fig. 4.7-1b. Plot of channel number in the projected ID spectrum vs MZ_{eff}^2.

A typical plot of ID vs energy is shown in Fig. 4.7-1a, corresponding to $\theta_{lab} = 15°$, $E_{lab} = 68.9$ MeV for ^{16}O ions incident on a carbon target of thickness 75 $\mu g/cm^2$. Here ID is defined as $(E + \Delta E)^{1.4} - E^{1.4}$ and is a measure of the particle identity. The traces due to C, N, and O have been identified by looking at their energy spectra. The energy spectra for the heavier ions were not recorded and their identity was made by several methods, the most accurate being a calculation of the low energy cutoff points of the traces using range energy tables[1] and the measured cutoff energies for C and O. The traces are C, N, O, F, Ne, Na, and Mg as indicated in Fig. 4.7-1a. All traces are well separated but an improvement[2] will be needed in the calculation of the ID in order that the ID of each particle trace remain constant with energy. It is not known yet if we can separate different isotopes of the same element.

A plot of channel numbers in the ID spectrum vs MZ^2_{eff} is shown in Fig. 4.7-1a. The Z_{eff} in this calculation is the effective charge of a heavy ion after it has passed through a sufficient thickness of material to reach its equilibrium charge distribution. It is defined as[1]

$$Z_{eff} = \gamma Z_{nuclear} = [1 - 1.85\, e^{-2\xi}]^{\frac{1}{2}}\, Z_{nuclear}$$

where

$$\xi = \frac{137\,\beta}{Z_{nuclear}} = \frac{137\, v}{cZ_{nuclear}} .$$

In the present calculation, v is the velocity corresponding to the highest energy observed for each particle.

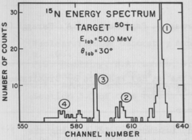

Fig. 4.7-2. Energy spectrum of ^{15}N ions from the reaction $^{50}Ti + {}^{16}O \rightarrow {}^{51}V + {}^{15}N$.

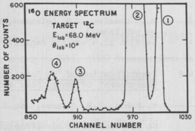

Fig. 4.7-3. Energy spectrum of ^{16}O ions from the oxygen bombardment of carbon.

The channel number is taken from a projection of the ID spectrum shown in Fig. 4.7-1a on the ID-axis. In the region from ^{12}C to ^{20}Ne this plot is clearly linear and provides a check on our mass identification.

Figure 4.7-2 shows the energy spectrum of ^{15}N ions from the reaction $^{50}Ti + {}^{16}O \rightarrow {}^{51}V + {}^{15}N$ at E_{lab} = 50.0 MeV and θ_{lab} = 30°. The numbers from 1 to 4 designate the reaction products $^{15}N + {}^{51}V$(g.s.), $^{15}N + {}^{51}V$(1.609), $^{15}N + {}^{51}V$(2.408 and 2.545) and $^{15}N + {}^{51}V$(3.28) respectively. This assignment is in agreement with that of Lemaire *et al.*[3]

The energy spectrum of ^{16}O ions at θ_{lab} = 10°, which results when a 75 μg/cm^2 thick carbon target is bombarded by 68.0 MeV oxygen ions, is shown in Fig. 4.7-3. The numbers 2, 3 and 4 designate the reaction products ^{16}O(g.s.) + ^{12}C (g.s.), ^{16}O(g.s.) + ^{12}C(4.44), and ^{16}O(6.05) + ^{12}C(g.s.). Number 1 is probably due to a contaminant and kinematically fits the reaction products ^{16}O(g.s.) + ^{28}Si(g.s.).

Of particular interest was the energy distribution of ^{15}N ions from a 50 μg/cm^2 thick ^{140}Ce target produced by 60.0 MeV incident oxygen ions, in that it corroborated the results of the single proton transfer reaction[4] obtained without identification techniques, even though the statistics in the present case were poor.

Because of the success of this investigation, it is proposed to use particle identification techniques in addition to the currently used singles counting method in the studies of nucleon and multi-nucleon transfer reaction induced by heavy ions, especially near the Coulomb barrier.

---

1. L.C. Northcliffe and R.F. Schilling, *Nuclear Data Tables*, Sec. A, *7*, 233 (1970).
2. Section 5.9 of this report.

3. M.C. Lemaire, J.M. Loiseaux, M.C. Marmaz, A. Papineau, and A. Faraggi (to be published).
4. Section 11.4 of this report.

4.8 Identification of ^{6}He Particles from the (α,^{6}He) Reaction by Simultaneous Measurement of Energy Loss and Time of Flight

M. Baker, J.R. Calarco, and J.G. Cramer

We have continued our efforts to study two-neutron pickup using the (α,^{6}He) reaction.[1] Even targets of very light nuclei are expected to produce very small fluxes of ^{6}He ions compared with those of alpha particles. This makes the identification of ^{6}He ions very difficult. Under these circumstances many experimenters have turned to the double particle identification method.[2,4] We have attempted to extend measurements of this type to lower outgoing particle energies by a simultaneous determination of "single" particle identification and mass.

A ^{9}Be target was bombarded with 42 MeV alpha particles from the University of Washington cyclotron. Reaction products were detected in a ΔE-E detector telescope consisting of a 35μ totally depleted silicon (ΔE) detector and a 1 mm lithium drifted silicon (E) detector. A timimg signal derived from the ΔE detector was used to start a time-to-amplitude converter (TAC). A signal derived from the oscillator of the cyclotron served to stop the TAC. The two energy signals and the time-of-flight signal were sent to the SDS 930 computer. Particle identification was determined using the $(E + \Delta)^b - (E)^b$ technique. Particle mass was derived from the relation $(E + \Delta E - E_0)(T_0 - T)^2$ where E_0 and T_0 were adjustable digital parameters. CRT oscilloscope displays of either particle identification, or mass, or the product of particle identification and mass vs total energy were available as 64 × 64 channel arrays.

The time resolution was improved compared to the previous runs[1] but difficulties were encountered in the mass determination caused by the incident alpha particle beam being extracted from more than one cyclotron orbit. When this occurs there is a transit time different of approximately 2 nsec through the beam transport system. For the flight path used satellite groups of elastic and inelastic alphas appeared in approximately the same region of the mass spectrum as that anticipated for mass A = 6 particles. Some success was achieved in reducing the magnitude of these groups by restricting the size of the beam as it emerged from the cyclotron but adequate mass identification was not obtained.

An experimental study of the (α,^{6}He) reaction on light nuclei where the double particle identification method was successfully employed has recently been reported.[3] The total thickness of our two thinnest available transmission counters has been ~85μ, permitting the redundant identification of ^{6}He ions of energies greater than about 13-14 MeV. The recent acquisition of two transmission detectors with thicknesses of 11 and 21 microns should make possible redundant or double particle identification with a three-counter telescope at ^{6}He energies as low as 7-8 MeV. An on-line program has been written[4] to perform this type of particle identification. Furthermore, it will now be possible to perform improved particle identification by insisting on consistency between time-of-flight information and redundant identification with a three-counter telescope.

1. Nuclear Physics Laboratory Annual Report, University of Washington (1970), p. 106.
2. F.S. Goulding, D.A. Landis, J. Cerny, and R.H. Pehl, IEEE Transactions on Nuclear Science, *NS-13*, No. 3, 514 (1966).
3. J.M. Arnold, and R.W. Bercaw, Bull. Am. Phys. Soc. *15*, 630 (1970).
4. Section 5.6 of this report.

4.9 A Single-Wire Position-Sensitive Proportional Counter for Magnetic Spectrograph Readout

M.P. Baker, J.R. Calarco, N.S. Chant, J.G. Cramer, and S. Hendrickson

A position-sensitive proportional counter of the type described by Borkowski and Kopp[1] has been constructed for use in the focal plane of the UW 90.6 cm Browne-Buechner Broad-range Magnetic Spectrograph.[2] The spectrograph, which has a specific energy dispersion dE/EdS of about 4.9×10^{-4} mm^{-1} is well matched to a readout device of this type, in that the anticipated position resolution of the counter is approximately equivalent to the expected energy resolution of the spectrograph. In particular, a 1.0 mm position resolution corresponds to 4.9 keV energy resolution at 10 MeV.

The detector has an active length of 197 mm and an active height of about 10 mm, the latter limited by a defining aperture in the spectrograph focal plane. The proportional counter is mounted on a track which follows the curvature of the focal plane, and the counter can be positioned anywhere along this track under external control. The entire track assembly can also be displaced back and forth externally to locate the focal plane empirically and to compensate for kinematic broadening effects when light targets are used.[2] In practice, the proportional counter has been positioned with its center approximately on the 90° position of the focal plane and the magnetic field varied rather than the counter position. In this configuration the counter spans an energy region of about ±5% of E_0, the energy of particles detected at the 90° position of the focal plane. Thus, the counter is sensitive to about the top 1 MeV region of a 10 MeV particle spectrum.

The position-sensitive detector consists of an inner assembly which does the actual counting and an outer pressure vessel which separates the approximately 1 atm of counter gas from the surrounding vacuum. The inner counter assembly is shown in Fig. 4.9-1. It consists of a 1/8" thick rectangular lucite frame supporting the position sensing element, a pyrolytic carbon-coated fused silica fiber 0.02 mm in diameter.[3] The end-to-end resistance of the fiber is about 1.5 megohms. The frame has a wire contact at each end to which the fiber is attached with conductive epoxy.[4] One of the wire contacts is under spring tension produced by a small leaf spring on the outside of the frame, so that the fiber is under continuous tension and is maintained in a taut position. The fiber is in close proximity on both sides to a pair of aluminized mylar electrodes which are formed by wrapping a sheet of aluminized mylar around one end of the frame and securing it in a tightly stretched position with pressure sensitive tape.[5] The mylar electrode and both ends of the center fiber are connected electrically to spring clips imbedded in the lucite frame which permit rapid connection and

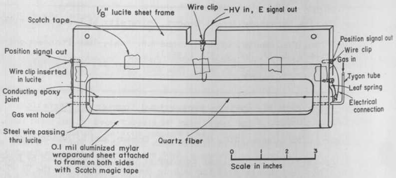

Fig. 4.9-1. Assembly Drawing of Inner Counter Assembly

replacement of counter assemblies. Counter gas consisting of 90% argon and 10% methane is injected directly into the counter assembly through a small hole drilled in one edge of the lucite frame. Gas exits around the edges of the mylar electrode and through another hole at the opposite end of the frame. The resistive central fiber and mylar electrodes form a distributed RC transmission line which filters out the high-frequency components of the counter pulse, producing a variation in rise-time of the pulse which depends on the horizontal position of the event.

An assembly drawing of the complete counter is shown in Fig. 4.9-2. The pressure vessel is constructed in a fairly modular form for flexibility and ease of modification. It has removable plates on the front, back, top, and bottom. The front plate forms the entrance window, which is a cylindrical surface with about a 3 cm radius of curvature with Havar[6] foil 6.4 microns in thickness cemented[7] to the aluminum plate. The window structure is constructed so that the window is as close to the counter assembly as possible, consistent with electrical insulation to about 2 kilovolts, to minimize energy loss of particles in passing through the gas outside the counter.

The top plate holds the feed-through BNC connectors which make electrical connections between the counter and the external electronics, and the support brackets for the inner counter assembly. The center feed-through connector is mounted on a removable circular plate so that it can be replaced by a high-voltage feed-through connector if bias voltages in excess of about 1.5 kilovolts are used. Wires from the three connectors slip into the spring clips on the counter assembly to provide positive electrical connections.

The bottom plate provides the two connections for the gas handling system. One connection brings the counter gas into the pressure vessel through a copper tube which extends to near the top of the inner cavity. A thin plastic tube about 5 cm long, which has been drawn out to a nozzle at each end, is press-fitted

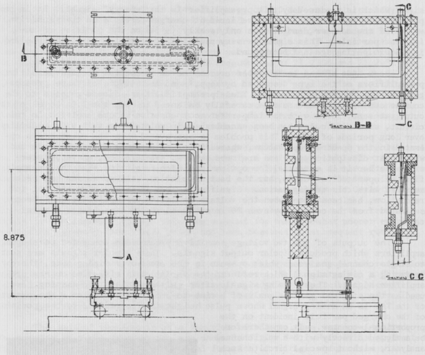

Fig. 4.9-2. Assembly Drawing of Complete Counter.

into the copper tubing. The other end of this tube is press-fitted into the hole in the side of the counter frame, thus insuring that fresh counter gas passes first through the inner counter before flowing out to the rest of the inner cavity. A second connection in the bottom plate conducts the gas out to an external gas trap where the gas is bubbled through diffusion-pump oil and into the atmosphere. The inside of the counter is thus maintained at atmosphereic pressure and the flow rate is adjusted by observing the rate at which bubbles are formed. The flow of gas is essential, for pronounced loss of counter gain has been observed when the gas flow has been interrupted for 15 minutes or so.

All three of the counter's electrical connections are brought out to preamplifiers. The aluminized mylar electrode of the inner counter assembly is connected to an ORTEC 190A charge-sensitive preamplifier (or a similar preamp suitable for solid-state detectors), and the negative bias voltage required by the counter is supplied through the normal bias connection of the preamplifier. The signal which is produced by this preamplifier is the "energy" signal. It is proportional to the energy lost by the incident charged particle in the sensitive volume of the counter, and depends only weakly (± 5%) on the position of the incident particle. This signal is very useful in determining particle type and in discriminating against background.

Both ends of the center fiber are connected to special voltage-sensitive preamplifiers of the type described by Kopp,[8] and the outputs of these preamps give the two "position" signals. These preamplifiers are direct-coupled to the counter center fiber and must be carefully balanced to keep the D.C. level of the output at zero. Even with the temperature compensation scheme employed in this circuit, some difficulty has been encountered in maintaining this D.C. stability over long periods of time. This problem is aggravated when the preamps are operated in the spectrograph vacuum, where direct adjustments cannot be made and where heat dissipation problems are more severe. We have not, as yet, determined whether it is essential for optimum position resolution that the preamplifiers be operated in vacuum, but the best resolution obtained so far has been measured with this configuration. Significant loss in signal size, if not in resolution, has been noted when the voltage sensitive preamplifiers have been separated from the counter by even 20 cm of RG 114/U low capacitance coaxial cable.

The outputs of the two voltage sensitive preamps are connected to shaping amplifiers which produce bipolar output signals. These bipolar signals are sent to single channel analyzers which operate in the cross-over timing mode, thereby producing a timing signal which reflects the variation in rise-time or the preamplifier signal. These timing signals after suitable delays and shaping, are used as the stop and start signals of a time-to-amplitude converter. The output of the TAC is an analog signal whose pulse height is proportional to the position of the charged particle incident on the proportional counter. It can therefore be analyzed directly with a multichannel analyzer, without special circuits such as division circuits, etc. Thus, except for the voltage-sensitive preamplifiers, the entire electronics system of the counter consists of standard nuclear electronics.

We have tested the counter both with a collimated radiothorium alpha source and in conjunction with the magnetic spectrograph. For these tests it was considered that the differences in emittance, entrance angle, and multiple scattering make resolution tests with the source of questionable value. Therefore, the source measurements were used primarily for linearity and end-effect tests, while resolution measurements were made primarily with the spectrograph. Fig. 4.9-3 shows the best reso-

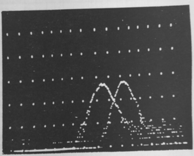

Fig. 4.9-3. Position spectra for NMR frequencies of 21.2396 MHz and 21.2451 MHz for elastic scattering of 9.0 MeV protons on gold at 60°.

lution obtained so far. Protons with an energy of 9.0 MeV were elastically scattered from a thin gold target and detected with the spectrograph positioned at an angle of 60°. The magnetic field of the spectrograph was changed until the elastic particle group was striking the counter approximately at its center. Then two measurements of the elastic group were made with the spectrograph set for magnetic fields corresponding to NMR frequencies of 21.2396 and 21.2451 MHz. This field shift is equivalent to an energy shift $\Delta E/E$ of 5.88×10^{-4} which, divided by the dispersion of the spectrograph at the 90° deflection position of 4.9×10^{-4} mm^{-1}, gives a position shift of 1.20 mm for the peaks. The peaks are separated by 32 channels, and the FWHM of the two peaks averages 16.5 channels, giving a position resolution of 0.62 mm FWHM. This corresponds to an energy resolution of 2.7 keV FWHM at 9.0 MeV incident proton energy.

This measurement was made with the magnet slits set to 50-50 mils vertical and 50-50 mils horizontal, which corresponds to a solid angle of 1.32×10^{-5} steradians. The resolution was observed to worsen by about a factor of three when the horizontal opening was increased by a factor of 10 to 500-500 mils or 1.32×10^{-4} steradians. This measurement was made when the Van de Graaff accelerator was extremely stable and the terminal ripple was less than 1 kilovolt. Since that time, a new belt has been installed in the machine and the terminal ripple is considerably worse. This may account for the somewhat poorer energy resolution (greater than 7 keV) which has been measured in subsequent runs, although other factors are also involved.

At least one counter assembly produced markedly poorer position resolution, and this was observable even with the alpha source. This counter was a "hurryup" job and the conductive epoxy curing time was speeded up by placing the counter assembly under a heat lamp. It is believed that the heating of the quartz fiber adversely affected its performance.

The gain of the counter as a function of bias voltage was investigated. The results of these measurements are shown in Fig. 4.9-4. Here it is apparent that the gain is roughly an exponential function of voltage which rises with a slope of 246 volts per factor of 10 in gain. Since the difference in energy loss in the counter between protons and alphas of the same energy is roughly a factor of ten, this represents the amount, about 250 volts, by which the bias voltage must be changed to optimize the bias voltage for one or the other kind of particle.

We will now enumerate the various difficulties which have been encountered in using the counter:

(a) Pressure Windows - The design of the counter is such that the rupture of a pressure window in vacuum has disastrous consequences for the inner counter assembly. Essentially, the whole counter is disemboweled into the vacuum system. On the first of several occasions on which this has occurred, oil from the gas trap was sucked back into the counter, reducing the counter which had just produced 0.6 mm position resolution to a frothy, oily mess. It is recommended that pressure windows be tested at 1½ atmospheres before they are used with a counter assembly, and that a double trap arrangement be used so that oil cannot be sucked into the counter.

(b) Preamps - As mentioned above, the voltage-sensitive preamplifiers have some D.C. stability problems which are particularly troublesome when they are used in vacuum. We have alleviated this problem to some extent, with the observation that the D.C. balance of the preamp can be set remotely by making small variations in the nominal 24 volt power supply voltage while monitoring the D.C. level of the preamp output. If the D.C. level is allowed to remain badly out of balance for a prolonged period the input FET is usually destroyed. Another preamp difficulty has been encountered at bias voltages above about 900 volts, where the counter has been observed to have infrequent but violent voltage breakdowns. Such sparks are well correlated with the loss of input FET's. A protective circuit at the input to the preamp is under consideration to alleviate this problem.

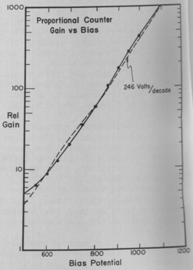

Fig. 4.9-4. Counter gain as a function of bias voltage.

(c) Shaping Amplifiers - The choice of shaping amplifiers is quite important to the operation of the counter, both in the resolution and the dynamic range of the device. The variation of risetimes produced by the counter is large compared to the time constants of most amplifiers. This causes amplitude variations in the amplifier output of up to 12 to one from one end of the counter to the other. This phenomenon is illustrated in Fig. 4.9-5, where we see oscilloscope traces of amplifier outputs. Here we see the variation in crossover point and amplitude for the two ends of the counter for an active filter amplifier with a 6 microsecond time constant (below) and a DDL amplifier with a 1 microsecond time constant (above). In the upper part of each trace is shown the energy signal for comparison, also illustrating its lack of variation with position. The time scale on the upper part of the figure is 0.5 μsec/cm and the lower, 5.0 μsec/cm. The time and amplitude variations of 15 different amplifier configurations have been studied and are illustrated in Fig. 4.9-6. We see that there is a general trend toward small amplitude variations with long time constants, as would be expected. Thus, to restrict the dynamic range of the output pulses to a value consistent with reliable operation of the timing single channel analyzers, it is necessary to use amplifiers with long time constants. This, consequently, restricts the counting rate at which the counter can be operated.

We have investigated the use of a center wire with a smaller resistance to reduce this problem, and find that the amplitude variations are indeed reduced,

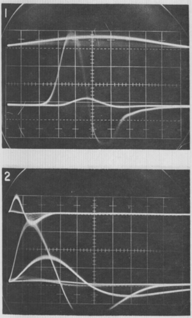

Fig. 4.9-5. Oscilloscope traces of amplifier output showing amplitude and time variations with position for Hamner NA-12D DDL (.7 μs) amplifier (top) and ORTEC 452 active filter (6 μs) amplifier (bottom).

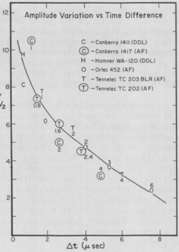

Fig. 4.9-6. Amplitude vs time variations for various amplifier types.

but the resolution is degraded at the same time.

(d) Background - We have found that the counter has a considerable background counting rate attributable to radiation from the Faraday cup, presumably neutrons. In some counters this background is randomly distributed in apparent position, in others tested it forms spurious "peaks" at particular "positions" of the counter, presumably regions where breakdown is most likely to occur. This is a serious problem, and can greatly limit the utility of the counter if it cannot be corrected.

Thus far, the only effective remedies have been to restrict measurements to relatively low energy protons, and to use massive shielding between the counter and the Faraday cup. Neither of these solutions is satisfactory, and others must be found. We intend to investigate the use of counter gases which contain no hydrogen, e.g., argon plus CO_2, and replace the aluminized mylar with thin aluminum to reduce the neutron sensitivity of the counter. This will eliminate the possibility of neutron-produced knock-on protons triggering the counter.

Another possibility is the use of multi-counter telescopes, with a coincidence requirement between counters. Such an arrangement might have the additional advantage of allowing the determination of the angle as well as the position of incident particles, thereby making possible digital corrections for the aberrations of the spectrograph and a corresponding enhancement in resolution and elimination of scattered background. This would, however, essentially double the electronic complexity of the detector system.

(e) End Effects - Nonlinearities near the ends of the counter have been observed, as shown in Fig. 4.9-7. Here, in the upper part of the figure, we see a position spectrum measured with an alpha source positioned at 1 cm intervals along the length of the counter. We see that the position linearity degenerates badly for the first and last 3 cm of the counter's length. By adding an RC termination network consisting of a 50 pf capacitor and 100K resistor to ground, at each end of the counter, we have reduced these effects, as shown in the lower part of Fig. 4.9-7.

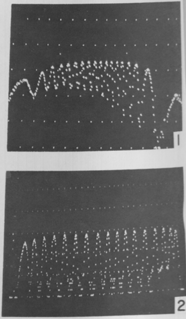

Fig. 4.9-7. Linearity measurement of counter, showing and effects with (bottom) and without (top) RC terminations.

These effects are also a function of amplifier time constant and this interaction has not been properly investigated as yet.

We intend to continue these investigations, and to construct counters which are longer so that more of the focal plane can be covered.

---

1. C.J. Borkowski and M.K. Kopp, IEEE Trans. on Nucl. Sci. *NS*17, No. 3, 340 (1970); *ibid.*, Rev. Sci. Instr. *39*, 1515 (1968).
2. D.K. McDaniels, W. Brandenberg, G.W. Farwell, and D.L. Hendrie, Nucl. Instr. and Meth. *14*, 263 (1961).
3. Manufactured by General Electric Manufacturing Research, Valley Forge, Pa.

4. ENT-105, Conductive Epoxy, Manufactured by Chromerics, Inc., 77 Dragon Ct. Woburn, Mass. 01801.
5. Scotch brand Magic Tape, Minnesota Mining and Mfg. Co., St. Paul, Minn.
6. Manufactured by Hamilton Precision Metals, Lancaster, Pa.
7. Permabond Cement, available from Universal Plastics Co., Seattle, Wash.
8. M.K. Kopp, Rev. Sci. Instr. *42*, 714 (1971).

---

5. COMPUTER SYSTEM

5.1 Computer System Expansion

N. Cheney, J. George, B. Lewellen, and F. Weiss

The computer expansion project began in late 1969 and described in last year's Annual Report has progressed to a point where all major units of the second computer system are on hand. The tasks remaining to be performed in order to bring the additional system up to an operational level include unit checkout (now in progress) and system integration. Due to the time required to design and build the interface for drum hardware, those units will not be included in this initial operating level. They are expected to be available several months after the second computer is running.

The final dual computer system configuration (Fig. 5.1-2) will vary considerably from that which was originally proposed (Fig. 5.1-1). As can be seen in Fig. 5.1-1, the original proposal required the two computers to share most of the peripherals and compete for their use. A somewhat complicated scheme was devised to ease this problem. Fortunately this scheme is no longer necessary, due to our purchase of a line printer, two magnetic tape units, and a teletype. These units are practically identical to their counterparts in the existing system and should present no interfacing problems when they are tied into the new system.

A 250K word drum and a 16K word core memory have also been added. It is expected that the software system will be stored on the 250K word drum, allowing the original 500K word drum to be used as general purpose storage. The 16K word core memory will replace the 8K word version in the new computer, improving its computing power and software compatibility with the existing computer.

It is believed the changes and additions described above will allow the two machines to operate more independently of one another and improve their overall computing capability.

Each of the pieces of hardware mentioned previously, i.e., the line printer, two magnetic tape units, teletype, 250K word drum, and 16K word core memory were purchased from Xerox Data Systems. The laboratory also obtained the following from XDS: A wired 930 Arithmetic/Control unit backplane, 930 control Console, TMCC "W" Buffer, power supplies, cabinets, and cabling -- all to be used in the new computer, and two Potter tape decks for spares support. All of this equipment is in good to new condition and was purchased at less than 5% of its cost when new. Funds for these purchases became available when the cost of semiconductors and other circuit components for the additional computer's circuit modules was less than originally anticipated.

The 450 circuit modules required for the expansion have been fabricated and checked out. Fabrication included artwork layout, etching, timing, component mounting (over 70,000 individual pieces), and flow soldering. Each module has been satisfactorily exercised in a test fixture. We were fortunate to have a

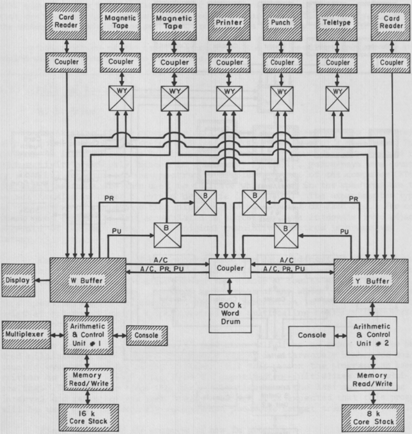

Fig. 5.1-1. Originally Proposed System. (Shaded units are the original system.)

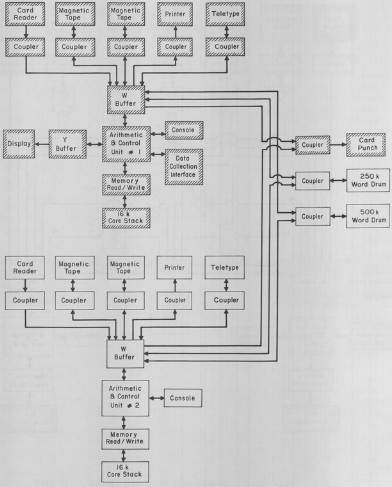

Fig. 5.1-2. Final System. (Shaded units are the original system.)

100% yield on the modules that reached the component mounting stage. That is, each module that had components mounted on it has gone satisfactorily through the subsequent fabrication and test steps and is now ready for use in the system.

Construction of the handler portion of the card reading hardware for the additional computer has been completed.

5.2 Lifetime Analysis Program

R. E. Marrs

An existing single parameter data collection program has been augmented with a routine which multiscales selected peaks or sections of a spectrum. The program is intended for use in situations where one or more detectors record the radioactivity previously induced in a target. Typically, gamma-rays are counted by a Ge(Li) detector and the spectrum is displayed on one of the computer CRT's. The digit switches are then used to indicate which lines in the spectrum are to be multiscaled in order to obtain half-life information. The experimenter types in the number of successive time bins and the size (time) of each bin. The computer then copies the data accumulated in successive time intervals into adjacent segments of the data array. The original cumulative spectrum is preserved intact.

Existing portions of the program plot the data and perform a least-squares Gaussian fit to the peak areas. Thus, in addition to a full spectrum, the program effectively gives the experimenter the number of counts accumulated in a peak per unit time vs time. As many as 50 peaks of any width, including the entire spectrum, may be multiscaled. The only restriction is that the size of the original spectrum plus the space required for multiscaling must fit into 8192 words of core.

The program is expected to be used when half-lives as short as a few hundred milliseconds are involved and when a target is alternately bombarded and counted over an extended period of time. For this reason the program has been written so that a "ready" pulse from the experiment re-initializes the multiscaling. The computer stops the data collection after the last multiscaling interval and waits for the next "ready" pulse. It is expected that this program will be used with the recently constructed pneumatic target transport system.[1]

Final testing of the program is now in progress.

---

1. See Sec. 3.1 of this report.

5.3 An On-Line Data Collection and Analysis Program for Single Parameter Experiments

M. Hasinoff and D. Patterson

The on-line data collection program[1] containing the light pen analysis package has been modified to provide space for more data storage and to allow for a more general background subtraction. The use of the light pen allows the experimenter to specify those channels which define a peak and its background region on a time sharing interrupt basis while the data is being collected. Since the ADC's are given the highest priorities in the interrupt list the background calculation being performed by the computer does not introduce any dead time into the data. The dead time is determined by the ADC conversion time plus the fixed time of 50 μsec required to process each event.

The present version of the program contains 6144 words of data storage and can accept data from up to 6 ADC's. All spectra are assumed to be of the same size, which can be up to 4096 channels. The digit switches are used to specify which spectrum is currently being displayed on the CRT scope and the peak whose parameters are to be entered or whose area is to be displayed. The data analysis includes the peak sum, the peak area corrected for background, and the peak cross section corrected for ADC dead time. Results of the calculation are displayed on the CRT scope along with the statistical errors of the above quantities.

A linear background has been assumed mainly for simplicity in programming since the analysis routine is written in SYMBOL, not FORTRAN. This is sufficient for most types of spectra but if a quadratic background is needed (e.g., to fit the Compton background in a Ge(Li) spectrum) it could easily be added as a FORTRAN subroutine to be called from the output subroutine. Six points are used to define a peak and its background region as indicated in Fig. 5.3-1.

The regions between points 1 and 2 between points 5 and 6 are averaged and then a straight line is drawn under the peak. The light pen is used to enter these points as start and end channels of the various regions; low background, high background, or peak region. The use of arbitrary background regions for each peak allows the experimenter to obtain his final results as soon as the run is completed except in the case where the peaks overlap. The agreement between

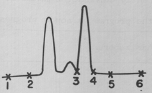

Fig. 5.3-1. Points used in defining the peak and background regions.

this on-line analysis and a post-run hand analysis is much better than 1% provided that a linear background is used in both analyses.

This program has been used to measure excitation functions and angular distribution for the reactions $^{40,48}Ca(^{16}O,^{16}O)^{40,48}Ca$ and $^{87}Rb(p,p_0)^{87}Rb$. In order to simplify the changing of the 6 light pen points for each peak, a light pen mode was added which increments all 6 points by a constant which is specified by a digit switch. As many as 6 detectors were used simultaneously and the reduction in data analysis time was found to be considerable.

---

1. Nuclear Physics Laboratory Annual Report, University of Washington (1970), p. 45.

5.4 A New Reaction Kinematics Program for the SDS 930 Computer

M. Hasinoff and H. Swanson

A new 2-body reaction kinematics program which contains the mass excesses of all the known nuclides in its mass library has been developed for the Laboratory's SDS 930 computer. Thus rather than specifying the masses for the reaction of interest (to 5 or 6 significant figures if keV accuracy is desired) one simply inputs the reaction itself, in conventional nuclear physics notation such as

U238(D,P)U239 or U238(D,P).

The program decodes the reaction title, determines the Z and A values for the four masses involved and computes the Q value for the reaction. This program is essentially the same as one written by S.L. Tabor and B.A. Watson[1] for the Stanford PDP 9 computer except for the subroutine which decodes the reaction title. This subroutine had to be rewritten since the binary storage of alphanumeric characters was not the same for the two machines.

As indicated above, the recoil particle need not be specified. Except for the forms A,D,N,P, and T, which are recognized as standard particles, each particle must be specified by its chemical symbol and its mass number.

In addition to calculating the energies of the reaction products (using the nonrelativistic formulas given in Nuclear Data Tables[2]) this program includes an optional energy-loss correction for the passage of the scattered particles through one or more foils before it enters the detector. This option is particularly useful when one is interested in stopping a heavy projectile in a foil placed in front of the detector and observing only the lighter reaction products which can pass through the foil. The foil is entered and decoded in the same fashion as the reaction elements. This energy-loss routine makes use of the effective charge formula for a particle moving through matter given by Booth and Grant:[3]

$$Z_{eff}^2 = Z^2 \gamma_{eff}^2$$

where $\gamma^2_{eff} = f(\epsilon Z^{-4/3})$,

$$f(x) = 1 - \exp(- 24.73x + 247.6x^2 - 131x^3),$$

ϵ = energy of moving ion in MeV/amu.

Input to the program is via the card reader or the teletype. The program output includes the lab angle, center-of-mass angle, energy, observed energy, kinematic broadening and solid angle ratio for both the outgoing particle and the recoil nucleus.

---

1. S.L. Tabor and B.A. Watson, Stanford Computer for Analysis of Nuclear Structure, Memo #29.
2. Nuclear Data Tables, Part 3, p. 161.
3. W. Booth and I.S. Grant, Nucl. Phys. *63*, 484 (1965).

5.5 An On-Line Program for Collecting Particle-Gamma Correlation Data Using Three ΔE-E Detector Arrays

D.M. Patterson

A three-parameter on-line particle identification program has been written to accomodate data collection from three ΔE-E detector arrays for particle-gamma correlation experiments. The program is written for the Laboratory's SDS 930 computer in the SDS assembly language SYMBOL. The main program features are: a) ΔE-ADC, E-ADC, and TAC-ADC inputs, b) ΔE routing to accommodate up to three ΔE-E detector array inputs, c) computer-calculated particle identification (ID) value using an exponential look-up table, d) three 512 channel energy spectra, selected by ID value and the occurrence of a TAC-ADC conversion, and a 256 channel TAC and ID spectra for each ΔE-E detector array, e) recording of selected raw event data on magnetic tape, f) on-line analysis of data using a light pen and live CRT data display, and g) two-parameter storage operation to aid in the selection of the optimum ID exponent, digital ID discriminator, and energy base level values.

The program was written to be as general as possible without sacrificing speed within the limitations imposed by the size of the computer memory storage. Data storage required about 8000 words of memory. This did not leave enough room for a program with all of the desired features, so the program was broken up into four logical sections and was operated as a CHAIN[1] program. In the CHAIN mode of operation, programs are recorded on magnetic tape in a self-loading form and can be selectively loaded into the computer under program control. The four chain programs in this case were a) data collection, b) end-of-run output, c) pre-run calibration and ID setup, and d) off-line data handling and data reduction routines. Since this program was written for the ^{3}He spin-flip experiments,[2] the more detailed discussion of its operation will be based on its use in collecting ^{3}He spin-flip data.

The program accepts data from three ADC's operated in a multiparameter mode. The maximum conversion sizes for the ADC's were: ΔE 512 channels; E 1024 channels; and TAC 256 channels. For an event to be considered valid, both a ΔE-ADC and E-ADC conversion had to be present. If a TAC-ADC conversion was also present, the event was considered gated (that is, a particle-gamma coincidence event). The digital ΔE and E values were added to obtain the total energy and a digital base level was subtracted from this value. Events with total energy less that the lowest digital base level were not stored in the data spectra, but they were scaled. Events with a processed energy value greater than 511 were stored in channel zero. The computer time required to process each event varied from about 123 μsec up to about 233 μsec depending upon the nature of the event. The processing time for each ungated event (no TAC) was about 182 μsec.

The ΔE-ADC could be externally routed so that data could be accepted from up to three independent ΔE-E detector arrays. When multiple arrays were used, the various analog signals were mixed externally before being sent to the ADC's. The program then used the ΔE route bits to determine which detector array the data was from and stored it accordingly.

The program calculated the function $(\Delta E + E)^x - E^x$ for each valid event with total energy (ΔE + E) above the lowest digital energy base level. A previously calculated table of N^x, where N is the channel number, was used to minimize the time required for the calculation. A 384 word lookup table was found sufficient for this purpose. The value of x (usually about 1.73) was selected so that the function was approximately constant for each particle type. The result of this calculation, the ID value, was used in conjunction with digital ID discriminator values to determine where the event was to be stored. There were three ID discriminator values for each ΔE-E array. Events with an ID value below the lowest ID discriminator were only scaled.

Three 512 channel arrays were available for data storage for each ΔE-E detector array. In the ^{3}He spin-flip experiment these were ungated ^{3}He, gated ^{3}He, and ungated ^{4}He energy (ΔE + E) spectra. The ^{3}He and ^{4}He arrays were allowed to have different digital energy base levels. In practice the maximum value of ΔE + E was somewhat greater than 1024; thus the energy base level had the same effect as a biased amplifier with a gain of 2. A 256 channel time (TAC) and ID spectra were also stored for each ΔE-E detector array. Since the information in these arrays was used strictly for monitoring purposes, it was stored on an available-time basis.

A program option allowed selected events to be stored on magnetic tape in raw form. This was facilitated by using two 128 word buffers for event data storage. After one buffer was filled, event data was stored in the other buffer while the first buffer was written on tape. The tape write program[3] was written such that it could operate at a lower priority than the ADC data acquisition.[4] Thus the tape write could proceed concurrently with data acquisition without introducing any noticeable dead time. In the ^{3}He spin-flip experiments, all gated events with ΔE + E above the lowest energy base level and ID above the lowest ID discriminator were stored on tape. All events with ID above the highest ID discriminator and ΔE + E above the lowest energy base level were also stored on tape. The event information written on tape was the ΔE-ADC conversion (including the route bits), E-ADC conversion, and TAC-ADC conversion.

Preliminary on-line data analysis was possible using a light pen and live CRT data display.[5] The light pen was used to specify peak start and end channels, peaks for special calculations, and selected data regions for expanded display. In this way spin-flip calculations were set up so that the experimenter could easily monitor the spin-flip probability and its statistical error as the data was being collected.

To facilitate the establishment of proper operating constants, a two-parameter $\Delta E + E$ vs ID data collection mode was also incorporated into the program. In this mode data were collected from each ΔE-E detector array in turn. The data were displayed in a 64×64 array. Thus one could visually check the flatness of the ID lines for the various particle types and adjust the ID exponent accordingly. After the ID exponent was established, the light pen was used to specify the ID discriminator values and energy base levels. Thus the experimenter could easily select the optimum operating constants by eye.

---

1. Nuclear Physics Laboratory Annual Report, University of Washington (1968), p. 165.
2. Sec. 10.4 of this report.
3. Nuclear Physics Laboratory Annual Report, University of Washington (1970), p. 45.
4. *Ibid.*, p. 41.
5. Nuclear Physics Laboratory Annual Report, University of Washington (1969), p. 142.

5.6 A Data Collection Program Using a Three-Counter Telescope for Redundant Particle Identification

J. G. Cramer

A data collection program has been written to perform particle identification using two transmission detectors (Δ_1 and Δ_2) and one detector in which the detected particle comes to rest (E). With a counter telescope of this type, three separate particle-identification criteria can be established by using for (Δ,E) in the identification algorithm the quantities $(\Delta_1,\Delta_2 + E)$, $(\Delta_1 + \Delta_2,E)$, and (Δ_2,E). The present program employs the first two of these three criteria to provide redundant particle identification, and also uses the ratio of the particle identification parameters thereby generated to require consistency between them. This permits stricter determination of particle type, as required in experiments where complete separation of particle groups is needed.

Basically, the program employs the structure of the Braithwaite Derandomizing Buffer program described in last year's Annual Report.[1] It forms three quantities, $E_T = \Delta_1 + \Delta_2 + E$, $ID_1 = (E_T)^{exp} - (\Delta_2 + E)^{exp}$, and $ID_2 = (E_T)^{exp} - (E)^{exp}$, where exp is an arbitrary exponent, approximately 1.73. The exponentiations are accomplished by means of a 2048 word lookup table which is generated before the data collection operation is begun. The program permits data collection in four two-parameter modes, ID_1 vs E_T, ID_2 vs E_T, ID_1/ID_2 vs E_T, and ID_1 vs

ID_2, so that gains, exponents, and digital windows can be set appropriately. The program also provides for data accumulation in a single parameter mode, with four 1024 channel spectra selected by four digital windows set on the average of ID_1 and ID_2.

It also permits printout of the one or two parameter arrays accumulated in the data collection phase of the program and collection and reanalysis of data on magnetic tape in an event-by-event format. Provisions are also made for correct identification of particles which do not penetrate the second transmission detector (Δ_2) and for expansion of the program to telescopes of four or more detectors for super-redundant identification.

---

1. Nuclear Physics Laboratory Annual Report, University of Washington (1970), p. 44.

5.7 A Modified DWBA Program to Calculate the Sub-Coulomb Nucleon Tunneling Cross Sections

K.G. Nair

A program called TRANSFER, which calculates stripping and pickup cross sections below the Coulomb barrier, is being written and tested. The theory is primarily based on the semi-quantal approximation for neutron tunneling proposed by Trautmann and Alder.[1] Briefly, this involves the simplification of the DWBA integral by approximating the external wave functions by Coulomb wave functions instead of the ordinary distorted radial wave functions obtained by solving the Schrodinger equation with optical potentials. In a more restricted version of the theory, when the incident energy is very much below the barrier, the radial wave functions can be replaced by their WKB approximations.

Preliminary testing of the program reproduces the essential features of sub-Coulomb transfer processes, e.g., strong backward peaking in the angular distributions and the increased probability of transfer for processes which involves better matching of the Coulomb parameter in the incident and exit channels. Modifications of this program under consideration are a) extension to proton transfer, b) generalization to multi-nucleon transfer, and c) inclusion of nuclear distortion as a correction factor for incident energies close to the Coulomb barrier.

---

1. D. Trautmann and K. Alder, Helv. Phys. Acta, *43*, 363 (1970).

5.8 Kinematics for Two- and Three-Body Final States

W.J. Braithwaite*

Although two-body reactions occur within a plane, it is convenient to specify all momentum vectors using three-dimensional rectangular coordinates. Such a formulation permits different orientations of the beam or the detected outgoing particles to be more easily described. Use of the rectangular coordinates to describe both position and momentum is convenient for finite-geometry kinematic calculations and results in greater speed of calculation since all transcendental functions (other than square root) are avoided.

The relativistic solution of the two-body kinematics problem is described below. Needed variables are: $E_0, \vec{P}_0$ (total laboratory energy and momentum), $\hat{P}_1$ (direction of detected particle), and A_1, A_2 (masses of the two outgoing particles: consistent with the relation

$$Q = \sqrt{E_0^2 - P_0^2} - A_1 - A_2).$$

Conservation of 4-momentum yields the following relations (in the laboratory):

$$\vec{P}_0 = \vec{P}_1 + \vec{P}_2 \Rightarrow P_0^2 + P_1^2 - 2(\vec{P}_0 \cdot \vec{P}_1) = P_2^2$$

$$E_0 = E_1 + E_2 \Rightarrow E_0^2 + E_1^2 - 2E_0E_1 = E_2.$$

Using the relation $E_k^2 = P_k^2 + A_k^2$ and equating on P_2^2 in the above, gives:

$$E_0^2 + A_1^2 - 2E_0\sqrt{P_1^2 + A_1^2} = P_0^2 - 2(\vec{P}_0 \cdot \vec{P}_1) + A_2^2$$

or $$E_0\sqrt{P_1^2 + A_1^2} = G + (\vec{P}_0 \cdot \hat{P}_1)P_1 \text{ with } G \equiv \tfrac{1}{2}(E_0^2 - P_0^2 + A_1^2 - A_2^2).$$

Squaring this last expression and collecting terms results in the following:

$$[E_0^2 - (\vec{P}_0 \cdot \hat{P}_1)^2]P_1^2 - 2(G\vec{P}_0 \cdot \hat{P}_1)P_1 + (E_0^2A_1^2 - G^2) = 0.$$

This quadratic equation for P_1 may give zero, one, or two solutions (branches). Momentum vectors ($\vec{P}_1$ and $\vec{P}_2$) are then constructed for each branch as follows: $\vec{P}_1 = P_1\hat{P}_1$ and $\vec{P}_2 = \vec{P}_0 - \vec{P}_1$.

A FORTRAN subroutine "TWOBOD" has been written to solve the two-body kinematics problem. Rectangular components of the 3-momenta are transferred through the arguments of the subroutine.

For a particular 3-body reaction, the kinematics can be calculated using the 2-body kinematics subroutine "TWOBOD" if the kinematic variables specified are direction for two of the three outgoing particles ($\hat{P}_1, \hat{P}_2$) and energy for one of them (E_1). Since

$$\vec{P}_1 = \hat{P}_1\sqrt{E_1^2 - A_1^2},$$

the momentum of one of the outgoing particles is known and thus the problem can be reduced to two-body form: $(\vec{P}_0 - \vec{P}_1) = \vec{P}_2 + \vec{P}_3$ and $(E_0 - E_1) = E_2 + E_3$. The left hand side of each expression is known, as well as the direction $\hat{P}_2$. Thus, "TWOBOD" may be used to calculate $\vec{P}_2$ and $\vec{P}_3$ using $(\vec{P}_0 - \vec{P}_1)$ and $(E_0 - E_1)$ as the "effective" total momentum and energy in the laboratory.

The FORTRAN program for relativistic 3-body reaction kinematics has been written which calls "TWOBOD" and provides a table of information.

This approach to 3-body kinematics has been found to be particularly useful in Monte Carlo calculations where finite geometry effects are calculated.

---

* Now at Department of Physics, Princeton University, Princeton, N.J.

5.9 Improved Calculation of Particle Identification from the ΔE and E Energy Signals of a Telescope

W.R. Wharton and H. Wieman

Old methods for calculating particle identification from the ΔE and E energy signals of a telescope have been found unsatisfactory for short-range particles such as ^{12}C, ^{15}N, and ^{16}O ions.[1] This paper examines ways to improve calculation of the particle identity and presents a new formula which allows fast accurate computation of the range-energy relationship for particles.

For long-range particles (p,d,t,^{3}He, and ^{4}He between 10-100 MeV) the range-energy relationship is well described by a power law:

$$R = a(E)^x \qquad (1)$$

where $x \approx 1.73$ independent of particle, and
a is a constant strongly dependent upon the type of particle.

From Eq. (1) , one can calculate a function to identify particles detected by a ΔE-E detector telescope.

$$PID = (\Delta E + E)^x - (E)^x = t/a \qquad (1a)$$

where PID = particle identity
t = thickness of ΔE detector.

Present programs in our laboratory calculate the PID using Eq. (1a) by referring to a table which stores the values $(I)^x$, where I is an integer. Events are separated into separate energy spectra according to the PID value irregardless of the energy. Therefore it is important that the PID be independent of energy for each particle.

The problem for short range particles is that Eq. (1) is invalid because the constant a and in turn PID become energy dependent. Figure 5.9-1 gives an example of the failure of Eq. (1) to reproduce the range energy relationship for

^{16}O. In order to correct the situation an equation has been formulated to more accurately fit the range-energy relationship for short-range particles:

$$R = a(E + b)^x \qquad (2)$$

where a,b, and x are constants.

For all ions so far tested, Eq. (2) gives excellent fits to the range-energy relationship. Table 5.9-1 presents the values of b and x for the best fits to the range-energy relationship[2] in aluminum upwards from about R = 2.7 mg/cm^2. R = 2.7 mg/cm^2 corresponds to the range of a 12 Si(Li) detector. The corresponding values for the energy over the range fitted are given in the last column. The goodness of the fit is represented by

$$\chi^2 = \frac{1}{N} \sum_{n=1}^{N} \frac{(R_{fit}(E_n) - R_{data}(E_n))^2}{(.05\ mg/cm^2)^2} .$$

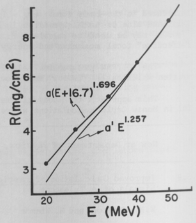

Fig. 5.9-1. The range-energy relationship[2] for ^{16}O is given by the dots. The fits using two different functional forms are labeled.

A $\chi^2 < 1$ indicates the fit should be acceptable for good particle identification. The table shows that all fits using Eq. (1),(with b = 0), were unacceptable whereas all fits using Eq. (2) were acceptable.

From Eq. (2), one can obtain a particle identification function:

$$PID = (\Delta E + E + b)^x - (E + b)^x = t/a. \qquad (2a)$$

The new constant b will cause no increase in memory requirements or in calculation time (Dead time). The constant b will simply be incorporated into a new table giving $(I + b)^x$. One can also use Eq. (2a) to nearly correct for any energy the particle may lose in deadlayers on the back side of the ΔE and the front side of the E detector, by simply adding the energy loss to the constant b.

Equation (2a) has not been tested during an on-line experiment, however by using Eq. (2a) significant improvements were made in the particle identification spectrum of ^{16}O, ^{15}N, and ^{12}C from an earlier experiment in which an 11μ ΔE detector was used. However, in order to make the PID energy independent for the separate particles, very large values of the constant b had to be used. The exponent x was chosen from Table 5.9-1, but the constant b was 36 MeV for ^{16}O, 29 MeV for ^{15}N, and 18 MeV for ^{12}C. No reason could be found why these values should be over twice as large as the values given for b in Table 5.9-1.

Often during an experiment it is necessary to look at two different particles simultaneously. This requires using different values for b and x in

Table 5.9-1. Results of fits to range-energy relationships for various particles.

ion	b (MeV)	x	χ^2	E_{min}-E_{max} (MeV)
^{1}H	.240	1.779	0.032	1 - 8
	--	1.692	61.9	1 - 8
^{4}He	1.358	1.795	0.034	2.8 - 20
	--	1.596	66.5	2.8 - 20
^{7}Li	3.64	1.807	0.058	5.6 - 35
	--	1.521	84.2	5.6 - 35
^{9}Be	5.83	1.758	0.035	6.3 - 36
	--	1.349	44.9	6.3 - 36
^{11}B	9.615	1.781	0.064	9.9 - 55
	--	1.352	66.3	9.9 - 55
^{12}C	11.916	1.764	0.022	15 - 60
	--	1.326	31.2	15 - 60
^{14}N	14.476	1.735	0.176	17.5 - 70
	--	1.290	26.3	17.5 - 70
^{16}O	16.70	1.696	0.120	20 - 80
	--	1.257	22.7	20 - 80
^{20}Ne	17.584	1.523	0.068	20 - 80
	--	1.11	10.9	20 - 80

Eq. (2a) to make the PID for each particle independent of energy. In Table 5.9-1 it is shown that the constant b increases and the exponent x decreases as the ion mass and charge increase. To simulate this simultaneous change in b and x we have added a term $C\Delta E$ to Eq. (2a). An iterative procedure has been applied to the spectrum of ^{16}O, ^{15}N, and ^{12}C, namely:

$$PID = (\Delta E + E + b)^x - (E + b)^x,$$

$$PID = PID + C_{PID}(\Delta E - \Delta E_0),$$

where C_{PID} is a constant depending on PID or the type of particle, and

ΔE_0 is a constant.

In this way we were able to make the PID for ^{16}O, ^{15}N, and ^{12}C simultaneously independent of energy. A program is being written where C will be stored in a 256 word array and the experimenter will be able to specify different values of C for such groups of particles, i.e., one value of C may be used for optimum separation of ^{12}C from ^{14}C for example, and another value of C used for optimum separation of ^{16}O and ^{18}O.

---

1. Section 4.7 of this report.
2. L.C. Northcliffe and R.F. Schilling, Nuclear Data Tables *7*, 233 (1970).

---

6. REACTIONS AND SCATTERING WITH LIGHT NUCLEI

6.1 Nucleon-Nucleon Final State Interactions in the Reactions $^3He(d,tp)p$ and $^3He(d,^3He\ n)n$

W.J. Braithwaite, D.R. Brown, J.R. Calarco, J.M. Cameron, R. Heffner, W. Jacobs, and D.W. Storm

A number of measurements have been made recently to determine the low energy nucleon-nucleon scattering parameters (the scattering length and effective range) using the interaction of the two nucleons of interest in three-body final-state reactions. The results obtained by Boyd *et al.*[1] by Bruckmann *et al.*[2] and by Niiler *et al.*[3] in their studies of p-p and p-n final state interactions in the reaction $p + d \rightarrow p + p + n$ have shown that these processes are describable in terms of parameters obtained from the low energy scattering of the two free nucleons in question.

A comparison of p-p,p-n, and n-n scattering parameters would yield information on the charge independence of the nucleon-nucleon force. Since direct n-n scattering experiments are not feasible at present, the only means of determining the n-n scattering length a_{nn} appears to be through the analysis of final state interactions of two neutrons.

The most accurate measurement of a_{nn} to date is that determined from the $\pi^- + d \rightarrow \gamma + n + n$ reaction.[4] In this case there is little interaction between the photon and the outgoing neutrons. These results have yielded a value of $a_{nn} = -18.42 \pm 1.53$ fm.

Van Oers and Slaus[5] have discussed the determination of a_{nn} from final state interactions when there are three strongly interacting particles present by using a comparison procedure. They propose that measurements be made of the p-p, p-n, and n-n final state interactions using mirror reactions and identical kinematical situations. In this case agreement of a_{pp} and a_{pn} with the appropriate free parameters would imply that the value of a_{nn} so obtained would also correspond to the free n-n scattering length.

The reaction $n + d \rightarrow p + n + n$ has been studied by Zeitnitz, Maschuw, and Suhr.[6] Since the p+d studies have yielded correct values for a_{pp} and a_{pn}, then this reaction should give a good value for a_{nn}. The n-n scattering length was determined to be $-16.4^{+2.6}_{-2.9}$ F.

In order to test charge independence to better than 1% in $\Delta V/V$ where V represents the two-nucleon potential, one needs to know the value of a_{nn} to better than about 1 F.[5] The previous measurements of a_{nn} suffer from poor statistics due to the use of low intensity beams.

We have observed the nucleon-nucleon final state interactions in the reactions

$$d + {}^3He \rightarrow t + p + p \qquad Q = -1.460$$

$$d + {}^3He \rightarrow {}^3He + p + n \qquad Q = -2.226$$

$$d + t \rightarrow t + n + p \qquad Q = -2.226$$

$$d + t \rightarrow {}^3He + n + n \qquad Q = -2.989.$$

These reactions have the advantage that they involve readily available beams of high intensity. They are complicated by the possible interactions of the outgoing nucleus with the outgoing nucleons. There may be additional complications due to various different and interfering reaction mechanisms in the primary $d + {}^3He$ and $d + t$ interactions. However it is hoped that a set of kinematic conditions can be found to minimize these effects so that the p-p and p-n final state interactions can be fit using known values of a_{pp} and a_{pn}. Then a reliable value for a_{nn} could be obtained with good statistics.

The reaction $d + {}^3He \rightarrow t + p + p$ was studied with deuterons of 20.45 MeV from the three stage Van de Graaff. The ^3He was enclosed in a cylindrical havar gas cell about 2½" high by 1½" diameter at a pressure of 1 atm. Tritons and protons were detected by two two-counter telescopes. Particle identification was done on both arms using an on-line look-up table technique. Coincident events were displayed three dimensionally -- number of events versus E_t versus E_p. True events are distributed along a kinematically allowed locus. When E_t reaches a maximum value the two protons have minimum relative momentum and interact producing an enhancement of events in this region. Events in this region were projected onto the E_p axis; such a projection is shown in Fig. 6.1-1. At E_p such that the relative momentum is zero, a minimum occurs due to Coulomb repulsion. As E_p deviates from this value to either side, the Coulomb force gives way to the attractive nuclear p-p force and strong enhancements occur. As E_p deviates further, the interaction dies away and the number of events is given by phase phase space arguments.

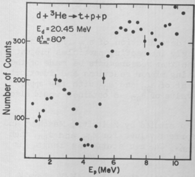

Fig. 6.1-1. Projection of $d+{}^3He \rightarrow t+p+p$ onto E_p axis. Minimum occurs where k_{pp}, the relative momentum between the two protons, goes to zero, due to Coulomb repulsion. As E_p deviates to either side enhancements are observed.

Similar results for $d+{}^3He \rightarrow {}^3He+p+n$ are shown in Fig. 6.1-2. In this case a ^3He and p were detected in coincidence at angles chosen to observe a p-n final state interaction. The data in the region of the enhancement were projected onto the E_p axis. The maximum enhancement

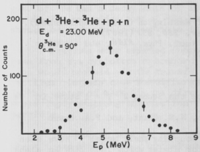

Fig. 6.1-2. Projection of d+^{3}He→^{3}He+p+n onto E_p axis showing p-n final state interaction enhancement.

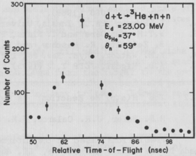

Fig. 6.1-3. Projection of d+t→^{3}He+n+n onto neutron time-of-flight axis. The peak occurs at the correct kinematic conditions for k_{nn} = 0 and corresponds to an n-n interaction.

occurs for E_p such that E_{pn} = 0; there is no Coulomb interaction in this case.

The reaction d + t → ^{3}He + n + n has been studied at E_d = 23 MeV using targets of tritiated titanium on platinum backings; the targets were supplied by ORNL. In this reaction a ^{3}He and a neutron are detected in coincidence. The neutron energy is determined by time-of-flight relative to the ^{3}He. Events were displayed versus $E_{^3He}$ and neutron time-of-flight. The portion of the kinematic locus in the region of the n-n final state enhancement was projected onto the time-of-flight axis. Fig. 6.1-3 shows the enhancement observed.

Attempts are being made to fit all three final state interactions using the theory of Watson[7] and Migdal[8] which treats the interaction of the two outgoing nucleons as being independent of the details of the primary reaction process. Fits to date are unsatisfactory, but it is not yet clear whether this is due to computational errors or some fundamental interference effect on the interaction process.

Some experimental difficulties have been encountered in studying the d + t → ^{3}He + n + n reaction. These include primarily the problem of defining a reaction plane between the target, the ^{3}He counter inside the chamber, and the neutron counter placed about 80" outside the chamber. A new chamber has been designed and built to minimize these problems and is discussed in Sec. 3.2 of this report.

1. D.P. Boyd, P.F. Donovan, and J.F. Mollenauer, Phys. Rev. *188*, 1544 (1969).
2. H. Brückmann, W. Kluge, H. Matthäy, L. Schänzler, and K. Wick, Phys. Letters *30B*, 460 (1969).
3. A. Niiler, C. Joseph, V. Valkovic, W. von Witsch, and G.C. Phillips, Phys.

Rev. *182*, 1083 (1969).
4. D. Nygren, Ph.D. Thesis, University of Washington (1968)(unpublished).
5. W.T.H. Van Oers and I. Slaus, Phys. Rev. *160*, 853 (1967).
6. B. Zeitnitz, R. Maschuw, and P. Suhr, Nucl. Phys. *A149*, 449 (1970).
7. K.M. Watson, Phys. Rev. *88*, 1163 (1952).
8. A.B. Migdal, JETP *1*, 2 (1955).

6.2 The $^3H(\alpha,p)^6He$ Reaction: A Search for the Second 2^+ T = 1 State in ^6He

M.P. Baker, J.R. Calarco, J.M. Cameron, N.S. Chant, and P.A. Russo

Predictions based on the intermediate coupling shell model[1-3] have been made in the mass 6 nuclei ^6He, ^6Li, and ^6Be for states which look like an alpha particle core plus two 1 p shell nucleons. These results give T = 1 states, in order $0^+,2^+,2^+,1^+,0^+$. The first two (the ground state and 1.80 MeV state in ^6He) are well known, but there is no consistent evidence for experimental observation of any of the three higher excited states using a variety of reactions. A preliminary search via two-nucleon transfer has been reported recently[5] for all three nuclei, as well as a detailed investigation of ^6He.[6]

Calculations based on the expected nuclear configurations indicate that those states above the first 2^+ can be excited by one nucleon pickup or two-nucleon stripping only insofar as these states mix with the ground or first excited state.[5] Of the two reactions, the two-nucleon stripping process is more sensitive to small admixtures.

These reactions are selective for the ground and first excited states because to lowest order in L-S coupling these have the 2 p shell nucleons in S = 0 space symmetric configurations whereas the three higher states are S = 1, L = 1.[1-3] In two-nucleon stripping, the two nucleons are most likely transferred in such space symmetric configurations. In one nucleon pickup from ^7Li, the residual nucleus must look like ^7Li less 1 p shell nucleon. The 3 p shell nucleons in ^7Li, however, are essentially in a pure configuration which is spatially symmetric in the exchange of any pair of nucleons. Thus we see that both reactions excite final states only through their space symmetric components.

These reactions then provide a sensitive experimental probe of the mixing coefficients in the wave functions and, therefore, of the residual nuclear interaction potential. Using different exchange mixtures in the residual interaction, the various theoretical works predict admixtures of space symmetric configurations into the second 2^+ T = 1 state in mass 6 from about 3%[1,2] to 30%.[3]

Consequently, investigations continue in search of high-lying states in mass 6 nuclei. The reason for the particular choice of ^6He is twofold. First, all three nuclei are unbound to three body breakup below the first 2^+ T = 1 state. However, if the final states are restricted to T = 1 nuclei (^6He and ^6Be) then the phase space background is reduced by elimination of the T = 0 three body breakup. Second, of the two T = 1 nuclei, ^6He and ^6Be, the corresponding states are expected to be somewhat more narrow in ^6He because the energy available for breakup is less; e.g., the g.s. of ^6He is stable (except to β decay) whereas the g.s. of ^{6}Be has a decay width of 100 keV, and while the first excited state of ^{6}He is 100 keV wide, that of ^{6}Be has a width of 1 MeV. Thus any higher states should be more easily observable in ^{6}He than in either ^{6}Li or ^{6}Be.

Previous work reported from this Laboratory[5] utilized the 42 MeV alpha beam from the cyclotron to bombard tritiated targets in the hope that the reaction would proceed via the transfer of two nucleons from the target to the projectile. In this case the differential cross-section should be backward peaked in the center of mass (in the direction of the incident triton). Forward peaking would imply a strong contribution from triton stripping from the incident alpha particle.

The earlier work did not include angular distribution measurements to check these hypotheses. Furthermore, there was high background due to (α,p) reactions on the backing material Ti and Pt. In separate runs, it was concluded that the bulk of this background (about 75-90%) was due to the lighter contaminant, Ti. This was consistent with the general observation that alpha induced

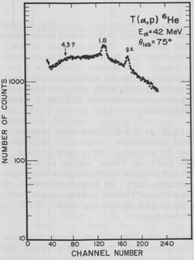

Fig. 6.2-1. Proton spectrum from (α,p) on tritiated titanium (∿0.5 mg/cm^{2}) on a platinum (∿2 mg/cm^{2}) backing. Since the ground state is particle stable all those protons under the ground state and at higher energies are from Ti or Pt.

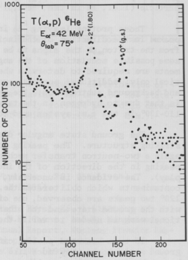

Fig. 6.2-2. Spectrum at same energy and angle as in Fig. 6.2-1,but with tritiated erbium (∿1 mg/cm^{2}) on a 2 mg/cm^{2} Pt backing. Ratio of peak to background for ground state is improved by a factor of 20 over Fig. 6.2-1.

reactions exhibit a 1/A character where A is the mass number.

New targets were obtained from ORNL, consisting of about 1 mg/cm^2 of erbium on a platinum backing (about 2 mg/cm^2). The erbium was then tritiated to a concentration of about one tritium atom per erbium atom. These targets were obtained in the hope that the erbium would provide lower background than titanium. The tritiated titanium target was about 0.5 mg/cm^2 titanium (tritiated to a 1:1 concentration) on a 2 mg/cm^2 platinum backing. The results of a comparison run are shown in Figs. 6.2-1 and 6.2-2. It is apparent that the erbium target gives much less background for a given amount of tritium. Since the ground state of ^{6}He is particle stable the background under the ground state is therefore used for the comparison. In this region the background is reduced by a factor of about twenty.

The investigation of the angular distribution of protons from the ^{3}He(α,p) ^{6}He reaction has proceeded with the tritiated erbium target. E_α = 42 MeV gives 18 MeV in the center of mass. The results are shown in Figs. 6.2-3 and 6.2-4 for the ground and first excited states of ^{6}He respectively. The cross section has been plotted versus $\theta_{c.m.}$ in the system in which the triton is the incident particle (i.e., as in the ^{4}He(t,p)^{6}He reaction).

Those protons leaving ^{6}He in the first excited state are strongly forward peaked in the direction of the incident triton indicating a two-neutron transfer from the triton to the alpha to be the dominant process. There appears to be some possible modulation of the angular distribution but more detailed measurements are required to determine whether it is real. The errors shown are statistical only; additional possible systematic errors are due to contaminant peaks and background subtraction. The main contaminant problem with the new backings is that due to hydrogen in the target. This makes measurements difficult around 110-130° in the c.m. system used to display the data.

The ground state angular distribution in Fig. 6.2-3 shows some rather striking structure. The peaking in the forward hemisphere (near 60°) indicates again a two-neutron transfer mechanism. There is evidence for a very strong peaking in the direction of the incident alpha particle (back angles in our display). The evidence is uncertain, however, due to alpha scattering on hydrogen contaminants which obliterates the spectrum around 120°. At angles backward of 120° two peaks are observed, one of which seems to be kinematically consistent with the ground state and the other with the hydrogen scattering peak. Additional work is needed to verify the backward peaking.

If this backward peaking can be demonstrated, it would indicate that the ground state looks very much like a ^{3}H - ^{3}H cluster while the first excited state has a character much more like an alpha plus two nucleons. Implications for the second 2^+ T = 1 state, however, are based on data on the first 2^+ state which suggests that investigation of the reaction via the two-nucleon transfer mechanism is the most logical approach.

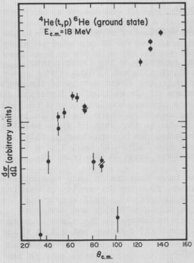

Fig. 6.2-3. Ground state angular distribution shows a peak at around 60°, but data at back center of mass angles indicate a strong backward peaking (direction of incident alpha) although these points are questionable due to contaminants.

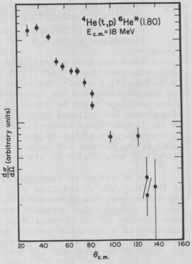

Fig. 6.2-4. Angular distribution of protons leaving ^{6}He in 1.80 MeV state. It is clearly forward peaked in direction of incident triton (0° c.m.).

1. A.N. Boyarkina, Bull. Acad. Sci. USSR Phys. Ser. *28*, 255 (1964).
2. S. Cohen and D. Kurath, Nucl. Phys. *73*, 1 (1965).
3. F.C. Barker, Nucl. Phys. *83*, 418 (1966).
4. T. Lauritsen and F. Ajzenberg-Selove, Nucl. Phys. *78*, 1 (1966).
5. M.P. Baker, J.R. Calarco, J.M. Cameron, N.S. Chant, and N. Mangelson, Bull. Am. Phys. Soc. *15*, 519 (1970); Annual Report, Nuclear Physics Laboratory, University of Washington (1970) p. 68.
6. R.H. Stokes and P.G. Young, Phys. Rev. *C3*, 984 (1971).

6.3 Isospin Impurity of the 5.36 MeV State in ^{6}Li

M. Baker, J.R. Calarco, J.G. Cramer, D. Oberg, W. Wharton, and D.H. Wilkinson

There has been a great deal of interest recently in the isospin non-conserving reactions $^{12}C(d,\alpha)^{10}B^*$ (1.74 MeV, 0^+; T = 1) and $^{16}O(d,\alpha)^{14}N^*$ (2.31 MeV, 0^+; T = 1).[1] Noble has suggested[2] that the direct nature of the angular distributions and the compound-nuclear nature of the excitation functions for these reactions might be explained by a two-step process consisting of a $(d,^{6}Li)$ pickup reaction followed by a $(^{6}Li,\alpha)$ stripping reaction. Here the ^{6}Li is in one of two isospin-mixed excited 2^+ states. The claim is that both of these seemingly contradictory pieces of experimental information can be explained by this model if one assumes ~5% isospin mixing between the $^{6}Li^*$ (4.57 MeV, 2^+;T = 0) and $^{6}Li^*$ (5.36 MeV, 2^+;T = 1) states at an intermediate stage in the reaction.

In an effort to test this hypothesis we have made preliminary measurements of the $^{9}Be(p,\alpha d)^{4}He$ reaction using 22 MeV protons from the University of Washington three-stage Van de Graaff accelerator. The target was a self-supporting ^{9}Be foil 215 $\mu g/cm^2$ thick obtained from ORNL. The alpha particles and deuterons were detected in coincidence using ΔE-E detector telescopes. The alpha counter consisted of a 35μ thick totally depleted silicon (ΔE) detector and a 3 mm thick lithium-drifted silicon (E) detector. The deuteron counter was composed of a 25μ thick ΔE detector and a 3 mm thick E detector.

Fast logic signals were derived from each ΔE detector and used to start and (with the appropriate delay) stop a time-to-amplitude converter. Events for which the four energy signals and the relative time signal satisfied a slow coincidence requirement were sent to the SDS 930 on-line computer for processing. Each of the five analog signals was converted to a channel number in a 2048 channel digital array. Each event was stored in a buffer and subsequently written on magnetic tape. Particle identification was performed for both telescopes by the computer using the $(E + \Delta E)^b - (E)^b$ method. Digital windows were set around the particles of interest in each identification spectrum and around the time peak in the relative time spectrum. Alpha-deuteron coincidences were then displayed on a CRT oscilloscope as a 64 × 64 channel E_d versus E_α array.

The basic objective of the experiment was to determine the degree of isospin mixing between the two 2^+ states in ^{6}Li by producing the T = 1 member of the pair and measuring the fraction of that state which decays into the isospin-forbidden, T = 0 (α + d) channel. The allowed particle decay of the T = 1 state is to the three-particle final state α + p + n. The $^{9}Be(p,\alpha)^{6}Li$ reaction was chosen as the primary reaction because previous measurements[3] have shown that this reaction populates the 5.36 MeV (T = 1) state quite strongly and the 4.57 MeV (T = 0) state only weakly. In order to insure the observation of decays via the T = 0 channel, deuterons must be detected in coincidence with the primary alpha particles. Alpha decay of the intermediate state can occur through either the T = 0 or T = 1 channel.

The earlier measurements of the $^{9}Be(p,\alpha)^{6}Li^*$ (5.36 MeV) reaction[3] indicate that the angular distribution is strongly forward-peaked and that the excitation function is reasonably flat. Thus the alpha counter was placed at a laboratory angle of 20° in order to enhance the counting rate and 22 MeV incident protons were used to minimize the target thickness effects on alpha energy resolution. If it is assumed that the decay of the ^{6}Li* (5.36 MeV) state is isotropic in the coordinate system in which the ^{6}Li* (5.36 MeV) is at rest, then the highest alpha-deuteron coincidence counting rate will be obtained if the deuteron detector is placed in approximately the direction of the recoiling ^{6}Li* (5.36 MeV) nucleus. With the alpha counter at 20° the deuteron counter was located at a laboratory angle of -135.8°.

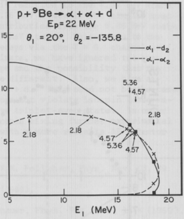

Fig. 6.3-1. Kinematic loci for the ^{9}Be(p,α,d)^{4}He and ^{5}Be(p,α,α_2)^{2}He reactions for α_1 = 20°, α_2 = -135.8°, and E_p = 22 MeV.

It was necessary to determine particle identification in the back-angle counter due to the anticipated alpha decays of the intermediate states. The expected kinematic loci for α_1 - d_2 and α_1 - α_2 coincidences for counter angles of 20° - (-135.8°) are shown in Fig. 6.3-1. The points at which enhancements above the three-body phase space background due to sequential decays of ^{6}Li* are anticipated are indicated with the appropriate excitation energies on both kinematic loci. At this pair of angles it is quite clear that particle identification in the back counter is desirable in order that the interpretation of the experimental results in what would be the regions of intersection of the two kinematic loci can be unambiguous. It is difficult in general to separate the α_1 - d_2 and α_1 - α_2 kinematic loci since both must be perpendicular to the E_{α_1} axis in a diagram like Fig. 6.3-1 at the same E_{α_1}.

The experimental results for α-d coincidences at θ_α = 20° and θ_d = -135.8° are illustrated in Fig. 6.3-2. The part of the kinematic locus for which data was collected is shown in the lower part of the diagram along with the expected positions of enhancements due to possible deuteron decays of ^{6}Li*. The events from the kinematic locus projected onto the alpha and deuteron energy axes are shown at the top and right of the diagram respectively. The number of deuterons observed in coincidence corresponding to the decay of the ^{6}Li* (2.18 MeV,$1 3^+$;T = 0) is ∿4% higher than that expected from a measurement of the singles cross section obtained with the same geometry. This number has been derived with the assumption that the state decays isotropically in the system where the ^{6}Li* is at rest and a phase-space contribution has been subtracted.

In Fig. 6.3-2 the cross section shows a substantial decline for alpha energies less than 16.5 MeV. For the energy region below the 2.18 MeV state in the projection onto the alpha energy axis in Fig. 6.3-2, phase-space calcula-

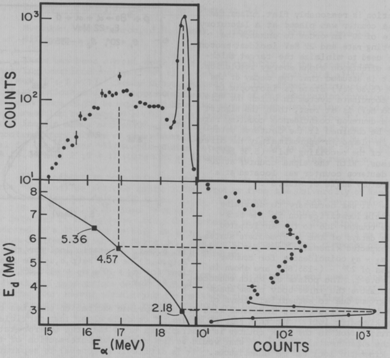

Fig. 6.3-2. Projections from the 3-body kinematic locus onto the alpha and deuteron energy axes for the coincidence data obtained at $\theta_\alpha = 20° - \theta_d = 135.8°$.

tions[4] indicate the continuum to be essentially flat. The drop-off with decreasing alpha energy (increasing deuteron energy) was probably due to a gradual decrease in efficiency in the ΔE detector in the deuteron telescope. Despite the fact that both detector telescopes were cooled, the ΔE detector in the deuteron telescope had a high noise level. As the deuteron energy increases the effect of the noise in the ΔE detector becomes more important since the energy deposited decreases.

With the uncertainty about the shape of the phase-space continuum it is difficult to assess directly the number of deuteron decays from the $^6Li^*$ (5.36 MeV) state. However, one can gain some insight by considering the relative strengths of the 4.57 and 5.36 MeV states in the singles and in the coincidence spectra. The cross section for the $^{9}Be(p,\alpha)^{6}Li^*$ reaction to the 4.57 MeV state is at most .06 times as large as that to the 5.36 MeV state in the singles spectrum. But in the coincidence spectrum, the contribution from the 5.36 MeV state appears to be at most equal to that of the 4.57 MeV state. This leads to the preliminary estimate that the 5.36 MeV state decays via the T = 0 channel at most about 7% of the time. In making this estimate, we have ignored the question of the efficiency of the deuteron telescope and the possibility that the substate populations of the two states might be different. Also, we have assumed that the 4.57 MeV state always decays to α + d. This need not be the case since α + p + n is energetically allowed and does not violate isospin conservation if the proton and neutron are in a relative triplet-even state. In order to obtain a more precise measurement of the isospin mixing further experimental study is planned at other pairs of angles and with a more reliable ΔE detector for the deuteron telescope.

---

1. J. Jänecke, T.F. Yang, W.S. Gray, and R.M. Polichar, Phys. Rev. *C3*, 79 (1971).
2. J.V. Noble, Phys. Rev. Letters *22*, 473 (1969).
3. Section 6.5 of this report.
4. D.P. Boyd, P.F. Donovan, and J.F. Mollenauer, Phys. Rev. *188*, 1544 (1969).

6.4 Inelastic Proton Scattering on ^{6}Li and ^{14}N to Study the Spin-Isospin Dependent Interaction

M. Baker, W.J. Braithwaite, J.G. Cramer, and E. Preikschat

The microscopic description of inelastic scattering requires a knowledge of the effective interaction before useful spectroscopic information can be extracted. The $^{6}Li(p,p')$ reaction leading to the 3.56 MeV state with $J^{\pi} = 0^{+}$ and T = 1 has been used[1] to study the spin-isospin dependent interaction. Since the ground state of ^{6}Li is 1^{+} and T = 0, the reaction involves a change in both spin and isospin. A recent study of this reaction at proton energies of 24 MeV included an analysis which assumed that it was dominated by the central spin-isospin exchange interaction.[1]

Recent calculations,[2] however, indicate that a tensor force may also be important in this reaction. By including a tensor component in the spin-isospin exchange interaction, satisfactory fits were obtained for forward angles.

More definitive experiments of this type could be done with polarized protons, since the spin exchange process is expected to produce sizable polarization asymmetries.[3] The availability of a polarized ion source has therefore provided motivation to measure the asymmetry of the reaction.

^{14}N is similar to ^{6}Li insofar as both are odd-odd nuclei with $J^{\pi} = 1^{+}$, T = 0 ground states. They also have low lying excited states with 0^{+} and T = 1, and could also be used in such a study.

In this preliminary experiment both ^{6}Li and ^{14}N were bombarded with unpolarized protons and the inelastic excitation of the first T = 1 state was

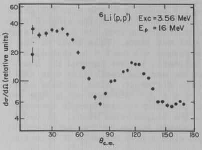

Fig. 6.4-1. Angular distribution of the 3.56 MeV state for the reaction ^{6}Li (p,p') with $J^\pi = 0^+$ and T = 1.

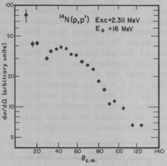

Fig. 6.4-2. Angular distribution of the 2311 MeV state of the reaction ^{14}N(p,p') with $J^\pi = 0^+$ and T = 1.

studied. Figure 6.4-1 shows the unnormalized angular distribution for ^{6}Li (p,p') 3.562 MeV. Figure 6.4-2 shows the angular distribution for the corresponding T = 1 level in ^{14}N(p,p') at 2.311 MeV and an incident energy of 16 MeV. The analysis in the latter case is made difficult because the peak of interest almost overlaps with the peak produced by elastic protons exciting the first excited state of ^{28}Si by inelastically scattering from the material of the detector.

Figure 6.4-3 shows a crude excitation function for ^{14}N(p,p) and ^{14}N (p,p') 2.311 MeV at lab angles of 50° and 90° and over an energy range from 15.0 to 17.5 MeV. Even though the elastic cross section excitation function varies smoothly, the inelastic excitation function shows large fluctuations. This indicates that a substantial contribution to the cross section is due to compound nuclear effects.

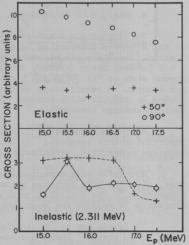

Fig. 6.4-3. Excitation function for the ground state and the 2.311 MeV T = 1 state of ^{14}N at lab angles of 50° and 90°.

We conclude that a similar polarized beam experiment on ^{14}N would be difficult to interpret because of compound nucleus contributions in this range of bombarding energies available with our polarized source.

---

1. S.M. Austin and G.M. Crawley, Phys. Letters *27B*, 570 (1968).
2. G.M. Crawley, S.M. Austin, W. Benenson, and V.A. Madsen, to be published.
3. V.A. Madsen (private communication).

6.5 A Study of the $^{9}Be(p,\alpha)$ Reaction

M.P. Baker, J.R. Calarco, D. Oberg, and W. Wharton

Previous studies[1-3] of the $^{9}Be(p,\alpha)$ reaction have been concentrated on those alpha groups populating the ground and first excited (2.18 MeV) states of ^{6}Li. We have initiated a study of this reaction for the purpose of exciting the known T = 1 states in ^{6}Li at 3.56 MeV (0^+) and 5.36 MeV (2^+) and any higher lying T = 1 states which might exist.

A number of attempts[4,5] have been made recently to search for higher lying T = 1 states in the mass 6 nuclei ^{6}He, ^{6}Li, and ^{6}Be. No consistent evidence has been found, however, for their existence. Although some experimenters have claimed to have found them[6,7] others have not seen them using the same reactions.[8]

Theoretical investigations of the nuclear configurations[9] of those states have indicated that they are excited in one nucleon pickup and two nucleon stripping reactions only insofar as they mix with the first two T = 1 states.[4] If this mixing is small and the states are essentially as predicted by L-S coupling, then the excitation will also be weak.

For this reason the $^{9}Be(p,\alpha)^{6}Li$ reaction appeared to be a likely tool to use in this search. The previous measurements[3] of the angular distributions for the ground and first excited states indicated that several reaction mechanisms were contributing comparably including ^{3}H pickup by the proton, alpha knockout, compound nucleus formation, ^{5}He stripping from ^{9}Be, and ^{6}Li knockout. Whereas the higher lying T = 1 states are excited by one and two nucleon transfer only if they mix with the lower ones, they might easily be populated through some of the mechanisms used to account for $^{9}Be(p,\alpha)$.

Furthermore, if the compound nuclear mechanism contributes significantly, then one should observe resonances in the excitation function for the T = 1 states whenever the center of mass energy corresponds to T = 1 resonances in the ^{10}B system. If such resonances can be excited then one might search for their decay to alpha plus higher lying T = 1 states in ^{6}Li.

Excitation functions were obtained for the ground state (1^+,T = 0), 2.18 MeV (3^+,T = 0), 3.56 MeV (0^+,T = 1), and 5.36 MeV (2^+,T = 1) states for incident protons of 12.0 to 22.4 MeV using two and three stage operation of the Van de Graaff. A typical spectrum is shown in Fig. 6.5-1 for 17.25 MeV bombarding energy. The targets were 215 $\mu gm/cm^2$ self supporting ^9Be foils obtained from ORNL. Alphas were detected using a two counter telescope employing a 35 μm silicon surface barrier detector for the ΔE counter and a laboratory built lithium drifted silicon detector for the E. Particle identification was performed on line in the SDS 930 computer using a lookup table technique.

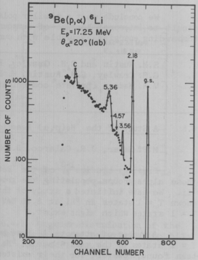

Fig. 6.5-1. Alpha spectrum from $^9Be(p,\alpha)^6Li$ for E_p = 17.25 MeV and θ_α = 20° in the laboratory. The C refers to a peak from $^{12}C(p,\alpha)$.

The excitation functions are shown in Figs. 6.5-2 - 6.5-5. All were obtained at a laboratory angle of 20°. Angular distributions were taken at E_p = 13.6 MeV, 14.5 MeV, 16.0 MeV, and 22.0 MeV. The excitation functions for the ground and first excited states decrease rather smoothly with increasing incident energy and show some broad structure. The broad structure might possibly be explained by a shift in the angular distribution peaks with increasing incident energy. However the present angular distribution data is not complete enough to test this. The 3.56 MeV excitation function shows a strong resonance at E_p= 13.25 MeV. This corresponds to resonance seen in $^7Li(^3He,\gamma_0)$[10] and perhaps also in $^9Be(p,\gamma)$.[11] Both reactions excite T = 1 negative parity resonances in ^{10}B which then can decay to the ground state by dipole emission. The 5.36 MeV excitation function does not show evidence for this resonance. This could be due to the fact that this state cannot be seen below E_p = 13.0 MeV because of the requirement that the alphas pass through the ΔE counter. More likely it is due to the fact that the excitation functions were studied at 20° in the laboratory. A typical angular distribution is shown in Fig. 6.5-6; this was taken at 22.0 MeV but the same general features were observed at other energies. At this angle the 5.36 MeV cross section is near a maximum while the 3.56 MeV cross section is near a minimum. This indicates that the 5.36 MeV state is probably being populated by direct mechanism, while the 3.56 MeV state is sensitive to the compound nucleus formation.

It would be interesting to study the resonance at 13.25 MeV with finer resolution for a range of angles in order to test this hypothesis. There is also weak indication of a possible resonance at 17.75 MeV which warrants further investigation.

To date we have seen no evidence in any of the spectra indicating the

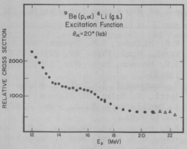

Fig. 6.5-2. The ground state excitation function. The triangles only refer to a different data run. The broad structure at E_p = 16.00 MeV may be accounted for by a shift in the structure in the angular distribution accompanying the increase in kR.

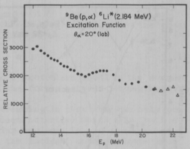

Fig. 6.5-3. The excitation function for the 2.18 MeV state. The broad resonance around 17.0 MeV is not understood. It is too narrow to be accounted for by the expected angular distribution shifts in that region.

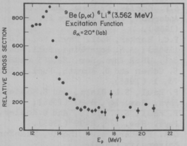

Fig. 6.5-4. The excitation function for the 3.56 MeV state. A sharp resonance is seen at E_p = 13.25 MeV which agrees with $^7Li(^3He,\gamma)$ and $^9Be(p,\gamma)$ work. There is evidence for a possible resonance at 17.75 MeV but a repeat run with fine resolution is required.

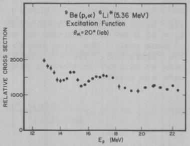

Fig. 6.5-5. The excitation function for the 5.36 MeV state. Some structure is observed which does not agree with that seen in the 3.56 MeV excitation function.

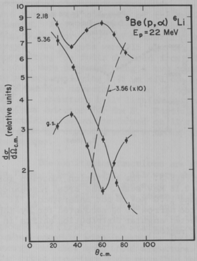

Fig. 6.5-6. Angular distributions at E_p = 22.0 MeV as a function of center of mass angle. The lines are to clarify the figure only. The 3.56 state was so weak at 22.0 MeV that only a rough estimate was obtained.

presence of any higher lying states in ^{6}Li.

1. H.R. Blieden, G.M. Temmer, and K.L. Warsh, Nucl. Phys. *49*, 209 (1963).
2. D.R. Maxson, Phys. Rev. *128*, 1321 (1962).
3. G. Gamborini, I. Iori, S. Micheletti, N. Molko, M. Pignanelli, and G. Tagliaferri, Nucl. Phys. *A126*, 562 (1969).
4. M.P. Baker, J.R. Calarco, J.M. Cameron, N.S. Chant, and N. Mangelson, Bull. Am. Phys. Soc. *15*, 519 (1970); Annual Report, Nuclear Physics Laboratory, University of Washington (1970), p. 68.
5. R.H. Stokes and P.G. Young, Phys. Rev. *C3*, 984 (1971).
6. C.J. Batty, B.E. Bonner, E. Friedman, C. Tschalär, L.E. Williams, A.S. Clough, and J.B. Hunt, Nucl. Phys. *A120*, 297 (1968).
7. B. Wakefield and B.E.F. Macefield, Nucl. Phys. *A114*, 561 (1968).
8. S.F. Eccles, C. Wong, and J.D. Anderson, Phys. Letters *20*, 190 (1966).
9. F.C. Barker, Nucl. Phys. *83*, 418 (1966); A.N. Boyarkina, Bull. Acad. Sci. USSR Phys. Ser. *28*, 255 (1964); S. Cohen and D. Kurath, Nucl. Phys. *73*, 1 (1965).
10. P. Paul, S.L. Blatt, and D. Kohler, Phys. Rev. *137*, B493 (1965); P. Paul, S.L. Blatt, and D. Kohler, Phys. Rev. *137*, B499 (1965).
11. G.A. Fisher, Ph.D. Thesis, Stanford University (1970).

6.6 A Comparison of the ^{6}Li(^{6}Li,^{6}He$_{g.s.}$)^{6}Be$_{g.s.}$ and the ^{6}Li(^{6}Li,^{6}Li$^*_{3.56\ MeV}$)^{6}Li$^*_{3.56\ MeV}$ Reactions

J.R. Calarco, J.G. Cramer, K.G. Nair, W.R. Wharton, and D.H. Wilkinson

Differential cross sections have been measured and compared for the ^{6}Li(^{6}Li,^{6}He$_{g.s.}$)^{6}Be$_{g.s.}$ and the ^{6}Li(^{6}Li,^{6}Li$^*_{3.56}$)^{6}Li$^*_{3.56}$ reactions at a laboratory energy of 32 MeV. The two reactions are expected to be approximately equal because the ground states of ^{6}He and ^{6}Be and the 3.56 MeV state of ^{6}Li form an isobaric multiplet of T = 1, and charge independence of nuclear forces is expected to be nearly valid. A comparison of these two reactions offers the possibility of testing a restricted form of charge independence:

$$(n - p) = \frac{1}{2}[(p - p) + (n - n)] \qquad (1)$$

where the nuclear forces between a neutron and a proton are equal to the average of the nuclear forces between two protons and the forces between two neutrons.

The two reactions studied here are interesting in that they can only proceed by a few select terms of the nucleon-nucleon potential which allow both a spin flip and an isospin flip of the interacting nucleons in each nucleus, so that the two $J^\pi = 1^+$, T = 0 lithium nuclei in the incident channel become two $J^\pi = 0^+$, T = 1 nuclei in the exit channel. Such terms of the nucleon-nucleon force are:

$$\vec{\tau}_i \cdot \vec{\tau}_j [V_{\sigma\tau} \vec{\sigma}_i \cdot \vec{\sigma}_j + V_{Ten,\tau} [3r^{-2}(\vec{\sigma}_i \cdot \vec{r})(\vec{\sigma}_j \cdot \vec{r}) - (\sigma_i \cdot \sigma_j)]. \qquad (2)$$

These terms come from the one pion exchange part of the nucleon-nucleon potential and have been measured to be somewhat smaller than the simple charge-exchange term $\vec{\tau}_i \cdot \vec{\tau}_j V_\tau$[2]. It is the hope of this experiment, then, that this particular view of the nucleon-nucleon potential will give us new information concerning terms violating charge independence in the nucleon-nucleon potential. The possibility exists that the reaction may go by more complicated mechanisms that cannot be simply described in nucleon-nucleon terms but would be written as appropriate terms in a macroscopic nuclear potential. In this case we would hope to learn more about the nuclear potential.

If Eq. (1) is valid, neglecting differences in distortion effects, we can predict a ratio for the two reactions:

$$\frac{d\sigma/d\Omega(^6Li^*_{3.56\ MeV} + {}^6Li^*_{3.56\ MeV})}{d\sigma/d\Omega(^6He_{g.s.} + {}^6Be_{g.s.})} = \frac{k_{^6Li^*}}{k_{^6He}} \; \frac{\langle 1010|00\rangle^2}{\langle 111\text{-}1|00\rangle^2} = 1.04. \qquad (3)$$

Differences from this ratio are expected because the ^6He and ^6Be ground states have different structures. The $^6He_{g.s.}$ is heavy-particle stable by 0.97 MeV and the $^6Be_{g.s.}$ is heavy-particle unstable by 1.37 MeV.

Preliminary results show striking differences in the cross sections for the two reactions. We first measured the elastic scattering and the $^6Li(^6Li,{}^6He)^6Be$ angular distributions at 32 MeV using a ΔE-E telescope and a monitor. After differences were found between the $^6Li(^6Li,{}^6He)^6Be$ data and earlier published results[3] on the $^6Li(^6Li,{}^6Li^*_{3.56\ MeV})^6Li^*_{3.56\ MeV}$ reaction, it was decided to measure both reactions simultaneously with the same ΔE-E telescope. A ΔE of 21μ or 35μ was chosen with an E of 200μ. An anti-coincidence detector was placed behind the E to reject all particles not stopped in the E. To measure the

$^6Li(^6Li,^6Li^*_{3.56})^6Li^*_{3.56}$ reaction it was necessary to observe the recoil ^6Li nucleus in coincidence with the ^6Li nucleus observed in the telescope, otherwise the reaction could never be observed because of the large continuum background in the ^6Li energy spectrum. Therefore a 25μ or 100μ Si(Li) transmission detector was placed at the correct angle to detect the recoil $^6Li^*_{3.56}$. Another detector was placed behind the recoil detector to reject all particles which pass through the first detector. Fast signals from the recoil-detector and the ΔE detector of the telescope were fed into the start and stop inputs of a TAC. A SCA window was liberally set (50 nsec wide) on the TAC output. Another SCA window was liberally set on the energy signal from the recoil detector. Slow coincidences were required between the TAC, ΔE, E, and recoil detectors along with anti-coincidences from the two anti-detectors. The resulting coincidence logic signal and the ΔE and E energy signals were each fed into an ADC on the SDS 930. The computer calculates the particle identification[4] (P.I.D.) as is shown in Fig. 6.6-1. A window was set to include the ^6He peak in the P.I.D. spectrum, and an energy spectrum was recorded for events falling inside the window (Bin 1). Another window was set to include the ^6Li peak in the P.I.D. spectrum and the events falling within the ^6Li window were separated into two Bins, Bin 4 if the coincidence ADC fired and Bin 3 if the coincidence ADC did not fire. The results from a typical run are shown in Figs. 6.6-1 and 6.6-2. The elastic peak in Bin 3 serves as a monitor and is also used to determine absolute cross section since the absolute cross section for elastic scattering has been accurately measured.[5]

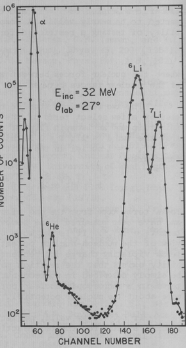

Fig. 6.6-1. A typical particle identification spectrum at $\theta_{lab} = 27°$. At more forward angles the ^6He and ^7Li peaks become stronger, improving the peak to valley ratio.

It was obviously necessary that there be a high coincidence efficiency so that essentially all events from the $^6Li(^6Li,^6Li^*_{3.56})^6Li^*_{3.56}$ reaction go into Bin 4 instead of Bin 3. In other words, for each ^6Li nucleus recorded in the telescope, the corresponding recoil ^6Li must be detected by the recoil detector and a true coincidence signal sent to the computer. A measurement of the coincidence efficiency is made before and after each $^6Li(^6Li,^6Li^*_{3.56})^6Li^*_{3.56}$ measurement. This is accomplished by moving the recoil detector to 90° with respect to

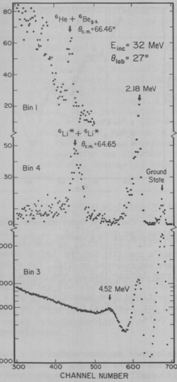

Fig. 6.6-2. Energy spectra corresponding to the run shown in Fig. 6.6-1.

Bin 1: includes P.I.D. channels 69-87
Bin 4: P.I.D. channels 137-163 with coincidences
Bin 3: 137-163 without coincidences

the telescope and measuring the coincidence efficiency for the elastic scattering. We have found that the coincidence efficiency is dependent upon good geometry and many elaborate procedures have been developed to assure a high efficiency and at the same time a reasonable counting rate. Usually a compromise is made between efficiency and counting rate so that the elastic efficiency is 95%. This corresponds to a calculated efficiency for the ^{6}Li(^{6}Li, ^{6}Li$^*_{3.56}$)^{6}Li$^*_{3.56}$ of about 90%. The reason the ^{6}Li(^{6}Li,^{6}Li$^*_{3.56}$)^{6}Li$^*_{3.56}$ reaction has a worse efficiency is because it is essentially a 4-body final state reaction. Before reaching the detectors, both ^{6}Li$^*_{3.56}$ nuclei photon decay changing their direction and momentum. One effect of the photon decay is clearly seen in Fig. 6.6-2 where the ^{6}Li* + ^{6}Li* peak is about twice the width of the ^{6}He + ^{6}Be peak. We have restricted the acceptance angle of the recoil counter and observed that the measured ^{6}Li(^{6}Li, ^{6}Li$^*_{3.56}$)^{6}Li$^*_{3.56}$ cross section drops faster than the measured elastic efficiency, confirming our calculation. However, we do not wish to depend upon an efficiency calculation when the correction is large. Therefore, we have developed procedures to assure a high efficiency.

The alignment of the beam collimaters, target holder, and detectors is checked to within a few mils with the use of an optical telescope. A small aperture is used in front of the telescope so that all particles detected from the target have a small angular spread (always less than 1° full spread). A larger aperture is put in front of the coincidence detector to allow detection of particles from the target over a larger angular range (usually about 5°). To measure different parts of the angular distribution, different shapes and sizes for the apertures are used. For example, when the telescope is at forward angles an ellipsoidal aperture is used such that the vertical angular spread is .4° and the horizontal spread is about .8°. In this case the vertical angular spread is kept low because the vertical angular spread for the corresponding recoil nuclei is:

$$0.4 \times \frac{\sin \theta_{recoil}}{\sin \theta_{telescope}} .$$

This number can become large as the telescope is moved forward in angle.

Self-supporting ^{6}Li targets as thin as 150 μg/cm^2 are used. The targets are made thin not only to improve resolution but also to diminish multiple-scattering effects. Multiple scattering significantly reduces the efficiency at forward angles where the recoil ^{6}Li has an energy less than 3 MeV. The root-mean-square scattering angle for multiple scattering is calculated to be[6]

$$\langle \theta^2_{lab} \rangle \approx \frac{5 \times 10^{-6}}{\cos \theta_{Rt}} \frac{t}{E_R^2} \text{(radians)}^2 \qquad (4)$$

where θ_{Rt} = angle of ^{6}Li recoil and normal of target

t = target thickness in μg/cm^2

E = recoil energy in MeV.

Equation (4) has been verified to within an accuracy of 20% by doing angular correlations on the elastic scattering.

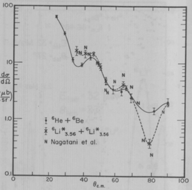

Fig. 6.6-3. Center of mass angular distributions for the ^{6}Li(^{6}Li,^{6}He$_{g.s.}$)^{6}Be$_{g.s.}$ and ^{6}Li(^{6}Li,^{6}Li$^*_{3.56}$)^{6}Li$^*_{3.56}$ reactions. Nagatani's results for the latter reaction are represented by N's. His errors were much larger than in the present experiment. The ^{6}Li(^{6}Li,^{6}Li$^*_{3.56}$)^{6}Li$^*_{3.56}$ cross sections have been divided by 2 to account for identical particles in the final state.

The ^{6}Li targets are never exposed to air. They are kept either in a vacuum or in an argon bath and transported to and from the scattering chamber in a special target lock. If the target oxidizes it usually warps. A warped target has been observed to cause errors in the detector angles as large as .5°. Angular correlation measurements are made on the elastic scattering to check horizontal alignment and verify that the target is not warped.

The partially completed center of mass angular distributions are shown in Fig. 6.6-3 along with the earlier results of Nagatani *et al.*[3] The ^{6}Li(^{6}Li,^{6}Li$^*_{3.56}$)^{6}Li$^*_{3.56}$ data has been divided by 2 to account for the fact there are two indistinguishable particles in the final state and the detector doesn't know which one it is seeing. The angular distributions should be symmetrical about 90° c.m. because the two particles in the incident channel are identical. As is seen in the figure there are two places where the cross sections don't agree: near 35° and 80° c.m. The difference near 35° is doubtful because the ^{6}Li$^*_{3.56}$ + ^{6}Li$^*_{3.56}$ data point at 35.4° has been subjected to a large efficiency correction. Before and after this data point was taken, the elastic efficiency was measured to be 66%. The inelastic efficiency was calculated to be 49%. It is planned to re-do the forward angles with better efficiency to verify the difference between the two cross sections. More data points must also be taken at the backward angles. An attempt will be made shortly to fit the angular distributions.

---

1. A. Bohr and B. Mottelson, *Nuclear Structure, Vol. 1* (W.A. Benjamin, Inc., New York, 1969).
2. V.A. Madsen, in Proceedings of the Conference on Nuclear Isospin, Ed. by John D. Anderson *et al.*(Academic Press, New York, 1969); E. Rose and P.D. Kunz, Phys. Letters *30B*, 231 (1969).
3. K. Nagatani, D.P. Boyd, P.F. Donovan, E. Beardsworth, and P.S. Assimakopoulos, Phys. Rev. Letters *24*, 675 (1970).
4. P.I.D. = $(E + \Delta E)^x - (E)^x$ where x is a parameter. H. Wieman revised the standard P.I.D. program to satisfy our coincidence requirements.
5. H.T. Fortune, G.C. Morrison, and R.H. Siemssen, to be published.
6. This equation was obtained from J.B. Marion, in *Nuclear Data Tables, Part 3*,(National Academy of Sciences National Research Council, Washington,D.C., 1960).

6.7 Investigation of Isospin Forbidden T = 3/2 Resonances in Light Nuclei Using a Polarized Proton Beam

J.G. Cramer, M. Hasinoff, E. Preikschat, G. Roth, and W.G. Weitkamp

During recent polarized ion source tests[1] a polarized proton beam of 5-20 nA has been obtained on target. This means the beam is intense enough to measure polarization excitation functions relatively quickly and simply.

We have investigated the use of polarization excitation functions in determining the presence and properties of narrow resonances. We have chosen several isospin-forbidden T = 3/2 resonances in ^{13}N and ^{17}F as subject of this investigation.

The measurement of the polarization asymmetry across the resonance is of interest since, in the case of a J = 0 target, it allows a unique determination[2-4] of the spin of the state. This is particularly useful when dealing with the isospin forbidden resonances in light nuclei because one is in effect investigating the properties of the lowest levels of the other members of the isospin multiplet, in our case ^{13}B, ^{13}O, ^{17}N, and ^{17}Ne. The level structure of these nuclei is not well known.

On the other hand, in cases where the spin of the parent state is known, the determination of the resonance spin through the shape of the polarization excitation function can provide strong evidence for identifying a given narrow resonance as the analog of the parent. For example, the ground state analog of ^{13}B and ^{13}O in ^{13}N should have $J^\pi = 3/2^-$, the ground state analog of ^{17}N and ^{17}Ne in ^{17}F should have $J^\pi = 1/2^-$, while any T = 2 ground state analog in a $T_z = 0$ nucleus, being even-even, must have $J^\pi = 0^+$, thus providing distinctive signatures for the identification of these resonances.

The aim of the present experiment is to establish the effectiveness of a polarized proton beam in the study of narrow resonances. Natural carbon and NiO_2

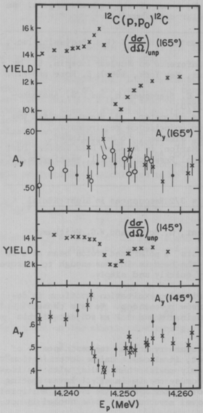

Fig. 6.7-1. Excitation function of ^{12}C (p,p_0) across the T = 3/2 analog resonance in ^{13}N. The differential cross sections and the polarization asymmetries A_y are shown at lab angles of 165° and 145°.

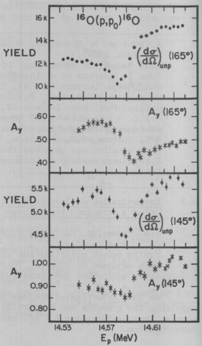

Fig. 6.7-2. Excitation function of ^{16}O (p,p_0) across the T = 3/2 analog resonance in ^{17}F. The differential cross sections and the polarization asymmetries are shown at lab angles of 165° and 145°.

targets were used to study three analog resonances, the 15.068 MeV level in ^{13}N and the 11.196 MeV and the 14.312 MeV levels in ^{17}F. The measurements were made with two left-right detector systems at lab angles of 145° and 165°. Figures 6.7-1 and 6.7-2 show the differential cross sections and the polarization asymmetries as a function of proton energy for two of the resonances. The results for the 11.196 MeV resonance were inconclusive and are not shown.

Although the $^{12}C(p,p_0)$ resonance shows up more strongly at 165° than at

145° with an unpolarized beam we find the reverse to be true with a polarized beam. The asymmetry shows about a 40% change in the 145° excitation curve but only a 5% effect at 165°.

In the case of the $^{16}O(p,p_0)$ resonance at E_p = 14.584 MeV the asymmetries show quite strong resonance effects at both angles.

These polarization excitation function measurements are being extended to a wider angular range, to other resonces in these nuclei, and to other isospin forbidden T = 3/2 and T = 2 states.

---

1. Refer to Sec. 2.1 of this report.
2. C.F. Moore and G.E. Terrell, Phys. Rev. Letters *16*, 804 (1966).
3. L. Veeser and W. Haeberli, Nucl. Phys. *A115*, 172 (1968).
4. G. Clausnitzer, R. Fleischmann, G. Graw, D. Proetel, and J.P. Wurm, Nucl. Phys. *A106*, 99 (1967).
5. G.M. Temmer, B. Teitelman, R. Van Bree, and H. Ogata, Proc. of the International Conf. on Nuclear Structure, Tokyo, 1967, p. 299.
6. J.L. Black, W.J. Caelli, D.L. Livesey, and R.B. Watson, Phys. Letters *30B*, 100 (1969).

---

7. NUCLEAR ASTROPHYSICS

7.1 Excitation Functions for $^{14}N(p,\alpha)^{11}C$ and $^{14}N(p,2\alpha)^{7}Be$

D. Bodansky, J. Cameron, W. Jacobs, and P.A. Russo

The reactions $^{14}N(p,\alpha)^{11}C$ and $^{14}N(p,2\alpha)^{7}Be$ are of interest in connection with the origin and abundance of the light elements Li, Be, and B (^{11}B and ^{7}Li are formed as decay products of ^{11}C and ^{7}Be). These elements are not formed in the main sequence of stellar evolution. Rather, they are produced by relatively high energy processes (sometimes loosely called "spallation" reactions) instead of low energy processes (thermonuclear reactions). Stellar nucleosynthesis of these light elements could take place by the action of high energy proton and alpha bombardment of the elements found near the stellar surface.[1] Or, possibly more likely,[2] due to interactions between galactic cosmic rays and the material of the interstellar medium. The reactions of protons on nitrogen have the lowest thresholds, by about 12 MeV, for production of these light elements in interactions of protons and the most abundant target nuclei: ^{12}C, ^{14}N, ^{16}O, and ^{20}Ne.

The excitation functions $^{14}N(p,\alpha)^{11}C$ and $^{14}N(p,2\alpha)^{7}Be$ are being studied by activation methods. Targets for the investigation of both of these reactions have been made of adenine ($C_5H_5N_5$) evaporated onto pure aluminum backings. It has been found that an additional thin film of polystyrene (dissolved in benzine) sprayed on the target inhibits the adenine from flaking and cracking, ensuring that the activity produced during activation stays localized near the beam spot. However, the targets are still susceptible to deterioration (e.g., thickness change) by the beam, so that the proton elastic scattering peak from nitrogen is monitored during bombardment in order to determine the average nitrogen thickness. This determination requires a knowledge of the absolute cross section for scattering of protons by nitrogen. Measurements of this cross section were made using a gas target over an incident proton energy range of 6 to 24 MeV, at appropriate monitoring angles. A normalization check was made by measuring the cross section (which is known very accurately) for the scattering of protons by hydrogen using the same gas target geometry. The $^{14}N(p,p)^{14}N$ elastic cross sections were thus determined absolutely to ±3%, enabling one to extract the product of beam flux and nitrogen thickness in the adenine targets to ±5%.

The reaction $^{14}N(p,2\alpha)^{7}Be$ has been studied over an incident proton energy range of 13 to 24 MeV. The 473 keV gamma radiation (half life of 53.6 days) was counted with a 3 x 3" NaI(Tℓ) crystal. No discernable long lived contaminant radiations were observed. The cross section rises rapidly from threshold (11.5 MeV) to a peak at about 20 MeV. The peak cross section is 46 ± 5 mb. This result is in agreement with similar measurements carried out at Orsay.[3]

The reaction $^{14}N(p,\alpha)^{11}C$ ($Q = -2.92$ MeV) has been studied over an incident proton energy range of 6 to 23 MeV. ^{11}C is a positron emitter of half life 20.3 minutes. There is a readily separable ^{13}N activity (half life = 10 minutes) produced in the reaction $^{14}N(p,d)^{13}N$ ($Q = -8.33$ MeV) and, to a much lesser extent, $^{12}C(p,\gamma)^{13}N$ ($Q = +1.94$ MeV). At high energies, the reaction $^{12}C(p,d)^{11}C$ ($Q = -16.5$ MeV) produces ^{11}C activity that must be accounted for and subtracted on the basis of separate carbon target bombardments. No other background activities were encountered. The targets were activated in the 60" scattering chamber and removed via a target lock for counting away from the bombardment area. A positron counter system, to count the annihilation gammas in coincidence, was constructed to hold and count the targets in a precise geometry.[4]

The cross section is found to exhibit strong fluctuations in the region between 6 and 10 MeV. Evidence for this has also been observed by Shrivastava *et al.*[5] A minimum is reached in the region of 9-10 MeV, after which the cross section rises to a broad maximum. At 14 MeV the cross section is approximately (±20%) 190 mb.

Further data runs are being taken for both of these reactions.

---

1. R. Bernas, E. Gradsztajn, H. Reeves, and E. Schatzman, Ann. of Physics (N.Y.) *44*, 426 (1967).
2. H. Reeves, W.A. Fowler, and F. Hoyle, Nature *226*, 727 (1970).
3. M. Epherre and C. Seide, submitted to The Physical Review.
4. See Sec. 414 of this report.
5. P.N. Shrivastava, E. Boreli, and B.B. Kinsey, Phys. Rev. *169*, 842 (1968).

7.2 Production of ^{6}Li and ^{10}B in Proton Bombardment of ^{13}C

D. Bodansky, D. Chamberlin, W. Jacobs, C. Ling, and D. Oberg

In analyses of the production of the light elements (Li, Be, and B) in stars or in the interstellar medium, it is usually assumed that the important targets are the most abundant nuclei, ^{12}C, ^{14}N, ^{16}O, and ^{20}Ne. For events involving the low energy tail (below, say, 25 MeV) of the cosmic ray or flare spectrum, the only member of this quartet which has low enough thresholds to give large yields is ^{14}N.[1] The present work is concerned with the possible additional contributions from ^{13}C, through the reactions $^{13}C(p,\alpha)^{10}B$ (Q = -4.06 MeV) and $^{13}C(p,2\alpha)^{6}Li$ (Q = -8.62 MeV). These reactions are initiated by protons (or heavy ions on hydrogen) at energies comparable to those for the ^{14}N reactions with protons, and there is no *a priori* reason to believe that the cross sections are very different from the two targets.

Knowledge of the ^{13}C and ^{14}N abundances is crucial to the assessment of the importance of these nuclei in light element production. Although the available information is very fragmentary, there is substantial evidence that the low $^{13}C/^{14}N$ ratio in the solar system is not a universally relevant guide. Within the solar system the abundance ratios are roughly: $C/N \sim 5$ and $^{13}C/^{12}C = 0.01$. In cosmic rays the C/N ratio is about 4.[2] However, the $^{13}C/^{12}C$ ratios may be as high as 0.15 (or more) in cosmic rays,[3] 0.25 to 0.50 in certain carbon stars;[4] and possibly 0.1 in some regions of the interstellar medium.[5] To further complicate the situation, it has been reported that N in high energy cosmic rays may be primarily ^{15}N,[6] although the solar system N is almost all ^{14}N. In view of the variations and uncertainties in these abundances, it is not possible to exclude ^{13}C as a contributor to light element production, and the determination of the ^{13}C reaction cross sections is desirable.

Exploration of the $^{13}C(p,\alpha)^{10}B$ reaction has assumed particular interest because of the suggestion by Reeves, Fowler, and Hoyle that most of the light element production takes place in the interstellar medium.[7] They further point out that the observed solar system $^{11}B/^{10}B$ ratio of 4 can be understood from reactions at high energies. Assuming ^{14}N to be the only contributor at low energies, they conclude that the galactic cosmic ray spectrum cannot be sharply peaked at low energies because a large low energy flux would produce ^{11}B through the $^{14}N(p,\alpha)^{11}C$ reaction and raise the $^{11}B/^{10}B$ ratio above 4. This argument, however, neglects the possible role of the $^{13}C(p,\alpha)^{10}B$ reaction at low energies which may act to reduce the $^{11}B/^{10}B$ ratio. In view of the fact that the direct observational determination of the galactic cosmic ray spectrum at low energies is obscured by poorly understood modulation effects of the solar wind, indirect evidence concerning the shape of the unmodulated spectrum is of great interest, and clarification of the contribution of ^{13}C is important.

A second specific interest in ^{13}C reactions is related to the abundance of Li. There are some indications that stars which contain extremely high amounts of Li also contain abnormally high amounts of ^{13}C.[4] It is difficult to identify the Li isotopes in these stellar spectra, but if one isotope predominates, it may be possible to make an identification.[8] High yields from the $^{13}C(p,2\alpha)^{6}Li$ reaction would suggest the desirability of looking for possible correlations between ^{13}C and ^{6}Li in stellar spectra, as a further step in establishing the detailed mechanisms of Li production.

Experimental studies of the $^{13}C(p,\alpha)^{10}B$ and $^{13}C(p,2\alpha)^{6}Li$ reactions have been started using protons from the tandem Van de Graaff accelerator. To permit particle identification by time-of-flight techniques, the beam was pulsed and bunched with the klystron buncher system.[9] Bunches as narrow as 0.7 nsec have been made possible by use of the direct extraction ion source.[10] The ^{13}C targets were prepared in this laboratory by the cracking of ^{13}C-enriched methyl iodide.[11]

The measurements of cross sections are being carried out using both single counter and coincidence techniques. In the single counter measurements, the particles are detected in a cooled 100-micron surface barrier detector, which is followed by a 2mm lithium drifted detector used to reject, by anti-coincidence, protons which pass through the first detector. All particles which stop in the first detector, in particular the ^{4}He, ^{6}Li, and ^{10}B nuclei, are identified by mass and energy from time-of-flight and pulse height information using an ET^2 data collection program in the on-line SDS 930 computer. The time-of-flight measurement was done with constant fraction timing,[12] which gave acceptable time resolution at energies as low as 500 keV (well below the energies at which time-pickoff systems[13] were found to be effective).

The observed ^{6}Li and ^{10}B yields directly give the cross sections of interest. However, for many angles and excitation energies the energy of the ^{10}B nuclei is too low for clean measurements, and the relevant cross sections can be more readily determined from the alpha particle groups corresponding to the ^{10}B recoil nuclei in question. The yields to bound states of ^{10}B (g.s.,0.72, 1.74, 2.15, and 3.59 MeV) can in principle be studied using just the alpha particles. However, for the 3.59-MeV state, the alpha particles are masked by alphas from the $^{12}C(p,\alpha)^{9}B$ reaction. To measure the cross section to this state, as well as contributions from unbound states, runs have been carried out in which recoil ^{10}B nuclei are looked at in coincidence with alpha particles.

It is not yet possible to quote absolute cross sections, because the data obtained is still fragmentary and because there have been some anomalies in the determination of the ^{13}C target thickness. For ^{6}Li production at incident proton energies of 12 MeV and 15 MeV, the total yield is strongly peaked in the forward direction over the bulk of the ^{6}Li spectrum. The ^{6}Li spectrum has little structure, although a distinct peak corresponding to the ($^{6}Li_{g.s.}$ + $^{8}Be_{g.s.}$) group is observed; the cross section for this group is relatively small and its angular distribution is rather flat. In studies of ^{10}B production, most extensively carried out at an incident energy of 15 MeV, it is found that the total yield is highest to the ^{10}B ground state, but that there are appreciable yields to all the excited bound states as well as to an unbound state, or states, near 5.17 MeV (presumably the T = 1 state at 5.17 MeV). It appears unlikely that other unbound states of ^{10}B make a major contribution, because no other strong groups are seen up to the threshold for proton emission at 6.59 MeV.

Plans for the future include the completion of existing measurements at incident proton energies of 9, 12, and 15 MeV and the extension of measurements to other energies.

---

1. See Sec. 7.1 of this report.
2. P. Meyer, *Annual Review of Astronomy and Astrophysics* (Annual Reviews, Inc., Palo Alto, 1969), Vol. 7, p. 1.
3. K. Kristiansson, G. Jonsson, and L. Malmqvist, *Proc. 11th Conf. on Cosmic Rays*, Budapest, 1969.
4. A. McKellar, *Stars and Stellar Systems* (University of Chicago Press, Chicago, 1960), Vol. 6, *Stellar Atmospheres*, p. 569; Y. Yamashita, *A Study of Carbon-Star Spectra Based on the C-Classification* (Pub. of the Dominion Astrophysical Observatory, Victoria, B.C., 1967), Vol. XIII, p. 5.
5. B. Zuckerman, P. Palmer, L.E. Snyder, and D. Buhl, Astrophys. J. *157*,L167 (1969).
6. N. Lund, B. Peters, R. Cowsic, and Y. Pal, Phys. Letters *31B*, 553 (1970).
7. H. Reeves, W.A. Fowler, and F. Hoyle, Nature *226*, 727 (1970).
8. G. Wallerstein (private communication).
9. Nuclear Physics Laboratory Annual Report, University of Washington (1967) p. 103.
10. Nuclear Physics Laboratory Annual Report, University of Washington (1970) p. 4.
11. See Sec. 3.5 of this report.
12. ORTEC: Constant Fraction Timing Discriminator-453; Timing Filter Amplifier-454.
13. ORTEC: Time Pickoff-260.

7.3 The Electromagnetic De-excitation of the 9.64-MeV State of ^{12}C

D. Bodansky, D. Chamberlin, C. Ling, D. Oberg, W. Trautmann, and D. Wilkinson

The helium burning process in stars, by which ^4He is converted into ^{12}C, proceeds in ordinary stars through the excited $J^\pi = 0^+$ state of ^{12}C at 7.66 MeV. However, in nucleosynthesis at very high temperatures,[1] which may occur in very massive or exploding objects, reactions proceeding through the 9.64-MeV $J^\pi = 3^-$ state of ^{12}C can become important. The ratio of the reaction rates for the two states is:

$$\frac{R(9.64)}{R(7.66)} = 7\, e^{-1.98/T}\, \frac{\Gamma(9.64)}{\Gamma(7.66)}$$

where the factor of 7 comes from the spin multiplicities of the states, the term 1.98 is the difference (in MeV) in the excitation energies, T is the temperature in MeV, and the Γ's are the widths for radiative transitions to bound states of ^{12}C.

The measured radiative width of the 7.66-MeV state is $\Gamma(7.66) = 2.8 \times 10^{-3}$ eV.[2] The radiative width for the 9.64-MeV state has not been measured, but is commonly taken in astrophysical calculations to be $\Gamma(9.64) = 10^{-2}$ eV, following estimates by Hoyle and Fowler.[3] With these widths, the 9.64-MeV state clearly can play no part in ordinary helium burning in stars, which takes place at temperatures of about 2×10^8 °K(T = 0.019 MeV). However, the situation is quite changed at the much higher temperatures which may be reached in exploding systems. The two rates become equal, given the widths cited above, at the not unattainable temperature of 7.1×10^9 °K(T = 0.61 MeV).

In view of the interest in synthesis processes at high temperatures, reasonably accurate knowledge of Γ(9.64) is desirable. It is at present not possible to make very precise theoretical estimates of Γ(9.64). The Weisskopf estimate for the width of the E1 transition from the 9.64-MeV state to the 4.44-MeV state of ^{12}C is 50 eV. The mean strength of isospin forbidden E1 transitions in the A-range 5 to 40 is 4×10^{-4} Weisskopf units,[4] suggesting a possible width in the neighborhood of $\Gamma(9.64) = 2 \times 10^{-2}$ eV, but the spread in strength is great (more than an order of magnitude either way) so that an experimental determination is obviously demanded.

An attempt is being made to determine Γ(9.64) experimentally, by exciting ^{12}C to the 9.64-MeV state in inelastic alpha particle scattering, and requiring a coincidence between the scattered alpha particles and recoiling ^{12}C nuclei. Such coincidences only occur for electromagnetic de-excitation of the excited ^{12}C. The radiative width can then be calculated from the measured radiative branching ratio, using the known total width of the 9.64-MeV state (34 keV). For example, a radiative width of 2×10^{-2} eV corresponds to a branching ratio of 0.6×10^{-6}.

Preliminary runs have been made using 24-MeV incident alpha particles and observing scattered alpha particles at 70°. The differential cross section for inelastic scattering to the 9.64-MeV state was found to be about 9 mb/sr (lab) for these conditions. With this cross section, it appears feasible to measure a branching ratio of 10^{-6}, provided that background events can be kept at a sufficiently low level. To date, the most pernicious background appears to arise from inelastic scattering of alpha particles in a ^{13}C target impurity, followed by breakup of the excited ^{13}C into ^{12}C (4.44-MeV state) and a neutron. Background from alpha particles has been held to a quite low level by using a thin (30 micron) detector for the ^{12}C nuclei, by rejecting longer range particles with an anti-coincidence detector, and by selecting mass 12 particles with time-of-flight information.

1. R.V. Wagoner, Astrophys. J. Suppl. *162*, 247 (1969).
2. F. Ajzenberg-Selove and T. Lauritsen, Nucl. Phys. *A114*, 1 (1968).
3. F. Hoyle and W.A. Fowler, Astrophys. J. *132*, 565 (1960).
4. S.J. Skorka, J. Hertel, and T.W. Retz-Schmidt, Nuclear Data, Sec. A, 2 *No. 4*, 347 (1966).

8.1 β-Decay of ^{8}Li and ^{8}B

D.E. Alburger* and D.H. Wilkinson

In the comparison of the β-decay of mirror pairs such as ^{8}Li, ^{8}B it is empirically found that the ratio $(ft)^+/(ft)^-$ is not unity but, usually, greater by 15% or so.[1] In the model of nuclear β-decay which treats the phenomenon as single-nucleon decay in the impulse approximation a $\beta^\pm$ asymmetry in Gamow-Teller decay may be expected of magnitude:

$$[(ft)^+/(ft)^-] - 1 \approx \frac{4}{3}\ |g_V/g_A| g_{IT}\ (W_0^{\ +} + W_0^{\ -})$$

where g_{IT} is the induced tensor coupling constant belonging, in the language of Weinberg, to a second class current. If nuclear β-decay is regarded as a many-body process then other second-class terms with unknown momentum dependence and associated with mesonic exchanges may be anticipated. If present experimental data are interpreted via the above expression we find $g_{IT} \approx 2 \times 10^{-3}$.

As an alternative to the above "fundamental" explanations of the $\beta^\pm$ asymmetry we have the possibility that the asymmetry arises because the nuclear wave functions of the mirror pair differ sufficiently, contrary to the dictates of charge independence; this is a "trivial" explanation. An experiment has been performed to separate one of the "fundamental" explanations, that of the induced tensor coupling, from the other two possibilities. ^{8}Li and ^{8}B decay to the very broad $J^\pi = 2^+$ state of ^{8}Be at a nominal energy of 3 MeV but in effect continuing for many MeV in excitation above this. ^{8}Be is everywhere unstable to decay into two alpha-particles whose energy then signal the excitation E_x in ^{8}Be to which β-decay led. If we call the excitation spectra $N(E_x)^+$ and $N(E_x)^-$ we expect $[N(E_x)^-/f^-]/[N(E_x)^+/f^+]$ to be a constant if the $(ft)^+/(ft)^-$ asymmetry is due to a "fundamental" but momentum-transfer-insensitive effect; we also expect this ratio to be approximately a constant if the "trivial" explanation is correct because the tightly-bound individual nucleons of ^{8}Be are little dependent on E_x until their thresholds are approached. If, however, the induced tensor explanation is correct, the above ratio will have the form $1 + \ \xi(W_0^+ + W_0^-)$ where ξ is determined by g_{IT}.

^{8}Li and ^{8}B were made at the Brookhaven National Laboratory Van de Graaff. $N(E_x)^\pm$ were measured with Si-counters and Fig. 8.1-1 shows the result. The full line, corresponding to $g_{IT} = 2 \times 10^{-3}$, is absolutely eliminated; statistical analysis gives $|g_{IT}| < 7 \times 10^{-3}$ at the 99% confidence level.

It therefore appears that the mirror asymmetry is due either to a momentum transfer-insensitive "fundamental" effect or to "trivial" nuclear structure causes (although in the latter case the effect is surprisingly large).

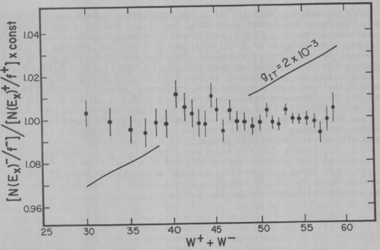

Fig. 8.1-1. Excitation spectra in ^{8}Li and ^{8}B β-decay divided by their respective f-values as a function of their summed energy release $W_0^+ + W_0^-$ and compared with arbitrary normalization. The full line is the slope to which the points should conform if the decays involved an induced tensor coupling constant of magnitude $g_{IT} = 2 \times 10^{-3}$.

---

* Brookhaven National Laboratory, Upton, New York.

1. D.H. Wilkinson, Phys. Letters *31B*, 447 (1970).

8.2 β-Decay of ^{11}Be

D.E. Alburger* and D.H. Wilkinson

^{11}Be is unique among the light nuclei in that the parity of its ground state is not that expected from the shell model. That the ground state might be of $J^{\pi} = 1/2^+$ as observed, rather than the $J^{\pi} = 1/2^-$ of the shell model, was made reasonable by the arguments of Talmi and Unna[1] based on the local systematics of the $2s_{1/2}$ state. Earlier studies of ^{11}Be[2] were incomplete insofar as the expected first-forbidden branch to the $J^{\pi} = 3/2^-$ state at 5020 keV had not been observed and the possible intrinsically-strong allowed transitions to positive parity states above the $^{7}Li + \alpha$ threshold had not been sought. In the latter context the possibility of a strong transition to the anti-analog in ^{11}B of the analog of the ground state of ^{11}Be is especially interesting.

^{11}B was made by ^{9}Be(t,p)^{11}Be at the Brookhaven National Laboratory Van de Graaff. Its decay was investigated using Ge(Li) and NaI(Tℓ) γ-ray detectors and Si α-particle detectors. Eight γ-ray transitions were measured including three weak γ rays with energies of 1772, 2893, and 5019 keV not observed previously in ^{11}Be decay. The relative γ intensities show that the 5020-state of ^{11}B is populated by a ^{11}Be first-forbidden β-ray branch of 0.28% (log ft = 7.94 ± 0.14), as well as by a cascade γ-ray branch of 4.1% from the ^{11}B 6793 keV state. Other previously observed β-ray branches were confirmed. Accurate energies were obtained for the ^{11}B states including a value of 7978.1 ± 1.9 keV for the 7th excited state. This is 18 keV lower than in previous reports. Delayed α particles were also found in ^{11}Be decay; the experimentally observed α-particle spectrum is a continuum extending from an instrumental lower limit of 0.3 MeV up to about 1.0 MeV and with a total α-particle intensity of 3.0% per decay. These α particles are not in coincidence with 478 keV γ rays from ^{7}Li. It is suggested that this β-ray branch of ^{11}Be proceeds to the 9870 keV $J^{\pi} = 3/2^{+}$ state of ^{11}B (log ft = 4.03 ± 0.15) followed by α-particle emission to the ground state of ^{7}Li, although an α-decay branch to the 478 keV state of ^{7}Li cannot be excluded. The experimental results are summarized in Fig. 8.2-1.

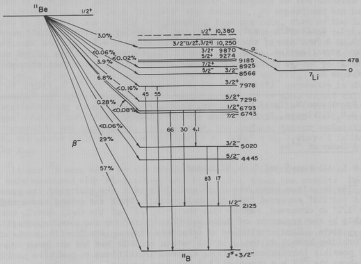

Fig. 8.2-1. β Decay of ^{11}Be.

An interesting feature is the weakness of the unique first-forbidden transition to the second excited state of ^{11}B (log ft > 10.9). This is at least 20 times slower than the average for $A \leq 40$. This probably reflects the accuracy of the simple Talmi-Unna model which regards ^{11}Be as a $2s_{1/2}$ neutron attached to the $J^\pi = 0^+$ ground state of ^{10}Be as unique parent. This description plus the usual $1p^{-1}$description for the low-lying ^{11}B states, including the one now in question, leads to an expected transition rate of zero. These descriptions also provide a nice qualitative explanation for the relative strengths of the three non-unique first-forbidden transitions to the ground, first-excited and third-excited states of ^{11}B: the transitions to the two lowest of these states are roughly of the same intrinsic strength while that to the third is an order of magnitude weaker whereas the squares of the (Cohen-Kurath) fractional parentage coefficients of these three states (in increasing order of excitation) for the ground state of ^{10}Be are 0.09, 0.12, and 0.005.

The question of the possible anti-analog of the analog in ^{11}B, at 12.57 MeV, of the ^{11}Be ground state is easily approached experimentally if the ^{11}Be state is indeed largely represented as described above because we then expect ^{11}B to decay to it with log ft ≈ 3.4. The $J^\pi = 1/2^+$ state at 6793 keV is an obvious candidate but is excluded because it has log ft = 5.9. No strong decay to a $J^\pi = 1/2^+$ state in the excitation range expected for the anti-analog is found. It appears probable that the simple anti-analog has mixed with $J^\pi = 1/2^+$ configurations derived from the "loose" attachment of $2s_{1/2}$ neutrons to low-lying $J^\pi = 1^+$ $T = 0$ states of ^{10}B. It is possible to construct a simple and self-consistent picture of this mixing that resolves the dilemma of the "missing" anti-analog and that also incorporates the observed strong transition to the $J^\pi = 3/2^+$ state at 9.87 MeV.

---

* Brookhaven National Laboratory, Upton, New York.

1. I. Talmi and I. Unna, Phys. Rev. Letters *4*, 469 (1960).
2. D.H. Wilkinson and D.E. Alburger, Phys. Rev. *113*, 563 (1959);D.E. Alburger, C. Chasman, K.W. Jones, J.W. Olness, and R.A. Ristinen, Phys. Rev. *136*, B916 (1964).

8.3 β-Decay of ^{13}B and ^{20}Na

D.E. Alburger*,G.T. Garvey†,D.R. Goosman*,K.W. Jones*,E.K. Warburton *,
D.H. Wilkinson, and R.L. Williams‡

The ft-values of positon emitters are systematically larger than those of their negaton-emitting mirrors.[1] In the course of investigating this problem it has been found that many β-decay half-lives are unreliably determined; discrepancies between values reported in the literature of 10 or 20 standard deviations are by no means uncommon. It is therefore of importance to re-determine at least those half-lives that are based on few measurements particularly when discrepancies are evident. Cases in point are the half-lives of ^{13}B and ^{20}Na. In the former case no accurate direct measurement existed but only a ratio[2] of the half-life to that of ^{12}B which, when combined with the (accurately known) half life of ^{12}B yielded $t_{1/2}$ (^{13}B) = 17.6 ± 0.4 msec. In the latter case values of $t_{1/2}$ (^{20}Na) of 408 ± 6 msec[3] and 448 ± 4 msec[4] were available.

We made ^{13}B by the reaction $^{11}B(t,p)^{13}B$ using 3.0 MeV tritons from the Brookhaven National Laboratory 3.5 MV Van de Graaff, and determined the decay of the ^{13}B using a plastic scintillator to detect the beta-particles. We found $t_{1/2}(^{13}B) = 17.33 \pm 0.17$ msec. We made ^{20}Na by the reaction $^{20}Ne(p,n)^{20}Na$ using 16.5 MeV protons from the Brookhaven National Laboratory second MP tandem Van de Graaff. A plastic scintillator was again used to detect the decay beta-particles. We found $t_{1/2}(^{20}Na) = 442 \pm 5$ msec.

In order to determine an accurate ft-value the energy released in the β-decay must also be known accurately. The mass of ^{13}B was well known but not that of ^{20}Na. We determined the threshold for the reaction $^{20}Ne(p,n)^{20}Na$ as 15.420 ± 0.009 MeV to which corresponds $^{20}Na - {}^{20}Ne = 13.892 \pm 0.009$ MeV.

Combined with other data these results yield:

$$(ft)^+/(ft)^-_{A=13} = 1.166 \pm 0.026$$

$$(ft)^+/(ft)^-_{A=20} = 1.054 \pm 0.023.$$

It is not yet clear whether these results and the similar data from other A-values[1] reflect a lack of mirror symmetry in the relevant nuclear wave functions (which is possible but would be surprising) or whether a fundamental β-decay interaction is involved. In the parameterization that represents the phenomenon as due to an induced tensor interaction of coupling constant g_{IT} (see report on β-decay of ^8Li and ^8B, Sec. 8.1) we would have:

$$g_{IT}(A = 13) = (2.6 \pm 0.5) \times 10^{-3}$$

$$g_{IT}(A = 20) = (1.5 \pm 0.6) \times 10^{-3}.$$

These values are consistent with the value $g_{IT} \approx 2 \times 10^{-3}$ that emerged from the overall survey.[1] It appears, however, that the induced tensor explanation is not correct but that we have either a wave function effect or a momentum-transfer-independent effect. In the latter event our present values for $(ft)^+/(ft)^-$ should be directly compared with the mean $(ft)^+/(ft)^-$ value derived from all 9 positon-negaton emitting mirror pairs namely:

$$(ft)^+/(ft)^-_{mean} = 1.13.$$

---

* Brookhaven National Laboratory, Upton, New York.
† Princeton University, Princeton, N.J.
‡ Johns Hopkins University, Baltimore, Maryland.
1. D.H. Wilkinson, Phys. Letters *31B*, 447 (1970).
2. A. Maranes, A.J.P.L. Policarpo and W.R. Phillips, Nucl. Phys. *36*,45 (1962).
3. J.W. Surrier, A.J. Armini, R.M. Polichar, and J.R. Richardson, Phys. Rev. *163*, 1091 (1967).
4. N.S. Oakey and R.D. Macfarlane, Phys. Rev. Letters *25*, 170 (1970), and private communication.

8.4 β-Decay of ^{25}Na

D.E. Alburger* and D.H. Wilkinson

The A = 25 system is interesting because it was there that rotational motion in light nuclei was first clearly demonstrated.[1] In ^{25}Mg the $J^\pi = 5/2^+$ ground state and the $J^\pi = 7/2^+, 9/2^+$ states at 1612 and 3400 keV, respectively, may form the beginning of a $K^\pi = 5/2^+$ strong-coupling rotational band (Nilsson orbit 5) while the $J^\pi = 1/2^+, 3/2^+, 5/2^+, 7/2^+$ states at 585, 975, 1965, and 2738 keV, respectively, may form the beginning of a $K^\pi = 1/2^+$ band (Nilsson orbit 9). These bands are signalled by their level sequences and by their appropriately enhanced E2 transitions. It is clear, however, from internal evidence, that band-mixing is taking place because, for example, the interband $J^\pi = 5/2^+ \rightarrow 5/2^+$ transition is several times stronger than would be expected if the bands were pure. A further $K^\pi = 1/2^+$ band (Nilsson orbit 11) may start with the $J^\pi = 1/2^+, 3/2^+$ states at 2562 and 2801 keV, respectively.

Further structural information may be sought from the β decay of ^{25}Na and from the $T = 3/2 \rightarrow T = 1/2$ gamma-decays in ^{25}Al. The ground state of ^{25}Na is $J^\pi = 5/2^+$ which already argues that strong $K^\pi = 3/2^+, 5/2^+$ band mixing (Nilsson orbits 7 and 5 respectively) has depressed the $J^\pi = 5/2^+$ state below the $J^\pi = 3/2^+$ band head of the expected $K^\pi = 3/2^+$ lowest band. Detailed measurements on ^{25}Na decay to excited states of ^{25}Mg have recently been made and analyzed[2] as have $T = 3/2 \rightarrow T = 1/2$ γ decays[3] in ^{25}Al. These results show that the situation is indeed a complicated one demanding J-dependent mixing between the two above-mentioned $K^\pi = 1/2^+$ bands in addition to that already noted between the $K^\pi = 5/2^+$ and $1/2^+$ bands. In particular, it is difficult to reconcile the ft-value for ^{25}Na decay to the $J^\pi = 3/2^+$ 975 keV state of ^{25}Mg (log ft = 5.05 ± 0.03) with that for decay to the $J^\pi = 5/2^+$ 1965 keV state (log ft = 6.00 ± 0.07) if those states are indeed members of a $K^\pi = 1/2^+$ band even when mixing with the other bands is allowed. If, in addition, the 2738 keV state is indeed of $J^\pi = 7/2^+$ and belongs to the same $K^\pi = 1/2^+$ band as the $J^\pi = 3/2^+$ and $5/2^+$ states just mentioned, as it is supposed to do, the experimental result of the present work, log ft > 6.5, becomes awkward to assimilate for the rotational model.

The recent work of Jones *et al.*[2] determined relative β-ray branching ratios to states of ^{25}Mg but, for the associated absolute ft-values and for the important ft-value to the ground state, had to rely on an early[4] determination of the ground-state branching ratio of unknown accuracy.

Our work had two objectives: (i) to determine the relative β branches of ^{25}Na to the excited states of ^{25}Mg and, in particular, to search for the β transition to the 2738 keV level; (ii) to determine the ground-state β branch.

^{25}Na was made by ^{23}Na(t,p)^{25}Na at the Brookhaven National Laboratory Van de Graaff and its radiations were investigated by means of Ge(Li), plastic, and NaI(Tℓ) detectors. From β-γ coincidence experiments the ^{25}Na β-ray branch to the ground state of ^{25}Mg is 62.5 ± 2.0%. Other β-ray and γ-ray branches were derived from the γ-ray spectrum and are in agreement with previous results. From both singles and γ-γ coincidence measurements a limit of <0.02% (log ft > 6.5) is placed on the β-ray branch to the 2738-keV $J^\pi = 7/2^+$ state of ^{25}Mg. The experimental results are summarized in Fig. 8.4-1.

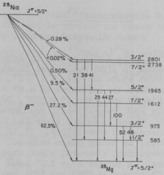

Fig. 8.4-1. β-decay of ^{25}Na.

Shell model calculations have been performed[5] in the $(1d_{5/2}-2s_{1/2})^{A-16}$ basis. This model predicts for the β-transitions to the ground, 975 , 1612 , 1965 , 2738 , and 2801 keV states the following log ft values which are individually followed by our respective experimental numbers (in parentheses): 4.33 (5.26); 4.55 (5.05); 4.42 (5.04); 5.62 (6.00); 6.14 (>6.5); 4.10 (5.20), respectively. The general trend of the theoretical numbers follows experiment quite closely: theory gives a satisfactory account of the relative transition strengths to the 975, 1965 , and 2738 keV states, in particular of the surprisingly weak decay to the $J^\pi = 7/2^+$ 2738-keV state. The strong-coupling collective model, which pictures these states as members of a $K^\pi = 1/2^+$ band, can only understand this situation in a complicated ad hoc manner; we may here be receiving the suggestion that the shell model, even in its present truncated form, provides an account of certain dynamical properties preferable to that of the collective model. Note that if an arbitrary addition of 0.7 were made to the above theoretical log ft values agreement between theory and experiment would become excellent and, in particular, that the experimental limit on the strength of the decay to the 2738 keV state would conform to theoretical expectation. This empirical factor of 5 is to be compared with the factor of 3 by which, typically, Gamow-Teller transitions calculated in the $(1d_{5/2} - 2s_{1/2})^{A-16}$ basis exceed in speed those calculated in the full $(1d_{5/2} - 2s_{1/2} - 1d_{3/2})^{A-16}$ basis (which cannot yet be applied to the A = 25 system).

---

* Brookhaven National Laboratory, Upton, New York.

1. A.E. Litherland, H. McManus, E.B. Paul, D.A. Bromley, and H.E. Gove, Can. J. Phys. *36*, 378 (1958).
2. A.D.W. Jones, J.A. Becker, R.E. McDonald, and A.R. Polette, Phys. Rev. *C1*, 1000 (1970).
3. G.C. Morrison, D.M. Youngblood, R.C. Bearse, and R.E. Segel, Phys. Rev. *174*, 1366 (1968).
4. D. Maeder and P. Staehelin, Helv. Phys. Acta *28*, 193 (1955).
5. J.B. McGrory, to be published.

8.5 Finite Nuclear Size and Radiative Corrections in the Construction and Assessment of Kurie Plots for Allowed Beta-Decay

D. H. Wilkinson

If only a small fraction of a beta-spectrum is available for Kurie plot analysis because of the existence of strong branches of lower energy it may become important to take into account finite nuclear size and radiative effects in the construction and assessment of the Kurie plot. Failure to do this may result in errors of many percent in the extraction of the intensity of the high energy beta-branch.

$$F(Z,W) = 2(1+\gamma)[\Gamma(2\gamma+1)]^{-2}(2pR)^{2(\gamma-1)}\, e^{\pi\alpha ZW/p}|\Gamma(\gamma + i\alpha ZW/p)|^2.$$

Use of F(Z,W) implies point charge electron wave functions, with no allowance for their curvature, evaluated at the nuclear surface together with neutrino wave functions evaluated at the nuclear centre. This requires correction in three respects: (i) electron wave functions appropriate to the finite nuclear charge distribution should be used; (ii) curvature of the lepton wave functions (finite de Broglie wave length effects) must be taken into account; (iii) the lepton wave functions should be appropriately integrated through the nuclear volume.

These effects have been considered elsewhere.[1] With:

$$F_0(Z,W) = \frac{2}{1+\gamma} F(Z,W)$$

we have

$$L_0 = [2p^2 F_0(Z,W)]^{-1} [f_1^{\;2} + g_{-1}^{\;2}]_{r=R}$$

where the f_1, g_{-1} are generated by the finite nuclear charge distribution. An accurate parameterization of L_0 has been given[1] that, to lowest order in the small quantities reads:

$$L_0 \approx 1 - \frac{7}{20}(\alpha Z)^2 - \frac{28}{15} WR\alpha Z - \frac{8}{15}\frac{R\alpha Z}{W} - \frac{1}{3}(pR)^2 \ldots \qquad (1)$$

Use of this L_0, or its more accurate version, then accomplishes simultaneously the first two corrections mentioned above: we replace F(Z,W) by $F_0(Z,W)L_0$ and replace f by $f(1+\varepsilon_{1,2})$; $\varepsilon_{1,2}$ derived from L_0, has been presented elsewhere.[1]

To effect the third correction we must reveal a prejudice about the nucleon wave functions involved. For the purposes of the present orientation we follow the earlier model[1] and take the nucleon wave functions as constant throughout the nuclear volume. To lowest order in the corrections the electron wave functions behave like:

$$f_1^{\;2}, g_{-1}^{\;2} \sim 1 - \frac{1}{3}\{[W + 3\alpha Z/(2R)]^2 - 1\}r^2$$

and the neutrino wave functions:

$$\psi_\nu^2 \sim 1 - \frac{1}{3}(W_0 - W)^2 r^2.$$

Allowance for integration through the nucleon volume then results in further replacing $F_0(Z,W)L_0$ by $F_0(Z,W)L_0 I$ where:

$$I = 1 + \frac{1}{5} R^2 [\frac{2}{3} \{[W + 3\alpha Z/(2R)]^2 - 1\} - (W_0 - W)^2]$$

and replacing $f(1 + \varepsilon_{1,2})$ by $f(1 + \varepsilon_{1,2} + \varepsilon_3)$; ε_3 has been presented elsewhere.[1]

Radiative corrections divide into two classes: the "inner" radiative corrections that, so far as nuclear beta-decay is concerned, merely renormalize the coupling constants, and the "outer" radiative corrections that affect the spectrum.[2] To order α the latter corrections may be represented by replacing $F(Z,W)$ by

$$F(Z,W)[1 + \frac{\alpha}{2\pi} g(W,W_0)]$$

which then entrains the replacement of f by $f[1 + \delta^R(Z,W_0)]$. $\delta^R(Z,W_0)$ has been presented elsewhere[2] and:

$$g(W,W_0) = 3 \ln M - \frac{3}{4} + 4[\frac{\tanh^{-1}\beta}{\beta} - 1][\frac{(W_0 - W)}{3W} - \frac{3}{2} + \ln\{2(W_0 - W)\}]$$

$$+ \frac{4}{\beta} L(\frac{2\beta}{1 + \beta}) + \frac{1}{\beta} [\tanh^{-1}\beta][2(1 + \beta^2) + \frac{(W_0 - W)^2}{6W^2} - 4 \tanh^{-1}\beta] \ldots$$

Here L(x) is the Spence function:

$$L(x) = \int_0^x \frac{\ln(1 - t)}{t} dt.$$

Putting together the above corrections leads to:

$$S(Z,W) = F(Z,W) \frac{2}{1 + \gamma} L_0 I[1 + \frac{\alpha}{2\pi} g(W,W_0)]$$

which should be used instead of $F(Z,W)$ in constructing Kurie plots, and to:

$$f_S = f[1 = \varepsilon_{1,2} + \varepsilon_3 + \delta^R(Z,W_0)]$$

which should be used instead of f in assessing Kurie plots, and so to:

$$\frac{N_S^t}{N_F^t} \approx [1 + \varepsilon_{1,2} + \varepsilon_3 + \delta^R(Z,W_0)] \frac{1 + \gamma}{2} \{(L_0 I)^{-1} [1 - \frac{\alpha}{2\pi} g(W,W_0)]\}_{W_1 \text{ to } W_0}$$

where N_S^t is the correct total number of events in the spectrum and N_F^t is the incorrect number that would be deduced by use of F(Z,W). W_1 is the energy above which the beta-spectrum is analyzed.

Figures 8.5-1 and 8.5-2 show the finite size correction for negatons and positons respectively using the low-Z approximation to L_0 of expression (1) above. Figure 8.5-3 shows the radiative correction.

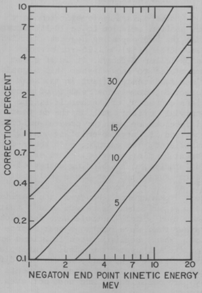

Fig. 8.5-1. The correction to the intensity for negaton emission due to the finite nuclear size effects. The correction is evaluated at $W_1=W_0$ and is positive i.e., the effect of applying the correction to data that have been reduced using F(Z,W) is to increase the estimated intensity. The numbers on the curves are the Z-values.

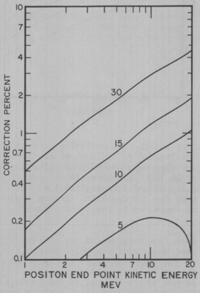

Fig. 8.5-2. The correction to the intensity for positon emission due to the finite nuclear size effects. The correction is evaluated at $W_1=W_0$ and is negative i.e., the effect of applying the correction to data that have been reduced using F(Z,W) is to decrease the estimated intensity. The numbers on the curves are the Z-values.

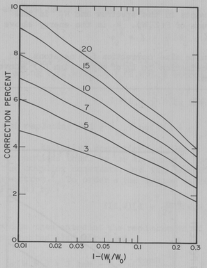

Fig. 8.5-3. The radiative correction to the intensity. The numbers on the curves are the electron end point kinetic energy in MeV. The correction is positive, i.e., intensities estimated without regard for the radiative effects should be increased by the amount shown.

1. D.H. Wilkinson, Nucl. Phys. *A158*, 476 (1970).
2. D.H. Wilkinson and B.E.F. Macefield, Nucl. Phys. *A158*, 110(1970).

8.6 Binding Energy Effects in Mirror Gamow-Teller β-Decay

D.H. Wilkinson

There is a systematic tendency for positon emission to be 10-15% slower than the corresponding negaton emission[1] i.e., $(ft)^+/(ft)^- \approx 1.15$ for mirror Gamow-Teller β-decays. It is of great importance to know whether this signals a new fundamental effect in the weak interaction, namely the reality of second class currents, or whether it is due to "trivial" effects such as the *de facto* differences between the positon-emitting body and its negaton-emitting analog associated, for example, with their different binding energies. Earlier careful studies of the binding energy effects[2] suggested that these could not be big enough to account for the experimental phenomenon. However, the earlier studies suffered the severe defect that they used single-particle wave functions rather than wave functions that reproduce the ft-values of the bodies in question. When realistic wave functions are used that involve several parent states p of the A-1 system the ensuing interplay of the many components to the total β-decay amplitude, each carrying its own different single-particle overlap $O_p(j_1j_2)$, the difference in the total $\beta^\pm$ moments is not simply related to the $O(j_1j_2)$ of any particular parent and need not even have the same sign as that for a single parent.

Good wave functions are available[3] for the 4 1p-shell systems A = 8,9,12 and 13 all of which have similar large energy releases and which show large and broadly concordant values of $(ft)^+/(ft)^-$. These wave functions are being used to evaluate the binding energy effect, the associated individual nucleon wave functions, different for each parent state, from whith the $O_p(j_1j_2)$ are derived, being evaluated in standard Saxon-Woods potentials with spin-orbit coupling adjusted in depth to give the separation energies appropriate to each parent state.

For the transition $J_i \rightarrow J_f; T_i \rightarrow T_i - 1$ we have:

$$\Lambda^{\frac{1}{2}} = N[3(2J_f + 1)(2 - 1/T_i)]^{\frac{1}{2}} \sum_{j_1 j_2} \sum_{p} (-)^{J_p+j_1+j_2} [(2j_1 + 1)(2j_2 + 1)]^{\frac{1}{2}} \times$$

$$\begin{Bmatrix} j_1 & j_2 & 1 \\ J_f & J_i & J_p \end{Bmatrix} \begin{Bmatrix} j_1 & j_2 & 1 \\ \frac{1}{2} & \frac{1}{2} & 1 \end{Bmatrix} \langle f\{|pj_2\rangle\langle i\{|pj_1\rangle \, O_p(j_1 j_2)$$

where J_p, j_1 couple to J_i; J_p, j_2 couple to J_f and $N = A - 4$ [log ft = 3.63 - log Λ].

This approach, while greatly superior to the earlier one[2] using a single parent (and single j-value) is still approximate and must be expected to exaggerate the magnitude of the actual effect. If we call the ft-value ratio computed in this way $[(ft)^+/(ft)^-]_B$ we have:

A	$(ft)^+/(ft)^-$	$[(ft)^+/(ft)^-]_B$
8	1.107±0.011	1.039
9	1.19 ±0.03	0.950
12	1.113±0.009	1.146
13	1.166±0.026	1.047

These theoretical numbers have not yet been corrected for transitions to excited states that are included in the experimental figures but this will not change things greatly. It is to be noted that the spread in theoretical ratios is greater than that in the experimental ratios; this is to be expected if the theoretical model indeed exaggerates the effect.

A further factor which is under computation, but for which results are not yet available, concerns the transformation suffered, in the β-transition, of the "rest of the nucleus" which has so far been regarded as a simple spectator. It is clear that this will also affect the ft-value ratio but the magnitude and sense of the correction are not yet known.

---

1. D.H. Wilkinson, Phys. Letters *31B*, 447 (1970).
2. R.J. Blin-Stoyle and M. Rosina, Nucl. Phys. *70*, 321 (1965).
3. S. Cohen and K. Kurath, Nucl. Phys. *73*, 1 (1965).

8.7 Parameterization of Relativistic Electron Wave Functions

R. E. Marrs and D.H. Wilkinson

It is usual to discuss allowed nuclear beta-decay through use of the Fermi function:

$$F(Z,W) = 2(1+\gamma)[\Gamma(2\gamma+1)]^{-2}\,(2pR)^{2(\gamma-1)}\,e^{\pi\alpha ZW/p}|\Gamma(\gamma+i\alpha ZW/p)|^2$$

which effectively evaluates at the nuclear radius R j = 1/2 wave functions generated by a point charge but without regard for their curvature (de Broglie wave length effect). For the most accurate work such as the evaluation of Fermi transitions and the comparison of mirror Gamow-Teller transitions it is necessary to generate the wave functions in a finite nuclear charge distribution of "realistic" type and to allow for the de Broglie curvature, i.e., use the higher terms in the expansion of the hypergeometric function. (It is also necessary to allow for the variation of the electron, and neutrino, wave functions through the nuclear volume).

These questions have recently been discussed[1] and the corrections to F(Z,W) presented in a parameterized form that makes their use in computation convenient and that also has advantages for analytical work. These parameterizations[1] effect corrections to F(Z,W) in the usual sense of continuing to refer the electron wave functions to the nuclear surface. This procedure arises historically because the point-charge wave functions diverge at the origin. However, wave functions generated in the field of a finite charge distribution are finite at the origin and it may be argued that their evaluation at the origin is preferable to their evaluation at the nuclear surface. The most recent and extensive numerical tabulation of relativistic electron wave functions generated by finite charge distributions[2] indeed refer to the origin. We are exploring methods of parameterizing these data as was done earlier[1] for the less-extensive tabulations referring to the nuclear surface. It is our intention to discover parameterizations that will suffice for all ranges of W that may be of eventual interest, i.e., up to $W \approx 50$ such as may be found far from the stability line throughout the periodic table. It is not yet clear whether the best solution will be a completely ad hoc parameterization or one guided by the theoretical expectation that is available for the lowest powers of αZ and WR.

1. D.H. Wilkinson, Nucl. Phys. *A158*, 476 (1970).
2 H. Behrens and J. Jänecke, *Landorf Börnstein Tables*, Group I, Vol. 4 (Springer, Berlin, Heidelberg, New York, 1969).

8.8 Double Electron Pair Creation

D.E. Alburger* and D.H. Wilkinson

Normal electron pair creation by a photon in the Coulomb field of a nucleus is a purely electromagnetic process that goes by diagrams such as:

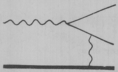

and that, in the extreme relativistic (ER) limit has the cross section (omitting constant terms):

$$\sigma_1 = Z^2 r_0^{\ 2} \ \alpha \ \frac{28}{9} \ln \frac{h\nu}{mc^2} \ .$$

As a higher-order process we may anticipate the occasional production of two electron pairs in a single photon-nucleus encounter through diagrams such as:

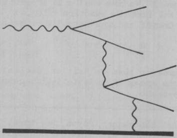

By simple counting of eγ vertices we should expect the probability for such double pair creation to be down on that for single pair creation by the factor R where $R \approx \alpha^{-2}$. Heitler[1] has, however, suggested that $R \approx \alpha^{-1}$ although he gives no reasoning. The only explicit estimate of σ_2, the cross section for double electron pair creation, appears to be that, deriving from an ER calculation,[2] of:

$$\sigma_{\gamma\gamma\rightarrow 2e^\pm} \approx \frac{40\alpha^2 r_0^{\ 2}}{9\pi} \ .$$

It has been pointed out[3] that this cross section may be simply related to that for double pair creation by photons:

$$\sigma_2 = Z^2 \frac{\alpha}{\pi} \left[\ln \frac{h\nu}{mc^2}\right]^2 \sigma_{\gamma\gamma\rightarrow 2e^\pm} ,$$

so that in the ER limit we have the prediction:

$$R_{ER} \approx [\frac{10}{7} (\frac{\alpha}{\pi})^2 \ \ln \frac{h\nu}{mc^2}]^{-1}$$

which contains the expected factor of α^{-2}.

Higher order processes are of some interest and promise to become more interesting. We have therefore undertaken a measurement, although not in the ER limit, in an attempt to determine R at 6.13 MeV.

When a Ge(Li) counter is irradiated by gamma-rays of high enough energy one sees a "full energy" peak and, due to pair creation followed by escape from the crystal of one or both annihilation quanta, "one escape" and "two escape" peaks . If the double pair creation process takes place we shall also see "three escape" and "four escape" peaks. [These will also arise from successive lower order processes, for example pair creation followed by bremsstrahlung from one of the electrons and a further pair creation so that if an experimental effect is seen the successive lower order processes must be eliminated before observation of the true double creation process may be claimed. This problem does not arise if only a limit is claimed.] We have used a 15 cc Ge(Li) counter irradiated with gamma radiation of 6.13 MeV from the reaction $^{19}F(p,\alpha)^{16}O$ at the Brookhaven National Laboratory Van de Graaff and have established a present limit:

$$R_{exp} > 6.5 \times 10^3.$$

This is about 50 times greater than the Heitler[1] estimate of α^{-1} but is still some 8 times less than the above ER estimate (which cannot be very reliable at 6 MeV) of Lipatov-Frolov-Serbo.

---

* Brookhaven National Laboratory, Upton, New York.

1. W. Heitler, *Quantum Theory of Radiation*, 3rd Edition (Oxford University Press, Oxford), p. 228.
2. L.N. Lipatov and G.V. Frolov, JETP Letters *10*, 254 (1969)(corrected by V.G. Serbo).
3. V.G. Serbo, JETP Letters *12*, 39 (1970).

9.1 Comparison of the (d,t) and (d,^{3}He) Reactions on ^{25}Mg at 21 MeV

M. Baker, J.R. Calarco, N.S. Chant, J.G. Cramer, D.L. Johnson, and H. Wieman

Direct reactions which proceed from a given initial state to analog final states serve as an experimental test of the charge independence of nuclear forces. Many experiments have been performed using light nuclei as targets where tritons and ^{3}He ions were detected simultaneously and the cross sections to analog final states determined.[1,2] This technique is advantageous in that the ratio of differential cross sections does not require the determination of target thickness, detector solid angle, or the number of particles incident on the target. These advantages are somewhat compromised by the necessity of performing particle identification under less than ideal circumstances, i.e., it is necessary to simultaneously separate tritons from deuterons and ^{3}He ions from alpha particles. Often the intensity of deuterons and alpha particles incident on the detector is much higher than that of the particles of interest.

For these direct reactions the differential cross sections are related in the following way:

$$\frac{d\sigma/d\Omega(t)}{d\sigma/d\Omega(^3He)} = \frac{k_t}{k_{^3He}} \frac{|M_t|^2}{|M_{^3He}|^2}.$$

If the reactions proceed by the direct transfer of a single nucleon (i.e., (d,t) and (d,^{3}He)) and if the nuclear states involved in the transition have "pure" isospin and the interaction conserves isospin, the theoretical ratio of the amplitudes is given by:

$$\frac{|M_t|^2}{|M_{^3He}|^2} = \frac{(0\ 0\ \frac{1}{2}\,\frac{1}{2}\,|\,\frac{1}{2}\,\frac{1}{2})^2 (T_t{+}\frac{1}{2}\ \ T_t{-}\frac{1}{2}\ \ \frac{1}{2}\,\frac{1}{2}\,|\,T_t T_t)^2}{(0\ 0\ \frac{1}{2}\,{-}\frac{1}{2}\,|\,\frac{1}{2}\,{-}\frac{1}{2})^2 (T_t{+}\frac{1}{2}\ \ T_t{+}\frac{1}{2}\ \ \frac{1}{2}\,{-}\frac{1}{2}\,|\,T_t T_t)^2} = \frac{1}{2T_t + 1}$$

where T_t is the isospin of the target.

Harris[3] has recently pointed out that the expression for the ratio of the differential cross sections is more complicated if one considers two-nucleon transfer reactions (i.e., (p,t) and (p,^{3}He)) to analog final states of the same isospin as the target. The reason is basically that if one considers other than $T_t = 0$ targets there are two total-isospin channels through which the reaction may proceed. For the deuteron-induced reactions there is only one.

In the (p,t)-(p,^{3}He) measurement of Hardy *et al.*[1] there is one experimental ratio of cross sections which is different from the theoretically expected value by more than one standard deviation. Using a ^{26}Mg target they obtained an experimental ratio of 2.50 ± .30 where the theoretical value was 1.86. This result could be merely a statistical fluctuation. If this is not the case, the result either yields information about the form of the isoscalar nuclear interaction or implies some degree of isospin non-conservation in the reaction.

In an attempt to minimize the number of possible explanations for this exceptional result we have performed an experiment which leads to the same final states but can proceed via only one isospin channel. The theoretically predicted result is therefore independent of the form of the isoscalar interaction.

We have measured differential cross sections for the $^{25}Mg(d,t)^{24}Mg^{*}(9.517; T = 1)$ and $^{25}Mg(d,{}^{3}He)^{24}Na(g.s.)$ reactions at laboratory angles between 10 and 60 degrees using 21 MeV deuterons from the University of Washington 3-stage Van de Graaff accelerator. The targets were constructed by evaporating isotopically enriched ^{25}Mg(99.2%) onto a 10 μg/cm^2 ^{12}C backing to a thickness of approximately 75 - 125 μg/cm^2.

The reaction products were detected by a ΔE-E telescope consisting of a 50μ thick totally depleted silicon (ΔE) detector and a 2 mm thick lithium-drifted silicon (E) detector. Coincident pulses from the two detectors were fed to the SDS-930 on-line computer where particle identification was determined numerically. Windows were established in the identification spectrum so that 1024 channel energy spectra for deuterons, tritons, ^{3}He's, and alpha particles could be collected simultaneously. The signal from a pulser triggered at a rate proportional to the incident beam flux was split and sent through attenuators to the preamplifiers of the ΔE and E counters. The relative sizes of the attenuators were chosen so that the amplified signals from the pulser woulc simulate a "particle" for which the value of $(E + \Delta E)^b - (E)^b$ was less than that for ^{3}He's but greater than that for tritons.

The particle identification spectrum obtained with the telescope at a laboratory angle of 40° is shown in Fig. 9.1-1. A line has been drawn through the data in the region of the hydrogen isotopes in an attempt to clarify the trend of the closely spaced data points. The deuteron-triton and ^{3}He-α separation is quite good, especially in view of the fact that the intensities of the particles of interest are approximately a factor of ten smaller than the adjacent particles in each case. The ^{3}He bin in the identification spectrum was chosen to include the pulser "particle". The pulse heights for the simulated E and ΔE signals were chosen so that the pulser events did not fall in a region of interest in the ^{3}He energy spectrum.

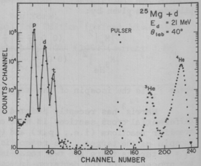

Fig. 9.1-1. Particle identification spectrum obtained at a laboratory angle of 40°.

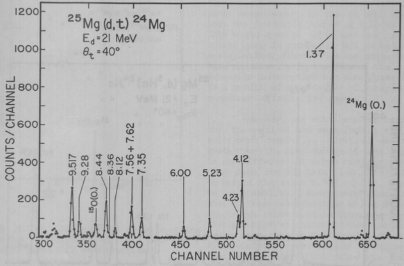

Fig. 9.1-2. Triton energy spectrum obtained at a laboratory angle of 40°.

The triton and ^{3}He energy spectra obtained at a laboratory angle of 40° are shown in Figs. 9.1-2 and 9.1-3 respectively. Lines have been drawn through the data points in the region of the prominent peaks to clarify the figures. Peaks resulting from reactions on the ^{12}C and ^{16}O contaminants are evident in the spectra and the known states[4] in ^{24}Mg and ^{24}Na which are clearly populated by these reactions are labeled with their excitation energies. There is one peak which appears in all the ^{3}He energy spectra whose origin is not certain. The energy variation of this group with angle is consistent with that of a state in ^{24}Na at an excitation energy of 2.90 MeV. There is no evidence for "feedthrough" of an alpha group in this energy region. Also, the Q values for the (d,^{3}He) reaction on the other isotopes of Mg which were present in the target are such that a very large cross section to what is now an unknown state in ^{25}Na or ^{23}Na would be required to produce the ^{3}He group observed. There is the possibility of detecting ^{3}He ions from other contaminants in this mass region, e.g., ^{23}Na or ^{27}Al. This is being carefully considered but the chances seem remote that this is the case. A more complete survey of the recent literature is in progress.

The recently discovered[5] 1.51 MeV state in ^{24}Na is populated quite strongly by this reaction. This is of some interest because this state is not populated by the ^{23}Na(d,p) reaction[6] but is observed in the ^{26}Mg(d,α) reaction.[5] It is hoped that an angular distribution for this state can be obtained from our data

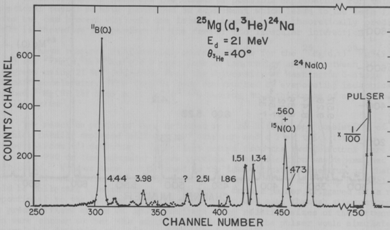

Fig. 9.1-3. ^{3}He energy spectrum obtained at a laboratory angle of 40°.

and spectroscopic information extracted. There is evidence for the analog of this 1.51 MeV state in some of the triton energy spectra obtained although the statistics are poor. This information could be useful as well since the Alberta group[7] was unable to find this state in ^{23}Na(d,n).

Angular distributions have been extracted from our energy spectra for the reactions which lead to the ^{24}Na ground state and its analog in ^{24}Mg. The differential cross sections for both reactions are plotted as a function of center-of-mass angle in Fig. 9.1-4. The ratio of differential cross sections integrated over center-of-mass angles from 10° to 70° is 0.484 ± 0.010 where the uncertainty is only that due to counting statistics. The theoretical calculation yields:

$$\frac{d\sigma/d\Omega(d,t)}{d\sigma/d\Omega(d,{}^{3}He)} = \frac{k_t}{k_{^3He}} \frac{1}{2T_t + 1} = 0.415.$$

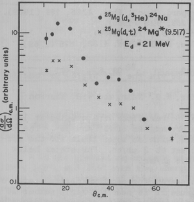

Fig. 9.1-4. Differential cross sections for the $^{25}Mg(d,{}^{3}He)^{24}Na(g.s.)$ and $^{25}Mg(d,t)^{24}Mg^{*}(0.517\ MeV)$ reactions.

Thus, our result is consistent with the Hardy measurement, in that we find more than the predicted number of tritons. This would seem to imply that the exceptional case in the Hardy data is neither a statistical fluctuation nor caused by some peculiarity in the form of the isoscalar interaction but more generally is a result of some degree of isospin nonconservation in the reaction.

However, one must consider both the theoretical and experimental results more carefully. First, if we integrate over the same center-of-mass angles in our differential cross sections as Hardy does for his data (i.e., 15-45°) we obtain the value 0.447 ± 0.010. Thus, we can numerically demonstrate what is obvious from consideration of Fig. 9.1-4; the triton cross section becomes relatively larger at center-of-mass angles larger than that at the position of the first minimum in the angular distribution. This observation raises the following question: Over what angular range should we perform the integration of the differential cross section? The obvious answer is that the angular range should be that for which the best theoretical results can be obtained. Hardy *et al.* claimed that the expression $k_t/k_{^3He}$ would reproduce the DWBA part of the integrated cross section ratio over their angular range of integration to better than 5%. Since the center-of-mass energy in our experiment is only ∿9-13 MeV we do not feel that $k_t/k_{^3He}$ is sufficiently accurate for analyzing our results.

If reliable DWBA calculations can be made, the ratio $k_t/k_{^3He}$ can be replaced by the ratio of integrated DWBA cross sections. Using optical model parameters from the literature,[8-10] calculation of these differential cross sections has been attempted using the program DWUCK. So far, the results have been highly dependent on the choice of optical model parameters for the outgoing particles. It is hoped that a suitable choice of optical model parameters can be made and a reliable region of angular integration determined.

---

1. J.C. Hardy, H. Brunnader, and Joseph Cerny, Phys. Rev. Letters *22*, 1439 (1969).
2. M. Gaillard, R. Bouché, L. Feuvrais, P. Gaillard, A. Guichard, M. Gusakow, J.L. Leonhardt, and J.R. Pizzi, Nucl. Phys. *A119*, 161 (1968).
3. Samuel M. Harris, Phys. Rev. *C1*, 362 (1970).
4. P.M. Endt and C. Van Der Leun, Nucl. Phys. *A105*, 1 (1967).
5. R. Jahr, J.A.H. Pfleger, and H. Zell, Phys. Letters *25B*, 113 (1967).
6. V.M. Zabegai, A.E. Melenevskii, O.F. Nemets, and V.N. Nemykin, Sov. J. Nucl. Phys. *11*, 155 (1970).

7. S.M. Tang, B.D. Sowerby, and D.M. Sheppard, Nucl. Phys. *A125*, 289 (1969).
8. C.M. Perey and F.G. Perey, Phys. Rev. *152*, 923 (1966).
9. R.N. Glover and A.D.W. Jones, Nucl. Phys. *81*, 268 (1966).
10. J.M. Joyce, R.W. Zurmühle, and C.M. Fou, Nucl. Phys. *A132*, 629 (1969).

9.2 Search for Negative Parity States of ^{42}Sc via the ^{39}K(^{6}Li,t)^{42}Sc Reaction

J.R. Calarco, J.G. Cramer, R.H. Heffner, K.G. Nair, and W.R. Wharton

The ^{39}K(^{6}Li,t)^{42}Sc and the ^{39}K(^{6}Li,d)^{43}Sc reactions were studied at laboratory energies of 26 and 32 MeV and laboratory angles of 25° and 35°. The cross sections were found to be discouragingly small, with an upper limit for the differential cross section to any state of ^{42}Sc set at 2 μb/sr. For states below 3 MeV excitation in ^{42}Sc the upper limit is 0.8 μb/sr.

The purpose of this experiment was to search for negative parity states of ^{42}Sc. The $^{42}_{21}$Sc$_{21}$ nucleus is interesting because it is near the magic number 20 for both protons and neutrons. The low lying negative parity states are described in shell model notation as 3 particle-1 hole states (3 particles in the 3p-1f shell and one vacancy in the 2s-1d shell), 5 particle-3 hole states, etc.

No negative parity states have been identified in ^{42}Sc although the isobaric analogs of the negative parity T = 1 states have been seen in ^{42}Ca.[1] The probable reason that these negative parity states have not been identified in ^{42}Sc is that few reactions favor formation of these states. We have chosen the reaction ^{39}K(^{6}Li,t)^{42}Sc in the belief that this reaction, if it is a direct three nucleon transfer reaction, will populate the negative parity states of ^{42}Sc much more strongly than the positive parity states. This will be true if the three particles are transferred as a cluster so that they all fall in the same major shell (3p-1f). If the cluster transfer mechanism is valid, the ^{39}K(^{6}Li,d)^{42}Sc reaction should preferably populate the positive parity 4 particle-1 hole states of ^{43}Sc. Indeed we found clearly identifiable peaks as large as 7 μb/sr in the energy spectrum which were at the correct energies to be identified with known positive parity states of ^{43}Sc. However, the resolution was about 120 keV and more work would be necessary to make unique identification of the peaks.

The experiment was carried out using a ΔE-E telescope to identify tritons and deuterons. The solid angle of acceptance of the detector was 2.2×10^{-4} sr. The target was KI on a 10 μg/cm^2 ^{12}C backing. Target thickness was measured from Coulomb scattering of ^{6}Li^{+++} from iodine. Because of the low cross sections we obtained all our data with a thick 320 μg/cm^2 KI target which caused an energy loss of 120 keV in the ^{6}Li^{+++} beam at 32 MeV. This coupled with kinematic broadening of around 70 keV made the resolution too poor for our data to be of much use. Although our Li-source[2] is capable of providing ≥ 1 μamp of ^{6}Li^{+++} on target, we found that the target rapidly degenerated with beams > 300 namp. Also, the elastic scattering of ^{6}Li from ^{127}I caused a high count rate of saturated pulses in the ΔE detector which spread out and shifted the I.D. spectrum, and to a lesser extent the energy spectra. Because of these problems, we found the experiment unfeasible at this time. If later it is possible to use the spectrograph with an enlarged acceptance angle, the experiment may be resumed.

---

1. R. Sherr, G. Crawley, and W. Benenson, Bull. Amer. Phys. Soc. *14*, 1222 (1969); R. Sherr, private communication.
2. Section 2.5 of this report.

9.3 Analog States in ^{88}Sr Observed with the Reaction ^{87}Rb(p,p$_0$)^{87}Rb

M. Hasinoff, K.G. Nair, and J.E. Spencer*

Additional measurements of the proton elastic scattering excitation functions for ^{87}Rb have been made. (The earlier work[1] has been reported in the Stanford Nuclear Physics Laboratory Annual Report.)

In the present experiment we have measured the p_0 yield at $\theta_{c.m.} = 90°$, 125°, 140°, and 165° over the energy regions 5.0 to 6.1 MeV and 7.3 to 8.3 MeV using $^{87}RbNO_3$ targets of thickness 50 and 150 μg/cm^2 respectively. The latter region was previously studied only in steps of 100 keV and the states seen in the (p,γ_0) and (p,γ_1) reactions[2] on ^{87}Rb were not observed. Since the proton partial widths must be known in order to extract the gamma decay widths for these levels we have undertaken these measurements. Another interest is the extension of the generalized optical potential model,[3] which has successfully described the ^{88}Sr + p system, by applying it to the neighboring systems of ^{89}Y + p and ^{87}Rb + p.

Figure 9.3-1 shows the data obtained for this reaction. The 4 lowest levels are produced by the coupling of the $d_{5/2}$ proton single particle orbital to the $(p_{3/2})^{-1}$ ground state configuration of ^{87}Rb which gives $1^-, 2^-, 3^-$, and 4^- states. The analog of the ^{88}Rb ground state at E_p = 5.09 MeV is known to be a 2^- level. By comparison with the (p,γ_0) and (p,γ_1) data we propose the spin ordering $2^-, 3^-, 4^-$, and 1^- for this quartet. The levels between 5.9 MeV and 7.3 MeV are more numerous than one would expect from coupling the $s_{1/2}$ and $d_{3/2}$ single particle proton orbitals to the $p_{3/2}{}^{-1}$ proton hole and thus it appears that these single particles states are fragmented by coupling to other open channels such as core excitations. All states observed in the (p,γ_0),(p,γ_1) or (d,p)[4] reactions between $E_x(^{88}Rb)$ = 2.1 → 3.1 MeV (E_p = 7.3 → 8.3 MeV) are seen in the (p,p_0) channel.

The analysis of these data to obtain the resonance parameters is in progress.

* Physics Department, Stanford University.

1. Nuclear Physics Laboratory Annual Report, Stanford University (July 1970), p. 58.
2. M. Hasinoff, Ph.D. Thesis, Stanford University, 1970.
3. J.E. Spencer, E.R. Cosman, H.A. Enge, and A.K. Kerman, Phys. Rev. *C3*, 1179 (1971).
4. J.A. Rapaport, M.N. Rao, R.L. Robinson, and J.L.C. Ford, Jr., Bull. Am. Phys. Soc. *14*, 1201 (1969).

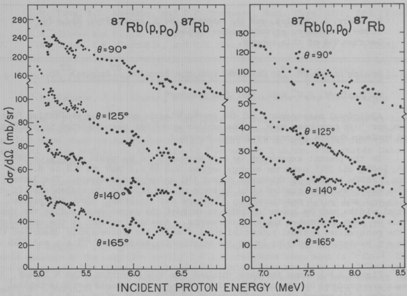

Fig. 9.3-1. Yield curves for the $^{87}Rb(p,p_0)^{87}Rb$ reaction at $\theta_{c.m.}$ = 90°,125°, 140°, and 165°.

9.4 Search for the Isospin Allowed Neutron Decay of the $T_>$ Giant Dipole Resonance in ^{90}Zr Using the Reaction $^{89}Y(p,n_A)^{89}Zr_A$

J.R. Calarco, M. Hasinoff, and H. Wieman

Several (p,γ) experiments[1,2] have recently observed a splitting of the giant dipole resonance into two main components which are predicted[3] to have different isospin quantum numbers. However the (p,γ) experiments do not determine the isospin of the observed levels since both $T_>$ and $T_<$ levels can decay to the ground state ($T = T_<$) by E1 radiation. Isospin selection rules prohibit the $T_>$ states from decaying by neutron emission unless such decays lead to the analog states in the residual nucleus.

In ^{90}Zr such an allowed neutron decay channel is available for the strong E1 $T_>$ level at E_x = 20.8 MeV since the lowest $T_>$ = 11/2 level in ^{89}Zr lies 8.0 MeV above the ^{89}Zr ground state or 19.96 MeV above the ^{90}Zr ground state. Although both $T_>$ and $T_<$ levels can decay to this analog state in ^{89}Zr (hereafter referred to as $^{89}Zr_A$), isospin and phase space factors favor the decay of the $T_<$ states to the more numerous $T_< = 9/2$ levels of ^{89}Zr. Thus it was felt that the observation of a resonance in the yield curve for the reaction $^{89}Y(p,n_A)^{89}Zr_A$ at E_p = 12.8 MeV would directly imply $T_> = 6$ for this state. Such a resonance in the n_A channel could also explain the increased width[2] of the 20.8 MeV state in ^{90}Zr compared to the 20 MeV state in ^{88}Sr where such n_A decay is energetically forbidden.

The (p,n_A) reaction has both a direct amplitude and a compound nuclear amplitude. Estimates of the compound nuclear amplitude have been made by Anderson and Kerman.[4] For the $^{56}Fe(p,n_A)$ reaction at E_p = 15 MeV they obtained a compound nuclear amplitude equal to the direct amplitude. In the case of the reaction $^{93}Nb(p,n_A)^{93}Mo$ they found the compound nuclear amplitude to be only 10% of the direct amplitude at E_p = 18.5 MeV. However an extrapolation to lower energies should increase the compound nuclear contribution to at least 20-30%. A similar value is expected for the $^{89}Y(p,n_A)^{89}Zr_A$ reaction.

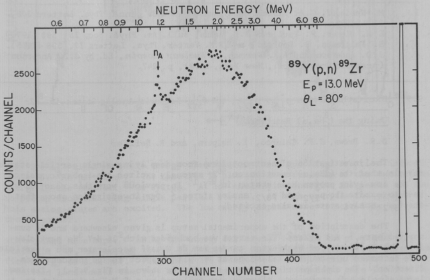

Fig. 9.4-1. Neutron time of flight spectrum from the reaction $^{89}Y(p,n)^{89}Zr$ measured at θ_L = 80°. The group labeled n_A corresponds to neutrons leading to the analog of the ^{89}Y ground state at 8.0 MeV in ^{89}Zr.

Contributions from states with other spins are expected to further reduce the 1^- resonance effect in the (p,n_A) channel since this reaction does not selectively pick out the 1^- states (unlike the (p,γ_0) reaction). However it is hoped that a resonance will still be observable in this reaction channel.

Figure 9.4-1 shows a neutron time of flight spectrum measured at $\theta_{lab} = 80°$ and $E_p = 13.0$ MeV. The detector was a 5" × 1" NE 213 liquid scintillator with a constant fraction discriminator tube base. Pulse shape discrimination was used to reject most of the gamma rays. The time resolution obtained for the gamma peak was 1.3 nsec. The n_A group shows up at channel 297 which corresponds to $E_n = 1.16 \pm 0.06$ MeV. The target was a rolled ^{89}Y foil ~ 1 mg/cm^2 thick. This produced a large gamma ray background due to the large forward angle scattering.

Preliminary results do not indicate any n_A resonance at $E_p = 12.8$ MeV. However we plan to repeat the experiment at several different angles using a thinner target (≈ 100 μg/cm^2). An angular distribution will also be measured to determine the angle which maximizes the contribution of the compound nuclear amplitude.

1. M. Hasinoff, G.A. Fisher, H.M. Kuan, and S.S. Hanna, Phys. Letters *30B*, 337 (1969).
2. E.M. Diener, P. Paul and J.F. Amann, Bull. Am. Phys. Soc. *15*, 593 (1970).
3. S. Fallieros, B. Goulard, and R.M. Venter, Phys. Letters *19*, 398 (1965).
4. J.D. Anderson and A.K. Kerman, in *Nuclear Isospin*, Ed. by J.D. Anderson (Academic Press, Inc., New York, 1969), p. 247.

9.5 Excitation of the $\bar{p}_{1/2}$, $\bar{p}_{3/2}$, and $\bar{f}_{5/2}$ Isobaric Analog States in ^{89}Zr Using the $(^3He,\alpha)$ Reaction

D.R. Brown, J.R. Calarco, I. Halpern, and R. Heffner

The investigation of neutron pickup from deep lying single particle states reveals that the $(^3He,\alpha)$ reaction on ^{90}Zr strongly excites the isobaric analogs of the low lying proton hole states in ^{89}Y.[1] In previous work this reaction was used to excite the $\bar{p}_{1/2}$ and $\bar{p}_{3/2}$ analog states.[2] Our investigation shows that the $\bar{f}_{5/2}$ analog state is also excited.

The description of the experimental setup is given elsewhere and is summarized here.[1] A 1 mg/cm^2 ^{90}Zr target was bombarded with 16 MeV ^3He particles from the University of Washington tandem Van de Graaff accelerator and α particles were detected in a counter telescope at 70° with respect to the incident beam direction. The alpha particle energy spectrum is shown in Fig. 9.5-1. The low lying single hole states are clearly seen followed by a 5 MeV region with no dominant structure. At excitation energies of 8.15 MeV, 9.62 MeV, and 9.82 MeV states identified as the analog states are strongly excited and the peaks due to ^{16}O and ^{12}C target contamination are also seen.

The $\bar{p}_{1/2}$ and $\bar{p}_{3/2}$ analog states were previously identified at excitation energies of 8.10 and 9.60 ± .08 MeV in good agreement with the two lowest analog

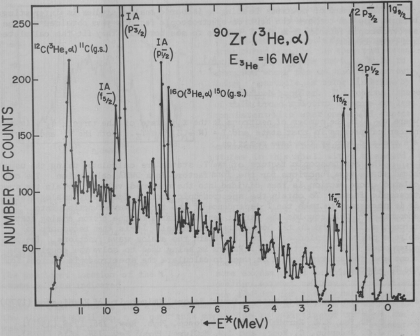

Fig. 9.5-1. Alpha particle energy spectrum for the $^{90}Zr(^{3}He,\alpha)$ reaction induced by 16 MeV ^{3}He particles. The spectrum is plotted as a function of the excitation energy in the residual ^{89}Zr system. At low excitation energies the peaks are due to pickup from low lying single particle states. At high energies the proton hole analog states are excited. The low energy alphas were truncated by an electronic cutoff.

state peaks seen here.[2] Using the energy difference between the $p_{\bar{1}/2}$ and $f_{\bar{5}/2}$ states in ^{89}Y, the analog to the $f_{\bar{5}/2}$ state is then predicted to lie at an excitation energy of 9.89 MeV. Thus the state excited here lies within 70 keV of the predicted location of the $f_{\bar{5}/2}$ analog state and on this basis we make its identification. The Coulomb separation energy calculated from these states using the ^{89}Zr-^{89}Y binding energies is $\Delta E_c = 11.73 \pm .03$ MeV which is in good agreement with the value $11.55 \pm .15$ MeV obtained by Anderson *et al.* from the (p,n) reaction on ^{89}Y.[3] (It should be noted that identification of the ℓ-value of a state from an angular distribution is not possible at this energy because all ℓ-values give the same backward peaked Coulomb stripping pattern.)

The pickup of neutrons leading to isobaric analog studies is interesting, because one can compare the neutron spectroscopic factors thus obtained and the spectroscopic factors from the $T_<$ states to see how well they fit the calculated sum rule limits:[4]

$$\sum S_{T_<} = \nu_{\ell,j} - \frac{\pi_{\ell,j}}{2T+1}$$

$$\sum S_{T_>} = \frac{\pi_{\ell,j}}{2T+1}$$

where $\nu_{\ell,j}$ is the number of neutrons in the ℓ,j state of the target, $\pi_{\ell,j}$ is the number of protons in that state and $T = (N - Z)/2 \equiv T_Z$. Both the $T_>$ and $T_<$ states are excited here by the same reaction.

The spectroscopic factors of the $T_<$ states are calculated using the usual bound state wave functions for the form factors in a DWBA calculation. The calculated cross section is then divided into the measured value to obtain the spectroscopic factor. To obtain the spectroscopic factors for the $T_>$ analog states it is necessary to take the T dependence of the target wave function into account.[5,6] This couples the parent neutron states to the proton analog states through a $\vec{T} \cdot \vec{t}$ term in the bound state potential. It is then necessary to solve a pair of coupled equations to obtain the analog wave functions. The computer code NEPTUN[7] written by T. Tamura is being used to solve the coupled equations and the solutions will be used to calculate the spectroscopic factors for the $T_>$ states.

---

1. Nuclear Physics Laboratory Annual Report, University of Washington (1970), p. 109.
2. C.M. Fou, R.W. Zurmühle, and J.M. Joyce, Phys. Rev. *155*, 1248 (1967).
3. J.D. Anderson, C. Wong, and J.W. McClure, Phys. Rev. *138*, B615 (1965).
4. J.B. French and M.H. Macfarlane, Nucl. Phys. *26*, 168 (1961).
5. R. Stock and T. Tamura, Phys. Letters *22*, 304 (1966).
6. R. Stock, R. Bock, P. David, H.H. Duhm, and T. Tamura, Nucl. Phys. *A104*, 136 (1967).
7. T. Tamura, private communication.

9.6 Evidence for Pickup of Neutrons from Deep Lying Single Particle States in ^{208}Pb Obtained Using the (^{3}He,α) Reaction

D.R. Brown, J.R. Calarco, I. Halpern, and R. Heffner

The large positive Q value of the (^{3}He,α) reaction (typically $\sim$ 13 MeV in heavier nuclei) may make it useful for studying nucleon pickup from deeply lying single particle states. The spectrum of α particles emitted at 70° in a bombardment of ^{208}Pb by 24 MeV ^{3}He particles is shown in Fig. 9.6-1. The data here have been plotted with a resolution of about 200 keV in order to smooth out statistical fluctuations to some degree.

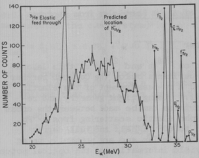

Fig. 9.6-1. α particle energy spectrum from the $^{208}Pb(^{3}He,\alpha)^{207}Pb$ reaction. The points represent the summation of the counts in five channels. The peaks above 32 MeV are the low lying single hole states in ^{207}Pb. At 23.6 MeV the ^{3}He elastic feedthrough peak is seen. The predicted location of the $h^{-}_{11/2}$ state is also indicated.

The very strongly excited states at low excitation are the $h^{-}_{9/2}$, $i^{-}_{13/2}$, f^{-} and p^{-} single neutron hole states. It is seen that there is a large weakly structured bump in the spectrum extending from just below the $h^{-}_{9/2}$ hole to energies where the emission of an outgoing particle is being hindered by the Coulomb barrier. The general shape of this broad spectrum is more or less consistent with what one would expect from neutron pickup in the 3s-2d shell. That is, if one calculates the pickup cross-sections from single particle states in this shell with a standard DWBA code and then spreads the resulting lines in energy, one reproduces reasonably well both the magnitude and general shape of the bump.[1] Unfortunately we cannot be very definite about the widths of these implied deeper hole states. For example, we show the expected location of the $h^{-}_{11/2}$ state which lies at the top of the s-d-g neutron shell, and although there is a very slight suggestion of some excess yield in this neighborhood, one can extract neither a total strength nor a width for the assumed $h^{-}_{11/2}$ line. There is also evidence for a peak around 30.5 MeV which falls in the middle of the expected shell gap. In part this may be due to splitting of the $h^{-}_{9/2}$ due to weak coupling with the $(f^{-}_{5/2} \times 4^{+})_{9^{-}/2}$ state,[2] but this mixing cannot account for the total width of this structure.

Some of the strength in this bump may not be due to single-hole strength at all. One suspects that there are contributions from multiple interactions in the nucleus by the passing projectile, giving rise to 2 particle-1 hole states, etc. We would like to find some criteria to help us determine the relative importance of multiple interactions in the excitation of higher states in direct reactions, but so far we have been unsuccessful.

1. Nuclear Physics Laboratory Annual Report, University of Washington (1970), p. 109.
2. S.M. Smith, P.G. Roos, C. Moazed, and A.M. Berstein, preprint.

9.7 Re-examination of Elastic Scattering of Alpha Particles from Isotopes of Pb and Bi

J.S. Blair, K. Ebisawa, and W.Q. Sumner

Previous alpha scattering experiments on ^{208}Pb and ^{209}Bi at this laboratory[1] and recent elastic alpha scattering experiments below the Coulomb barrier at the University of Minnesota[2] have prompted a re-measurement of the elastic scattering from several isotopes of Pb and Bi. Using tight geometry and requiring beam-energy stability, precise comparisons can be made between the cross sections of the various isotopes. 42 MeV alpha elastic scattering from ^{204}Pb, ^{206}Pb, ^{208}Pb and ^{209}Bi was measured from 16° to 60° in half and full degree steps. The extracted cross sections are quite similar and are presently being analyzed. It is hoped that this data will yield information on the optical potential near the nuclear surface and perhaps information on nuclear radii.

---

1. J. Alster, Phys. Rev. *141*, 1138 (1966).
2. J.S. Lilley, private communication.

9.8 Evidence for ^{5}He and ^{5}Li Production in High Energy α Particle Bombardment of Heavy Nuclei

D.R. Brown, J.R. Calarco, I. Halpern, and R. Heffner

The thesis work of G. Chenevert of this laboratory[1] has raised a number of interesting questions about the interaction of high energy helium ions with heavier nuclei. One of Chenevert's more puzzling results is the broad structure seen in the spectra of outgoing α particles when α particles are used as incident projectiles. These spectra are found to exhibit a broad plateau extending from a residual excitation of 9 MeV to an excitation of 25 MeV (at 65 MeV incident energy) or 31 MeV (at 90 MeV incident energy). Relevant portions of typical spectra, observed at various angles, are shown in Fig. 9.8-1. In corresponding studies of the ^{3}He,^{3}He' reaction, the spectra were also found to rise up sharply at ∿ 9 MeV excitation, but with ^{3}He they fell off quite rapidly and continuously from this point, showing no back edge at 25-30 MeV as in the ^{4}He spectra.

Attempts to explain the structure and angular distribution of the plateau have been made in terms of a nucleon-knockout model and in terms of a model involving the excitation of nuclear surface oscillations. So far neither of these models has been able to account for the observations. It has recently been suggested to us[2] that part of what one sees in (α,α') spectra may come from (α,^{5}He) or (α,^{5}Li) reactions, i.e., from pickup reactions where the emerging particle separates into a nucleon plus α particle soon after leaving the nucleus ($\tau_{1/2}$ ∿ 10^{-21}sec).

There are some simple kinematic features of such pickup/breakup reactions that one can compare with the observed spectra. Let E_0 be the kinetic energy of the A = 5 emerging particle and let E_R be the resonance energy of this particle's "ground" state. The laboratory energy of an α particle sent off at θ to the original emission direction (θ being measured in the c.m. system) is

$$E_{lab} = 0.8E_0 + 0.2E_R + 2\sqrt{0.16\ E_R E_0}\ \cos\theta .$$

If the breakup is isotropic in the c.m. system, i.e., if $dN/d\cos\theta$ = constant, it follows that dN/dE_{lab} is constant from

$$E_{lab}^{min} = (\sqrt{0.8E_0} - \sqrt{0.2E_R})^2$$

to

$$E_{lab}^{max} = (\sqrt{0.8E_0} + \sqrt{0.2E_R})^2$$

and zero outside this range. The spectrum is therefore a plateau of width,

$$W = 4\sqrt{0.16E_R E_0}.$$

For ^5He, $E_R \sim 1$ MeV and for an incident energy of 65 MeV, E_0 should be about 55 MeV if the α particle is picking up the most loosely bound neutrons. With these values E_{lab}^{min} is 39 MeV which corresponds very closely to the location of the "high residual excitation" edge of the observed spectrum. The width of the observed spectrum is however about 50% greater than the value of W given above. It is our present view that the observed plateaus arise from superpositions of two effects, the pickup/breakup mechanism here described plus a spectrum due to normal inelastic scattering. This view is supported by the observation (Fig. 9.8-2) that if one subtracts the pickup/breakup spectrum in a self-consistent way from the observed spectrum, the residual spectrum looks very much like that seen in the (^3He,$^3He'$) reaction.

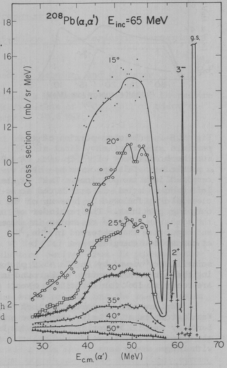

Fig. 9.8-1. Alpha spectra observed at a number of angles in the bombardment of ^{208}Pb with 65 MeV α particles. The portion of the spectrum corresponding to the excitation of discrete low-lying levels is shown only for the 30° data.

That is, it seems as though "normal" inelastic scattering is rather similar for ^3He and ^4He but that the ^4He,$^4He'$ reaction shows the additional contribution arising from the instability of the pickup product ^5He. This kind of account for the $^4He'$ spectra is more consistently carried out in terms of a ^5He intermediate rather than a ^5Li intermediate (where E_R is about twice as large) and it leads one to suspect that the (α,^5He) reaction is rather more probable than (α,^5Li).

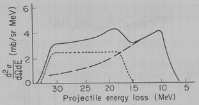

Fig. 9.8-2. The mesa-portion of the particle spectrum (heavy line) at 22° for the bombardment of ^{208}Pb with 90 MeV α particles. This spectrum has been decomposed into two portions. That at the left (shown dotted) is attributed to nucleon pickup followed by breakup of the outgoing particles. The remainder of the spectrum (dashed) resembles in shape and magnitude that observed in ^{3}He,$^{3}He'$ at comparable energies.

To test and confirm the above ideas we are presently working on two coincidence measurements to be performed with the 42 MeV α beam of our cyclotron:

$$\alpha + {}^{208}Pb \rightarrow {}^{207}Pb + ({}^{5}He) \rightarrow {}^{207}Pb + \alpha + n \qquad (1)$$

and

$$\alpha + {}^{208}Pb \rightarrow {}^{207}T\ell + ({}^{5}Li) \rightarrow {}^{207}T\ell + \alpha + p. \qquad (2)$$

In these reactions, the final α particle is emitted within a few degrees of the original direction of the A = 5 pickup product. The nucleons are emitted into a rather narrow cone, (θ ∿ 22° for the ^{5}He pickup), most of them appearing near the surface of this cone. The kinematics is therefore very favorable for the detection of these events. The α particles are detected by a solid state counter telescope and the neutrons by an NE 213 scintillator viewed by an RCA 4522 photomultiplier. We have succeeded in reducing the photon and neutron background in this detector to reasonable levels and are ready to look for coincident events arising from the pickup/breakup reaction.

We are also preparing to look for the breakup products of ^{5}Li, here at Washington and at Berkeley where the available incident energy is higher. At Berkeley we will be working again with Dr. Hendrie with whom we collaborated in the original investigation of inelastic scatterings of ^{3}He and ^{4}He particles with large energy loss.[3]

1. Gary M. Chenevert, Ph.D. Thesis, University of Washington, 1969 (unpublished).
2. H. Morinaga, private communication.
3. G.M. Chenevert, N.S. Chant, I. Halpern, C. Glashausser, and D.L. Hendrie (to be published).

10.1 Measurement of the Substate Cross Sections in the Inelastic Scattering of Protons from $^{40}Ca(3.73\ MeV, 3^-)$

J. Eenmaa, T. Lewellen, D. Patterson, F. Schmidt, and J. Tesmer

During the past year we have undertaken a series of experiments to measure the substate cross sections of the 3.73 MeV 3^- state of ^{40}Ca. All of these experiments utilized an incident proton energy of 20.3 MeV.

The experiments involve measurement of the $(p,p'\gamma)$ angular correlation function for several different gamma detector geometries. In each case, the correlation function was measured by detecting the inelastically scattered protons in coincidence with the de-excitation γ-rays. The protons were detected with a liquid-nitrogen (LN_2)-cooled 5-detector array. The detectors were 3 mm Si(Li) with defining apertures subtending a full angle of 2° in-plane and a half angle of ∿3° out-of-plane. They were placed at 10° intervals on a brass block which was attached to a LN_2 dewar. The block allows the LN_2 to circulate behind each detector. The dewar and LN_2 supply system is described elsewhere.[1]

Gamma rays were detected by a 5" × 4" NaI(Tℓ) crystal coupled to an RCA 4522 photomultiplier.[2] Fast timing signals were derived from the proton detectors with direct coupled fast preamplifiers built at the laboratory.[3] The coincidence events were detected with a standard fast-slow circuit. Time-to-amplitude converters (TACs) were used to detect the fast coincidences. The time spectra from the TACs were gated by the inelastic protons and the de-excitation energy γ-rays with energies over 0.511 MeV. The full-width at half-maximum of the coincidence peaks in the gated time spectra were typically 2 nsec or less. The fast-slow coincidence resolving time (peak base width) was ∿10 nsec. The data were taken on-line with the SDS computer. Five time and five proton spectra, each containing 256 channels, were collected in the computer by a program that also calculates and displays the correlation values and their statistical errors during data collection.[4]

In general, the correlation function (referred to z axis along $\vec{k}_{inc} \times \vec{k}_f$ (see Fig. 10.1-1) has the form

$$W(\phi_p,\phi_\gamma\theta_\gamma) = \frac{7}{8\pi}[A(\phi_p,\theta_\gamma) + B_1(\phi_p,\theta_\gamma)\cos[2\phi_\gamma - \delta_1] \quad (3)$$

$$+ B_2(\phi_p,\theta_\gamma)\cos[4\phi_\gamma - \delta_2] + B_3(\phi_p,\theta_\gamma)\cos[6\phi_2 - \delta_3]].$$

The parameters B_1, B_2, and B_3 are rather complicated expressions involving reduced rotation matrices and off-diagonal terms of the density matrix. However, the leading term has a somewhat simpler form

$$A(\phi_p,\theta_\gamma) = C_0(\theta_\gamma)S_0(\phi_p) + C_1(\theta_\gamma)S_1(\phi_p) + C_2(\theta_\gamma)S_2(\phi_p) + C_3(\theta_\gamma)S_3(\phi_p)$$

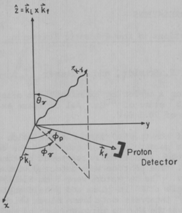

Fig. 10.1-1. The coordinate system used in particle-gamma correlation studies. The beam is along the x-axis.

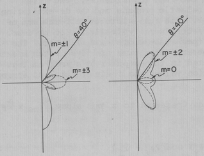

Fig. 10.1-2. Octupole radiation patterns.

where S_i is the probability for exciting the $|i|$-th substates with an unpolarized beam. The C_i coefficients can be easily expressed in terms of reduced rotation matrices.

If one can determine the various S_i, then the substate cross sections are given by

$$\sigma_i = S_i\left(\frac{d\sigma}{d\Omega}\right)_{3^-} .$$

For a gamma detector with a circular aperture centered on the z-axis, Eq. (1) becomes

$$W_{z\text{-axis}} = a_0S_0 + a_1S_1 + a_2S_2 + a_3S_3 \quad (2)$$

where the a_i terms include the appropriate integerations for θ_γ to take into account the finite solid angle subtended by the γ detector. Our γ detector has a polar acceptance angle of 5°. Considering the octupole radiation patterns (Fig. 10.1-2), and our acceptance angle, the vast majority of events detected should be from the m = ±1 substate. When the a_i are calculated, this is in fact the case, and one can write

$$W_{z\text{-axis}} \simeq \frac{7}{8\pi} S_1.$$

Although this result is similar to the case of spin-flip probability for 2^+ states,[5] the Bohr theorem, when applied to a $0^+ \rightarrow 3^- \rightarrow 0^+$ transition, predicts that only the even substates are populated by spin-flip processes. Thus, in the present instance, $S_0 + S_2$ is the spin-flip probability, not S_1.

When the gamma detector is placed in the reaction plane, the correlation function retains all the terms of Eq.(1). However, if measurements at a number of γ angles (θ_γ) are taken for each proton angle, a least-squares fitting program can yield a reasonably accurage value for A, as well as for the other parameters We then have an equation of the form

$$A = b_0S_0 + b_1S_1 + b_2S_2 + b_3S_3 \qquad (4)$$

where the b_i include solid angle corrections.

We also have the normalization condition that

$$S_0 + S_1 + S_2 + S_3 = 1 \qquad (5)$$

so that if another measurement can yield a number for an equation of the general form of Eq. (4), we can extract S_0, S_1, S_2, and S_3.

To get this measurement, a new gamma detector system (termed the mid-plane detector) is currently being built and is described in Sec. 4.6 of this report. Since the z-axis and in-plane correlation measurements do not emphasize the even substates, a gamma polar angular range of 25°-40° was selected as ideal for the new detector (see Fig. 10.1-2). Also, in order to minimize the necessary data collection time, the new detector will integrate over ϕ_γ. This measurement will give us our fourth equation; viz.,

$$W_{\text{mid-plane}} = C_0S_0 + C_1S_1 + C_2S_2 + C_3S_3.$$

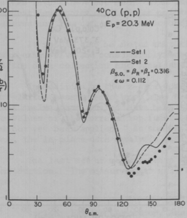

Fig. 10.1-3. Elastic Cross Section

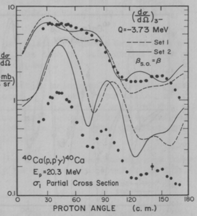

Fig. 10.1-4. Inelastic Cross Section

The series of measurements will thus enable us to extract the substate cross sections σ_0, σ_1, σ_2, and σ_3, as well as the spin-flip probability $P_{sf} = S_0 + S_2$, and the in-plane correlation parameters B_1, B_2, B_3, δ_1, δ_2, and δ_3. These quantities should provide a stringent test of the DWBA collective model as applied to a 3^- state, and will supplement conclusions recently arrived at as a result of similar measurements for 2^+ states.[6]

The experimental program began with the measurements of the elastic and inelastic cross sections (Figs. 3 and 4). The inelastic cross section agrees quite well with data published by Schaeffer.[7]

We generated a preliminary set of optical model parameters to fit the elastic cross section data with the optical model search code OPTIM1.[8] No attempt has yet been made to fit the asymmetry data published by Blair *et al.*[9] (Figs. 10.1-5 and 10.1-6). As shown in Fig. 10.1-3, our optical parameters, labeled set 2, fit the elastic data quite well but differ in phase from the prediction obtained from parameters published by Schaeffer, labeled set 1. Table 10.1-1 lists the two sets of parameters and Fig. 10.1-5 shows the elastic polarization predictions.

The predictions of the inelastic cross section and asymmetry (Figs.10.1-4 and 10.1-6) are the result of preliminary DWBA calculations made with the code of H. Sherif[10] and include the full Thomas form of the spin-orbit potential. Again, sets 1 are the predictions based on Schaeffer's parameters, sets 2 is based on our parameters. Neither set does particularly better than the other in

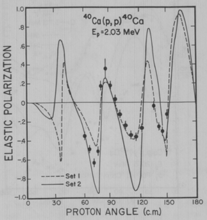

Fig. 10.1-5. Elastic asymmetry

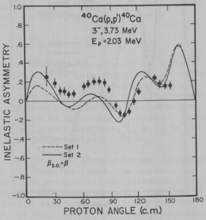

Fig. 10.1-6. Inelastic asymmetry

Table 10.1-1. Optical model parameters for ^{40}Ca + p elastic scattering.

Set 1 Schaeffer's parameters
Set 2 Parameters generated by OPTIM1

Set	V_A	WV_A	W_{SA}	$V_{so}R$	$V_{so}I$	R_A	R_I	R_S	R_C	A_A	A_I	A_S
1	43.22	0.0	5.49	3.25	.58	1.25	1.25	1.15	1.15	.65	.62	.55
2	43.64	0.0	5.51	4.34	.80	1.302	1.248	0.999	1.25	.520	.686	.243

predicting the inelastic cross section.

Figure 10.1-4 also shows the data and predictions based on Eq. (3). If one considers set 2, the prediction agrees quite well with the data in general shape. In fact, the fit is quite good if the prediction is normalized to the data. The reason for the disagreement in magnitude has not been completely determined yet.

However, a major source of error currently exists in the overall normalization of the z-axis correlation data due to the correction made for the efficiency of the gamma detector. This correction involves the product of the efficiency and effective solid angle of the gamma detector. Currently, the detection systems in use have not been calibrated for energies greater than 1.37 MeV. In the next few months calibration points in the energy range of 3 to 4 MeV will be measured and the data adjusted accordingly.

It should also be noted that the DWBA calculations done to date are by no means exhaustive and considerably more work will be done on calculations after all the data collection and final analysis is complete.

In addition to the z-axis correlation function measurements, the in-plane correlation measurements have also been completed. For each proton angle, at least twelve gamma angles have been measured. The data has been analyzed for the values of the correlation function, but the least squares fitting technique has not yet been applied. As soon as the calibration of the gamma detector is done, the in-plane data analysis will be completed.

The last set of measurements will use the new mid-plane detector now under construction. The measurements will hopefully be complete by September of this year.

1. Nuclear Physics Laboratory Annual Report, University of Washington (1966), p. 83.
2. Nuclear Physics Laboratory Annual Report, University of Washington (1970), p.32.

3. Nuclear Physics Laboratory Annual Report, University of Washington (1970), p. 30.
4. Nuclear Physics Laboratory Annual Report, University of Washington (1970), p. 45.
5. F.H. Schmidt, R.E. Brown, J.B. Gerhart, and W.A. Kolasinski, Nucl. Phys. *52*, 353 (1964).
6. J.R. Tesmer, Ph.D. Thesis, University of Washington, 1971 (unpublished).
7. R. Schaeffer, Nucl. Phys. *A132*, 186 (1969).
8. D. Zorstadt, Problem OPTIM1, Report Cyc-6835, University of Colorado, Boulder, Colorado.
9. A.G. Blair *et al.*, Phys. Rev. *1*, 444 (1970).
10. H. Sherif, Ph.D. Thesis, University of Washington, 1968 (unpublished).

10.2 ^{24}Mg, ^{60}Ni, ^{64}Ni, ^{92}Mo(p,p'γ) Proton Spin Flip at 20 MeV

J. Eenmaa, T. Lewellen, D. Patterson, F.H. Schmidt, and J.R. Tesmer

The z-axis proton-gamma angular correlations in the excitation of the first 2^+ states of ^{24}Mg (1.37 MeV), ^{60}Ni (1.33 MeV), ^{64}Ni (1.34 MeV), and ^{92}Mo (1.54 MeV) have been measured at an incident proton energy of 20.0 MeV. The method is similar to that described in earlier reports and publications.[1,2]

The general expression for the angular correlation between inelastically scattered particles and subsequent de-excitation gamma rays can be written as

$$W = \sum_{MM'} \rho_{MM'} \, \eta_{M'M}$$

where the matrix $\eta_{M'M}$ describes the de-excitation of the 2^+ state, while $\rho_{MM'}$ may be expressed as

$$\rho_{MM'} = \sum_{\mu_i \mu_f} T(\mu_i \mu_f M) T^*(\mu_i \mu_f M')$$

where $T(\mu_i \mu_f M)$ is the amplitude for exciting the state $|2M\rangle$, and μ_i and μ_f are the spin projections of the incident proton and the inelastically scattered proton, respectively. Measurements of W can thus be used to determine the elements of $\rho_{MM'}$. These elements may, in turn, be predicted by various interaction theories, as, for example, by collective model DWBA (considered herein), thus providing a very stringent test of these theories.

If the z-axis is chosen to lie perpendicular to the reaction plane, the Bohr theorem states that only the M = ±1 substates are populated in the spin-flip process.[3] The z-axis correlation is defined by evaluating the expression for W at $\theta_\gamma = 0$. The result is

$$W(\theta_\gamma = 0) = \frac{5}{8\pi} (\rho_{11} + \rho_{-1-1}) = \frac{5}{8\pi} S_1 .$$

S_1 is the probability that proton spin flip has occurred.

Measurements of the elastic and inelastic scattering differential cross sections and spin-flip probabilities were made over a large angular range. The data for ^{24}Mg, ^{60}Ni, and ^{64}Ni are presented in Figs. 10.2-1 through 10.2-3. Also shown in the figures is the M = ±1 substate cross section

$$\sigma_1 = S_1 \frac{d\sigma}{d\Omega}$$

where $d\sigma/d\Omega$ is the differential scattering cross section for the 2^+ state as a whole. The ^{92}Mo data is currently being analyzed and will be included in a later report.

The measured spin-flip probabilities for ^{60}Ni and ^{64}Ni display a prominent peak (∿30%) at backward angles. There is also some structure at forward angles. These features are similar to earlier measurements on ^{58}Ni and ^{54}Fe, and seem to be characteristic of nuclei studied in this mass region at this energy.[1,4,5] For ^{24}Mg, the back-angle peak is rather broad and appears to be double-humped. There is also a smaller peak (∿15%) at ∿40°.

Also shown in the figures are optical model calculations for the elastic scattering and collective model DWBA calculations for the inelastic scattering performed with the code of H. Sherif.[6] The DWBA calculations include the full Thomas form of the spin-orbit potential in the interaction potential.[7]

Two sets of optical model parameters were investigated for each element. There parameters are presented in Table 10.2-1. The first set, labeled A, are derived from the "standard" optical model of Becchetti and Greenlees.[8] These parameters give fairly good fits to the elastic scattering data, although there are some deviations at the backward

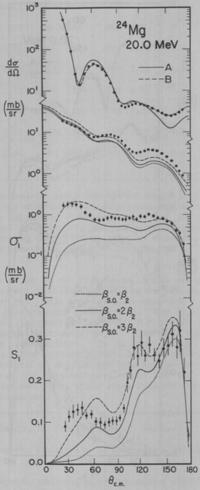

Fig. 10.2-1. ^{24}Mg elastic and inelastic differential scattering cross sections, σ_1 partial cross section, and spin-flip probabilities. β_2 = 0.49.

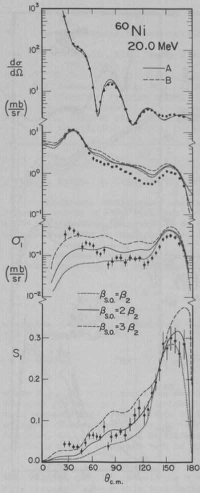

Fig. 10.2-2. ^{60}Ni elastic and inelastic differential scattering cross sections, σ_1 partial cross section, and spin-flip probability. β_2 = .24.

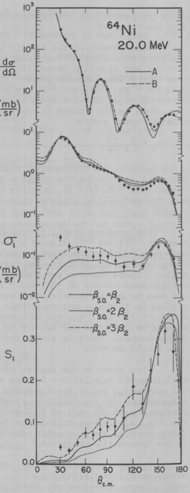

Fig. 10.2-3. ^{64}Ni elastic and inelastic differential scattering cross sections, σ_1 partial cross section, and spin-flip probability. β_2 = .20.

Table 10.2-1. Optical Model Parameters

	Set	US	WS	WD	RS	RI	RSP	AS	AI	ASP	RC	χ^2
^{24}Mg	A	49.30	1.70	6.80	1.17	1.32	1.01	.750	.510	.750	1.25	27.3
	B	46.23	5.50	3.14	1.19	1.43	1.08	.715	.387	.550	1.25	1.8
^{60}Ni	A	52.10	1.70	7.60	1.17	1.32	1.01	.750	.560	.750	1.25	6.2
	B	52.02	2.75	6.46	1.18	1.27	.984	.710	.582	.670	1.25	3.6
^{64}Ni	A	53.40	1.70	8.30	1.17	1.32	1.01	.750	.600	.750	1.25	14.0
	B	52.10	1.46	7.76	1.19	1.26	1.04	.690	.613	.716	1.25	2.3

angles. The second set, labeled B, was obtained by using the optical model search code OPTIM-I to optimize the fit to the elastic scattering data. In all cases, the elastic scattering fits could be improved. However, except for the case of ^{24}Mg, the required parameters changes were slight, and did not necessarily lead to better fits for the inelastic scattering data. Also, since no elastic polarization data was used in the parameter search the value of this procedure could be considered somewhat questionable.

The inelastic scattering predictions shown in the figures are those using the parameters of set A. Better fits to inelastic scattering data have been reported if β_{SO} is made larger than β_2.[6,7,9,10,11] This increases the relative strength of ΔU_{SO} with respect to the whole perturbation potential ΔU. The figures show the effect of this variation in the interaction potential for predictions of the total inelastic differential cross sections, the $M = \pm 1$ partial differential cross sections, and the spin-flip probabilities. In all cases, the general features of the data are reproduced. The spin-flip data, in particular, is strongly suggestive of the increased strength of ΔU_{SO} in the interaction potential. This feature is not so obvious from the data and predictions for the total inelastic scattering differential cross sections, since these include contributions from the other, non-spin flip substates.

1. W.A. Kolasinski, J. Eenmaa, F.H. Schmidt, H. Sherif, and J.R. Tesmer, Phys. Rev. *180*, 1006 (1969).
2. Nuclear Physics Laboratory Annual Report, University of Washington (1968), p. 82.
3. A. Bohr, Nucl. Phys. *10*, 486 (1959).
4. Nuclear Physics Laboratory Annual Report, University of Washington (1970), p. 85.
5. D.L. Hendrie, C. Glashausser, J.M. Moss, and J. Thirion, Phys. Rev. *186*, 1188 (1969).
6. H. Sherif, Ph.D. Thesis, University of Washington, 1968 (unpublished).
7. H. Sherif and J.S. Blair, Phys. Letters *26B*, 489 (1968).

8. F.D. Becchetti and G.W. Greenlees, Phys. Rev. *182*, 1190 (1969).
9. J. Eenmaa, F.H. Schmidt, and J.R. Tesmer, Phys. Rev. *28B*, 321 (1968).
10. J. Raynal, Proceedings of the 3rd International Symposium on Polarization Phenomena of Nucleons, Quebec, 1969, p. 75.
11. J.R. Tesmer, Ph.D. Thesis, University of Washington, 1970 (unpublished).

10.3 ^{54}Fe(p,p'γ) Angular Correlation Measurements at 19.6 MeV

J. Eenmaa, T.K. Lewellen, R.E. Marrs, D.M. Patterson, P.A. Russo, F.H. Schmidt, and J.R. Tesmer

The in-plane and z-axis (spin-flip) correlations for the first 2^+ (1.409 MeV) of ^{54}Fe have been measured. The z-axis correlation measurement has been previously reported.[1] The purpose of these measurements was to further examine differences between ^{54}Fe and nuclei such as ^{56}Fe and ^{58}Ni. The differences have been observed by Glashausser *et al.*[2] in the inelastic asymmetries for the 2^+ states. Hendrie *et al.*[3] have measured the z-axis correlations of both ^{54}Fe and ^{56}Fe at 19.6 MeV and found few differences. The DWBA collective model calculations predict the inelastic asymmetries for nuclei such as ^{56}Fe and ^{58}Ni very well but do not agree with the forward-angle asymmetry data for ^{54}Fe. Our correlation measurements were undertaken in hopes of clarifying this situation.

An angular correlation measurement, whether in-plane or z-axis, consists of detecting the number of inelastically scattered protons (exciting the 2^+ state) in coincidence with the de-excitation γ-rays as a function of the angle between their directions of propagation. A calibrated γ detector was used to obtain absolute correlation values. The experimental arrangement has been described previously.[4]

The z-axis and in-plane correlations were combined to yield the substate probabilities and substate cross sections. These results are very similar to those for ^{12}C and ^{58}Ni.[4,5]

The in-plane parameters, however, have proven to be more interesting than expected. The in-plane correlation function can be written as

$$W(\theta_\gamma = \pi/2,\phi_\gamma) = 5/16\pi[A + B \sin^2 2(\phi_\gamma - \varepsilon_2) + C \sin^2(\phi_\gamma - \varepsilon_1)]$$

where parameters A,B,C,ε_1 and ε_2 are determined by the measurement. In this form the parameters B and ε_2 depend on non-spin-flip amplitudes while C and ε_1 are spin-flip dependent. Parameter A depends on all the amplitudes.

We have found that parameter A is very sensitive to the form of the spin-dependent coupling potential, ΔU_{SO}, used in the collective model calculations. Parameter A, the spin-flip probability, S_1, and the inelastic asymmetry data[3] are shown in Fig. 10.3-1 along with the collective model predictions.

The DWBA collective model calculations were made with the code of Sherif and Blair.[6] This program allows the form of ΔU_{SO} to be varied. In particular, the full-Thomas form of the coupling potential can be used. In addition, the

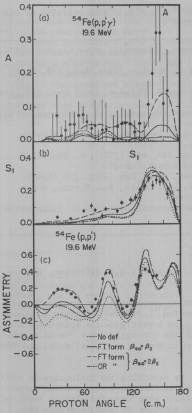

Fig. 10.3-1. a) The parameter A for the in-plane correlation function; b) the spin-flip probability, S_1, as determined by z-axis correlation measurements; c) the inelastic asymmetry. The curves are drawn for various DWBA collective model calculations.

strength (or deformation) of U_{SO} can be varied.

The predictions were made with the standard optical parameters of Becchetti and Greenlees.[7] Two forms of ΔU_{SO} were used. One form, labeled "OR" is similar to that proposed by Fricke *et al.*[8] The other form, labeled "FT", is the full-Thomas form. The deformation parameter, β_{SO}, is used to change the strength of ΔU_{SO}. It has been customary to set $\beta_{SO} = \beta_2$, the deformation for the central optical potential. For the curves in Fig. 10.3-1 labeled "No def", $\beta_{SO} = 0$; i.e., $\Delta U_{SO} = 0$, although spin-dependent forces still act in the elastic channels. Predictions are also shown for $\beta_{SO} = \beta_2$ and $\beta_{SO} = 2\beta_2$. The latter value does not necessarily imply a greater deformation of ΔU_{SO}; but represents a convenient means of increasing the strength.

Two conclusions can be drawn from the comparison of the predictions to the experimental data: 1) The full-Thomas form of ΔU_{SO} is superior, particularly for A. 2) $\beta_{SO} = 2\beta_2$ improves the fits to all the data, particularly to the asymmetry and parameter A. The spin-flip probability is not greatly affected by the form of ΔU_{SO}. This reflects the well known fact that spin flip is mainly produced by spin-dependent distortions in the elastic channels.

An increase in β_{SO} has been suggested by several authors as a means of improving asymmetry predictions for data at higher energies.[6,8] Recently, Raynal,[9] basing his calculations on a microscopic description, has shown that ΔU_{SO} for ^{54}Fe should have β_{SO} increased.

Parameter A for ^{58}Ni is also better fit by the full-Thomas form. However, the differences in the asymmetry fits between ^{54}Fe and ^{58}Ni are resolved only if $\beta_{SO} = 2\beta_2$ for ^{54}Fe.

The remaining in-plane parameters for ^{54}Fe are fairly insensitive to the form of U_{SO} and are very similar to those of ^{58}Ni.

---

1. Nuclear Physics Laboratory Annual Report, University of Washington (1970), p. 85.
2. C. Glashausser, R. de Swiniarsky, and J. Thirion, Phys. Rev. *164*, 1437 (1967).
3. D.L. Hendrie, C. Glashausser, J. Moss and J. Thirion, Phys. Rev. *186*,1188 (1969).
4. Nuclear Physics Laboratory Annual Report, University of Washington (1970), p. 82.
5. J.R. Tesmer, J. Eenmaa, T. Lewellen, D.M. Patterson, and F.H. Schmidt, Bull. Am. Phys. Soc. *14*, 1220 (1969).
6. H. Sherif and J.S. Blair, Phys. Letters *26B*, 489 (1968); H. Sherif, Ph.D. Thesis, University of Washington, 1968 (unpublished).
7. F.D. Becchetti, Jr. and G.W. Greenlees, Phys. Rev. *182*, 1190 (1969).
8. M.P. Fricke, R.M. Drisko, R.H. Bassel, E.E. Gross, B.J. Morton, and A. Zucker, Phys. Rev. Letters *16*, 746 (1966).
9. J. Raynal, Proceedings of the 3rd International Symposium on Polarization Phenomena of Nucleons, Quebec, 1969.

10.4 ^{24}Mg(^{3}He,^{3}He'γ) Spin Flip at 24.0 MeV

J.G. Cramer, J. Eenmaa, T.K. Lewellen, R. Marrs, D.M. Patterson, and J.R. Tesmer

The z-axis (spin-flip)[1] ^{3}He-gamma angular correlation for scattering of 24.0 MeV ^{3}He from ^{24}Mg exciting the first excited (1.368 MeV,2^+) state has been measured. The purpose of this measurement is to investigate the spin-dependence of the ^{3}He-nucleus interaction and to extract the strength of the ^{3}He spin-orbit potential depth. The latter is of particular interest for optical model and DWBA collective model calculations.

The spin-flip probability is measured by detecting the inelastically scattered ^{3}He particles in coincidence with de-excitation gamma-rays emitted perpendicular to the reaction plane. The ^{3}He particles were detected with an array of three ΔE-E detector telescopes. The defining aperture on each telescope was about 2.5° wide by about 4.5° high (full angle), and the telescopes were mounted 20° apart. The gamma-rays were detected with a lead-shielded 5" × 4" NaI(Tℓ) crystal coupled to an RCA 4522 photomultiplier.[2] A lead collimator with a geometric half-angle of acceptance of 9° was placed in front of the NaI(Tℓ) crystal. The absolute efficiency of the gamma-ray detector for 1.368 MeV gamma rays has been experimentally determined to an accuracy of about 2%. Fast timing signals were derived from the E detectors with direct-coupled fast preamplifiers[3] and from the saturated anode pulse of the photomultiplier tube. The coincidence events were determined with a standard fast-slow coincidence circuit using a time-to-amplitude converter (TAC) to detect the fast coincidences. The ΔE, E, and TAC analog signals were sent to ADC's of the SDS 930 computer system. The ΔE and E signals were gated by events which deposited more than about 1.5 MeV in both detectors of an ΔE-E telescope. This signal was also used to gate the TAC signal provided a gamma-ray above about 0.7 MeV had been detected and a TAC conversion had occurred. The data were collected using an on-line particle identification program which permitted collection of particle-gamma correlation data from three independent ΔE-E telescopes.[4] The program stored all particle-gamma coincidence gated events on magnetic tape, allowing complete re-analysis of the gated data after a run. Gated and ungated particle spectra were stored during a run. The number of true coincidence events were determined by comparing the ratio of the gated and ungated inelastic peak areas to the ratio of the gated and ungated elastic peak areas. Since the TAC was operated at 100 nsec full scale, the fast time resolution was 100 nsec during a run. This resolving time could be reduced by about a factor of two by setting a SCA window around the time peak.

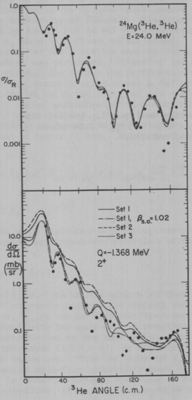

Fig. 10.4-1. ^{24}Mg elastic and inelastic cross sections. $\beta_2 = 0.34$ and $\beta_{so} = 2.04$ for the inelastic cross section predictions unless noted otherwise.

The post-run analysis was carried out by reconstructing the time spectra for events in a selected energy and particle type region. The number of true coincidence events were determined by comparing the number of counts in a time peak region with those in a flat time background region. The time peak region was established by summing the gated time spectra for a series of runs. The full width at the base of the gated time peak was approximately 11 nsec. Thus a factor of five to ten improvement was obtained in the fast coincidence resolving time. In addition, the error introduced by accidental subtraction is smaller when the gated time spectra is used. This is especially true if the elastic cross section is smaller than the inelastic cross section, as it is for most angles between 80° and 165° in this experiment.

Fig. 10.4-2. ^{24}Mg spin-flip cross section and spin-flip probability. β_2 = 0.34 and β_{so} = 2.04 unless noted otherwise.

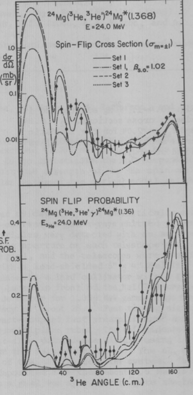

The measured cross sections and spin-flip probability are shown in Figs. 10.4-1 and 10.4-2. The error due to counting statistics is indicated for all points with errors larger than the size of the dots. All cross sections were multiplied by a factor of 1.1 since this consistently improved the optical model fit to the forward angle elastic data. This correction is comparable to the uncertainty in target thickness and uniformity. Note that the inelastic cross section is out of phase with the elastic cross section as prescribed by the Blair phase rule for strongly absorbed particles. The spin-flip probability was calculated assuming equal populations of the m = 0, +2, and -2 substates for the gamma detector solid angle correction. The uncertainty introduced by these substates is about ±0.02 for each point. The spin-flip data has not been corrected for the effects of the finite particle detector solid angle.

Predictions are shown for three slightly different sets of optical model parameters (see Table 10.4-1). The parameters of Set 1 and Set 3 were optimized by fitting the elastic scattering cross section using the optical model search program OPTIM-I (CYC-6835) obtained from the University of Colorado. The starting parameters for Set 1 were those obtained by Baugh[5] for 29 MeV ^{3}He scattering from ^{24}Mg. During the search, r_o, V_{so}, and r_c were held fixed and all other parameters were allowed to vary. The parameters of Set 2 are the same as Set 1 with the exception of V_{so}. No additional search was performed. Parameter Set 3 was obtained with V_o, V_{so}, r_{so}, a_{so}, and r_c fixed. The search was performed with V_{so} = 2.5 MeV. It might be noted that while the search program showed a definite preference for values of r_{so} and a_{so} near those of Set 1 the effect on the elastic fit was small. It was found that better fits could be obtained for the forward angle data if the nine back angle data points were excluded. The optimum parameters for this case produced deeper oscillations at forward angles; but they also raised the back angle prediction by about a factor of two. The form of the optical potential used was:

$$U(r) = V_c(r) - V_o f(r,R_o,a_o) - iWf(r,R_i,a_i) + \left(\frac{\hbar}{m_\pi c}\right)^2 V_{so} \frac{1}{r}\frac{d}{dr} f(r,R_{so},a_{so}) \vec{\sigma} \cdot \vec{L}$$

where $f(r,R,a) = [1 + \exp((r - R)/a)]^{-1}$ and $R_N = r_N A^{1/3}$.

The DWBA collective model calculations were performed with a computer program written by H. Sherif[6] which uses a deformed spin-dependent potential of the full Thomas form, i.e.,

$$(\hbar/m_\pi c)^2 V_{so} \vec{\sigma} \cdot [\vec{\nabla}\rho(\vec{r}) \times \vec{\nabla}/i],$$

where $\rho(\vec{r})$ is the nuclear matter density function. One of the options of Sherif's code allows one to choose different deformation parameters for the central and spin-orbit parts of the interaction. That is, β_{so}/β can be different from one. Shown in Fig. 10.4-1 and 10.4-2 are predictions with two spin-orbit strengths and two values of ADEF = β_{so}/β. The main contribution to the back angle spin-flip probability peak comes from the distorted waves (ADEF = 0). As ADEF is increased, the height of the back angle peak decreases. Thus the value of V_{so} implied by matching the height of the back angle spin-flip probability peak depends to some extent on the value of ADEF. In order to produce structure in the more forward angle spin-flip probability predictions, it appears that a value of

Table 10.4-1. Optical Model Parameters for $^{24}Mg + ^{3}He$ at 24.0 MeV

Set	V_o	r_o	a_o	W	r_i	a_i	V_{so}	r_{so}	a_{so}	r_c
1	152.8	1.15	0.744	18.87	1.70	0.883	2.5	1.62	0.507	1.30
2	152.8	1.15	0.744	18.87	1.70	0.883	3.0	1.62	0.507	1.30
3	150.0	1.16	0.732	17.65	1.74	0.913	3.0	1.10	0.719	1.30

ADEF around six is required. This is also seen to produce a better fit to the spin-flip cross section between 70° and 140°. The effect of using different spin-orbit geometry parameters is demonstrated by parameter Set 3. This set produces the best fit to the inelastic cross section at forward angles. However, the forward angle spin-flip cross section prediction has much less structure than the data. It should also be noted that while Set 2 and Set 3 produce about the same height for the back angle spin-flip probability peak, the back angle spin-flip cross section predictions differ by what would amount to 0.5 MeV in the spin-orbit potential.

The results of these calculations indicate that the spin-orbit potential for 24.0 MeV ^{3}He on ^{24}Mg is between 2.0 MeV and 3.5 MeV. This conclusion agrees with that of a previous spin-flip measurement on ^{12}C[7] and ^{3}He elastic polarization measurements on ^{12}C at 31.6 MeV,[8] and 18 and 20 MeV.[9] The lower limit of 2.0 MeV is slightly above the upper limit suggested by ^{3}He elastic polarization measurements on ^{12}C at 40 MeV.[10] There are strong indications that the strength of the ^{3}He spin-orbit interaction in DWBA collective calculations should be larger than that implied by the optical model parameters. A similar conclusion has been reached by Sherif[6] and Tesmer[11] for proton inelastic scattering. In comparing the spin-flip probability and elastic polarization predictions (not shown), it appears that the spin-flip probability is at least as sensitive, if not more sensitive, to the strength of the spin-orbit potential than is the elastic polarization. More calculations are planned to investigate the above conclusions.

1. F.H. Schmidt, R.E. Brown, J.B. Gerhart, and W.A. Kolasinski, Nucl. Phys. *52*, 353 (1964).
2. Nuclear Physics Laboratory Annual Report, University of Washington (1970), p. 32.
3. *Ibid.*, p. 30.
4. Section 5.5 of this report.
5. D.J. Baugh, Nucl. Phys. *A131*, 417 (1969).
6. H. Sherif, Ph.D. Thesis, University of Washington, 1968 (unpublished).
7. D.M. Patterson and J.G. Cramer, Phys. Letters *27B*, 373 (1968).
8. J.B.A. England, R.G. Harris, L.H. Watson, D.H. Worledge, and J.E. Evans, Phys. Letters *30B*, 476 (1969).
9. W.S. McEver, T.B. Clegg, J.M. Joyce, E.J. Ludwin, and R.L. Walter, Phys. Rev. Letters *24*, 1123 (1970).
10. R.L. Hutson, S. Hayakawa, M. Chabre, J.J. Kraushaar, B.W. Ridley, and E.T. Boschitz, Phys. Letters *27B*, 153 (1968).
11. J.R. Tesmer, Ph.D. Thesis, University of Washington, 1971 (unpublished).

10.5 ^{3}He Spin Flip in the Reaction $^{58}Ni(^3He, ^3He')$ at 22.5 MeV

J.G. Cramer, J. Eenmaa, T. Lewellen, D.M. Patterson, and J.R. Tesmer

Measurements have been made of the z-axis (spin-flip) ^{3}He-gamma angular correlation in which 22.5 MeV ^{3}He particles are inelastically scattered by ^{58}Ni to populate the first excited state of ^{58}Ni. The purpose of this experiment was to obtain information about the ^{3}He spin-orbit force by extending ^{3}He spin-flip measurements to medium-weight nuclei which are better described by optical model and DWBA collective model calculations.

Spin-flip data were obtained at 5° intervals from 125° to 165°, but unfortunately the statistical errors of the data are 50% or greater due to the small back-angle cross section for this reaction. There is evidence for a peak around 155° where the spin-flip probability is between 0.05 and 0.15. The back-angle spin-flip cross section is a factor of 10 to 20 smaller than that measured for ^{24}Mg at 24 MeV.[1]

Exploratory DWBA collective model calculations have been performed using two different sets of optical model parameters. One set used a real potential depth of 180 MeV[2] and the other set a real potential depth of 149 MeV.[3] The DWBA calculations using the 180 MeV parameter set with V_{so} = 3.0 MeV predict a maximum spin-flip probability of .068, while the DWBA calculation using the 149 MeV parameter set with V_{so} = 7.0 MeV predict a maximum spin-flip probability of .005. Both of these values are consistent with the experimental results reported here, although the 180 MeV set is preferred.

In view of the low spin-flip cross section, it is estimated that at least 72 hours of beam time would be required to obtain 10% statistics for a back angle spin-flip data point. Thus it is probably not feasible to obtain spin flip data with the accuracy required to make definitive statements about the ^{3}He spin-orbit potential in the Ni region.

---

1. Section 10.4 of this report.
2. D.E. Rundquist, M.K. Brussel, and A.I. Yavin, Phys. Rev. *168*, 1287 (1968).
3. E.R. Flynn and R.H. Bassel, Phys. Rev. Letters *15*, 168 (1965).

10.6 $^{12}C(\alpha,\alpha'\gamma)$ Out-of-Plane Angular Correlation Measurements

J. Eenmaa, T.K. Lewellen, D.M. Patterson, F.H. Schmidt, and J.R. Tesmer

In-plane angular correlation measurements for the reaction $^{12}C(\alpha,\alpha'\gamma)^{12}C^*$ $(4.44, 2^+)$ have been performed by Hayward at 22.750 MeV, and have been reported on earlier.[1-3] These data yield the substate amplitudes a_0, a_{+2}, a_{-2}, and the relative phase δ_2 (see Sec. 10.7 of this report). Since the 2^+ excited state decays via quadrupole (E2) radiation, the de-excitation radiation from the m = 0 substate is absent in the reaction plane and the relative phase $\delta_0 = \varepsilon_0 - \varepsilon_{-2}$ cannot be extracted from the in-plane data alone. On the other hand, if a value of θ_γ other than $\pi/2$ is chosen for the angle of measurement, the parameter δ_0 can, in principle, also be extracted since the correlation function measured out-of-plane contains all the parameters, a_0, a_{+2}, a_{-2}, δ_2, δ_0. In practice, however, the parameters are mixed in such a way as to make such an analysis extremely difficult. If, however, the correlation function is measured both in the reaction plane and at some angle to the plane, the parameters, a_0, $a_{\pm 2}$, δ_2 can be determined from the reaction plane data and used to analyze the more complex data measured outside the plane. The procedure that one might follow for such an analysis has been given by Cramer and Eidson.[4]

In order to perform the out-of-plane measurement, to complement the in-plane measurements of Hayward, a gamma-ray detector carriage and associated shielding was designed and fabricated so as to allow the positioning of the gamma-ray detector at $\theta_\gamma = 40°$, measured from the polar angle. This equipment was designed for use in the 24 inch diameter general purpose scattering chamber. It is described in detail in Sec. 3.3 of this report.

The out-of-plane correlation measurements were then performed at 35 alpha-particle scattering angles between 15° and 165°. At each alpha-particle scattering angle, correlations were measured at from 8 to 15 azimuthal gamma-ray angles (ϕ_γ) between 0° and 180°. In some cases, as a check on the geometrical alignment of the equipment, measurements were also performed on the opposite side of the beam, i.e., at $\phi_\gamma = \phi_\gamma + 180°$. The incident beam energy was 22.750 MeV and the target was a self-supporting 200 $\mu g/cm^2$ carbon foil. The combined in-plane and out-of-plane data are currently being analyzed following the procedure outlined in Ref. 4.

1. Nuclear Physics Laboratory Annual Report, University of Washington (1968), p. 3.
2. Nuclear Physics Laboratory Annual Report, University of Washington (1969), p. 16.
3. T.D. Hayward, Ph.D. Thesis, University of Washington, 1969 (unpublished).
4. J.G. Cramer and W.W. Eidson, Nucl. Phys. *55*, 593 (1964).

10.7 $^{58}Ni(\alpha,\alpha'\gamma)^{58}Ni^*$(1.45 MeV) Angular Correlation Measurements at E_α = 23.25 MeV

J. Eenmaa, T.K. Lewellen, D.M. Patterson, F.H. Schmidt, and J.R. Tesmer

Absolute measurements of angular correlations between inelastically scattered alpha particles and de-excitation gamma rays in the reaction $^{58}Ni(\alpha,\alpha'\gamma)$ $^{58}Ni^*$ (1.45 MeV,2^+) have been performed at an incident alpha particle energy of 23.25. Initial in-plane measurements and the description of the experimental procedure have been reported earlier.[1] Since then, the in-plane measurements have been extended to cover the complete angular range from $\phi_{\alpha'}$ = 30° (lab) to $\phi_{\alpha'}$ = 170° (lab). Out-of-plane measurements, at θ_γ = 40°, have also been performed for $\phi_{\alpha'}$ = 35° (lab) to $\phi_{\alpha'}$ = 82.5° (lab) at 2.5° intervals. The procedure for the out-of-plane measurements is described in Sec. 10.6 of this report and the analysis of these data is currently in progress. The following discussion will refer only to the in-plane correlation data.

The angular correlation function for inelastically scattered alpha particles from an even-even nucleus and the co-planer de-excitation gamma rays in a $0^+ \rightarrow 2^+ \rightarrow 0^+$ transition can be expressed as:[2]

$$W(\theta_\gamma = \pi/2, \phi_\gamma; \phi_{\alpha'}) = \frac{5}{16\pi}[(1 - a_0^2) - 2a_{+2}\, a_{-2} \cos(4\phi_\gamma - \delta_2)]$$

where the $a_m (m = 0, \pm 2)$ represent the magnitudes of the complex transition amplitudes,

$$T_m / \sqrt{\sum_m |T_m|^2} = a_m e^{i\varepsilon_m},$$

for the excitation of the m'th substates of the 2^+ state, and δ_2 is the relative phase, $\delta_2 = \varepsilon_2 - \varepsilon_{-2}$.

Measurements of the in-plane correlation function with a gamma-ray detector of known efficiency enables one to determine, absolutely, the parameters a, $a_{\pm 2}$, $a_{\mp 2}$, and δ_2. The ambiguity between the a_{+2} and a_{-2} parameters, which arises because the expression for W is symmetric in a_{+2} and a_{-2}, can be removed only by means of a polarization-sensitive angular correlation measurement.[3,4]

Optical model and collective model DWBA calculations have been performed. Six sets of optical model potentials were obtained by using the optical model search code OPTIM-I to fit the elastic scattering data. These potentials correspond to the well-known discrete ambiguities in the real potential depth which arise from the place-equivalence of the asymptotic solutions and correspond to a discrete number of nodes of the wave function inside the nucleus. These potentials are listed in Table 10.7-1. All of these potentials give about the same

Table 10.7-1. Optical Model Parameters

Set	V_R	R_R	A_R	W_{VI}	R_I	A_I	R_C
1	20.7	1.72	0.49	15.6	1.28	1.10	1.40
2	43.8	1.66	0.52	9.0	1.73	.30	1.40
3	67.8	1.59	0.52	12.5	1.58	.38	1.40
4	104.0	1.48	0.56	18.0	1.48	.14	1.40
5	129.3	1.49	0.54	18.4	1.50	.19	1.40
6	162.8	1.47	0.53	19.7	1.52	.22	1.40

quality fits to the elastic scattering differential cross-section. Set 1 has the lowest real potential depth of about 21 MeV, while Set 6, with $V_R \sim 160$ MeV, corresponds to about 4x single nucleon potential. Collective model DWBA calculations were performed for each set of potentials. The predictions shown in the figures are those for Sets 1 and 6. The other sets of potentials give fits intermediate between these two extremes.

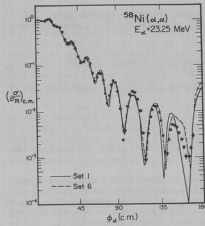

Fig. 10.7-1. Elastic scattering differential cross section, and optical model predictions.

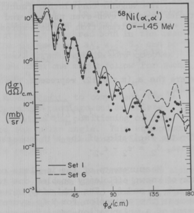

Fig. 10.7-2. Inelastic scattering differential cross section, and collective model DWBA predictions.

Figures 10.7-1 and 10.7-2 show the data and predictions for the elastic and inelastic differential scattering cross sections. While the predictions of Sets 1 and 6 give the same quality fits to the elastic scattering, the predictions of Set 1, for the inelastic scattering, are definitely superior at the backward angles. The remaining figures (10.7-3 - 10.7-5) show the angular correlation data and the corresponding DWBA predictions.

The data, as well as the fits, for the phase angle, δ_2, (Fig. 10.7-3) oscillate about the adiabatic phase angle (shown by the diagonal line), and pass through the adiabatic phase angles at the maxima of the inelastic differential cross sections. These oscillations become more marked as one goes toward the backward angles. Again Set 1 is superior in that the data do not exhibit the violent behavior predicted by Set 6. Figure 10.7-4 shows the substate populations a_0^2 and $a_{+2}^2 + a_{-2}^2$ and the corresponding substate cross-sections. The oscillations in the partial cross sections are much more marked than for the total inelastic differential cross-section. Again Set 1 seems to give the better fit, both with regard to magnitudes and phases. Figure 10.7-5 shows the measured magnitude of the nuclear polarization, $P_n = a_{+2}^2 - a_{-2}^2$. The top curves show the predicted polarization with the correct sign. The correlation data only gives us the magnitudes but not the sign of the polarization and these data and fits are shown in the lower half of the figure. Again, Set 1 seems to give the better fits. Because the magnitude of the inelastic cross-section is so low, it doesn't appear feasible to attempt to remove the ambiguity between a_{+2} and a_{-2} by doing a polarization measurement.

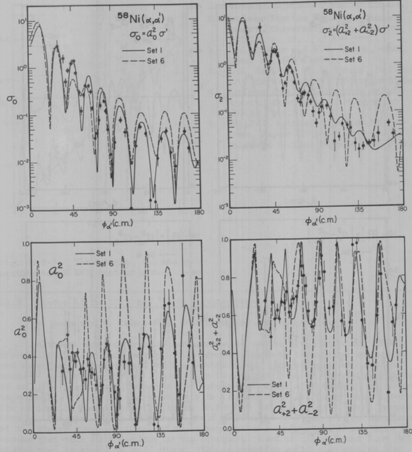

Fig. 10.7-4. Substate populations and partial cross-sections and collective model DWBA predictions.

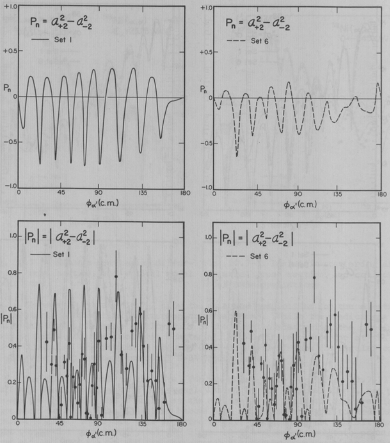

Fig. 10.7-5. Nuclear polarization and collective model DWBA predictions.

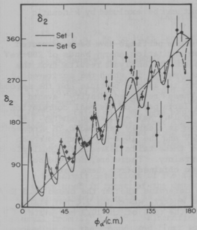

Fig. 10.7-3. Phase angle, δ_2, and collective model DWBA predictions.

1. Nuclear Physics Laboratory Annual Report, University of Washington (1970), p. 88.
2. J.G. Cramer and W.W. Eidson, Nucl. Phys. *55*, 593 (1964).
3. T.D. Hayward, Ph.D. Thesis, University of Washington, 1969(unpublished).
4. Nuclear Physics Laboratory Annual Report, University of Washington (1969), p. 16.
5. OPTIM-I, Optical Model Search Program, Report CYC-6835, University of Colorado Nuclear Physics Laboratory.

10.8 Status of the 10.3 MeV ^{12}C State Experiment

D. Bodansky, D. Chamberlin, W. Trautmann, and D. Wilkinson

Although numerous studies have been made of the level structure of ^{12}C around 11-MeV excitation energy, full agreement between theoretical approaches and experimental results has not been established. For example, the cluster model[1,2] predicts a pair of 2^+ states in this region, one of them being a member of an alpha-cluster band based on the deformed 0^+ state at 7.66 MeV. In several experiments,[3-5] β-decay of ^{12}B and ^{12}N to a broad state in ^{12}C has been observed, its excitation energy and width being 10.3 ± 0.3 MeV and 3.0 ± 0.7 MeV, respectively. The spin-parity assignment could be limited to 0^+ or 2^+. On the basis of the Wigner sum rule, 0^+ seems to be more probable. However, if one were to assume that this state belongs to the rotational band of the deformed 7.66 MeV state, then it should be a 2^+ state. This assumption would also explain the large width as a result of the strong deformation.[5,6] An effort to determine the spin of the 10.3 MeV state has been undertaken, using alpha-alpha angular correlation methods.

^{12}C nuclei of a thin carbon target have been excited by a 24-MeV alpha-particle beam. The scattered alpha-particles have been observed and identified in coincidence with the alpha-particles from the $^{12}C \rightarrow {}^8Be + \alpha$ breakup. The inelastic alpha-particle detector was held at 20°(lab) and the breakup alpha particle detector was varied in angle from 25° to 150°(lab). Alpha particles resulting from ^8Be breakup are also observed but can be excluded by kinematic considerations.

Angular distributions for the second alpha particle have been extracted from the coincidence spectra, and plotted for excitation energy bands of 200-keV width from 9.5 to 14.5 MeV. A major problem for the analysis results from the fact that the coincidence spectra also contain events in which the scattered alpha particle is observed in the detector for the second particle and the second alpha is then found in the other detector. These "reversed identity" events appear as peaks in the spectra and obscure a large part of the real correlation pattern, in particular the region from 11.5 to 14.5-MeV excitation energy. At 9.6 MeV the correlation function of a 3^- state is clearly reproduced, in agreement with other works.[7,8] The tails of the 9.6-MeV and the 10.8-MeV groups overlap in the region around 10.3 MeV. A subtraction of these tails leaves a residual yield comparable in height to the statistical uncertainty. Therefore, no evidence for the observation of the 10.3 state has yet been obtained from these data.

Further investigations are planned to determine whether the broad 10.3 MeV state can still be seen near 9 MeV excitation energy, where the 9.6-MeV state should have fallen off rapidly enough so that the tail of the 10.3-MeV state could become predominant.

1. R.K. Sheline and K. Wildermuth, Nucl. Phys. *21*, 196 (1960).
2. K. Wildermuth and W. McClure, in *Springer Tracts in Modern Physics, Vol. 41,* Ed. by G. Hohler (Springer-Verlag, Berlin, 1966).
3. C.W. Cook *et al.*, Phys. Rev. *111*, 567 (1958).
4. D.H. Wilkinson *et al.*, Phys. Rev. *130*, 1953 (1963).
5. D. Schwalin and B. Povk, Nucl. Phys. *89*, 401 (1966).
6. H. Morinaga, Phys. Letters *21*, 78 (1966).
7. R.A. LaSalle *et al.*, Phys. Letters *5*, 170 (1963).
8. O.V. Borniof *et al.*, Sov. Journal of Nucl. Phys. *4*, 227 (1967).

11. REACTIONS WITH OXYGEN IONS

11.1 $^{12}C(^{16}O,\alpha)^{24}Mg$ to High Excitation Energies in ^{24}Mg

D. Bodansky, D. Chamberlin, C. Ling, and D. Oberg

In order to study further the highly excited states in ^{24}Mg (in the region of 15 to 18 MeV) which were found to be populated in the $^{12}C(^{16}O,\alpha)^{24}Mg$ reaction,[1] the experiment was extended to include measurement of α-α angular correlations. The excited states of ^{24}Mg were expected to decay primarily by alpha particle emission to ^{20}Ne. If the first alpha particle is detected at 0°, the angular distributions of the second alpha particle can be used to directly determine the spin and parity of the ^{24}Mg states which have undergone transitions to the ground state of $^{20}Ne(0^+)$.

To permit detection of the first alpha particle at 0°, a 44 mg/cm^2 gold foil was placed in front of the detector to stop the incident ^{16}O beam (about 48 MeV in most runs) as well as scattered ^{16}O and ^{12}C nuclei. The second alpha particle was detected in coincidence with the first, over a (laboratory) angular interval from 12° to 33°. Kinematic bands were observed corresponding to events proceeding to the ground and first excited states of ^{20}Ne. While this work was still in a quite preliminary stage, we became aware of the very similar work being carried out by the Yale group.[2] In view of the similarity of approach, the very substantial progress already made at Yale, and our interest in other projects, it seemed unwise to pursue this program further at the present time.

1. Nuclear Physics Laboratory Annual Report, University of Washington (1970), p. 149.
2. A. Gobbi, P.R. Maurenzig, L. Chua, R. Hadsell, P.D. Parker, M.W. Sachs, D. Shapira, R. Stokstad, R. Wieland, and D.A. Bromley, Phys. Rev. Letters *26*, 396 (1971).

11.2 Two-Neutron Transfer Reactions in the Vicinity of the Coulomb Barrier Using the Reaction $(^{18}O,^{16}O)$

M. Hasinoff, M. Lau, K.G. Nair, J. Pedersen, and W. Reisdorf

Two-nucleon transfer cross sections are known to be strongly nuclear structure dependent and allow therefore sensitive tests of current microscopic theories for nuclear wave functions.[1] In the past, two-nucleon transfer reactions have been predominantly induced using light projectiles ($A \leq 6$) such as in (t,p) reactions. The present availability of heavy ion beams in tandem Van de Graaff accelerators makes it possible to investigate two-nucleon transfer induced by heavier projectiles. A program was initiated which uses the reaction $(^{18}O,^{16}O)$ for two-neutron transfer studies. The success of one-nucleon transfer studies using heavy ion beams with energies in the vicinity of the Coulomb barrier[2] leads us to confine ourselves in this preliminary study to this energy region.

Several advantages are expected from this type of study:

a) restriction to energies in the vicinity of the Coulomb barrier will allow the use of theoretical techniques well established in Coulomb excitation studies and recently[3] applied to nucleon transfer reactions as well. It is hoped that the influence of nuclear fields on the incoming and outgoing waves is small enough to allow a simplified treatment such as described in Ref. 3, thus circumventing existing difficulties of optical models in heavy ion scattering.[4] The relatively large values ($\sim$ 50) of the Coulomb parameter $Z_1Z_2e^2/\hbar v$ justify the use of semiclassical approximations for the particle trajectories as a first orientational step in the data analysis; b) in relation with the above it is hoped that reliable spectroscopic factors will be obtained in these studies; c) a certain number of potentially interesting phenomena particular to heavy ion scattering are expected. First one may mention a possible difference between two-nucleon fransfer using (t,p) versus (A,A - 2) reactions with A > 6: whereas in the former projectile the s-part in the intrinsic two-nucleon wave function is dominant, it is conceivable that in some heavier projectiles significant fractions of d(ℓ = 2)-parts have to be taken into account for the intrinsic two-nucleon wave function. This should yield extended information on two-nucleon correlations in nuclei. A second prospect has been pointed out by Dietrich,[5] namely possible strong enhancement of two-nucleon transfer between nuclei known to have strong pairing vibrations.

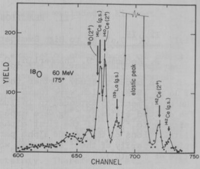

Fig. 11.2-1. Energy spectrum at 175° obtained with ^{18}O (60 MeV) incident on ^{140}Ce.

We have started our study choosing ^{140}Ce as target. The advantages of this choice are readily seen: The reaction $^{140}Ce(^{18}O,^{16}O)^{142}Ce$ involves the transfer of a two-nucleon system between two closed neutron-shell cores (N = 8 and 82) and consequently substantial simplifications for the theoretical interpretation are expected. Another favorable factor is the near equality and low value of the two-neutron binding energies for both cores ($B_{2n}(^{18}O)$ = 12.19 MeV, $B_{2n}(^{142}Ce)$ = 12.65 MeV).

In a first experiment a set of six surface barrier detectors were arranged at backward angles ranging from 175° to 150° relative to the beam axis. A natural Ce target of $\sim$20 μg/cm^2 on 90 μg/cm^2 Ni was exposed to a well collimated ^{18}O beam ($\sim$ 200 nA). An energy spectrum obtained at 175° and at incident energies of 60 MeV (laboratory system) is shown in Fig. 11.2-1. All significant peaks can be identified through kinematic relationships as indicated by the arrows in the figure. A relatively large cross-section for two-nucleon transfer to the ground and first excited (2^+) state of ^{142}Ce was observed. All transfer reactions are confined to backward angles. At 175° the cross-section for elastic scattering was found to be (86 ± 2)% of the Rutherford cross-section. The ratio of the elastic versus the two-neutron transfer cross-section is 109 ± 7 and 192 ± 17 (at 175°) for the first 2^+ (Q = -0.19 MeV) and the ground state (Q = +0.46 MeV) of ^{142}Ce respectively. The strong probability for the excitation of the 2^+ state in ^{142}Ce may indicate the possibility of a two-step process (Coulomb excitation followed by transfer or vice versa). A surprisingly large one-neutron transfer cross-section to the ground state of ^{141}Ce was also observed. It is comparable to the cross-sections for Coulomb excitation to the first excited states of ^{18}O and ^{140}Ce. The importance of angular momentum matching at these incident energies is apparent: only reactions with $-3 \leq Q \leq 3$ MeV were seen with sizable statistical weight.

---

1. N.K. Glendenning, Phys. Rev. *137*, B102 (1965); I.S. Towner and J.C. Hardy, Adv. in Phys. *18*, 401 (1969).
2. L.J.B. Goldfarb, in *Nuclear Reactions Induced by Heavy Ions*, ed. by R.Bock and W.R. Hering (North-Holland Publishing Co., Amsterdam, 1970), p. 115.
3. D. Trautmann and K. Alder, Helv. Phys. Acta *43*, 363 (1970).
4. J.S. Blair, in *Nuclear Reactions Induced by Heavy Ions*, ed. by R. Bock and W.R. Hering (North-Holland Publishing Co., Amsterdam, 1970), p. 27; D.A. Bromley, *ibid.*, p. 27
5. K. Dietrich, Phys. Lett. *32B*, 428 (1970).

11.3 Measurements of ^{48}Ca + ^{16}O and ^{40}Ca + ^{16}O Elastic Excitation Functions

M. Hasinoff, T. Lewellen, K.G. Nair, D. Potter, R. Vandenbosch, and W. Wharton

We have initiated a series of experiments to study the elastic excitation functions of ^{16}O from calcium isotopes above the Coulomb barrier. The motivation for these experiments was to see if the ideas proposed[1] to explain the large differences[1,2] in the elastic scattering of ^{18}O + ^{18}O as compared to ^{16}O + ^{16}O could be successfully extended to other systems. It was suggested that the critical angular momentum parameter of the ℓ-dependent potential proposed by Chatwin *et al.*[4,5] could be estimated from consideration of only the direct reaction channels expected to be strongly coupled to the elastic channel. Calculations based on the relative Q-values of the inelastic and alpha-transfer channels predict that there will be stronger ℓ-dependence for ^{40}Ca than for ^{48}Ca. However, the differences expected are not nearly as large as between the elastic scatterings of ^{16}O + ^{16}O and ^{18}O + ^{18}O.

The experimental setup consisted of a multi-detector array with six 100 thick surface barrier detectors arranged at the lab angles of 30°,60°,70°,80°, 90°, and 100°. The target thicknesses were 31 μg/cm^2 ^{40}Ca and 97 μg/cm^2 ^{48}Ca on 15 μg/cm^2 carbon backings. Excitation functions were measured from E_{lab} = 25.0 MeV to 45.0 MeV for ^{40}Ca and from E_{lab} = 25.0 MeV to 50.0 MeV for ^{48}Ca. The intervals were varied from 1.0 MeV to 5.0 MeV depending on the energy region. The absolute excitation functions for ^{48}Ca and ^{40}Ca are shown in Figs. 11.3-1 and 11.3-2. Corrections were made for the energy loss in the targets and the small amount of ^{40}Ca impurity (15.7%) in the ^{48}Ca target. The continuous lines in the figures are only to guide the eye. In Fig. 11.3-1, the dashed line connecting the open squares is an interpolated excitation function taken from the ^{40}Ca results to correspond to the center of mass angle of 119.2°. It is evident from these two excitation functions at $\theta_{c.m.}$ = 119.2°, that the strong absorption

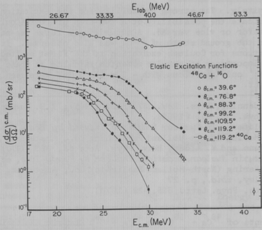

Fig. 11.3-1. Elastic excitation functions of $^{48}Ca + ^{16}O$.

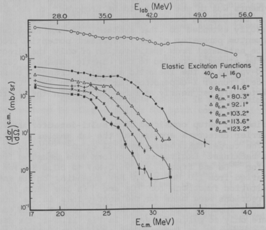

Fig. 11.3-2. Elastic excitation functions of $^{40}Ca + ^{16}O$.

radius[3] of ^{48}Ca is larger than that of ^{40}Ca by about 0.2 F.

We have also measured elastic angular distributions for ^{48}Ca + ^{16}O at E_{lab} = 35.0 MeV from θ_{lab} = 20° to 100° and for ^{40}Ca + ^{16}O at E_{lab} = 35.0 MeV, 36.3 MeV and 38.4 MeV. The latter are being analyzed. The ^{48}Ca + ^{16}O elastic angular distribution is shown in Fig. 11.3-3. The lines are calculated curves using the optical model code LOP.[1] The dashed line corresponds to a standard optical model fit with V = 35.0 MeV, W = 2.5 MeV, R = 7.46 F, R_c = 7.2 F, and a = 0.67 F. The continuous line is calculated using an ℓ-dependent potential with V = 35.0 MeV, W = 2.5 MeV, R = R_c = 7.2 F, a = 0.75 F, and ℓ_c = 13.3. The geometries of the real and imaginary potentials were the same in both cases. We are now in the process of calculating the excitation functions with the same set of parameters.

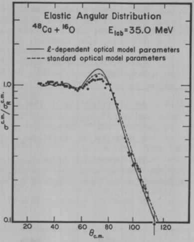

Fig. 11.3-3. Elastic angular distributions of ^{48}Ca + ^{16}O at E_{lab} = 35.0 MeV.

Finally, we tried to look for the resonance structure expected on the basis of the ℓ-dependent optical model prediction in the region of E_{lab} = 37.0 MeV to E_{lab} = 42.0 MeV at extreme back angles for the ^{16}O elastic scattering from ^{40}Ca. For this purpose, we used an annular surface barrier detector 700μ thick at a distance of 6.13" from the target (θ_{lab} = 178.7°). In addition, four regular 100μ thick surface barrier detectors and one 35μ thick planar detector were placed at regular intervals on a platform so as to cover the back angles from 120° to 160°. The measured energy spectra consisted of all particles which could be stopped in these detectors. They showed pronounced peaks at all incident energies. The excitation functions of these peaks indicated resonances near E_{lab} = 36.3 MeV and E_{lab} = 38.4 MeV. However, a comparison of the kinematic positions of these peaks obtained from the ^{40}Ca and ^{48}Ca spectra at different angles, indicated that these were alpha-particles produced in the reaction ^{12}C + ^{16}O → ^{4}He + ^{24}Mg and were originating from the carbon backings of the targets. With the present experimental setup we were unable to identify the ^{16}O elastic peaks from ^{40}Ca and ^{48}Ca at back angles.

Further experiments are planned to reduce the excessive contributions to the energy spectrum from carbon by choosing different target backings. In addition, a suitable combination of a thin transmission detector (e.g., 11μ - 20μ thick) with a thicker detector (e.g., 100μ thick) behind it, will be used to exclude the longer range alpha particles.

1. R.W. Shaw, Jr., Ph.D. Thesis, University of Washington, 1970 (unpublished).

2. R.H. Siemssen, J.V. Maher, A. Weidinger, and D. Bromley, Phys. Rev. Letters, *19*, 369 (1967).
3. J.S. Blair, Phys. Rev. *95*, 1218 (1954).
4. J.S. Eck, R.A. Chatwin, K.A. Eberhard, R.A. LaSalle, A. Richter, and D. Robson in *Nuclear Reactions Induced by Heavy Ions*, ed. by R. Bock and W.R. Hering (North-Holland Publishing Co., Amsterdam, 1970), p. 80.
5. R.A. Chatwin, J.S. Eck, A. Richter, and D. Robson, *ibid.*, p. 76.

11.4 An Investigation of the Nucleon Transfer Reactions Induced in ^{140}Ce by 60 MeV ^{16}O Ions

J.S. Blair, M. Hasinoff, K.G. Nair, W. Reisdorf, and W. Wharton

The importance of transfer reactions induced by heavy ions below the Coulomb barrier as a tool for the extraction of relatively accurate spectroscopic information has been stressed in recent years by Buttle and Goldfarb[1] and by

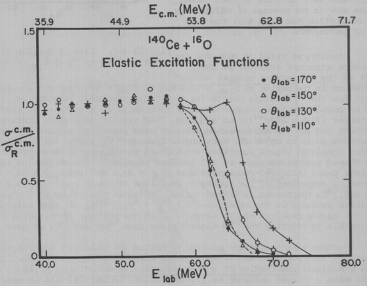

Fig. 11.4-1. Elastic excitation functions of ^{140}Ce + ^{16}O. The continuous lines are only intended to guide the eye.

Trautmann and Alder[2] among others. Consequently, there has been an increased activity in this field lately starting with the work reported by Barnett and Phillips[3] who observed neutron and proton transfers below the barrier induced by 69.1 MeV ^{16}O ions in ^{208}Pb.

In the present work we tried to study sub-Coulomb nucleon transfer reactions induced by 60 MeV ^{16}O ions in ^{140}Ce with a view to investigating the reaction mechanisms as well as spectroscopic factors of levels excited by these reactions. This is a continuation of the work reported last year.[4]

The experimental setup was essentially the same as in the previous work except that six surface barrier detectors were simultaneously used instead of four. These were mounted in an array at angular intervals of 10° each and an extra detector was kept at a fixed angle of 90° to serve as a monitor. The target thickness was 24.0 μg/cm^2 and the average solid angle subtended at the detectors was 1.08×10^{-3} sr. First of all, the elastic excitation functions were measured from E_{lab} = 40.0 MeV to 72.0 MeV at intervals of 2.0 MeV each and at the laboratory angles of 110°, 130°, 150°, and 170°. The ratio of the elastic to Rutherford cross sections as a function of incident energy is shown in

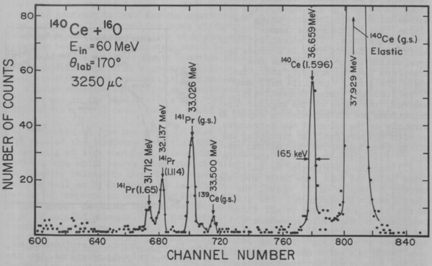

Fig. 11.4-2. Energy spectrum of all the heavy ions stopped in the detector at θ_{lab} = 170°. The arrows indicate the kinematically allowed positions of peaks corresponding to the reactions which leave the residual nuclei in the states shown near the appropriate peaks.

Fig. 11.4-1. The transfer cross sections decrease rapidly with incident energy and to get reasonable yields the incident energy has to be high. However, to take advantage of the formalisms of sub-Coulomb transfer theories, the incident energy has to be below the Coulomb barrier. It was decided on the basis of these curves that E_{lab} = 60.0 MeV is the optimum incident energy to study the transfer reactions.

All energetically allowed heavy ion reaction products were stopped in the detectors and counted. A typical energy spectrum at θ_{lab} = 170° is shown in Fig. 11.4-2. A very careful energy calibration was made using the elastic scattering of ^{16}O ions of energies 40.0 MeV, 45.0 MeV, 52.2 MeV, 55.0 MeV, and 60.0 MeV. All the peaks in the spectra were identified from kinematics using the energy calibration after proper corrections for the energy loss in the target were applied. The elastic peak and the inelastic peak due to the first excited state of ^{140}Ce (1.596 MeV, $J^{\pi} = 2^{+}$) were easily identified at all angles. In addition, Fig. 11.4-1 also shows peaks corresponding to the final reaction products of ^{17}O(g.s.) + ^{139}Ce(g.s.), ^{15}N(g.s.) + ^{141}Pr(g.s.), ^{15}N(g.s.) + ^{141}Pr (1.114 MeV), and ^{15}N(g.s.) + ^{141}Pr(1.65 MeV). Angular distributions for the last three reactions were measured and the results are shown in Fig. 11.4-3. The errors indicated are due to statistics only. The strong backward peaking characteristic of sub-Coulomb transfer reactions is evident in all cases. The dashed lines are calculated using the simple transfer theory of Lemmer[5] for ℓ = 0 transitions. The normalization is arbitrary. Clearly this is a crude approximation in our case, since the ℓ-transfers involved are 3,6, and 1 for the ^{141}Pr(g.s.),^{141}Pr(1.114 MeV) and ^{141}Pr(1.65 MeV) states respectively. However, the shapes of the angular distributions are not expected to depend as strongly on the value of the ℓ-transfer as with the more familiar stripping and pickup reactions above the Coulomb barrier. The continuous line in the ^{141}Pr (g.s.) angular distribution is calculated using the DWBA code DWUCK with the correct ℓ-transfer of 3. Again, the normalization is arbitrary. The shapes of the calculated curves in all these cases are in reasonable agreement with the experimental trend. However it is not clear at this point that the DWBA code DWUCK is a valid one to use in the present case to extract spectroscopic information.

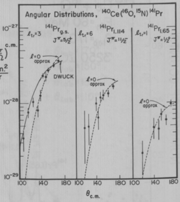

Fig. 11.4-3. Angular distributions of the proton stripping reactions. The explanations of the continuous and dashed lines are given in text. The ℓ-transfer assignments are from angular momentum considerations and the J^{π} assignments are those due to generally accepted ^{140}Ce(^{3}He,d)^{141}Pr data.

Therefore, a program is being written[6] specifically for heavy ion induced nucleon transfer below the Coulomb barrier. It is hoped that more quantitative information regarding the reaction mechanisms, relative spectroscopic factors, etc., can be obtained using this code when the analysis is complete.

---

1. P.J.A. Buttle and L.J.B. Goldfarb, Nucl. Phys. *78*, 409 (1966).
2. D. Trautmann and K. Alder, Helv. Phys. Acta, *43*, 363 (1970).
3. W.R. Phillips and A.R. Barnett, in *Nuclear Reactions Induced by Heavy Ions*, ed. by R. Bock and W.R. Hering (North-Holland Publishing Co., Amsterdam, 1970).
4. Nuclear Physics Laboratory Annual Report, University of Washington (1970) p. 108.
5. R.H. Lemmer, Nucl. Phys. *39*, 680 (1962).
6. Sec. 5.7 of this report.

11.5 Coupled Channels Analysis of Heavy Ion Elastic Scattering

R. Vandenbosch

In an investigation of the elastic scattering of ^{18}O off ^{18}O reported last year[1] it was found that the 90° excitation function for this reaction is in striking contrast to that for the scattering of ^{16}O off ^{16}O. The former system does not exhibit the striking gross structure exhibited in the latter case, and has much smaller cross sections at higher energies. We suggested[2] that the differences between the two systems could be qualitatively understood on the basis of the relative ease for direct reaction channels to carry away the angular momentum associated with a grazing collision in the elastic entrance channel. An analysis showed that the Q value differences between the two systems would lead to angular momentum inhibition of directly-coupled channels in the case of ^{16}O + ^{16}O but not in the case of ^{18}O + ^{18}O. If the direct-reaction channels are inhibited the elastic cross section would be expected to be unusually large.

Looked at from the point of view of the optical model, it is primarily the size of the imaginary potential which determines the magnitude of the elastic scattering at high energies. Since the imaginary potential is determined by interactions which remove flux from the elastic entrance channel, the size of W is directly related to the direct-reaction channels coupled to the entrance channel, as well as by interactions leading to intermediate states which eventually result in compound nucleus formation. A more quantitative approach to studying the effect of competing direct reaction channels on the elastic cross section is that of coupled channels.[3] At the present time one only knows how to properly treat inelastic excitations with this approach. The coupled channels approach has been quite successful in describing scattering of light particles from either vibrational or permanently deformed nuclei. It has also been applied to the elastic and inelastic scattering of heavy ions at high energy.[4] The nuclear potential, assumed to follow the nuclear shape, is expanded in terms of deformation parameters. If only the real part of the potential is assumed to be deformed, the coupling is said to be real, and if the imaginary part of the potential is also deformed the coupling is called complex. It has been suggested[5] that only real coupling need be considered if all of the important direct-reaction channels are treated explicitly in the coupled-channels calculation. It is perhaps appropriate at this point to raise a warning note about the appropriateness of such a description for the interaction of two heavy ions. It is not at all clear that such a simple description adequately describes all of the important degrees of freedom of two finite sized deformable objects. On the other hand our interest in this model will be to explore the effects on the elastic channel, and hopefully the details of the effect on the elastic channel will depend primarily on the amount of flux removed from the elastic channel and less sensitively on the exact form of the form factor of interaction, assuming that the overall strength of the coupling has been chosen to reproduce observed inelastic cross sections.

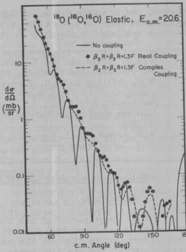

Fig. 11.5-1. Comparison of coupled-channels calculations of elastic scattering angular distribution with optical model calculation (no coupling). The coupling is to a 2^+ state at 2 MeV and a 3^- state at 6 MeV excitation energy.

We first describe some sample coupled channels calculations performed to explore the effects of various parameters on the elastic cross sections. The geometry of the potential used in these calculations is essentially that of the Maher *et al.*[6] optical model fit to $^{16}O + ^{16}O$. Figure 11.5-1 compares the calculated elastic cross section assuming large deformation parameters for both the 2^+ and 3^- states with the elastic cross section given by the same optical potential in the absence of coupling. The effect of coupling with this potential is to damp the oscillatory structure in the angular distribution, with more of the structure washed out if complex rather than real coupling is assumed. There is also some shift in the peak positions in this example. The relative effects of the inelastic scattering to the 2^+ and 3^- states in ^{16}O as compared to ^{18}O is shown in Fig. 11.5-2. The βR values are taken from the literature[4,7] or, in the case of the 2^+ state in ^{18}O, from an analysis of $^{16}O + ^{18}O$ inelastic scattering. The structure is more strongly damped in ^{18}O due to the less negative Q value and the larger deformation of the 2^+ state. The larger deformation parameter for the 3^- state in ^{16}O as compared to ^{18}O somewhat weakens the direction of the effect of 2^+ states. The alpha transfer channels, which are not included in this calculation, are expected to play a dominant role for the high partial waves for ^{18}O.

A useful way to illustrate various effects on the different partial waves is to plot the S matrix elements in the complex plane. The scattering matrix element for the ℓ^{th} partial wave is defined by $S_\ell = e^{2i\delta_\ell}$, where δ_ℓ is the nuclear phase shift. In Fig. 11.5-3 we plot the S matrix elements for the sample calculation shown in Fig. 11.5-2. One can see that the stronger coupling to states in

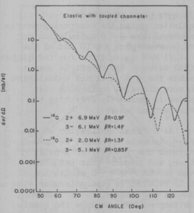

Fig. 11.5-2. Sample coupled channels calculations illustrating the relative effects of the inelastic scattering to the 2^+ and 3^- states in ^{16}O as compared to ^{18}O. A vibrational model with complex coupling was used. The calculation assumed non-identical particles.

^{18}O as compared to ^{16}O has resulted in stronger absorption for the partial waves corresponding to grazing collisions, $\ell \sim 16$.

The dependence on Q-value alone is exhibited by the dotted and dashed curves in Fig. 11.5-4. A more negative Q-value results in the coupled channel to be less effective in damping the cross section. The relative importance of coupling on the low and high partial waves is also demonstrated in the figure. In this com-

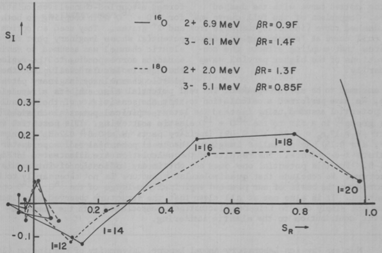

Fig. 11.5-3. The S-matrix elements for the even partial waves are plotted for the sample calculations shown in Fig. 11.5-2. The lines connecting the points are simply to guide the eye. The arc starting from S_R = Re S_ℓ = 1.0 is the locus of points expected in the absence of absorption.

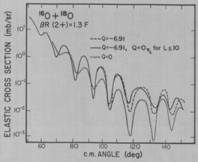

Fig. 11.5-4. Illustration of the Q-value dependence on the elastic scattering assuming coupling to a 2^+ deformed state. The damping associated with a more favorable Q value is shown by comparison of the dotted curve with the dashed curve. Comparison of the full curve and the dashed curve (indistinguishable from the full curve at forward angles) demonstrates that coupling affects the contributions of the higher partial waves primarily.

parison we have performed a synthetic calculation using the scattering-matrix elements of the Q = 0 calculation for partial waves with $\ell \leq 10$ and of the Q = -6.91 MeV calculation for the higher partial waves. The result is seen to resemble the Q = -6.91 MeV calculation much more closely, confirming that coupling is primarily affecting the higher partial waves.

As a final application of the coupled-channels approach, we have investigated the proposal of Scheid, Greiner, and Lemmer[8] that structure observed in the $^{16}O + ^{16}O$ excitation function is related to quasimolecular states. Following the suggestion of Imanishi,[9] who attempted to reproduce the quasimolecular structure in $^{12}C + ^{12}C$ at low energies by considering coupling to the 2^+ state in ^{12}C, Scheid *et al.* have performed a coupled-channels calculation for $^{16}O + ^{16}O$ with coupling to both 3^- and 2^+ states. They used an optical potential whose imaginary part for the elastic channel was assumed to vanish at a radius corresponding to the region of the "quasimolecular" well. For the inelastic channel the imaginary potential was assumed to be surface-peaked. The real potential also exhibits a repulsive core. We have performed a calculation to test the sensitivity of their result to the potential assumed, using instead the latest empirical potential obtained by the Yale group[10] in a fit to the $^{16}O + ^{16}O$ elastic scattering. This potential (real part: $V = 17, r_o = 1.35$, $a = 0.49$; imaginary part: $W = 0.8 + 0.2\,E_{c.m.}$, $r_o = 1.27$, $a = 0.15$) has a smaller imaginary than real potential radius parameter to simulate ℓ-dependence. The results of the calculation are illustrated in Fig. 11.5-5. For this potential one does not obtain any indication of intermediate structure. We conclude that quasimolecular structure is not necessarily to be expected on the basis of our present empirical knowledge of the $^{16}O + ^{16}O$ optical potential. It is also not at all clear that the structure observed experimentally is not simply due to Ericson fluctuations, associated with the compound-elastic contribution to the elastic scattering.

---

1. Nuclear Physics Laboratory Annual Report, University of Washington (1970), p. 95.
2. R.W. Shaw, Jr., R. Vandenbosch, and M.K. Mehta, Phys. Rev. Letters *25*, 457 (1970).
3. T. Tamura, Rev. Mod. Phys. *37*, 679 (1965). We are indebted to Professor Tamura for making his JUPITER code available to us.

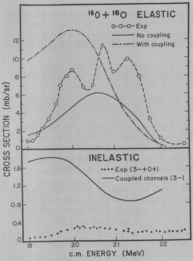

Fig. 11.5-5. Comparison of the coupled-channels calculation of the elastic and inelastic cross sections for $^{16}O + ^{16}O$. Also shown is the calculated elastic cross section in the absence of coupling. The deformation parameters used were $\beta_2 R = 0.9$ F and $\beta_3 R = 1.4$ F. The experimental data is from Maher *et al.*, Ref. 6. A recent remeasurement[11] of the inelastic cross section is in much better agreement with the calculation.

4. R.H. Bassel, G.R. Satchler, and R.M. Drisko, Nucl. Phys. *89*, 419 (1966).
5. G.H. Rawitscher, Symposium on Heavy Ion Scattering, Argonne, Ill. (1971).
6. J.V. Maher, M.W. Sachs, R.H. Siemssen, A. Weidinger, and D.A. Bromley, Phys. Rev. *188*, 1665 (1969).
7. J.C. Hiebert and G.T. Garvey, Phys. Rev. *135*, B346 (1964);B.G. Harvey *et al.*, Phys. Rev. *188*, 712 (1966).
8. W. Scheid, W. Greiner, and R. Lemmer, Phys. Rev. Letters *25*, 176 (1970).
9. B. Imanishi, Nucl. Phys. *A125*, 33 (1969).
10. A. Gobbi, W. Reilly, R. Wieland, and D.A. Bromley, International Conference on Heavy Ion Physics, Dubna, USSR (1971)
11. P.P. Singh, Symposium on Heavy Ion Scattering, Argonne, Ill. (1971).

12.1 Competition between Neutron and Gamma Ray Emission following (d,d') Reactions

D. Bodansky, J.R. Calarco, J.M. Cameron, D.D. Chamberlin, C. Ling, and D. Oberg

The investigation has been continued of neutron and gamma ray competition in the decay of the compound nucleus formed following the (d,d') reaction. In addition to ^{61}Ni, which was the first target studied in this work, we have also used as targets ^{25}Mg, ^{57}Fe, ^{91}Zr, and ^{119}Sn. The most extensive data has been taken for ^{61}Ni and ^{25}Mg, where a number of combinations of detector angles have been explored; for the other targets both the deuteron and neutron counters have been restricted to 90° to the beam direction (on opposite sides of the beam).

The basic approach of the experiment has been to look at neutrons in coincidence with inelastic deuterons. The deuteron energy determines the excitation energy of the intermediate residual nucleus. In the region of interest this nucleus will emit neutrons to discrete states of the final nucleus and the energies of neutrons are measured from the neutron flight times. In the most recent runs, the neutron observations have been supplemented by observations of the spectrum of gamma rays in coincidence with the inelastic deuterons.

The experimental arrangement now consists of a three-counter telescope (ΔE,E and anti) for deuteron detection, used in coincidence with either the neutron counter (a 5" × 1" NE213 liquid scintillator) or the gamma counter (a 3" × 3" NaI crystal). It is possible to use both the neutron counter and gamma counter simultaneously, but not in coincidence with each other. The coincidences between deuterons and neutrons or gamma rays are established by time-of-flight (TOF) systems, employing the deuteron signals as start pulses and the neutron or gamma signals as stop pulses. The processed analog signals of ΔE and E (for the deuteron) together with combinations of either (a) a neutron TOF signal, a scintillator pulse shape discrimination signal, and a scintillator pulse height signal or (b) a gamma TOF signal and a gamma energy signal, are presented to the computer ADC's. Particle identification is performed on-line in the computer, and for deuteron events the full array of signals is recorded event-by-event on magnetic tape. To monitor the experimental runs, a variety of live displays may be presented on the computer oscilloscope. In the latest configuration, two 32 × 64 channel arrays are displayed; one of neutron TOF vs deuteron energy and one of gamma energies vs deuteron energy. For data analysis a 64 × 64 channel array of any selected pair of signals can be retrieved from the magnetic tape; it is also possible to impose any desired pulse height criteria upon the remaining coincident signals.

The fractional neutron yield to the different states of the final nucleus is obtained from the plot of neutron TOF vs deuteron energy, by summing over the kinematic bands corresponding to the discrete (d,d'n) groups, correcting for detector efficiency and solid angle, and normalizing to the (d,d') yield. It is assumed in this calculation that the neutron yield is isotropic; this assumption is consistent with results of measurements made in which the neutron detector angle is varied. Results obtained in this way for ^{61}Ni are shown in Fig. 12.1-1, for a case in which the deuteron detector is at 90°.

When the ^{61}Ni excitation energy is sufficiently low, the neutron decay to the first excited state at 1.33 MeV can be independently determined by measuring the 1.33 MeV gamma ray yield. When more highly excited states of ^{60}Ni are accessible, the situation becomes more complicated, but the 1.33-MeV gamma ray yield remains a rather good measure of total neutron decay to excited states of ^{60}Ni, because the excited states below 4 MeV decay primarily through the 1.33 MeV state.[1] This gamma ray yield, independently normalized, is also displayed in Fig. 12.1-1. In general the neutron and gamma ray results are qualitatively consistent. Quantitative comparisons are at the moment difficult to make because of large statistical and systematic uncertainties in the gamma ray data. It is hoped that future runs will reduce these uncertainties.

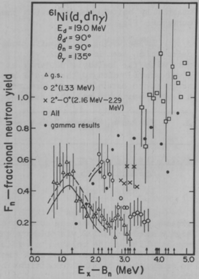

Fig. 12.1-1. Fractional neutron yield as a function of available neutron energy (i.e., excitation energy minus the neutron binding energy). The different symbols designate neutron yields to different states of ^{60}Ni as well as yields from gamma data (see text). The arrows indicate thresholds for the different decay channels.

A simple approach to the interpretation of the neutron yield may be made by calculating the spin distributions of the d + ^{61}Ni system and the excited ^{61}Ni* on the basis of the statistical model, using deuteron transmission coefficients generated from an optical model code. Given the ^{61}Ni* spin distribution and a set of conventional gamma widths and neutron transmission coefficients, a further statistical model calculation gives the fractional neutron yield. The results of such a calculation is shown in Fig. 12.1-1 as a solid line. The neutron yields are quite sensitive to the spin populations, but, because for most spin states emission is either overwhelmingly via neutrons or overwhelmingly via gamma rays, the calculated yield is not very sensitive to the neutron and gamma ray widths. In Fig. 12.1-1 the calculated neutron yield is slightly lower than the observed yield. As low spin states favor neutron emission, better agreement would be obtained were it assumed that (d,d') events led to lower spins than implied by a statistical model calculation. This is not an unreasonable assumption, because in the high l-transfer region, the (d,d') yield may be somewhat depleted by (d,p) and (d,n) reactions. When the 20% of the events corresponding to highest spins of the d + ^{61}Ni system are removed from consideration, predicted yields are in substantially better agreement with the measurements, as displayed as the dotted curve of Fig. 12.1-1.

In assessing the significance of the agreement between measurement and calculation seen in Fig. 12.1-1, it would be of interest to examine analogous data with the inelastic deuteron at other angles where the amount of non-statistical contribution to the (d,d') reaction is enhanced differently. Work is in progress to obtain data at forward deuteron angles where direct interaction plays a larger part, but reliable data are not as yet available.

---

1. S. Raman, Nuclear Data Sheets for A = 60, Nuclear Data B2-5-45 (1968).

12.2 The High Energy Gamma Ray Spectra from 16 MeV Deuteron Bombardment of Various Nuclei

I. Halpern and D.L. Johnson

From observations of the high energy gamma spectrum (E_γ > 10-12 MeV) one expects to learn something about the mechanism involved in the de-excitation of highly excited nuclei via primary gamma transitions. These studies give information which can be related to radiative capture when the primary transitions go to bound final states. The high energy part of the gamma spectrum can be used to study these primary transitions because here they predominate over gamma rays from other reactions. Light nuclei may however have certain strong gamma rays due to non-primary transitions.

The high energy spectra from bombardments with high energy alpha particles and ^{3}He nuclei seem to indicate the predominance of compound nuclear formation followed by statistical emission of the primary quanta. The shape of such statistical emission should be essentially that of an exponential level density modulated by the inverse cross section between the states involved. The best estimate for the shape of the inverse cross section is that of the giant dipole resonance. The resulting spectral shape should be a decreasing exponential with a sharp drop-off above 14-16 MeV. Drake *et al.*[1] have observed such spectral shapes from alpha and ^{3}He bombardments leading to the same compound nucleus ^{64}Zn.

Bombardment with protons to produce the same energy in ^{64}Zn produces spectra which are quite different indicating a different mechanism. The proton spectra for the same excitation energy in ^{64}Zn (∿ 29.5 MeV) extends to about 26 MeV which is 5 MeV higher than from the ^{3}He bombardment. In addition, strong lines to certain excited states were observed in other proton bombardments.

It was expected that since the deuteron is a composite particle as is the alpha and ^{3}He nucleus, it should also produce high energy spectra via the compound nucleus. A survey run was performed to see if these high energy gamma rays could be observed in the presence of the large neutron background produced by the deuteron beam.

The detector was a 3ϕ" × 5¼" NaI crystal inside an 8ϕ" × 12" NaI anti-coincidence annulus. About 13" of polyethylene was placed between the target and detector to reduce the number of target neutrons that hit the detector. The random background due to room neutrons typically accounted for more than 90% of all events. To be able to see the true gamma spectrum below 12 MeV the time-of-flight technique was used to separate the prompt gamma spectrum from that produced by prompt and random neutrons. Preliminary results indicate that the high energy spectra appear to have about the same shape as those of the alpha and ^{3}He bombardments leading to the same excitation energy. Figure 12.2-1 shows the high energy portion of the pulse-height spectrum produced by 16 MeV deuterons incident on ^{63}Cu. A semi-logarithmic plot emphasizes the basically exponential shape with a knee at about 15 MeV. The figure also shows the detector response to a 15.1 MeV gamma ray. The excitation energy of the ^{65}Zn compound nucleus formed in this reaction is about 29.9 MeV. This spectrum compares quite well to spectra of the compound system ^{64}Zn at about the same excitation energy produced by alpha and ^{3}He bombardments and not like that from the proton bombardment. The 90° gamma spectra produced by bombardment with 16 MeV deuterons has been observed with the following targets: ^{9}Be,^{11}B,^{12}C,^{16}O,^{27}Al,V,^{59}Co,NatNi,^{63}Cu,^{89}Y,^{93}Nb,^{116}Sn,^{165}Ho,^{181}Ta, and ^{209}Bi. Except for ^{11}B (the 15.1 MeV line from ^{12}C) no targets show any pronounced lines above 10 MeV. In a typical run the spectrum extends to approximately 10 MeV below the maximum gamma energy possible whereas for proton bombardments the spectra extend 5 MeV or more higher. It appears that at excitations in the region of 23-33 MeV the non-statistical mechanisms do not give large contributions to the high energy gamma yield.

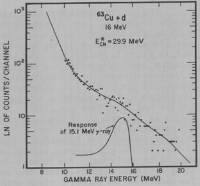

Fig. 12.2-1. The high energy part of the pulse height spectrum of gammas from the reaction ^{63}Cu plus 16 MeV deuterons. The detector response to a 15.1 MeV gamma ray is also shown.

---

1. D. Drake, S.L. Whetstone, and I. Halpern, Phys. Letters *32B*, 349 (1970).

12.3 Systematics of Angular Distributions in Fast Proton Capture

I. Halpern and R. Heffner

We have examined some of the photon angular distributions in fast proton capture which have been reported in the literature for light[1-4] and medium weight[5] nuclei. Our object was to see whether the main features of such distributions can be understood in terms of present-day views of the capture process and to explore the use of such distributions to help resolve problems which remain in our picture of nucleon capture.

The current model for fast nucleon capture involves two amplitudes for the capture process,[6,7] one corresponding to a direct radiative transition to a bound state by the incident nucleon and the other to a non-radiative transition to the same state accompanied by the excitation and subsequent de-excitation of a collective state in the target. The radiations from the direct capture and from the decaying collective state are emitted coherently. However, there is an important difference between these two amplitudes which has implications about the forward-folding of the photon distributions which is sometimes observed. The radiation associated with the incoming proton itself is emitted from a rapidly moving charge, but the radiation from the induced dipole oscillation in the target (the E1 oscillation is the main multipole excited) comes from relatively slow moving charges. The classical radiation pattern of a charge accelerating in the direction of its velocity contains the forward-folding factor $(1 - \beta \cos \alpha)^{-4}$ where α is the angle of observation with respect to the particle motion and βc is the particle velocity when it is radiating. The forward-folding factor associated with a proton radiating as it accelerates across the edge of a nucleus is even larger than this. The recoil of the target nucleus contributes an amplitude about half as big as the proton's and opposite to it. Since this amplitude comes from a slowly moving charge, it has negligible fore-aft asymmetry and therefore the effective proton amplitude ($A_{proton} - A_{recoil}$) is relatively more forward folded than it would be in the absence of the recoil effect.

When the photon emitted by a captured proton is in the giant resonance region,[6] it can be shown that the amplitude associated with the polarization and depolarization of the target is about three times that associated with the proton (including the recoil amplitude mentioned above). Since the polarization amplitude arises from slow charges, we expect no striking fore-aft asymmetry when photons are emitted with near-resonance energies. This seems to be borne out by the data (Fig. 12.3-1) where somewhat smoothed excitation functions have been plotted along with the values of the coefficients in the angular distribution $W_\gamma(\theta) = 1 + a_1P_1(\cos \theta) + a_2P_2(\cos \theta) + \cdots$. It is seen that in all five examples, a_1 (which measures the forward folding) is small in the region of the giant resonance. In three cases it is seen to rise to rather large values as one goes to energies above the giant resonance. It would be of interest to study the angular distributions at still higher energies to see whether a_1 remains large. If the origin of the forward folding is due predominantly to a kinematic effect as we are suggesting, the value of a_1 should stay up as the energy is raised.

For two of the targets in the figure, it is seen that a_1 remains negligibly small throughout the range of measurements. For these two targets it happens that a_2 is either small or positive whereas for the other three targets (where a_1 does increase at higher energy) a_2 has an average value which is large and negative. The following connection between a_1 and a_2 suggests itself. Where a_2 is large and negative, the angular distribution peaks at 90°. It is the sort of distribution that is emitted classically when the acceleration and velocity of the emitter are parallel. It therefore corresponds to protons incident on the nucleus with small impact parameters (low ℓ values). Furthermore, when the acceleration and velocity of a radiating charge are parallel, the forward-folding is large (see above). However when the impact parameter approaches the nuclear radius (i.e., $\ell \sim kR$) then the acceleration and velocity are perpendicular and one can show classically that the forward-folding becomes rather small. Thus we are led to

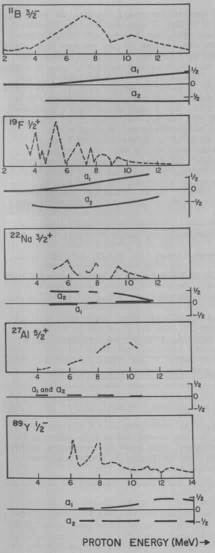

Fig. 12.3-1. Energy dependence of the coefficients a_1 and a_2 of the angular distributions of photons to 0^+ ground states of residual nuclei when protons are captured by the five nuclei shown. The data here are somewhat smoothed versions of those in the literature.[1-5] In each case the energy dependence of the cross-section is shown (dashed line). It may be possible to understand some features of the patterns for a_1 and a_2 in terms of general classical considerations (see text).

expect that when the ℓ's important in the capture are small, a_1 will be large and when they are large, a_1 will be small. The amount of forward-folding depends therefore on whether the target and residual spins are nearly equal or rather unequal. It will be of interest to examine other cases to see whether this classically-suggested connection between a_1 and a_2 holds up. One is encouraged to look for such general connections by the fact that a_1 and a_2 seem to remain rather constant with energy despite strong ups and downs in the cross-section. If it turns out that one can in this way identify targets for which there is very little a_1 arising from kinematic origins, such targets might be especially useful in a search for genuine E2 - E1 interference, i.e., for a mapping of the E2 strength function in the target nucleus. Similarly, if the non-vanishing a_1 in Fig. 12.3-1 is purely kinematic in origin, arising entirely because of the incident protons' speed, it follows that the corresponding value of a_1 in fast neutron capture would be vanishingly small since here the neutron itself does not radiate. Only the (slow moving) recoiling nucleus radiates. In short n capture would be more useful than p capture for the study of E2 strengths in nuclei since the signature for E2 (the E1 - E2 interference in the angular distribution) would not be masked by what appears to be a simple kinematic effect. We are therefore studying the feasibility of undertaking the measurement of capture gamma ray angular distributions following fast neutron capture.

---

1. R.G. Allas, S.S. Hanna, L. Meyer Schützmeister, and R.E. Segel, Nucl. Phys. *58*, 122 (1964).
2. R.E. Segel, Z. Vager, L. Meyer Schützmeister, P.P. Singh, and R.G. Allas, Nucl. Phys. *93*, 31 (1967).
3. R.C. Bearse, L. Meyer Schützmeister, and R.E. Segel, Nucl. Phys. *A116*, 682 (1968).
4. P.P. Singh, R.E. Segel, L. Meyer Schutzmeister, S.S. Hanna, and R.G. Allas, Nucl. Phys. *65*, 577 (1967).
5. M. Hasinoff, Ph.D. Thesis, Stanford University, 1970 (unpublished).
6. G.E. Brown, Nucl. Phys.*A95*, 339 (1964).
7. C.F. Clement, A.M. Lane, and J.R. Rook, Nucl. Phys. *66*, 273,293 (1965).

12.4 The Radial Dependence of the Nucleon-Nucleus Force Responsible for E1 Excitations of Target Nuclei

I. Halpern

A paper is being prepared for publication which presents a microscopic derivation of the strength and spatial dependence of the force with which an incident nucleon electrically polarizes a nucleus. This work has been done in collaboration with V.A. Madsen of Oregon State University and J. Zimányi of the Central Research Institute for Physics, Budapest, Hungary.

12.5 A Search for Spin-Flip E1 Gamma Ray Transitions from Isobaric Analog Resonances in ^{209}Bi and ^{90}Zr

D.R. Brown, J.R. Calarco, M. Hasinoff, and R. Heffner

It has been found that the measured E1 matrix elements for a gamma transition between an isobaric analog resonance (IAR) and a low-lying bound state is reduced compared to the pairing model estimate. The reduction factor for the transition from the $2f_{7/2}$ IAR (E_x = 14.95 MeV) to the $2d_{5/2}$ ground state in ^{141}Pr was found to be about 3.9.[1] This degree of hindrance was shown to be consistent with a microscopic random-phase-approximation calculation in which a particle-hole interaction proportional to the matrix element $\langle r \rangle$, the E1 matrix element, was assumed.[2] Thus the hindrance of the IAR transition was attributed to out-of-phase admixtures of the associated collective state (here the giant dipole resonance) into both the IAR and the final bound state.

It would be of interest to extend these types of measurements to transitions where different types of residual interactions might be studied. We sought to do this by measuring a spin-flip E1 transition from an IAR, whereby the interaction $\langle \sigma \times r \rangle$ might be studied. One such measurement of a spin flip E1 transition in ^{89}Y has been reported with the interesting result that the matrix element is about 4 times larger than the single particle estimate.[3]

We chose to investigate the reactions ^{208}Pb(p,γ)^{209}Bi and ^{89}Y(p,γ)^{90}Zr. The gamma rays were detected using a 20 cm^3 Ge(Li) detector. For the ^{208}Pb(p,γ)^{209}Bi reaction we sought to measure the transition strength from the $3d_{5/2}$ IAR ($E_x \simeq$ 20.3 MeV) to the $2f_{5/2}$ second executed state (E_x = 2.83 MeV) of ^{209}Bi. We also tried to measure the transitions in ^{90}Zr from the $(d_{3/2},p_{1/2}^{-1})_{2^-,1^-}$ IAR to the low lying single particle states in the p-shell. In neither reaction, however, could we obtain a suffient γ-yield within a reasonable data collection time. The primary experimental limitation on the counting rate for the resonance transitions of interest was the large overall counting rate. This overall rate was most probably due to gamma rays deriving from neutron capture following (p,n) reactions in the target and thus could not be reduced to a tolerable level.

---

1. H. Ejiri *et al*, Nucl. Phys. *A128*, 388 (1969).
2. H. Ejiri, private communication.
3. P. Richard *et al.*, Phys. Letters *29B*, 649 (1969).

12.6 Delayed Ground State Rotational Band Transitions following Compound Reactions in Deformed Nuclei

I. Halpern and H. Wieman

In his thesis study[1] in this Laboratory S.M. Ferguson found that a significant fraction ($\lesssim$ 10%) of the ground band radiations in even-even rare earth nuclei, which are produced in (α,xn) reactions, comes out delayed. More specifically, forty-two MeV α's were used in the bombardments and it was found that some of the ground band radiation appeared as late as ∿ 30 ns after each beam burst.

The fraction of delayed to prompt ground band radiations was largest for the lower transitions. It is assumed that the large angular momentum input into the nucleus is responsible for the delay which occurs in some higher levels which feed the ground band.

We have made preparations for an experiment to study this phenomenon further. Using the Van de Graaff accelerator with heavy ions we plan to achieve angular momentum inputs comparable to those obtained with 42 MeV α's. We plan to begin with a carbon beam which will be produced using the direct extraction ion source by mixing a small percentage of methane with the hydrogen source gas. A variable leak has been ordered for this purpose. We have also obtained isotopically enriched ^{160}Gd, ^{154}Sm, and ^{150}Nd which we will make into self-supporting targets.

---

1. S.M. Ferguson, Ph.D. Thesis, University of Washington, 1969 (unpublished).

13.1 Spin Isomers of the Shape Isomer ^{237m}Pu

W. Jacobs, M. Mehta, P.A. Russo, J.R. Tesmer, and R. Vandenbosch

Previous experiments have indicated the presence of more than one spontaneous fission isomer in ^{237}Pu. The purpose of the present investigation was to confirm these findings and to characterize as fully as possible the isomers observed.

The reactions $^{235}U(\alpha,2n)^{237m}Pu$ and $^{237}Np(d,2n)^{237m}Pu$ were studied with 24-27 MeV alphas and 11 meV deuterons using chopped and bunched alpha and deuteron beams from the two-stage Van de Graaff and pulsed alpha beams from the cyclotron. Experimental details have been published.[1-3]

The very short-lived component formerly assigned to ^{237m}Pu[4] has been attributed to ^{238m}Pu based upon evidence obtained in this experiment[3] and elsewhere.[5] The other two delayed fission components, both identified as ^{237m}Pu, have been assigned half lives of 82±8 nsec and 1120±80 nsec. Figure 13.1-1 is one example of the two-component decay curves from which these numbers were derived. Isomer ratios and delayed-to-prompt ratios have been obtained for both isomers in the three bombarding cases. These values appear in Table 13.1-1.

It is shown from the relationship between the relative yields of the short- and long-lived isomer and the initial excitation and angular momentum of the compound nucleus that the observed trend in the yield ratio cannot be due to an energetic effect caused by a significant difference in excitation and must be attributed to angular momentum. The dependence of the isomer ratio on the angular momentum of the compound nucleus indicates that the observed trend in the yield ratio cannot be an energetic effect caused by a significant difference in excitation and must be attributed to angular momentum. The dependence of the isomer ratio on the

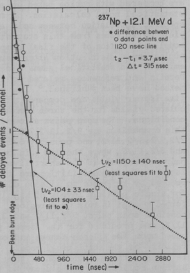

Fig. 13.1-1. Two-component decay curve of ^{237m}Pu from the 12.1 MeV deuteron bombardment of ^{237}Np with 3.7 μsec intervals between beam bursts. The 1150±140 nsec dotted line is the least squares fit to the short-lived points after subtraction of the long-lived contribution.

Table 13.1-1. Isomer Ratios for ^{237m}Pu

Target	Projectile	σ_{long} / σ_{prompt}	σ_{long} / σ_{prompt}	σ_{long} / σ_{prompt}	$\sigma_{delayed}$ / $\sigma_{spallation}$
^{235}U	24 MeV α's	5.61	6.3±3.2	11.9±3.2	300±60
^{235}U	27 MeV α's	2.65	1.9±0.9	4.5±0.9	180±40
^{237}Np	12.1 MeV d's	2.59	4.5±1.9	7.1±1.9	

angular momentum of the compound nucleus shows that the long-lived state has the higher spin. This is illustrated in Fig. 13.1-2 where the observed ratios are compared with ratios based on a statistical model calculation. A more specific correlation between spin and yield ratio comes from this statistical model calculation of the final compound nuclear spin distribution after neutron emission and statistical gamma decay. Details and references related to this method have been published.[3] The relative isomer yields are compared with calculated yields for the three bombarding conditions. The spin pairs allowed by this comparison are 9/2,11/2;7/2,11/2; 7/2,9/2;5/2,11/2; and possibly 5/2,9/2 and 3/2,11/2, where the low spin of the pair corresponds to the short-lived isomer. These possibilities are further reduced by reference to Nilsson diagrams for single particle levels of highly deformed nuclei in this mass region. Two possible spin pairs, 5/2,11/2 and 3/2, 11/2, are predicted for the isomer pair based upon the Nilsson scheme and on the validity of the statistical model. It is assumed that penetration of the inner barrier followed by gamma decay to the ground state is a non-competitive mode of decay for ^{237m}Pu.[3]

A determination of the deformation of the second well is possible by identification of one of the isomers as the 11/2⁻ state if the criterion is maintained that this state must lie close to the Fermi surface at the appropriate deformation. The steepness of

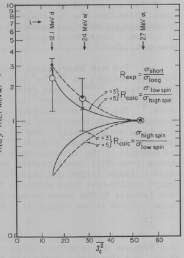

Fig. 13.1-2. Ratio of isomer ratio for each bombardment to the isomer ratio for the 27 MeV alpha particle bombardment as a function of the mean square initial compound nuclear spin. The open circles are the experimental results. The solid line is the theoretical result for spin pairs 3/2,11/2 and 5/2,9/2 with a spin cutoff parameter, σ, of 3. The dashed line is the theoretical result for the same spin pairs with =5. The error in the 27 MeV alpha experimental point has been propagated into the error in the other two experimental points.

this $11/2^-$[505] single particle state with deformation results in a fairly well-defined deformation of 0.60 0.04.

It is quite likely that the presence of this $11/2^-$ state near the Fermi surface is associated with the observation of anomalously long-lived isomers in ^{236}Pu and ^{238}Pu. These isomers have anomalously large excitation energies (≈ 4 MeV rather than ≈ 2.8 MeV) and presumably are two-quasiparticle states.[1]

It is also interesting to note that although the specialization energy associated with the $11/2^-$ isomer in ^{237}Pu would be much too large, based on single particle calculations for reflection-symmetric shapes,[6] to observe a spontaneous fission branch, if asymmetric shapes are considered,[7] the expected specialization energy is much reduced for this state.

---

1. R. Vandenbosch and K.L. Wolf, in *Physics and Chemistry of Fission,* (International Atomic Energy Agency, Vienna, 1969).
2. Nuclear Physics Laboratory Annual Report, University of Washington (1970),p. 137.
3. P.A. Russo, R. Vandenbosch, M. Mehta, J.R. Tesmer, and K.L. Wolf, Phys. Rev. *3*, 1595 (1971).
4. K.L. Wolf, Ph.D. Thesis, University of Washington, 1969 (unpublished).
5. S.C. Burnett, H.C. Britt, B.H. Erkkila, and W.E. Stein, Phys. Letters *31B*, 523 (1970).
6. S.G. Nilsson, G. Ohlen, C. Gustafson, and P. Möller, Phys. Letters *30B*, 437 (1969).
7. C. Gustafsson, P. Möller, and S.G. Nilsson (private communication,1971).

13.2 Threshold Determination for Spontaneous Fission Isomers of ^{237m}Pu

M. Mehta, D.W. Potter, P.A. Russo, R. Vandenbosch, and R. Wilson

The identification of two isomers with different spins and half-lives has led to an interest in determining the relative excitation energies of the two isomers. Interest in the relative energies is motivated by the possibility of gamma decay from one isomer to the other, and also by possible interpretation of the different half-lives in terms of specialization energy effects.

An attempt to determine the relative thresholds using the ^{235}U(α,2n) reaction is in progress. Plastic fission track detectors, chosen because of high sensitivity, are placed along a tightly collimated trajectory of the recoiling compound nuclei. A four-sided recoil chamber has been constructed providing an overall detection efficiency which is 4 times greater than that obtained by electronic timing with semiconductor detectors. Considerable difficulty was encountered with Makrofoil of 0.85 mg/cm^2 thickness was used. Large and irreproducible backgrounds were observed. The experiment is being repeated with foils of 1.1 mg/cm^2 thickness.

13.3 Investigation of Delayed Gamma Decay of the ^{238}U Shape Isomer

J.R. Calarco, R.H. Heffner, W. Jacobs, J. Pedersen, P.A. Russo, and R. Vandenbosch

The liquid drop model demonstrates that the total nuclear potential energy increases and passes through a saddle point as a nucleus undergoes prolate distortions from the equilibrium configuration. The Strutinsky prescription incorporates single particle corrections in the liquid drop potential. The result is a second minimum in the nuclear potential energy in the vicinity of the saddle point deformation.[1] The process of delayed fission is ascribed to a decay from the second minimum via tunneling through the outer barrier which lies, typically, at a deformation, β, near 0.7.[2]

The known shape isomers occur in greatest numbers in the plutonium isotopes which frequently exhibit multiple isomerism corresponding to more than one state in the second minimum. Fewer instances of delayed fission have been observed among the isotopes of uranium, and none have been positively identified as isotopes of neptunium. Furthermore, isomer ratios (delayed fission to spallation cross section ratios) for delayed fission in uranium isotopes are smaller than those typical of plutonium delayed fission although delayed fission half lives for the even-even uranium isotopes are longer than any observed for even-even plutonium isotopes.[3] This suggests that a competitive mode of decay, penetration of the inner barrier followed by a gamma cascade to the ground state of the first minimum, is the dominant decay mode for the uranium and neptunium isotopes.

Investigation of the gamma branch as a decay mode for the shape isomer ^{238m}U has been undertaken. The half life and cross section for ^{238}U delayed fission have been measured at this laboratory[3] using the ^{238}U(d,pn) reaction to produce the isomer ^{238m}U decays by delayed fission with a half life of approximately 200 nsec. The isomer ratio is $\approx 10^{-5}$, an order of magnitude lower than observed for plutonium isomers.

The spin and parity of the shape isomer in ^{238m}U is expected to be 0^+, and consequently a significant branching ratio for decay of the isomer to the first excited 1^- and 2^+ states in the normally deformed ^{238}U nucleus is anticipated. These states are lying at 0.676 MeV and 0.045 MeV respectively.

The experimental design is based upon identification of lines in a gamma spectrum which decay with a half life of 200 nsec and lie within the 0.5-3.0 MeV range. Cross sections are expected to be of the order of 25 to 50 microbarns based on relative even-even uranium and plutonium isomer ratios.

A deuteron beam from the direct extraction ion source of the two-stage Van de Graaff accelerator has been pulsed at frequencies between one and ten kHz with beam bursts 50 to 100 nsec wide. The low duty cycle prevents buildup of long-lived activities due to delayed gamma rays in fission fragments. The target, a natural uranium foil 3.68 mg/cm^2, was bombarded with 1-5 na of 17 MeV deuterons to produce the ^{238}U(d,pn)^{238m}U reaction. The target was located within two inches of the gamma detector, a 20 cc Ge(Li) crystal at $\theta_{lab} = 90°$.

The data has been collected using an existing program modified for this experiment. A fast timing signal derived from signals out of the gamma detector stops a TAC which has been started by the oscillator signal from the beam chopper. The TAC output produces a time spectrum which is observed over a microsecond range and stored in the computer. The time spectrum is divided into anywhere from two to sixteen bins, and the energy spectrum associated with each bin is stored separately.

Early attempts at data collection have concentrated on reduction of gamma and neutron background between beam bursts. Some progress has been made through endeavors which include various techniques of shielding. Initial background cross sections at 1 MeV were about 5 times larger than cross sections anticipated for the delayed gamma lines.

---

1. V.M. Strutinsky, Nucl. Phys. *A95*, 420 (1967).
2. K.L. Wolf, Ph.D. Thesis, University of Washington, 1969 (unpublished).
3. K.L. Wolf, R. Vandenbosch, P.A. Russo, M.K. Mehta, and C.R. Rudy, Phys. Rev. *6*, 2096 (1970).

13.4 The Emission of Third Particles in Nuclear Fission

I. Halpern

A review paper on this subject (being prepared for the Annual Review of Nuclear Science) is nearing completion.

---

14. RESEARCH PERFORMED BY USER OR VISITOR GROUPS

14.1 Pion-Nucleus Cross-Sections

J.R. Calarco, I. Halpern, M. Hasinoff, and R. Marrs

We have begun to plan for experiments to be performed at LAMPF in collaboration with Prof. Mark J. Jakobson and co-workers of the University of Montana and Dr. D.C. Hagerman and his colleagues of the Los Alamos Laboratory. A proposal has been submitted to the AEC by Prof. Jakobson which describes the motivations and proposed methods for the study of total cross-sections of pions on various nuclei at energies up to 300 MeV. We are also looking into possible measurements of double charge exchange cross-sections on nuclei.

14.2 Total Body Calcium Studies in Humans Using Neutron Activation Analysis

C. Chesnut*, J.D. Denny*, G. Hinn*, R. Murano*, W.B. Nelp*, H.E. Palmer*, and T. Rudd*

The experiments to determine the accuracy of our system in estimating total

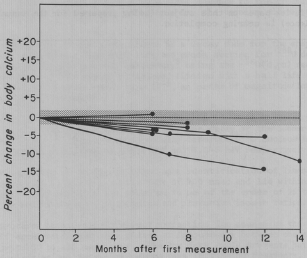

Fig. 14.2-1. Serial loss of body calcium - renal osteodystrophy hemodialysis patients.

body calcium by neutron activation analysis and whole body counting are now complete. A total of six cadavers were irradiated, ashed and chemically analyzed for calcium. One cadaver differed greatly from the others in that the amount of ^{49}Ca induced in him was about 20% less than would be predicted from his skeletal mass.

This result was explained by the fact that he was preserved by a solution containing 4% borax which is about 10% boron by weight while the other cadavers were not. The large cross section of boron for thermal neutrons (514 barns) decreased the effective thermal neutron flux to his skeleton by approximately 20%, thus explaining the discrepancy. The accuracy of the system calculated for the other five subjects is ±5%.

Investigations of the pathophysiology and therapy of various groups of patients with metabolic bone disease using total body neutron activation analysis to measure total body calcium are continuing with some patients followed for nearly two years. One hundred forty-seven studies on 105 patients have been completed and the initial results have been enlightening.

The patients with chronic renal failure maintained by hemodialysis on the artificial kidney have had a mean loss of total body calcium of about 7% of their total body calcium with two subject having a 12% and 14% loss respectively over a one year period (Fig. 14.2-1). Measures are now being taken to attempt to prevent

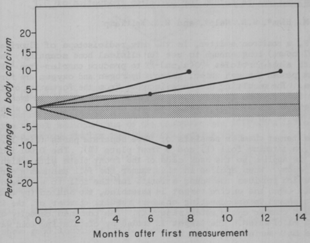

Fig. 14.2-2. Serial change in body calcium - renal transplants.

this calcium loss.

Of the three kidney transplant patients who have had repeat measurements, two have had positive calcium balance after surgery while one has had a 10% loss of total body calcium after transplantation (Fig. 14.2-2). The patient with the large loss of calcium is suffering from persistent hyperparathyroidism post transplant.

Over thirty patients with osteoporosis have had initial total body calcium determination and the effect of various drugs on their calcium balance will be monitored in them using neutron activation analysis.

Two NASA volunteers who underwent 16 weeks of bed rest as simulated weightlessness had no significant change in their total body calcium during the period as measured by neutron activation analysis before and after bed rest.

Future plans involve primarily following the above groups of patients with neutron activation analysis to evaluate various types of therapy and to study other individuals with problems in whom total body calcium determination would be of clinical usefulness or of special interest.

---

* Department of Nuclear Medicine, University of Washington.

14.3 A High Pressure Method for Cyclotron Production of ^{18}F

G.M. Hinn*, W.B. Nelp*, and W.G. Weitkamp

^{18}F, a positron emitter, is the only radioisotope of fluorine with a half life (1.87 hours) long enough to use for clinical bone scanning. Water is bombarded with alpha particles $^{16}O(\alpha,pn)^{18}F$ to produce carrier-free ^{18}F. When an alpha beam passes through water, gaseous hydrogen and oxygen are formed through radiolysis. The resulting pressure increase from the formation of these gases can cause foil rupture at pressures in excess of 60 psi.[1] To avoid this problem a high pressure containment vessel has been designed which will withstand internal pressures up to 160 psi.

The target chamber consists of three separate parts (Fig. 14.3-1): a back plate (A), a titanium foil (F) and a front plate (B). The 0.001 inch thick titanium foil is applied to the back side of the front plate with a high temperature resistant epoxy. When applied in this manner the foil assumes a curved radius of one inch which provides the added strength for the foil to withstand pressures up to 160 psi. When the entire target is assembled, two sealed (by means of a viton O ring not shown) interconnecting chambers result: chamber c_1, the irradiation chamber, and chamber c_2, a water reservoir. The combined capacity of both chambers is 15 ml of water. The target is cooled by circulating cold water across the entire back surface of plate A.

During bombardment the 42 MeV alpha beam is maintained at a current of 20 to 25 μA.

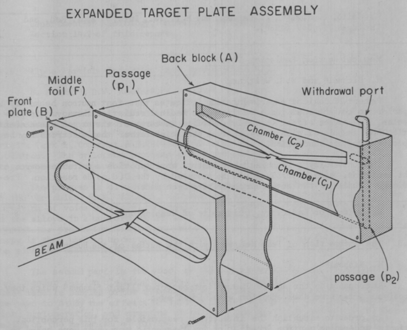

Fig. 14.3-1. High pressure ^{18}F production cell.

At the end of bombardment a needle valve is opened and the internal pressure forces the target solution out of the chambers and through a .22 u millipore filter and into a vented sterile multidose collecting vial.

An average yield of 6.2 mCi/μA-h or 194 mCi/75 min at a beam current of 25 μA has been attained using this method. A theoretical yield of 10 mCi/μA-h was calculated from previously published cross sections[2] and is slightly higher than the experimental results.

Negligible amounts of radiocontaminants (0.16 uCi of ^{48}V) have been detected from recoil reactions off the titanium foil. The final product has been sterile and shown good localization in bone.

---

* Department of Nuclear Medicine, University of Washington.
1. J.C. Clark and J.D. Sylvester, Int. J. Appl. Rad. and Isotopes *17*, 151 (1966).

2. K. Saito, T. Nozaki, T. Tanaka, and M.T. Fal, Int. J. Appl. Rad. and Isotopes *14*, 357 (1963).

14.4 Medical Neutron Radiation Therapy

H. Bichsel* and W.G. Weitkamp

Recent biological experimentation indicates that fast neutron beams may be superior to conventional gamma radiation in medical radiation therapy. In particular, the oxygen effect (usually described in terms of the oxygen enhancement ratio OER) associated with heavy charged particles rather than electrons may be exploited in this connection.

The University of Washington cyclotron would provide a suitable source of fast neutrons, which probably would be produced by the $D(d,n)^3He$ reaction. Preliminary studies of the entire problem have been made.

* Department of Radiology, University of Washington.

14.5 The Interaction of Fast Neutrons with the Retina of the Human Eye

H. Bichsel*

Astronauts on the Apollo Spaceflight reported "light flashes" which they perceived after some dark adaption with closed eyes.

In order to establish the interaction responsible for this perception, patients undergoing neutron irradiation for diagnostic purposes[1] were asked to report any light perception experienced during the course of the irradiation.

The experience by all four subjects was described quite vividly, mostly in terms of a resemblance to fireworks. Distinct streaks of light were reported.

Our current interpretation is the following: Heavy charged particles [recoil protons, recoil nuclei, alpha particles produced by nuclear reactions (e.g., $^{16}O(n,\alpha)$] interact directly with the retina, producing the impression of light perception.

The longest tracks observed were over 1 mm long (corresponding to the range of protons over 10 MeV). Alpha particles producing tracks of this length would have an energy of about 40 MeV. Since the neutron spectrum used does not contain energies above 25 MeV, alpha particles of this energy could not be produced.

It is remarkable that some tracks were observed to have a structure; they were wider at one end. This may be due to the increase in energy loss (stopping power) with reduced particle velocity.

* Department of Radiology, University of Washington.
1. Section 14.2 of this report.

14.6 Alpha Particle Injection into Reactor Materials

D. Kramer*, D.W. Keefer*, K.R. Garr*, A. Pard*, and C.G. Rhodes*

Alpha-particle irradiations of fast-reactor cladding and structural materials are being carried out under a program at Atomics International sponsored by the AEC-DRDT called "Irradiation Damage in Cladding and Core Structural Material", Task 2, Contract A.T.(904-3)-842 using the University of Washington's cyclotron. The cyclotron provides a fast and convenient method of introducing large concentrations of helium into various cladding candidates.

The program is divided into two sections; the first is the investigation of the variables, flux, fluence, temperature, and helium concentration, on the formation of voids in stainless steel. The cyclotron is used to implant helium in the alloys in a uniform manner at a low temperature. This is followed by accelerator proton irradiation to produce voids in the material. Electron microscopy is then used to ascertain the effects of the above mentioned variables on the size and distribution of the produced voids.

The second part is the study of high-temperature helium embrittlement in fast-breeder reactor cladding alloys. Helium is deposited uniformly in small sheet tensile samples prior to mechanical testing. Light and electron microscopy are used to study the effects of various thermo-mechanical treatments on the motion, agglomeration, and trapping of helium atoms and to determine the effect of helium on the mechanism of failure in the alloy.

* Atomics International, Canoga Park, California.

14.7 Nuclear Orientation of I = 13/2 Mercury Isomers*

R.J. Reimann†, C.C. Chan†, and M.N. McDermott†

The University of Washington 60" cyclotron has been used to produce I = 13/2 Hg isomers for study by an optical pumping technique. Measurements of the ratios of the nuclear magnetic resonance frequencies of the isomers to that of ^{199}Hg contained in the same sample cell have been made for 11h ^{193m}Hg, 40h ^{195m}Hg, 24h ^{197m}Hg, and the much shorter lived 44m ^{199m}Hg.

Early experiments were done on ^{197m}Hg which was produced by bombarding commercially pure Au foils measuring 4" × 3/4" × .005" with 21 MeV deuterons. A reaction cross section of 300 mb[1] leads to the estimate that 10^{13} to 10^{14} atoms were produced by typical beam exposures of 25 μA for 4 hours. All of the above isomers were produced in later experiments by bombarding commercially pure .002" Pt targets with 42 MeV α particles degraded by .01" of Al. Slightly greater amounts of ^{193m}Hg were produced by undegraded 42 MeV α's incident on .005" targets. For the short-lived ^{199m}Hg, exposures of 30 μA were made for 3 hours, which corresponds to roughly 3 mean lives.

The mercury produced in these foils was distilled into 1" cylindrical quartz sample cells under vacuum. Such cells (also containing stable ^{199}Hg as a reference) were then placed in the center of a stable homogeneous magnetic field of about 650 gauss and illuminated with either right or left circularly polarized 2537 Å resonance radiation directed along the magnetic field. This light was produced by electrodeless discharge lamps which contained isotopically separated mercury. The spectra of the lamps were shifted by a magnetic field to coincide with the absorption spectrum of the isotope being studied. A portion of the angular momentum of the absorbed circularly polarized light is transferred to the nuclei via the atomic hyperfine interaction, thereby orienting them. The intensity of the scattered light which was polarized parallel or perpendicular to the static field was monitored in a direction at 90° to the pumping light. An rf field perpendicular to the static field was swept slowly through the Larmor precession frequencies of the nuclei causing them to disorient. The resulting change in the monitored light intensity showed a characteristic resonance lineshape. The signal was digitized and stored in a PDP 8/I computer as a function of the applied rf frequency.

The main information provided by this technique is the ratio of nuclear resonance frequencies to that of the reference, ^{199}Hg. These ratios can then be combined with available values of the magnetic dipole hyperfine interaction constants[2] to yield differential hyperfine anomalies. The results of this research are tabulated below. These values are in agreement with the less precise values of Moskowitz *et al.*[3] for the longer-lived isomers.

Isotope	$\nu/\nu(199)$	${}_{m}\Delta_{199}(^3P_1)$
193m	0.1609411(5)	+0.01060(3)
195m	0.1588454(4)	+0.01042(4)
197m	0.1562657(3)	+0.01012(36)
199m	0.1542921(8)	?

The anomaly is not evaluated for ^{199m}Hg because the dipole interaction constant is unknown. A current project, therefore, is to measure this constant by the level-crossing technique. Shell model calculations are underway which should produce values of the nuclear dipole moments and hyperfine structure anomalies to compare with our measurements.

---

* Work supported in part by the National Science Foundation.
† Department of Physics, University of Washington.
1. R. Vandenbosch and J.R. Huizenga, Phys. Rev. *120*, 1313 (1960).
2. Nuclear Data Tables *5*, 564 (1969).
3. P.A. Moskowitz, C.H. Liu, and H.H. Stroke, Bull.Am.Phys. Soc.*15*,1676(1970).

14.8 Fission Fragment Angular Momentum in Charged Particle Induced Fission

W. Loveland*, Y.S. Shum*, and D.W. Hill*

As part of a continuing study of primary fission fragment angular momentum, measurements of fragment isomer ratios in charged particle induced fission have been made. The experimental techniques used have been discussed elsewhere.[1] The measured values of the isomer ratios and the primary fragment angular momentum inferred from them are summarized in Table 14.8-1. The interpretation has been done using the Vandenbosch-Huizenga formalism. The energy available for the neutron-γ-ray cascade that de-excites the fragments and the spin cutoff parameters were inferred using measured data on ν(A) for charged particle induced fission, the Wing-Fong mass formula and the superconductor model calculations of Vonach, Vandenbosch, and Huizenga.[2] The primary conclusions reached are:

(a) As the (Z,A) of the fissioning system decrease, the primary fragment angular monentum, J, increases.

(b) The magnitude of J in charged particle induced fission is greater than the J values inferred for low energy induced fission.

(c) The magnitude of J doesn't seem to be strongly correlated with the initial compound nuclear angular momentum.

Table 14.8-1

Fission Fragment Isomer Ratios and Angular Momentum in Charged Particle Induced Fission.

Reaction Studied	Fragment Studied	Isomer Ratio $\left(\frac{\sigma_m}{\sigma_m + \sigma_g}\right)$	J
^{238}U(35 MeV α,f)	^{134}Cs	0.52 ± 0.02	11 ± 1
^{232}Th(20 MeV d,f)	^{134}Cs	0.64 ± 0.01	13 ± 1
^{232}Th(10 MeV p,f)	^{95}Nb	0.040	12
^{226}Ra(19 MeV d,f)	^{134}Cs	0.20 ± 0.05	7 ± 2
^{209}Bi(35 MeV α,f)	^{115}Cd	0.98 ± 0.12	15 ± 1
	^{115}Cd	0.9 ± 0.2	13 ± 4
	^{95}Nb	0.030	15

* Oregon State University, Corvallis, Oregon.

1. Nuclear Physics Laboratory Annual Report, University of Washington (1970), p. 160.
2. H. Vonach, R. Vandenbosch, and J.R. Huizenga, Nucl. Phys. *60*, 70 (1964).

14.9 Particle-Induced Fission of Elements Below Po

R. Williams*, R. Kieburtz*, and E.F. Neuzil*

The Department of Chemistry at Western Washington State College consistently utilizes the cyclotron at the University of Washington in its studies of the particle-induced fission of elements below Po. In the past year work has continued on the 41 MeV alpha-particle induced fission of the element Ta. Our previous studies with elements below Po showed a rather consistent narrowing of the fission fragment mass distribution curve as the atomic number of the target material was lowered. Extrapolation of the results predicts that Ta should fission with the formation of only 2 or 3 fission fragments. Results appear to confirm this prediction. The fission fragment mass distribution curve is very narrow (width at one half maximum: 2±1 amu) indicating the production of very few fission fragments. A complicating factor in determining the total fission cross section for Ta is the presence of charge distribution. Charge distribution is known to occur in the fission of elements in the region of Ta. The effects of charge distribution make the determination of the fission fragment cross-sections very difficult.

Also presently being research is the effect of angular momentum on low-to-moderate energy particle-induced fission. In connection with this research the cyclotron has been used mostly for the bombarding of Au with deuterium ions.

---

* Western Washington State College, Bellingham, Washington.

14.10 Silver Radionuclides in Biota from the Pacific Ocean

T.M. Beasley* and E.E. Held*

Silver-108m and 110m were reported in biota from the Pacific Ocean. It was suggested that the ratio $^{110m}Ag/^{108m}Ag$ would be useful as a tracer of environmental processes based on two assumptions: (a) most of the radiosilver was produced during the 1961-62 nuclear test series, and (b) the radiosilver was produced solely by thermal neutron activation of stable silver. Silver and cadium irradiated in the cyclotron provided empirical evidence of other pathways of ^{108m}Ag, ^{110m}Ag production. In addition, the irradiated silver provides a ^{108m}Ag source which is not commercially available.

---

* Laboratory of Radiation Ecology, University of Washington

---

15. APPENDIX

15.1 Nuclear Physics Laboratory Personnel

Faculty

Eric G. Adelberger, Assistant Professor[1]
John S. Blair, Professor
David Bodansky, Professor
John G. Cramer, Associate Professor
Arthur W. Fairhall, Professor
George W. Farwell, Professor; Vice President for Research
James B. Gerhart, Professor
I. Halpern, Professor
Wilhelm R. Hering, Visiting Senior Research Associate[2]
J. Daniel Larson, Visiting Scholar[3]
Madhukar K. Mehta, Visiting Professor[4]
Fred H. Schmidt, Professor
Robert Vandenbosch, Professor
Denys H. Wilkinson, Battelle Distinguished Professor[5]

Research Staff

John R. Calarco, Research Associate
John M. Cameron, Research Associate[6]
Nicholas S. Chant, Research Associate[7]
Michael D. Hasinoff, Research Associate
Jørgen Pedersen, Research Associate
Ekkehard Preikschat, Research Associate
Willibrord N. Reisdorf, Research Associate
Derek W. Storm, Research Associate[8]
William G. Weitkamp, Senior Research Associate, Technical Director, Nuclear Physics Laboratory

Laboratory Supervisory Personnel

Harold Fauska, Research Electronics Supervisor; Assistant Technical Director, Nuclear Physics Laboratory
John W. Orth, Accelerator Engineer; Assistant Technical Director, Nuclear Physics Laboratory

Predoctoral Research Associates

Chemistry

Clifford Rudy[9]
Phyllis A. Russo
Robert W. Shaw, Jr.[10]

Physics

Michael P. Baker
Wilfred J. Braithwaite[11]
Douglas R. Brown
David Chamberlin
Juri Eenmaa
Robert H. Heffner
William A. Jacobs
David L. Johnson
Thomas K. Lewellen
Ching C. Ling
Roscoe E. Marrs
K. Gopinathan Nair
Dennis L. Oberg
Donald M. Patterson
William Q. Sumner[12]
Joseph R. Tesmer
Wolfgang Trautmann[13]
William R. Wharton
Howard E. Wieman

Research Assistants

Chemistry

Pui-Hing Lau
Douglas W. Potter

Physics

Katsuyuki Ebisawa
Andrew Eng[14]
Sidney Hendrickson[14]
Kwok-Leung Liu[14]
Herbert F. Swanson
Harvey J. Willenberg[14]

Full-Time Technical Staff

Accelerator Operators

Barbara L. Lewellen

Accelerator Technicians

Carl E. Linder
Georgia J. Rohrbaugh
George E. Saling

Chemists

Joanne M. Heagney
Shirley Kellenbarger

Design and Drafting

Peggy Douglass, Graphics Aide
David W. Gough, Designer
Lewis E. Page, Draftsman

Electronics Technicians

Laverne H. Dunning
Kyum-Ha Lee[15]
Norman G. Ward

Engineering and Physics

Noel R. Cheney, Computer Systems Engineer
Judith E. George, Engineering Aide[14]
Rod E. Stowell, Field Engineer
Gary W. Roth, Physicist

Developmental Machinists

Norman E. Gilbertson
Charles E. Hart, Foreman
Gustav E. Johnson
Edwin P. McArthur[16]
Byron A. Scott
Anthony Virant, Leadman
Allen L. Willman

Administrative Staff

N. Lynn Avedovech[14]
Diane Florian
Jennifer S. Osterman[14]
Susan E. Lambert[14]
Helene G. Turner, Administrative Secretary

Part-Time Technical Staff

Jack R. Davis[14]
Robert A. Falk[14]
David O. Hall[14]
Walter E. Lindsay[14]
William R. Mallgren[14]
Peter S. Rabinovitch[14]
Eric Schnellman[14]
Fred Weiss

---

1. On leave; at Princeton University, Princeton, N.J.
2. Permanent address: Max Planck Institute, Heidelberg, Germany.
3. Permanent address: Brookhaven National Laboratory, Upton, New York.
4. Permanent address: Bhabha Atomic Research Centre, Trombay, Bombay, India.
5. Permanent address: Oxford University, England.
6. Now at University of Alberta, Edmonton, Alberta, Canada.
7. Now at University of Minnesota, Minneapolis, Minnesota.
8. Now at Columbia University, New York.
9. Now at Kansas State University, Manhattan, Kansas.
10. Now at Princeton University, Princeton, N.J.
11. Now at Princeton University, Princeton, N.J.
12. Now at Purdue University, Lafayette, Indiana.

13. Predoctoral Research Associate without stipend.
14. Terminated.
15. Transfer to Child Development and Retardation Center, University of Washington.
16. Transfer to Physical Medicine and Rehabilitation, University of Washington.

15.2 Advanced Degrees Granted, Academic Year 1970-1971

W.J. Braithwaite: Ph.D. "Light-Nucleus Reactions with Definite Isospin Leading to Correlated Proton-Neutron Final States"

C.R. Rudy: Ph.D. "Heavy Ion Emission from Light Nuclei"

R.W. Shaw, Jr.: Ph.D. "The Nuclear Elastic Scattering of Identical Oxygen Isotopes"

J.R. Tesmer: Ph.D. "Proton-Gamma Angular Correlation Studies of ^{12}C, ^{58}Ni, and ^{54}Fe"

15.3 List of Publications

"A study of some (p,t) and (p,^{3}He) reactions induced by 49.5 MeV polarized protons", J.M. Nelson, N.S. Chant, and P.S. Fisher, Nucl. Phys. *A156*, 406 (1970).

"Excitation energy dependence of neutron yields and fragment kinetic energy release in the proton-induced fission of ^{233}U and ^{238}U", C.J. Bishop, R. Vandenbosch, R. Aley, R.W. Shaw, Jr., and I. Halpern, Nucl. Phys. *A159*, 129 (1970).

"Mass determinations of the neutron-deficient nuclides ^{88}Zr and ^{140}Nd by (p,2n) threshold measurements", P.A. Russo and R. Vandenbosch, Nucl. Phys. *A159*, 153 (1970).

"Substate Populations and Nuclear Polarization Produced by Inelastic Alpha-Particle Scattering on Carbon-12", T.D. Hayward and F.H. Schmidt, Phys. Rev. *C1*, 923 (1970).

"Spontaneous Fission Isomerism in Uranium Isotopes", K.L. Wolf, R. Vandenbosch, P.A. Russo, M.K. Mehta, and C.R. Rudy, Phys. Rev. *C1*, 2096 (1970).

"$^{20}Ne(p,t)^{18}Ne$ Reaction as a Test of the ^{18}Ne and ^{20}Ne Wave Function", J. L'Ecuyer, R.D. Gill, K. Ramavataram, N.S. Chant, and D.G. Montague, Phys. Rev. *C2*, 116 (1971).

"Particle-Hole States in ^{208}Pb with Configuration $(d_{5/2},j^{-1})$", J.G. Kulleck, P. Richard, D. Burch, C. Fred Moore, W.R. Wharton, and P. von Brentano, Phys. Rev. *C2*, 1491 (1970).

"Energy Dependence of Quasi-Free Scattering in Deuteron Breakup by Protons", D.J. Margazioti, G. Paic, J.C. Young, J.W. Verba, J.M. Cameron, D.W. Storm, and T.A. Cahill, Phys. Rev. *C2*, 2050 (1970).

"Decay of ^{11}Be", D.E. Alberger and D.H. Wilkinson, Phys. Rev. *C3*, 1492 (1971).

"Spin Isomers of the Shape Isomer ^{237m}Pu", P.A. Russo, R. Vandenbosch, M. Mehta, J.R. Tesmer, and K.L. Wolf, Phys. Rev. *C3*, 1595 (1971).

"Decay of ^{25}Na", D.E. Alburger and D.H. Wilkinson, Phys. Rev. *C3*, 1957 (1971).

"Spin Dependence in the Excitation of the First 2^+ State of ^{54}Fe", J.R. Tesmer and F.H. Schmidt, Phys. Rev. Letters *26*, 857 (1971).

"Elastic Scattering of ^{18}O by ^{18}O", R.W. Shaw, Jr., R. Vandenbosch, and M.K. Mehta, Phys. Rev. Letters *25*, 457 (1970).

"β Decay of ^{8}Li and ^{8}B: The Second-Class Current Problem", D.H. Wilkinson and D.E. Alburger, Phys. Rev. Letters *26*, 1127 (1971).

"A comparison of polarization analyzing powers of two-nucleon transfer reactions leading to mirror final states", J.M. Nelson, N.S. Chant, and P.S. Fisher, Phys. Letters *31B*, 445 (1970).

"Spectra of High-Energy Photons Emitted from the Compound System ^{64}Zn in Various Nuclear Reactions", D. Drake, S.L. Whetstone, and I. Halpern, Phys. Letters *32B*, 349 (1970).

"On the effective charge factor for the radiative capture of fast nucleons", J. Zimányi, I. Halpern, and V.D. Madsen, Phys. Letters *33B*,205 (1970).

"Isomer in ^{174}Hf", H. Ejiri, S.M. Ferguson, R. Heffner, and H. Wieman, in *Proceedings of International Conference on Radioactivity in Nuclear Spectroscopy*, (Nashville, Tennessee, 1969).

"Nuclear Polarization of $^{12}C^*(4.44)$ Nuclei Excited by Inelastic Alpha Scattering", F.H. Schmidt and T.D. Hayward in *Symposium on Nuclear Reaction Mechanisms and Polarization Phenomena,1969* (University of Laval Press, Quebec 1970), p. 275.

"An Improved Method of Calculating Finite Range Effects in Two-Nucleon Transfer Reactions", N.S. Chant and N.F. Mangelson in *Symposium on Nuclear Reaction Mechanisms and Polarization Phenomena,1969* (University of Laval Press, Quebec, 1970), p. 281.

"A Comparison of Polarization Analyzing Powers of Two Nucleon Transfer Reactions Leading to Mirror Final States", J.M. Nelson, N.S. Chant, and P.S. Fisher in *Symposium on Nuclear Reaction Mechanisms and Polarization Phenomena,1969* (University of Laval Press, Quebec 1970), p. 387.

"Study of the Energy Dependence of the p-p Quasi-Free Scattering in the Reaction D(p,2p)n", W.J. Braithwaite, J.M. Cameron, D.W. Storm, D.J. Margaziotis, G. Paic, J.G. Rogers, J.W. Verba, and J.C. Young in *The Three Body Problem in Nuclear and Particle Physics*, Ed. by J.S.C. McKee and P.M. Rolph (North Holland, Amsterdam, 1970), p. 407.

Publications in Press or Submitted for Publication:

"The University of Washington Lamb-Shift Polarized Ion Source", E. Preikschat, G. Michel, G.W. Roth, J.G. Cramer, Jr., and W.G. Weitkamp, to be published in *Proc. 3rd International Symposium on Polarization Phenomena in Nuclear Reactions,* Madison, Wisc. (1970).

"A High Pressure Non-Catalytic Method for Cyclotron Production of ^{18}F", G.M. Hinn, W.B. Nelp, and W.G. Weitkamp (submitted to J. Appl. Radiat. Isotopes).

"Electric quadrupole transitions from high spin states in the beta-vibrational band of ^{154}Gd", S.M. Ferguson, R. Heffner, and H. Ejiri (to be published in Phys. Letters).

"Energy Dependence of Quasi-Free Scattering in the D(p,pn)p Reaction", W.J. Braithwaite, J.R. Calarco, J.M. Cameron, and D.W. Storm (to be published in Phys. Rev.).

"Search for a State in ^3He via the $p + d \rightarrow p + d^*$ Reaction", W.J. Braithwaite, J.M. Cameron, D.W. Storm, and T.A. Tombrello (submitted to Phys. Rev.).

"Gross Structure in the Spectra of Helium Ions Inelastically Scattered from Heavy Nuclei with Large Energy Loss", G. Chenevert, N.S. Chant, I. Halpern, C. Glashausser, and D.L. Hendrie (submitted to Phys. Rev. Letters).

"Breit-Wigners Viewed through Gaussians", D.H. Wilkinson (to be published in Nucl. Instr. and Meth.).

"Finite nuclear size and radiative corrections in the construction and assessment of Kurie plots for allowed Beta-decay", D.H. Wilkinson (to be published in Nucl. Instr. and Meth.).

Papers Given at Meetings and Conferences:

"Mechanisms for Reactions Involving Heavy Ions in the Entrance and/or Exit Channel", R. Vandenbosch, Gordon Research Conference on Nuclear Chemistry, New London, New Hampshire, June 1970.